

Diagenetic Controls on Hydrothermal Fluid Flow in the Osiris, Isis, and Isis East
Carlin-Type Gold Showings, Nadaleen Trend, Yukon

by

Neil I. Beaton

A thesis submitted in partial fulfillment of the requirements for the degree of

Master of Science

Department of Earth and Atmospheric Sciences
University of Alberta

©Neil I. Beaton, 2015

Abstract

Following ATAC Resources Ltd.'s 2010 discovery of the gold prospects in the Nadaleen Trend (Central Yukon), company geologists and consultants determined that Precambrian carbonate rocks within the trend contain large endowments of gold located in the hinges of anticlines and fault zones. Subsequent studies revealed that additional gold mineralization is found away from these structures, spatially associated with "dolomitization fronts", i.e. lithological contacts between dolomite and other units.

Geochemical studies reveal that the carbonate host rocks of the Nadaleen Trend precipitated in anoxic, ferruginous seawater during the Ediacaran Period. Large volumes of dolomite and pyrite were generated during near-surface diagenesis, and the pyrite became enriched in trace metals. During further burial, calcite veining and stylolitization occurred. This preceded a base metal mineralization event in which a second generation of dolomite formed; this process created significant new porosity and permeability in the host rocks. Further calcite veining and a second generation of stylolitization subsequently occurred. This was post-dated by the ore stage which consisted of the precipitation of gold-bearing arsenian pyrite and a third generation of dolomite. Ore fluids travelled vertically along faults and laterally into Permeable zones associated with saddle dolomite and stylolites. Gold-bearing fluids travelled through these conduits until they encountered pyrite grains, at which point a sulfidation reaction occurred. This reaction resulted in deposition of gold-bearing arsenian pyrite on the pre-existing grains of pyrite. Since the first two generations of pyrite occur most commonly in dolomite rather than limestone, gold mineralization occurred preferentially in dolomite. A post-ore stage occurred consisting of calcite, realgar, and orpiment.

Electron microprobe analysis and laser ablation inductively coupled plasma mass spectrometry reveals that the hydrothermal fluids were reducing and acidic, and thus were capable of dissolving carbonates to create porosity. Carbon, oxygen, and strontium isotopic data on calcite and dolomite indicate that the hydrothermal fluids isotopically equilibrated with the host rocks. The mineralization present in the Nadaleen Trend has geological features similar to those of world-class Carlin-type gold deposits, a class of gold deposits modelled after the Carlin Trend in Nevada.

Preface

The project for this MSc. thesis was coordinated by Dr. Sarah Gleeson of the University of Alberta (U. of A.) and ATAC Resources Ltd. (ATAC). The author spent the summer of 2012 working in Nadaleen Camp of Central Yukon and collecting core samples for the thesis. Half-core from all drill holes was sent to ALS Minerals in Vancouver by Archer, Cathro and Associates (AC) to examine whole-rock geochemistry of the rocks. These Au grades were used as a guide for sample selection, and ultimately 502 rock samples from seven drill holes were collected. Rocks were then sent to Edmonton and the study commenced in September 2012.

Rock sample collection from Nadaleen Camp was a collaborative effort between the author and Dr. Gleeson, and sample selection for all subsequent analytical methods was conducted by the author. Hand sample and petrographic studies were carried out by the author, and the subsequent analytical techniques were conducted by the author with guidance by University of Alberta (U. of A.) or University of Calgary (U. of C.) faculty and staff. Cathodoluminescence microscopy (CL) was conducted with the assistance of Judy Schultz (U. of A.), electron microprobe analysis (EMPA) with Andrew Locock (U. of A.), laser ablation secondary ion mass spectrometry (LA-ICP-MS) with Yan Luo, secondary ion mass spectrometry (SIMS) with Richard Stern (U. of A.), and strontium isotope analysis with Chiranjeeb Sarkar (U. of A.). Samples for bulk carbon, oxygen, and sulfur isotopic data were selected by the author and sent to the U. of C. where they were analyzed by Steve Taylor. All data presented in this thesis were collected by the author, and all figures and tables were made by the author unless otherwise indicated.

Acknowledgments

I would like to acknowledge Dr. Sarah Gleeson for her guidance, support, and patience throughout this master's thesis. Beginning with a minimal geochemistry background, it was with her guidance and experience that I managed to complete this complex geological and geochemical study. I would also like to acknowledge Julia Lane, Rob Carne, Joan Carne, and the rest of the AC and ATAC crew for their collaborative insight into my thesis and the Nadaleen gold project. There are numerous other U. of A. staff and faculty members who have been of utmost importance to my studies including Judy Schultz for assistance with CL microscopy, Andrew Locock of the EMPA lab, Yan Luo of the LA-ICP-MS Lab, Richard Stern of the CCIM Lab, Chiranjeeb Sarkar for strontium isotopic studies, and Steve Taylor (U. of C.) for carbon, oxygen, and sulfur isotopic studies. I would also like to acknowledge Michael Rogers, Laurence Pryer, Joe Magnall, Merilie Reynolds and Yannick Bussweiler for their willingness to provide scientific insight into my thesis project.

Funding for this thesis was provided by ATAC and a Collaborative Research and Development Grant to Sarah Gleeson from the Natural Sciences and Engineering Research Council of Canada (NSERC).

Table of Contents

Chapter 1 - Introduction	1
1.1 Gold Deposits in Yukon	1
1.2 Carlin-type Gold Deposits	4
1.2 Thesis Aims and Outline	5
Chapter 2 - Diagenetic Controls on Hydrothermal Fluid Flow in the Osiris, Isis, and Isis East Carlin-Type Gold Showings, Nadaleen Trend, Yukon	6
2.1 Introduction	6
2.2 Regional Geology	8
2.3 Local geology	9
2.3.1 Stratigraphy of the Nadaleen Trend	9
2.3.2 Structural History of the Nadaleen Trend	12
2.3.3 Mineralization in the Nadaleen Trend	13
2.4 Methods and analytical techniques	14
2.4.1 Petrography and Cathodoluminescence Microscopy	14
2.4.2 EMPA	14
2.4.3 LA-ICP-MS	15
2.4.4 Bulk Carbon and Oxygen Isotopes	16
2.4.5 Secondary Ion Mass Spectrometry	16
2.4.6 Strontium Isotopes	17
2.4.7 Sulfur Isotopes	18
2.4.8 Whole-rock Geochemistry	18
2.5 Results	19
2.5.1 Logs and Cross section	19
2.5.2 Petrology and Paragenesis (hand specimen, thin section, CL)	22
Host Rocks	22
Near-Surface Diagenesis Stage (Stage I)	24
Base Metal Mineralization Stage (Stage II)	26

Intermediate Diagenesis Stage (Stage III)	27
Ore Stage (Stage IV)	29
Post-Ore Stage (Stage V)	30
2.5.3 EMPA	32
Carbonate EMPA	32
Host Rocks and Near-Surface Diagenesis Stage (Stage I).....	32
Base Metal Mineralization Stage (Stage II)	34
Intermediate Diagenesis Stage (Stage III).....	35
Ore Stage (Stage IV)	38
Post-Ore Stage (Stage V)	38
Sulfide EMPA	38
Host Rocks and Near-Surface Diagenesis Stage (Stage I).....	39
Base Metal Mineralization Stage (Stage II)	41
Ore Stage (Stage IV)	42
2.5.4 LA-ICP-MS	45
Carbonate LA-ICP-MS	45
Host Rocks and Near-Surface Diagenesis Stage (Stage I).....	46
Base Metal Mineralization Stage (Stage II)	49
Intermediate Diagenesis Stage(Stage III).....	49
Ore Stage (Stage IV)	51
Post-Ore Stage (Stage V)	51
Pyrite LA-ICP-MS	55
Near-Surface Diagenesis Stage (Stage I)	56
Base Metal Mineralization Stage (Stage II)	59
Ore Stage (Stage IV)	59
2.5.5 Bulk Carbon and Oxygen Isotopes	59
Host Rocks and Near-Surface Diagenesis Stage (Stage I)	59
Base Metal Mineralization Stage (Stage II)	62

Intermediate Diagenesis Stage (Stage III).....	62
Ore Stage (Stage IV)	62
Post-Ore Stage (Stage V)	62
2.5.6 SIMS.....	63
Host Rocks and Near-surface Diagenesis Stage (Stage I).....	64
Base Metal Mineralization Stage (Stage II)	65
Intermediate Diagenesis Stage (Stage III).....	67
Ore Stage (Stage IV)	67
Post-Ore Stage (Stage V)	67
2.5.7 Sr isotopes	69
Host Rocks	70
Base Metal Mineralization Stage (Stage II)	70
Intermediate Diagenesis Stage (Stage III).....	70
Ore Stage (Stage IV)	71
Post-Ore Stage (Stage V)	71
2.5.8 Sulfur Isotopes.....	72
Near-Surface Diagenesis (Stage I)	72
Base Metal Mineralization Stage (Stage II)	73
Ore Stage (Stage IV)	73
2.6 Discussion	74
2.6.1 Host Rocks	74
2.6.2 Near-Surface Diagenesis Stage (Stage I).....	76
2.6.3 Base Metal Mineralization Stage (Stage II).....	78
2.6.4 Intermediate Diagenesis Stage (Stage III)	81
2.6.5 Ore Stage (Stage IV)	82
2.6.6 Post-Ore Stage (Stage V)	83
2.6.7 Controls on Hydrothermal Fluid Flow	84
2.6.8 Deposit Model and Controls on gold Mineralization.....	86

2.6.9 Comparison with Carlin-type Gold Deposits	89
Chapter 3 Conclusions	92
3.1 Implications for Exploration	94
Works Cited	95
Appendix A – Stratigraphic Logs	107
Appendix B – EMPA Operating Conditions.....	108
Appendix C – Whole-rock Geochemistry Gold Grades	109
Appendix D – EMPA Data	116
Appendix E – LA-ICP-MS Data	140
Appendix F – SIMS Data.....	176

List of Tables

Table 1. Selected carbonate LA-ICP-MS data **48**

Table 2. Selected sulfide LA-ICP-MS data **57**

Table 3. Bulk C and O isotope data..... **60**

Table 4. Sr isotope data **69**

Table 5. S isotope data..... **72**

Table 6. Features of Carlin-type Gold Deposits compared with Nadaleen Trend **89**

Table 7. Pyrite composition in Nadaleen and Carlin Trend **90**

Table 8. EMPA operating conditions **108**

List of Figures

Figure 1. Geologic map of Yukon and Rackla Gold Belt	2
Figure 2. Geologic map of the Eastern Nadaleen Trend	3
Figure 3. Geologic map of Yukon and Rackla Gold Belt with detailed lithologies.....	7
Figure 4. Schematic model for Nadaleen Basin architecture	10
Figure 5. Correlation of Windermere stratigraphy with Isis and Isis East	11
Figure 6. Stratigraphic logs of Osiris holes and representative samples	19
Figure 7. Stratigraphic logs of Isis and Isis East holes and representative samples.....	20
Figure 8. Cross section of Isis East hole OS-12-120.....	21
Figure 9. Images for host rocks	23
Figure 10. Paragenetic Sequence.....	24
Figure 11. Images for Stage I	25
Figure 12. Images for Stage II.....	27
Figure 13. Images for Stage III	28
Figure 14. Images for Stage IV	29
Figure 15. Images Stage V	31
Figure 16. Carbonate paragenetic stages with corresponding data table.....	33-34
Figure 17. X-Y plots for Carbonate EMPA data.....	36
Figure 18. Zoned dolomite images with corresponding EMPA data	37
Figure 19. Ternary plot of sulfides.....	39
Figure 20. Sulfide paragenetic stages with corresponding EMPA data	40-41
Figure 21. X-Y plots for sulfide EMPA data	43
Figure 22. EMPA elemental maps of pyrite grains	44
Figure 23. Carbonate LA-ICP-MS craters and corresponding data	45-46
Figure 24. LA-ICP-MS data for carbonate phases	50
Figure 25. LA-ICP-MS data for carbonate phases cont'd.....	52
Figure 26. REY plots for carbonate phases	53
Figure 27. X-Y plots of carbonate LA-ICP-MS data	54

Figure 28. Sulfide LA-ICP-MS craters and corresponding data	55-56
Figure 29. X-Y plots of sulfide LA-ICP-MS data.....	58
Figure 30. Bulk C and O isotope plot.....	61
Figure 31. SIMS C and O images with corresponding data.....	63-64
Figure 32. SIMS C and O isotope plots.....	66
Figure 33. SIMS C and O data vs. EMPA data.....	68
Figure 34. Sr isotope data vs. EMPA data	70
Figure 35. S isotope data	73
Figure 36. Controls on hydrothermal fluid flow	85
Figure 37. Schematic Model for Host Rocks and Stage I	86
Figure 38. Schematic Model for Stage II	87
Figure 39. Schematic Model for Stage IV	88

Chapter 1 - Introduction

1.1 Gold Deposits in Yukon

Gold has existed as a minor constituent of the Earth ever since its formation 4.54 billion years ago. Throughout Earth's history, geological processes such as mantle convection and plate tectonics have redistributed this gold, transporting and concentrating some of it at, or near, the Earth's surface. These economic accumulations of gold occur in many geological settings, including surficial (e.g. placer), orogenic vein systems in cratons, magmatic hydrothermal systems associated with volcanic arcs (e.g. porphyry Cu-Au deposits), and sedimentary-hosted gold deposits (e.g. gold bearing sedimentary exhalative deposits and Carlin-type systems). Yukon, Canada has a rich gold mining history; the Klondike Gold Rush attracted thousands of people to the Yukon and Alaska at the end of the 19th century to mine placer gold. More than one hundred years later, gold deposits in the Yukon are still of great economic significance; approximately \$45 million was spent on mineral exploration in Yukon in 2013, and 76% of these expenditures were on gold exploration (Pigage et al., 2014). Since 2006, when multiple gold discoveries were made by Vancouver-based ATAC in the 1,700 km² Rackla Gold Belt (Fig. 1a), the area has been the focus of exploration programs. The Rau Trend is located in the western end of the Rackla Belt and hosts the Tiger gold and the Ocelot silver-lead-zinc prospects (Fig. 1b). The Nadaleen Trend, in the eastern end of the Rackla Belt, hosts seven gold prospects.

Recently, ATAC's exploration focus has been in the 50 km-long Nadaleen Trend (Fig. 1b). Mineralization in the Nadaleen Trend was discovered in 2010 by ATAC during regional bedrock mapping where outcrops containing abundant realgar were discovered. Subsequent soil sampling revealed gold in soil anomalies, which led to regional drilling and the discovery of high-grade gold prospects. Within the Nadaleen Trend, there are seven major zones of gold mineralization: Conrad, Osiris, Isis, Isis east, Amon, Anubis, and Sunrise (ATAC Resources Ltd., 2011a; 2012a; 2012b; 2013; 2014). This study focuses on the Osiris, Isis, and Isis east zones which lie in the 1.5 km² area in the eastern Nadaleen Trend shown in Figure 2.

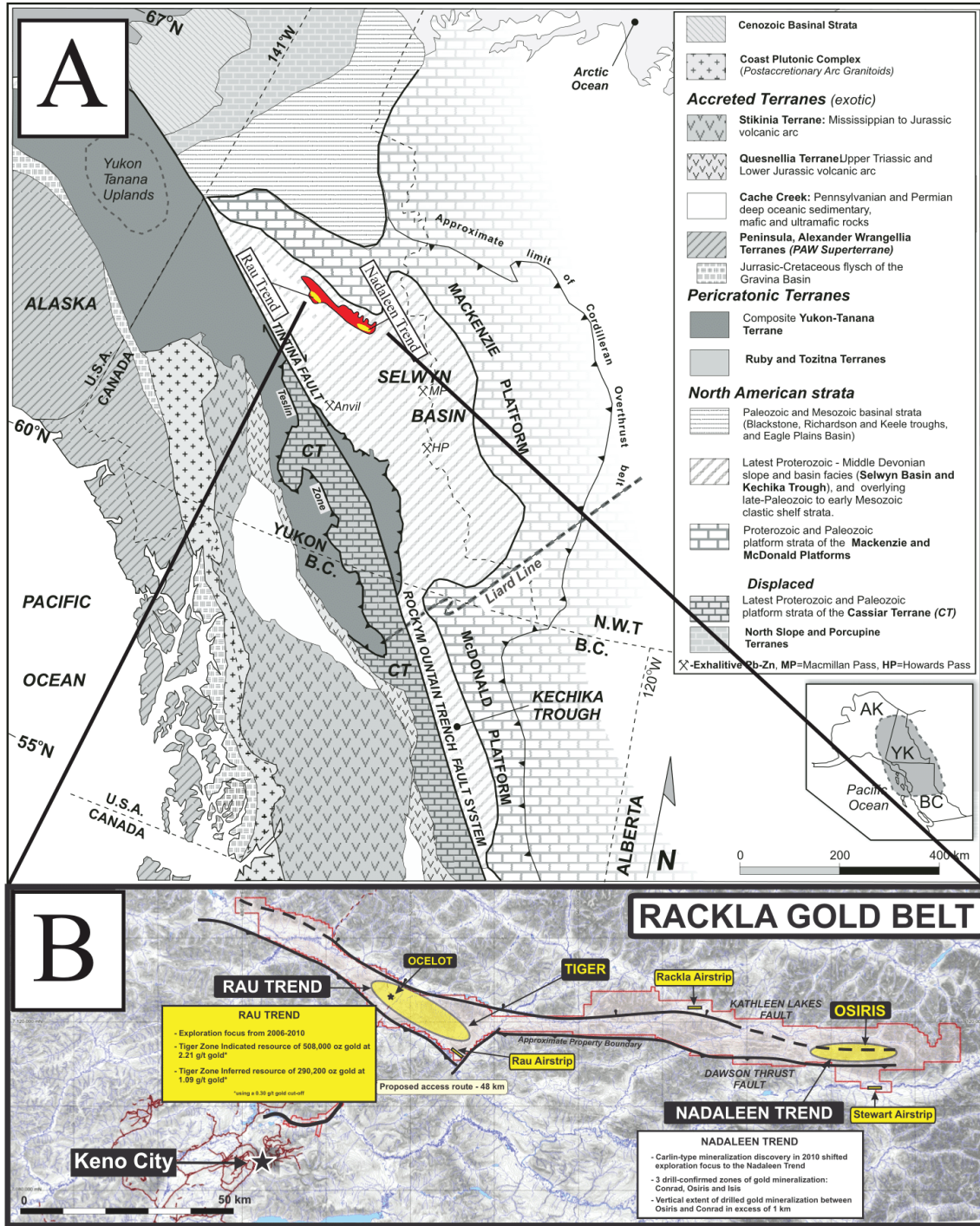


Figure 1. A) Geologic Map of the Yukon showing location of the Rackla Gold Belt Nadaleen Trend (modified after Mair et al., 2006). B) Map of the Rackla Gold Belt showing the locations of the Rau Trend and the Nadaleen Trend (modified after ATAC Resources Ltd., 2011b).

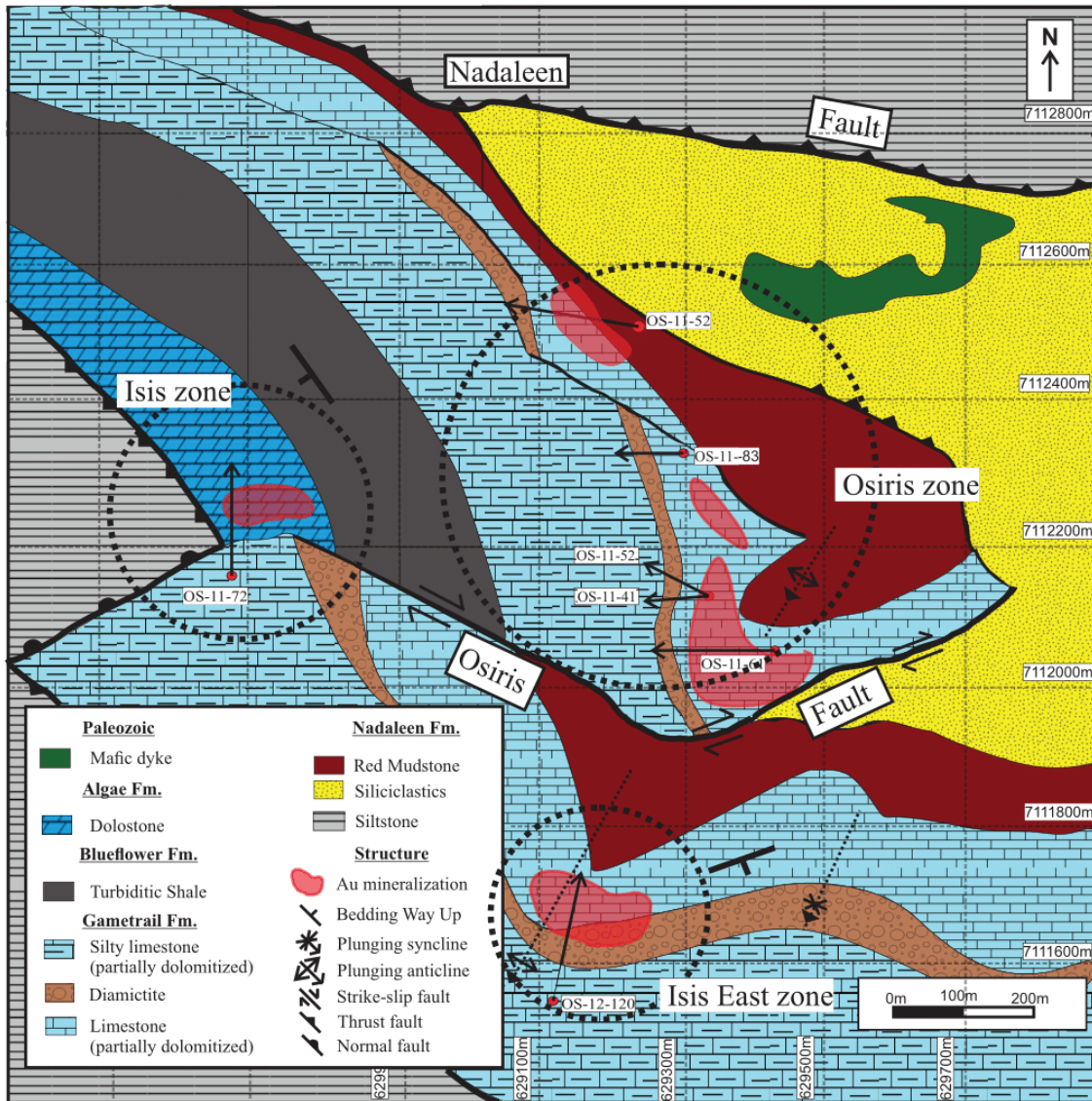


Figure 2. Map of the area of study in the Eastern Nadaleen Trend with locations of the Osiris, Isis, and Isis East zones. Modified after ATAC Resources (2013). Directions of plunge and directions of fault motion are from Palmer (2014).

Studies by company geologists (ATAC) and consultants have suggested that the gold mineralization is hosted in Ediacaran, silty, carbonate rocks (Colpron et al., 2013). Some of the highest gold grades are found in brecciated zones in limestone and dolostone (Tucker et al. 2013), as well as in the hinges of anticlines; in these areas carbonate has been removed (decarbonatized) and silicification has occurred. Gold is also found at stratigraphic contacts of limestone with dolostone, a.k.a. “dolomitization fronts” (Gleeson, 2012). It has been suggested that gold occurs in arsenic-rich rims on euhedral and framboidal pyrite grains (Acosta-Gongora and Gleeson, 2011).

The work by ATAC indicated that the style of mineralization in the Nadaleen Trend is strikingly similar to the gold mineralization in the Carlin Trend of Nevada, U.S.A., which is one of the premier areas of gold mining and production in the world. “Carlin-type Gold Deposits” (CTGDs) occur in clusters and have huge gold reserves, with several deposits in the Carlin Trend containing more than ten million ounces of gold (Cline et al., 2005). There are CTGDs in other parts of the world such as the Zimudang Gold Deposit in China and the Alšar District in Macedonia, but up until recently, no CTGDs have been discovered in Canada. Therefore, ATAC’s discovery of the prospects in the Nadaleen Trend with the first Carlin-Type gold mineralization to be discovered in Canada is of great interest for gold exploration in the Yukon. Gaining an understanding of the geological history and the diagenetic history of the sedimentary host rocks in the Nadaleen Trend will be fundamental in understanding the spatial distribution of gold in the area. To fully understand the gold deposits of the Nadaleen Trend, the geological characteristics of CTGDs must first be addressed. The next section (Ch. 1.2) will provide a brief literature review on CTGDs to provide context for this study on gold mineralization in the Nadaleen Trend.

1.2 Carlin-Type Gold Deposits

Gold mineralization in the Carlin District of northeast Nevada was discovered in the 1960s, and in the last 50 years it has become one of the largest producers of gold in the world, with production of over 50 Moz (Price and Meeuwig, 2004). The host rocks in the Carlin district comprise Paleozoic silty carbonate strata which are exposed beneath the Late Devonian to early Mississippian Roberts Mountain thrust fault. Structural controls may also be important in the Carlin District, as most of the gold is found in Silurian-Devonian carbonates beneath the Roberts Mountain thrust fault (Bakken, 1990). The current structural configuration of the Carlin District is complex, owing to a series of deformational events spanning from the Late Devonian to the Late Cretaceous (Roberts et al., 1958; Ketner 1977; Theodore et al., 2004; Cline et al., 2005) that ultimately affected hydrothermal fluid flow and subsequent gold mineralization between 42 and 36 Ma (Cline et al., 2005).

The orebodies are silty limestones which have been decarbonatized, argillized (i.e. new clay minerals have been introduced), brecciated, and faulted. The occurrence of gold within pyritic silty carbonates is controlled by sedimentological and mineralogical processes. Gold in the Carlin district occurs as invisible sub-micron gold associated with arsenian pyrite (Cline et al., 2005).

The gold-bearing hydrothermal fluids had temperatures that ranged from 180-240°C (Cline and Hofstra, 2000), salinities of 2-3 wt. % NaCl, and abundant H₂S (Cline et al., 2005), which is important as gold was likely transported as a bisulfide species (Emsbo et al. 2003; Cline and Hofstra, 2000; Benning and Seward, 1996). Ore fluids travelled vertically and

laterally along faults (Radtke et al., 1980; Kuehn and Rose 1992; Stenger et al. 1998; Hickey et al., 2014a) and deposited gold in the Eocene, between 36 and 42 Ma (Hofstra et al., 1999; Arehart et al., 2003; Tretbar et al., 2000), suggesting there is spatial and temporal overlap of CTGDs with regional extension and volcanism (Ilchik and Barton, 1997; Hofstra et al., 1999). It has been suggested that the duration of ore genesis was <15 to 45 ka, and that the gold flux was 30 to 80 kg/yr (Hickey et al., 2014b). The origin of the gold-bearing fluids is debated, as some have argued for a metamorphic/magmatic source (Muntean et al., 2011; Cline and Hofstra, 2000), and others have suggested a meteoric water source where meteoric fluids scavenged gold from sedimentary rocks (Ilchik and Barton, 1997). The gold is commonly found in arsenian pyrite rims which nucleated on earlier-formed euhedral or framboidal pyrite (Wells and Mullens, 1973; Arehart et al., 1993; Scott et al., 2009; Barker et al., 2009). Some authors have suggested a key factor is the presence of iron-rich silty carbonates, as it is the sulfidation of iron that is thought to have controlled ore deposition (Hofstra et al., 1991).

Decarbonatization, argillization, and silicification of carbonates are also important steps in mineralization, and these processes created voids in which significant volumes of gold ultimately were deposited (Cline and Hofstra, 2000; Cline et al., 2005; Bakken, 1990; Emsbo et al., 2003). Much of the gold is associated with other ore-stage minerals including pyrite, marcasite, quartz, kaolinite, dickite and illite as well as late ore-stage minerals such as realgar and orpiment (Cline et al., 2005).

1.3 Thesis Aims and Outline

The Nadaleen Trend contains the first Carlin-type gold mineralization to be discovered in Canada, and the implications of the discovery may be very economically significant. Carlin-type gold deposits typically have a strong structural control on mineralization but the diagenetic history of the host-rocks may affect fluid flow away from feeder structures and, therefore, control the tonnage of the deposits. The main aims of this master's thesis were to determine how the diagenetic and cementation history of the Nadaleen Trend has affected the migration of gold-bearing hydrothermal fluids, and to determine the spatial distribution of dolomite and gold deposition.

This paper-based thesis consists of three chapters. This chapter (Chapter 1) serves as a broad introduction to the project and to CTGDs. Chapter Two presents the results of the research, and will be published as a scientific paper. Chapter Three is a broad conclusion chapter that outlines the major conclusions of the research and contains suggestions for future research.

Chapter 2 - Diagenetic Controls on Hydrothermal Fluid Flow in the Osiris, Isis, and Isis East Carlin-Type Gold showings, Nadaleen Trend, Yukon

2.1 Introduction

Sediment hosted gold mineralization was discovered in 2010 in the Nadaleen Trend of central Yukon. The Nadaleen Trend is located 185 km ENE of Mayo, Yukon, near the eastern margin of the Rackla Gold Belt (Fig. 3). There has been significant gold mineralization discovered in seven prospects within the Nadaleen Trend: Osiris, Isis, Isis East, Conrad, Anubis, Sunrise, and Amon. Intersections in drill cores include 27.43 m grading 6.28 g/T in the Isis East zone (ATAC Resources Ltd., 2012b) and 26.12 m grading 6.08g/T in the Osiris zone (ATAC Resources Ltd., 2011a). The age of the mineralization is unknown but has been constrained to be between 74 and 42 Ma at the Conrad Prospect (Tucker, 2015). The origin and controls on gold mineralization in the Nadaleen Trend are not fully understood, but there are a number of studies being carried out to gain a better understanding of the geologic history of the area. It is evident that there is a structural control on mineralization; at Conrad the high grade mineralization is associated with faults, and in Osiris there is significant mineralization found in the hinges of anticlines (Palmer, 2014). There are many areas of the Nadaleen Trend where gold mineralization is not associated with faults or folds but rather, is associated with “dolomitization fronts” i.e. lithologic boundaries between dolostone and limestone (Gleeson, 2012).

ATAC has concluded that this area contains the first Carlin-type gold showings to be discovered in Canada. There are many features of the Nadaleen Trend that bear similarity to the Carlin District of Nevada: silty carbonate host rocks, presence of regional thrust faults, and evidence of decarbonatization, silicification, and brecciation of the host rock associated with gold mineralization. Tucker (2015) suggested that decarbonatization of host carbonates and subsequent silicification and brecciation are processes that accompanied gold mineralization. The orebodies are commonly shear- and breccia-zones infilled with jasperoid, calcite, realgar, and orpiment (Tucker, 2015). Gleeson (2012) suggested that dolomitization may have also acted as a control on mineralization. The overarching objective of this study was to determine how the diagenetic and cementation history of the Nadaleen host rocks ultimately affected hydrothermal fluid flow in the Osiris, Isis, and Isis East zones of the Nadaleen Trend.

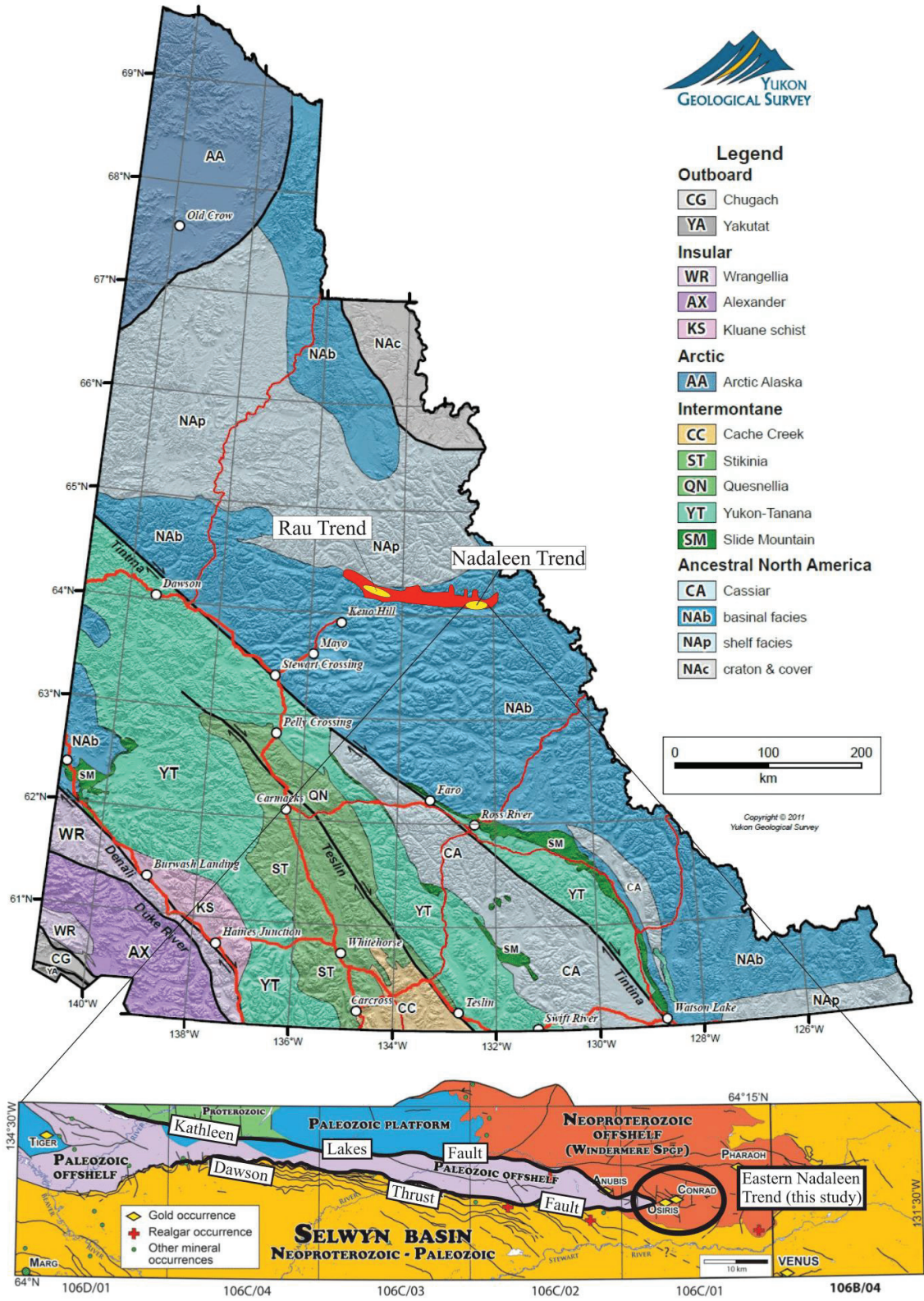


Figure 3. Map of the Yukon with location of Rackla Belt and Nadaleen Trend. The circled area in the lower part of the figure shows the location of the Osiris zone. Modified after Colpron et al. (2013).

The diagenetic and cementation history of the host and mineralized units were investigated via petrography, CL, EMPA, and LA-ICP-MS. The source of the hydrothermal fluids and other components were investigated through stable isotope studies of carbon, oxygen, strontium, and sulfur. Finally, a genetic model was constructed for the studied deposits.

2.2 Regional Geology

The geological history of Yukon is protracted, comprising crustal extension, orogenesis, and cratonization of the supercontinent Laurentia, followed by Neoproterozoic to Mesozoic sedimentation, and the Mesozoic accumulation of accreted terranes (Thorkelson et al., 2005; Mair et al., 2006). Cratonization of Laurentia possibly began at 2.0 Ga and the last major tectonic and magmatic events of the Laurentian craton occurred roughly 1.84 Ga (Thorkelson et al., 2005; Norris and Dyke, 1997). Laurentia may have been connected to another continent at the time, or continents, such as Australia (Bell and Jefferson, 1987), Antarctica (Moores 1991; Dalziel, 1991), Siberia (Sears and Price, 2000), South China (Li et al., 1995), or Rodinia (Colpron et al., 2002). Approximately 1.7 billion years ago, attenuation of Laurentia occurred, forming a passive margin or intracratonal basin in which sediments of the Wernecke Supergroup were deposited. This marks the beginning of the development of the Mackenzie Platform, a succession of four Supergroups (Wernecke, Pinguicula, Mackenzie, Windermere; Fig. 1). An extensional event occurred at ~1.38 Ga, during which rocks of the Pinguicula Supergroup were deposited. The Mackenzie Mountains Supergroup was then deposited on a platform extending from the Canadian Shield to the Amundsen basin (Rainbird et al., 1996). Overlying the Mackenzie Mountains Supergroup is the Windermere Supergroup, a 5 to 7 km thick package of basal rift deposits, glacial diamictites, siliciclastics, and carbonates. The base of the Windermere Supergroup is thought to represent synrift sedimentation between 762 and 728 Ma, during the breakup of the supercontinent Rodinia (Mair et al., 2006), between 755 and 700 Ma (Windgate and Giddings, 2000; Powell et al., 1993).

Overlying the Windermere Supergroup, on the western flank of North America, sedimentation continued from the Neoproterozoic to the Mesozoic. These sediments are now preserved as the Selwyn Basin sedimentary package (Mair et al., 2006). The supercontinent Laurentia began to break up roughly 575 Ma (Colpron et al., 2002). Allochthonous terranes were accreted to the west coast of North America from the Early Jurassic to the Late Cretaceous (Mair et al., 2006; Monger et al., 1982; Coney et al., 1980), deforming the sedimentary rocks and causing mid-Cretaceous plutonism (Armstrong, 1988). The NW-SE-trending Tintina Fault separates rocks of ancestral North America (to the NE) and the accreted terranes (to the SW; Fig. 1). In the Northern Selwyn Basin there is a structural trend called the Rackla Gold Belt. The Rackla Gold Belt is an E-W-trending structural trend at the northern margin of the Selwyn Basin (“basinal facies” on Fig. 3), which also fringes on the Windermere Supergroup. The major structural features in the Rackla Belt are the Dawson Thrust Fault and the Kathleen Lakes Fault (Moynihan et al.,

2014; Fig. 3). The Rackla Belt can be divided into five stratigraphic facies domains: the Selwyn Basin, Paleozoic offshore carbonates, the Windermere Supergroup, Paleozoic platform carbonates, and the Neoproterozoic Wernecke and Pinguicula Supergroups, as shown in Figure 3 (Colpron et al., 2013). The Neoproterozoic to Upper Paleozoic Selwyn Basin sedimentary rocks comprises mostly clastic rocks, and occurs in the hanging wall of the Dawson fault (yellow unit to the south of the fault). To the north of the Dawson fault Ordovician-Permian offshore carbonates and shales (purple unit) are exposed and are bounded by the E-W trending Dawson Thrust and Kathleen Lakes faults. Neoproterozoic offshore siliciclastic and carbonates of the Windermere Supergroup (red unit) are found in the eastern footwall of the Dawson Thrust. Ordovician to Devonian platform carbonates are located to the north of the Kathleen Lakes fault (blue unit), and Proterozoic rocks of the Wernecke and Pinguicula Supergroups are also found north of the Kathleen Lakes fault; the green unit at the western end of the Nadaleen Trend (Colpron et al., 2013).

2.3 Local geology

2.3.1 Stratigraphy of the Nadaleen Trend

Colpron et al. (2013) have suggested that in the Neoproterozoic there was a basement high (Fig. 4) that controlled sedimentation into two sedimentary basins: the Nadaleen Basin (containing the Windermere Supergroup) and the Hyland basin (containing the Yusezu Formation). The Windermere Supergroup comprises basal rift deposits and glacial diamictites which are overlain by siliciclastics and carbonates (Narbonne and Aitken, 1993). The sedimentary rocks of base of the Windermere Supergroup were deposited in an intracontinental rift setting between 740 and 723 Ma during the Sturtian glaciation (Eisenbacher, 1981; Ross et al., 1995; Colpron et al., 2002), whereas the upper rocks of the Windermere Supergroup were deposited in a passive margin setting. The Windermere Supergroup consists of the following sedimentary packages, in order from oldest to youngest: Coates Lake Group, Rapitan Group, Twitya, Ice Brook/Keele, Sheepbed, Nadaleen, Gametrail, Blueflower, and Risky Formations (Fig. 5). Colpron et al. (2013) have suggested that the limestones of the Osiris and Isis East zones of the Nadaleen Trend (Fig. 2) are part of the Gametrail Formation. This correlation was made based on lithologic correlations, and the fact that Ediacaran fauna have been discovered in the Gametrail Formation. The Gametrail Formation has been described as a 320m thick dolomitized carbonate cap overlying deep-water mudrocks (Aitken, 1989). The Gametrail Formation formed as part of a transgressive systems tract during a time in which carbonates with very low $\delta^{13}\text{C}$ values were forming (the "Shuram negative carbon isotope excursion", herein referred to as the Shuram Excursion; Macdonald et al., 2013).

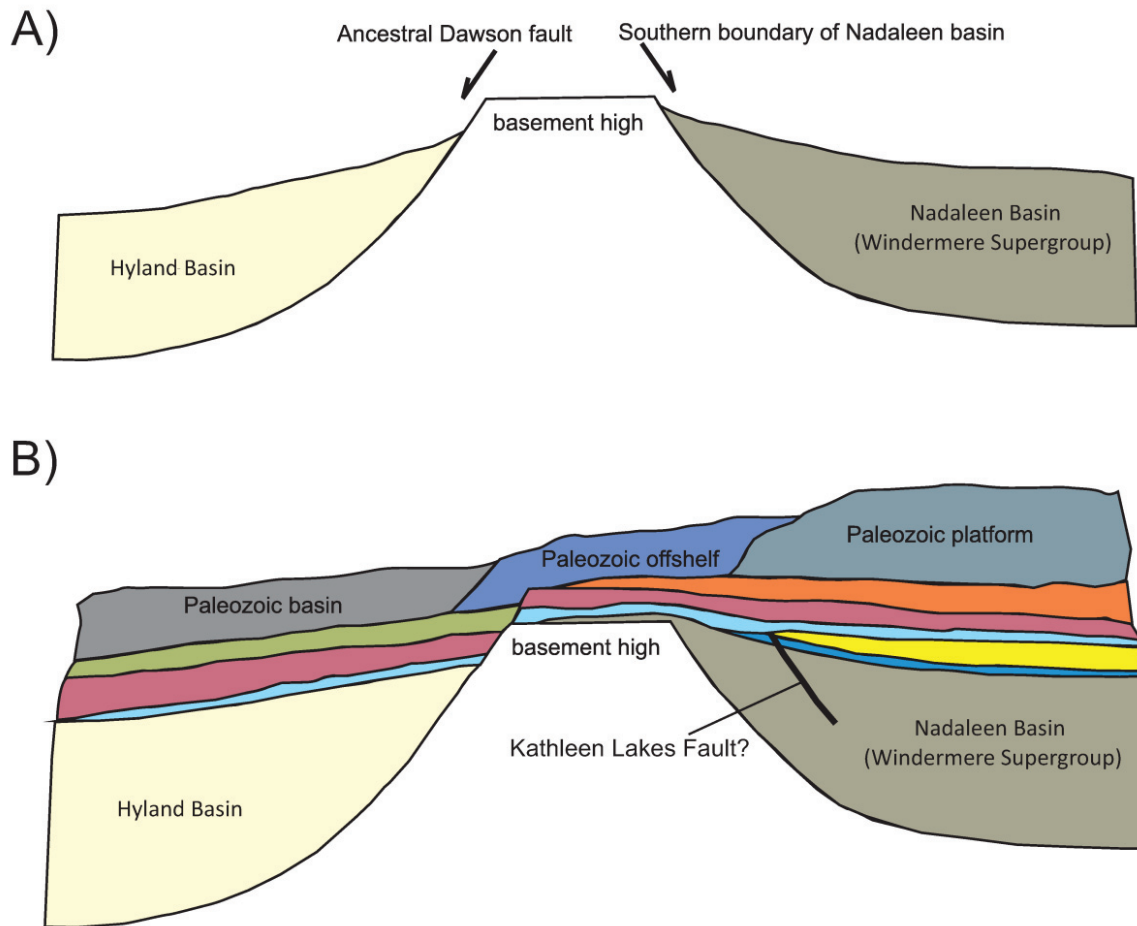
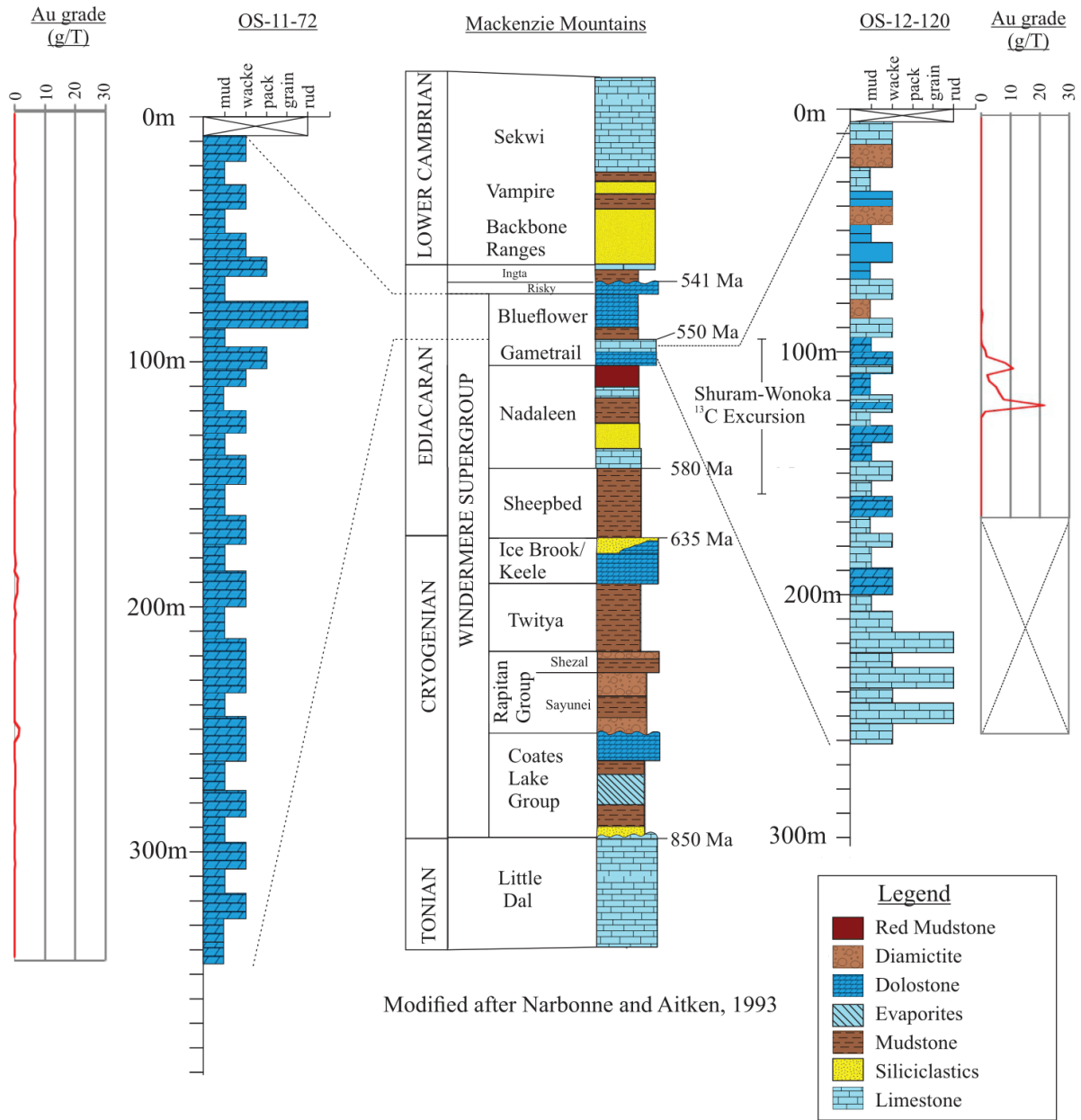


Figure 4. Cross section of stratigraphy modified after Colpron et al. (2013). Basement high is vertically exaggerated.

Overlying the Gametrail Formation is the Blueflower Formation which is dominated by dark shales and turbiditic sandstones (Fig. 2, 5; Narbonne and Aitken, 1993). This is overlain by the Algae formation, a package of limestones and dolostones which is contemporaneous with the Risky Formation (Fig. 5; Moynihan et al., 2014). The carbonates in the Isis zone are part of the Blueflower Formation (Fig. 2, 5). Overlying the Blueflower Formation are the Risky and Ingta Formations (Fig. 5), which represent the top of the Windermere Supergroup. These two units are not present in the Eastern Nadaleen Trend in Figure 2. Beneath the Gametrail Formation is the Nadaleen Formation, which is reached in deeper parts of the Osiris and Isis East holes. Following deposition of the rocks of the Windermere Supergroup, sedimentary rocks were continually deposited over the basement high (Fig. 4B) throughout the Paleozoic.



Modified after Narbonne and Aitken, 1993

Figure 5. Stratigraphy of Isis East hole OS-12-120 and Isis hole OS-11-72 with Mackenzie Mountains stratigraphy. Whole-rock geochemistry gold grades of drill holes indicated by red lines. Gold grades were not determined for OS-12-120 below 175m. Units in Nadaleen Trend drill holes have been correlated with the Gametrail Formation (Colpron et al., 2013). Isis East hole OS-12-120 (and all drill holes in Osiris) are part of the Gametrail Formation whereas Isis hole OS-11-72 is part of the Blueflower Formation. Modified after Narbonne and Aitken (1993) and Moynihan et al. (2013). Dates are from MacDonald et al. (2013).

2.3.2 Structural History of the Nadaleen Trend

The Nadaleen Trend is delineated by the roughly E-W-trending Dawson Thrust Fault and the Kathleen Lakes Fault. These faults wane to the east, with both faults terminating near the eastern Nadaleen Trend (Fig. 3; Moynihan et al., 2014). The overall structural style in the area is NNE-vergent fold-thrust deformation, although the area of study in eastern Nadaleen Trend (Fig. 2) occurs in a triangle zone that is not seen to the east or west and is bounded by S- and N-vergent reverse faults in the north and south, respectively (Palmer, 2014). This 6 km² eastern Nadaleen area contains the following features: (1) generally southerly-dipping bedding, (2) several hundred-meter scale, open to tight chevron folds that plunge moderately to steeply to the SSW, WSW, SE, and E, (3) the E-trending dextral Osiris Fault, (4) the steeply NNE-dipping Nadaleen Fault zone and (5) the late N-trending dextral Conrad Fault (Palmer, 2014). These structural features are oblique to the overall trend of the Nadaleen area and the Rackla Belt. Not all of these features are present in the 1.5 km² area of this study. The dip of the bedding is variable due to the folding, there is a chevron fold in the Isis East zone but not Osiris, the Osiris fault has been folded and trends in several directions, the steeply-dipping Nadaleen fault is present, and the Conrad fault is not present here.

Palmer (2014) suggested that the obliquity of the area in the eastern Nadaleen Trend is due to a basement structure that obstructed NNE-vergent fold-thrust movement to the west of the eastern Nadaleen trend. The rigid basement structure responsible for this obliquity is the basement high shown in Figure 4, and likely had different rheological properties than the overlying sediments. This obstruction resulted in strike-slip motion seen in the Nadaleen trend (Palmer, 2014). The repeated stratigraphy of the Osiris and Isis East zones is due to strike-slip faulting (Fig. 2). Palmer (2014) suggested that the current structural configuration of the eastern Nadaleen Trend is the result of four deformation events. Event D1 was characterized by NNE-SSW directed shortening; D2 by NW-SE-directed shortening and dextral shear; D3 by N-S-directed shortening; and D4 by minor N-trending dextral strike-slip.

2.3.3 Mineralization in the Nadaleen Trend

There are seven areas of gold mineralization in the Nadaleen Trend: Osiris, Conrad, Isis, Isis East, Amon, Anubis, and Sunrise; the highest gold grades are in Osiris and Conrad. In the Conrad zone, gold is commonly associated with brecciated, decarbonatized, silicified, and realgar-, orpiment-, and calcite-mineralized shear zones (Tucker, 2015).

There is a clear structural control on mineralization, as there is significant gold mineralization in S- to SSW-plunging anticlines in the Osiris, Isis East, and Conrad zones (Palmer, 2014; Tucker, 2015; Fig. 2). The reverse faults of the triangle zone acted as aquitards, funneling gold-bearing hydrothermal fluids updip into the Nadaleen host rocks (Palmer, 2014). Once these fluids reached the Nadaleen host rocks, they were concentrated into the hinges of S- to SSW- plunging anticlines. The nearby Conrad zone (also in the eastern Nadaleen Trend) was studied by Tucker (2015) to determine the nature of the mineralization. The principal gold host rocks in the Conrad zone are decarbonatized silty carbonates which are also commonly silicified and brecciated. Gold in the Conrad zone is hosted in arsenic-rich pyrite growth rims surrounding pre-existing pyrite grains (Tucker, 2013). Gleeson (2012) reported that there is significant gold mineralization near dolomitization fronts (Fig. 5), and that the gold occurs as “invisible gold” in the rims of pyrite. A report by Acosta-Gongora and Gleeson (2011) suggested that in Osiris, there are grains of pyrite with rims of “fuzzy” arsenian pyrite, which is the place of residence of gold in CTGDs.

The circled area in the Windermere Supergroup (Fig. 3) shows the location of the Eastern Nadaleen Trend; the area of focus in this study. Figure 3 shows a map of the area of study in the Eastern Nadaleen Trend, indicating the location of the Osiris, Isis, and Isis East Carlin-type gold zones. As shown in Figure 2, seven drill holes were studied for this master’s thesis. Five of these drill holes are in Osiris (OS-11-41, OS-11-52, OS-11-61, OS-11-80, and OS-11-83), one is in Isis (OS-11-72), and one is in Isis East (OS-12-120).

2.4 Methods and analytical techniques

A total of 502 rock samples were collected from 7 diamond drill holes from the eastern Nadaleen Trend during the summer of 2012. Five of the drill holes are in the Osiris zone, one is in the Isis zone, and one is in the Isis east zone (Fig. 2). Extra stratigraphic logs are shown in Appendix A.

2.4.1 Petrography and Cathodoluminescence Microscopy

Detailed descriptions of all rock samples were made. Composition, sedimentary features, veining, mineralization, and any cross-cutting relationships were noted in each sample. Of the 502 rock samples, 115 were made into standard thin sections (27 by 46 mm) at Vancouver GeoTech Labs. Plane-polarized (PPL), cross-polarized (XPL), and reflected light (RL) microscopy were used to further characterize each sample. Limestone host rocks were classified according to the Dunham carbonate nomenclature system. Dolomite phases were classified according to the nomenclature system of Gregg and Sibley (1984). Cathodoluminescence microscopy was then carried out on a subset of thin sections in the University of Alberta U-Pb Geochronology Laboratory with the help of Judy Schultz. The CL microscope used consists of a cathode ray tube connected to a thin section chamber. Photomicrographs of the CL response were taken in a dark room with 30-second exposure, and sample chamber pressure of 70-73 mTorr. Cathodoluminescence microscopy was useful in identifying carbonate phases and distinguishing one carbonate phase from another (i.e. dolomite 2 from dolomite 3). Mineral phases were identified and assigned to paragenetic Stage I, Stage II, Stage III, Stage IV, or Stage V. Stages I and III were defined according to the diagenetic classifications of Machel (1999), which describes near-surface, shallow, intermediate, and deep diagenetic features. Deep diagenetic features were not recognized in this thesis. The other paragenetic stages were defined according to mineral assemblages and cross-cutting relationships as outlined below.

2.4.2 EMPA

Electron Microprobe Analysis was conducted with a JEOL 8900 instrument at the University of Alberta Electron Microprobe Lab to determine major and minor element compositions of carbonate and sulfide minerals. Samples were coated with a conducting film of carbon by Dr. Andrew Locock. The EMPA techniques employed were electron dispersive spectrometry (EDS), wavelength dispersive spectrometry (WDS), X-Ray elemental mapping, backscattered electron (BSE) imaging, and secondary electron (SE) imaging. Electron dispersive spectrometry was used for semi-quantitative determination of the elemental composition of minerals, and WDS was then used to quantitatively determine major and minor element concentrations of these minerals. X-ray elemental mapping, BSE imaging and SE imaging were used to qualitatively examine the spatial distribution of selected elements in minerals. Operating conditions of the electron beam

during WDS analysis were set depending on the material being analyzed (see Appendix B). Several analytical crystals were used to cover a wide range of x-ray wavelengths: Pentaerythritol (PET), lithium fluoride (LIF), thallium acid phthalate (TAP), and a layered dispersive element (LDE). The concentrations of specific elements were calibrated to the following standards for carbonate analyses: sanbornite and barite for Ba, dolomite for Mg and Ca, strontianite for Sr, rhodonite for Mn, albite for Na, willemite and sphalerite for Zn, and siderite for Fe. For sulfides, the standards used were: pyrite and Fe metal for Fe and S, Galena for Pb, indium arsenide and gallium arsenide for As, stibnite and Sb metal for Sb, thallium selenide for Tl, zinc sulfide for Zn, Cu metal for Cu, Ag metal for Ag, Sanbornite for Si, cadmium selenide for Cd and Se, and Ni metal for Ni.

2.4.3 LA-ICP-MS

Laser ablation inductively coupled plasma mass spectrometry was conducted at the University of Alberta Arctic Resources Lab to determine the trace element concentration in carbonate minerals and pyrite. A Resonetics Laser Ablation system equipped with a 193 nm argon fluoride excimer laser was used with a Thermal XR ICP-MS run at medium mass resolution. For carbonate analyses, a beam diameter of 120 μm , laser frequency of 10 Hz and laser energy of 120 mJ were used. For pyrite analyses, a beam diameter of 23 μm , laser frequency of 10 Hz, and laser energy of 100 mJ were used. The background scan and ablation times were 40 and 30 seconds for carbonates, respectively, and 30 and 40 seconds for pyrite. Reference material NIST 612 was used for carbonates and MASS-1 for pyrite. Several additional reference materials (NIST 610 and MACS-3 for carbonates, NIST 612 for pyrite) were also analyzed for comparison with previously reported values. Accuracy was tested by ablating NIST 610, NIST 612, MASS-1, and MACS-3 reference materials and comparing elemental concentrations with those listed on the GEOREM website. Accuracy ranged from 5 to 15 %. A single Faraday detector was used to detect isotopes based on their mass-to-charge ratio. In carbonates, isotopes analyzed include ^{42}Ca , ^{26}Mg , ^{45}Sc , ^{47}Ti , ^{49}Ti , ^{51}V , ^{52}Cr , ^{55}Mn , ^{57}Fe , ^{59}Co , ^{60}Ni , ^{61}Ni , ^{65}Cu , ^{66}Zn , ^{75}As , ^{85}Rb , ^{88}Sr , ^{89}Y , ^{90}Zr , ^{95}Mo , ^{98}Mo , ^{107}Ag , ^{109}Ag , ^{111}Cd , ^{114}Cd , ^{121}Sb , ^{123}Sb , ^{137}Ba , ^{139}La , ^{140}Ce , ^{141}Pr , ^{146}Nd , ^{147}Sm , ^{153}Eu , ^{157}Gd , ^{159}Tb , ^{163}Dy , ^{165}Ho , ^{166}Er , ^{169}Tm , ^{172}Yb , ^{175}Lu , ^{197}Au , ^{205}Tl , ^{207}Pb , ^{209}Bi , ^{232}Th , and ^{238}U . In pyrite, isotopes analyzed include ^{51}V , ^{52}Cr , ^{55}Mn , ^{59}Co , ^{60}Ni , ^{61}Ni , ^{65}Cu , ^{66}Zn , ^{75}As , ^{95}Mo , ^{98}Mo , ^{107}Ag , ^{109}Ag , ^{111}Cd , ^{114}Cd , ^{121}Sb , ^{123}Sb , ^{137}Ba , ^{139}La , ^{197}Au , ^{202}Hg , ^{205}Tl , ^{204}Pb , ^{207}Pb , and ^{209}Bi . For the remainder of this thesis, these components will be reported as just the element, rather than the isotope. Any reported Cd, Sb, Mo, Ag, and Pb will refer to ^{114}Cd , ^{123}Sb , ^{98}Mo , ^{109}Ag , and ^{207}Pb , respectively. Iolite software was used to process the raw mass spectrometer data. Calcium concentration, as determined by EPMA, was used as the internal standard for carbonates whereas Fe concentration was used as the internal standard for pyrite. Detection limits were calculated using Iolite. The rare earth elements and Y (REY) were normalized to mean Post-Archean Australian Shale (PAAS) concentrations from Pourmand et al. (2012). Lower limits of quantitation were

calculated using $LLQ = 3.333 \text{ LLD}$ (Perkins and Pearce, 1995). LA-ICP-MS data below the LLQ were not heavily relied upon. Cerium anomalies were calculated as $Ce/Ce^* = Ce_{PAAS}/(0.5La_{PAAS} + 0.5Pr_{PAAS})$ where $X_{PAAS} = [X]_{sample}/[X]_{PAAS}$ (Zhou et al., 2012).

2.4.4 Bulk Carbon and Oxygen Isotopes

Samples were prepared for C and O isotopic analysis at the U. of A. using a hand drill to powder 20-30 mg of vein and mineralized material. Sample powders were sent to the Isotope Science Laboratory at the University of Calgary, and analyzed by Steve Taylor. Samples were digested in anhydrous phosphoric acid at 25°C and the CO₂ reactant was analyzed in a Thermo Finnigan Gasbench mass spectrometer coupled to a Delta Vplus to determine ¹⁸O/¹⁶O and ¹³C/¹²C ratios. Internal lab reference materials were tested at the beginning and end of each set of samples to normalize the data and to correct for any instrument drift. The internal lab standards were regularly calibrated against international standards to assure accuracy of δ¹³C and δ¹⁸O values relative to VPDB and VSMOW, respectively. The sample analyses are precise to 0.2 ‰ (1σ) for both δ¹³C and δ¹⁸O values.

2.4.5 Secondary Ion Mass Spectrometry

The following methodology summary was written by Richard Stern. Rock samples exposed in polished thin-sections were prepared for in situ SIMS oxygen and carbon isotope analysis at the CCIM lab, University of Alberta. Twenty regions of interest (2 – 3 mm diameter) from various thin-sections (80 μm thick) were extracted by diamond coring, and then cast together in epoxy along with calcite and dolomite reference materials (RM) into CCIM mount M1299. The mount was then lightly polished with diamond compounds to achieve a uniformly flat surface. After cleaning with soap and de-ionized water, the mount was coated with gold prior to scanning electron microscopy (SEM) using the CCIM Zeiss EVO MA15 instrument, operating at 15 and 20 kV and 3 – 4 nA beam current.

Oxygen isotope ratios (¹⁸O/¹⁶O) were determined first in dolomite and then calcite using the IMS-1280 multi-collector ion microprobe at CCIM. Primary beam conditions included the use of 20 keV ¹³³Cs⁺ ions focused to form a probe with diameter ~10 μm and beam current ~ 1.5nA which was rastered during analysis to form a sampled area ~15 x 20 μm. The primary beam was rastered 22 x 22μm for 60 s prior to analysis to clean the surface of Au and contaminants and implant Cs. The normal incidence electron gun was utilized for charge compensation. Negative secondary ions were extracted through 10 kV into the secondary column (Transfer section). Conditions for the Transfer section included an entrance slit width of 122 μm, field aperture of 5 x 5 mm, and a field aperture-to-sample magnification of 100x. Automated tuning of the secondary ions in the Transfer section preceded each analysis. The energy slit was fully open. Both ¹⁶O⁻ and ¹⁸O⁻ were analyzed simultaneously in Faraday cups (L'2 using 10¹⁰ Ω amplifier, and H'2 with 10¹¹ Ω) at mass resolutions of 2000 and 2275, respectively. Mean count rates for ¹⁶O⁻ and ¹⁸O⁻ were typically 2.0 x 10⁹ and 4 x 10⁶ counts/s, respectively, determined over a 75 – 100 s

counting interval. The analytical protocol interspersed analyses of unknowns with in-house end-member dolomite and calcite reference materials (CCIM dolomite S0202 with $\delta^{18}\text{O}_{\text{VSMOW}} = +26.65 \text{ ‰}$; calcite S0119 with $\delta^{18}\text{O}_{\text{VSMOW}} = +23.41 \text{ ‰}$; R. Stern, unpublished data) in a 4:1 ratio. Instrumental mass fractionation (IMF) for $^{18}\text{O}/^{16}\text{O}$ was $\sim -8.5 \text{ ‰}$ for dolomite and $\sim -2 \text{ ‰}$ for calcite, determined precisely for each analytical session from utilizing all the replicate analyses of the RMs. The standard deviation of multiple measurements of $^{18}\text{O}/^{16}\text{O}$ ratios in S0202 was 0.10 ‰ and for S0119 was 0.12 ‰ , after small corrections for systematic within-session IMF drift ($<0.3 \text{ ‰}$). Final uncertainties are reported at 95% confidence level (2σ) and propagate within-spot counting errors, between-spot errors to account for geometric effects, and between-session error that accounts for uncertainty in the mean IMF for the session. The data exclude any uncertainties related to possible biases due to measuring unknowns with significantly different major element compositions to the RMs, such as dolomite with significant Fe content. The total uncertainties in $\delta^{18}\text{O}_{\text{VSMOW}}$ dolomite average about $\pm 0.25 \text{ ‰}$ (2σ) per spot, and for calcite $\pm 0.3 - 0.4 \text{ ‰}$. Individual analyses are reported relative to VSMOW.

Carbon isotope analyses were conducted on spots adjacent to the preceding O-isotope analyses using similar primary beam and secondary column parameters. Negative secondary ions $^{12}\text{C}^-$ and $^{13}\text{C}^-$ were analyzed simultaneously in a Faraday cup (L'2 using $10^{11} \Omega$ amplifier) and electron multiplier (EM), at mass resolutions of 2000 and 2900, respectively. Mean count rates for $^{12}\text{C}^-$ and $^{13}\text{C}^-$ were typically 1.0×10^7 and 1.2×10^5 counts/s, respectively, determined over a 90 s counting interval. As for O-isotopes, analyses of the dolomite and calcite RMs were carried out regularly during the sessions (CCIM dolomite S0202 with $\delta^{13}\text{C}_{\text{VPDB}} = +2.92 \text{ ‰}$; calcite S0119 with $\delta^{13}\text{C}_{\text{VPDB}} = -1.64 \text{ ‰}$; R. Stern, unpublished data), and processed collectively over the sessions (3 for dolomite, 1 for calcite). The session standard deviations of $^{13}\text{C}/^{12}\text{C}$ ratios for S0202 were $0.15 - 0.28 \text{ ‰}$ and for S0119 was 0.30 ‰ , after corrections for linear within-session IMF drift due to the ageing of EM (ranging from 1 ‰ to 4.5 ‰ over an individual session). The total uncertainties in $\delta^{18}\text{O}_{\text{VSMOW}}$ dolomite average about $\pm 0.5 \text{ ‰}$ (2σ) per spot, and for calcite $\pm 0.6 \text{ ‰}$. Individual analyses are reported relative to VPDB. There were matrix effects due to the high Fe content of the dolomites. The $\delta^{18}\text{O}$ values of these high-Fe dolomites were corrected using data from Fayek et al. (2001).

2.4.6 Strontium Isotopes

Stable isotopes of strontium in calcite and dolomite were analyzed by Chiranjeeb Sarkar at the University of Alberta. Twenty-seven rock powder samples were prepared by using a hand drill to extract 0.1 to 0.2 mg of powder per sample from veins and areas of mineralization. The samples were dissolved in HCl, and any solid (sulfide) residue was removed by decanting the carbonate the solution into another container. Column chemistry was used to separate Sr from other elements in solution. Strontium isotopes (^{84}Sr , ^{86}Sr , ^{87}Sr , and ^{88}Sr) were detected using Faraday cups in a Neptune plus multicollector

inductively coupled plasma mass spectrometer (MC-ICP-MS) and $^{87}\text{Sr}/^{86}\text{Sr}$ ratios were calculated from this. The reference material used was SRM987, a universally accepted Sr standard. There was one sample with very low Sr content; the isotopic composition of this sample was analyzed by a secondary electron multiplier.

2.4.7 Sulfur Isotopes

Twenty-five samples of pyrite were prepared for sulfur isotope analysis by hand drilling 10 to 20 mg of powder per sample from well-constrained rock samples. These samples were then sent to the University of Calgary Isotope Science Laboratory where their sulfur isotopic compositions were analyzed by Steve Taylor. Samples were introduced to a combustion furnace at 1050°C and the SO_2 from the reaction was separated from other gases using a gas chromatography column. The SO_2 was then analyzed by a Delta+XL mass spectrometer which collected masses of 64, 65 and 66 amu and the $^{34}\text{S}/^{32}\text{S}$ ratio was determined. Internal lab standards were analyzed every 10 samples. The $\delta^{34}\text{S}$ values were calculated relative to Vienna Canon Diablo Troilite (VCDT). The sample analyses are precise to 0.3 ‰ (1σ).

2.4.8 Whole-rock Geochemistry

Core from the seven drill holes in this study were sent to Australian Laboratory Services (ALS) minerals in Vancouver for whole-rock geochemical analysis. Gold concentrations for every 3.05 meter interval were determined by the Au-AA26 ore method. In this method, fire assay fusion is used for sample decomposition and the sample is then analyzed by atomic absorption spectrometry. These gold grades were used as a guide for sample selection to ensure that gold-mineralized and non-mineralized samples were collected. Gold grades for all seven drill holes are listed in Appendix C. Concentrations of 47 other elements were determined via method ME-MS61m, but these data were not used in this master's thesis.

2.5 Results

2.5.1 Logs and Cross section

Locations of all drill holes studied are shown in Figure 2. Drill holes OS-11-41, OS-11-52, OS-11-61, OS-11-80, and OS-11-83 are in Osiris; OS-11-72 is in Isis; and OS-12-120 is in Isis East. Lithologic logs (with representative samples) of six of these drill holes are presented in Figures 5, 6 and 7. These drill holes comprise mostly interbedded limestone (wackestone and lime mudstone) and dolostone, and there are minor amounts of diamictite and rudstone.

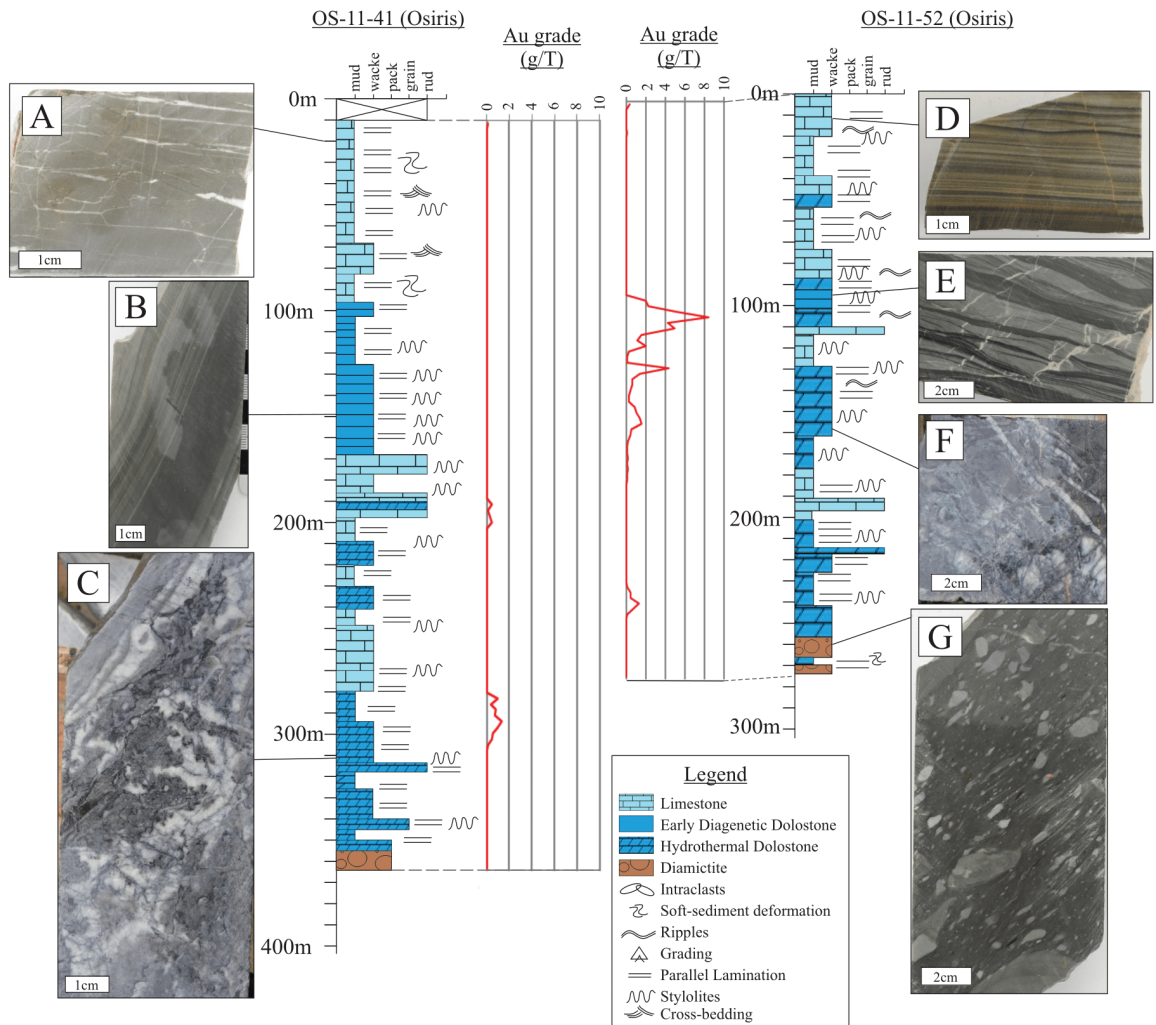


Figure 6. Lithologic logs of Osiris holes OS-11-41 and OS-11-52 with images of hand samples. Note gold mineralization at dolomitization fronts. A) Massive limestone with calcite veins. B) Laminated near-surface diagenesis dolostone. C) Hydrothermal dolostone with veins of dolomite. D) Laminated limestone. E) Laminated limestone with ripples. F) Hydrothermal dolostone. G) Diamictite

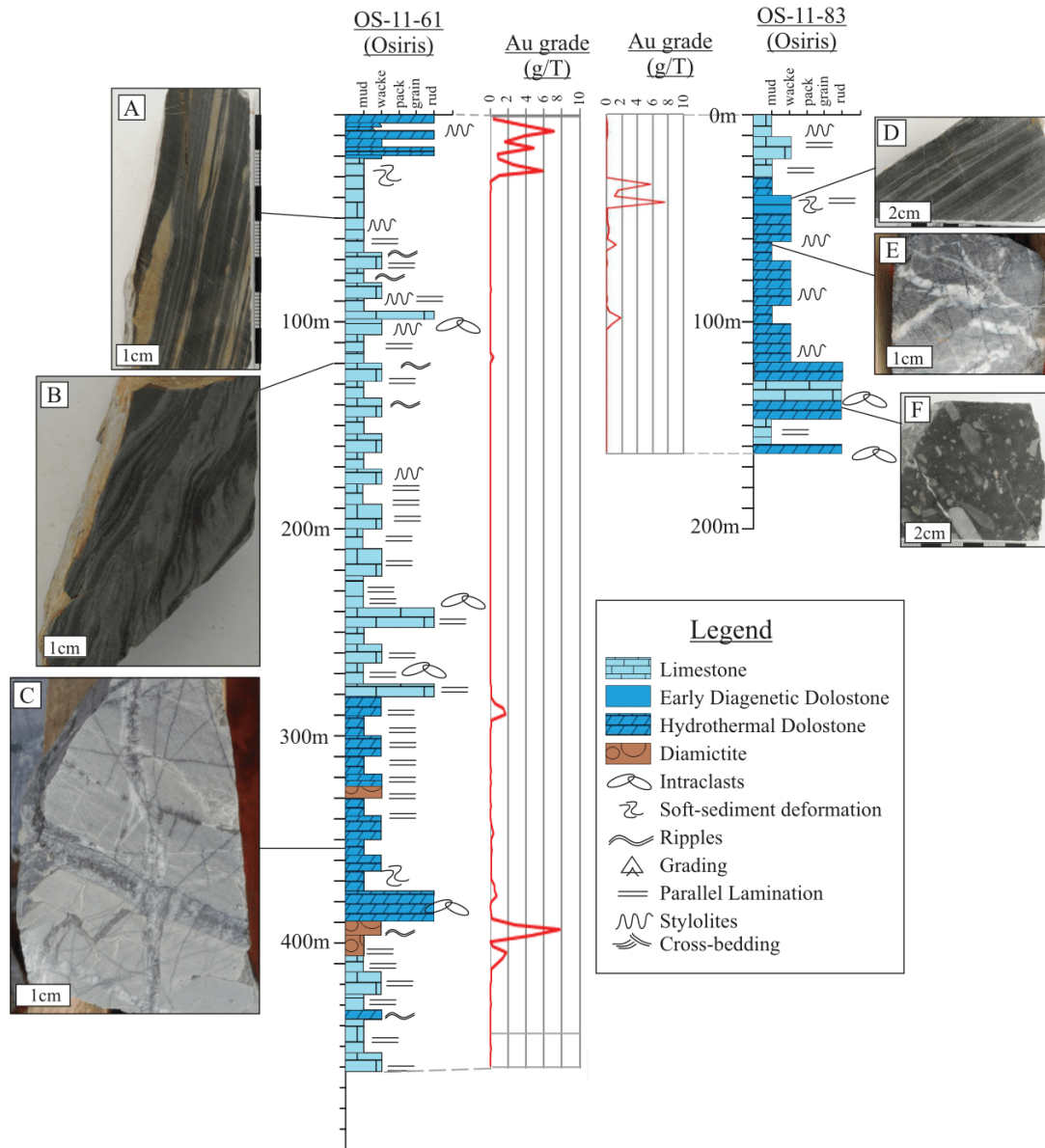


Figure 7. Lithologic logs of Osiris holes OS-11-61 and OS-11-83 with images of hand samples. Note gold mineralization at dolomitization fronts in OS-12-120. Gold grades in OS-11-72 are very low. A) Laminated limestone. B) Rippled limestone. C) Hydrothermal dolostone. D) Laminated near-surface diagenetic dolostone. E) Hydrothermal dolostone. F) Dolomitized Diamictite.

There is a correlation between gold grade and dolomitization fronts. There are two main types of dolostone in the Nadaleen Trend: fine-grained, fabric retentive dolostone and coarse-grained, fabric destructive dolomite interpreted to be hydrothermal in origin (section 2.5.2). Gold grades from whole-rock geochemistry for all drill holes are listed in Appendix C. From the above images, it is evident that dolomitization is an important factor in the distribution of gold. The most strongly mineralized drill holes are OS-12-120, OS-

11-52, OS-11-61, OS-11-80, and OS-11-83 with maximum gold grades of 21.7, 8.46, 7.15, 18.55, and 7.57 g/T, respectively. Gold grades of OS-12-120 are presented in the cross-section in Figure 8.

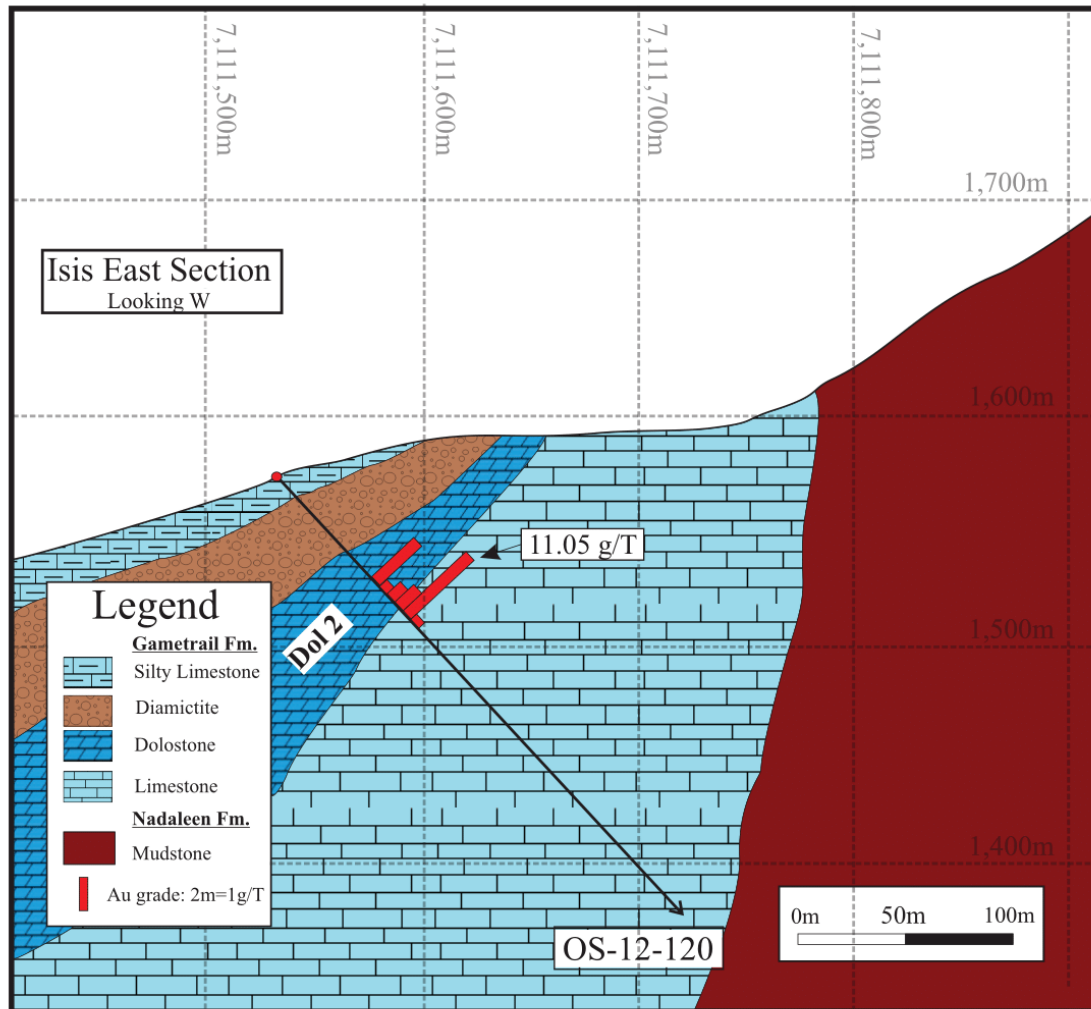


Figure 8. Cross-section of Isis east hole OS-12-120. All rocks of this drill hole are in the Ediacaran Gametrail Formation. Note the mineralization at/near the dolomitization front. Modified after ATAC Ltd. (2013).

Drill holes OS-11-72 and OS-11-41 are the least mineralized, with maximum gold grades of 1.41 and 1.32 g/T, respectively. Isis hole OS-11-72 is purely dolostone, so there are no dolomitization fronts in this hole. For this reason, less emphasis was placed on Isis for this study. As shown in Figure 7, there is some gold mineralization in OS-11-72, but it is low-grade compared to the dolomitization front-associated mineralization in some of the other

holes (see Appendix C). Osiris hole OS-11-41 has very low gold grades, but it is nonetheless concentrated at dolomitization fronts.

2.5.2 Petrology and Paragenesis (hand specimen, thin section, CL, EMPA imaging)

The host rocks are described below, and some representative samples are shown in Figure 9. A total of five paragenetic stages have affected the host rocks (Figure 10). There is a near-surface diagenetic stage (Stage I), a base metal mineralization stage (Stage II), an intermediate diagenesis stage (Stage III), a gold ore stage (Stage IV), and a post-ore stage (Stage V).

Host Rocks

The general stratigraphy of the study area is laid out in Figure 3. The dominant host rocks of the Osiris and Isis East zones are lime mudstones, wackestones, rudstones, and diamictites (Fig. 9). Lime mudstone and wackestone are commonly interbedded or interlaminated with one another; the darker grey layers are lime mudstone and the lighter grey layers are wackestone (Fig. 9a, 9b, 9c). Wackestones consist of 60 to 80 % micrite matrix, 17 to 37 % calcite grains, and ~3 % detrital clasts (Fig. 9f, 9i). Lime mudstones consist of 80 to 95 % micrite matrix and 5 to 20 % calcite grains (Fig. 9f, 9h). Common sedimentary features in wackestone and lime mudstone include laminations (Fig. 9a, 9b), symmetric to asymmetric ripples (Fig. 9a, 9b), and dewatering structures (Fig. 9c). The most common detrital grains are quartz, apatite, K-feldspar, and zircon (Fig. 9f, 9i); in most cases, detrital grains are immature (i.e. poorly sorted, angular with low sphericity). Rudstones consist of 80 to 90 % coarse grains and 10 to 20 % fine matrix (Fig. 9d). Both the coarse grains and the matrix of rudstone comprise either wackestone or lime mudstone. Coarse grains in rudstone are angular to sub-angular with poor sphericity, and are commonly imbricated (Fig. 9d). Diamictites consist of 20 to 50 % coarse clasts and 50 to 80 % fine matrix (Fig. 9e). The coarse clasts are composed of lime mudstone, wackestone or dolostone, and the fine matrix comprises either lime mudstone or wackestone. Clasts in the diamictites are sub-angular to sub-rounded with low to high sphericity, and are poorly sorted (Fig. 9e).

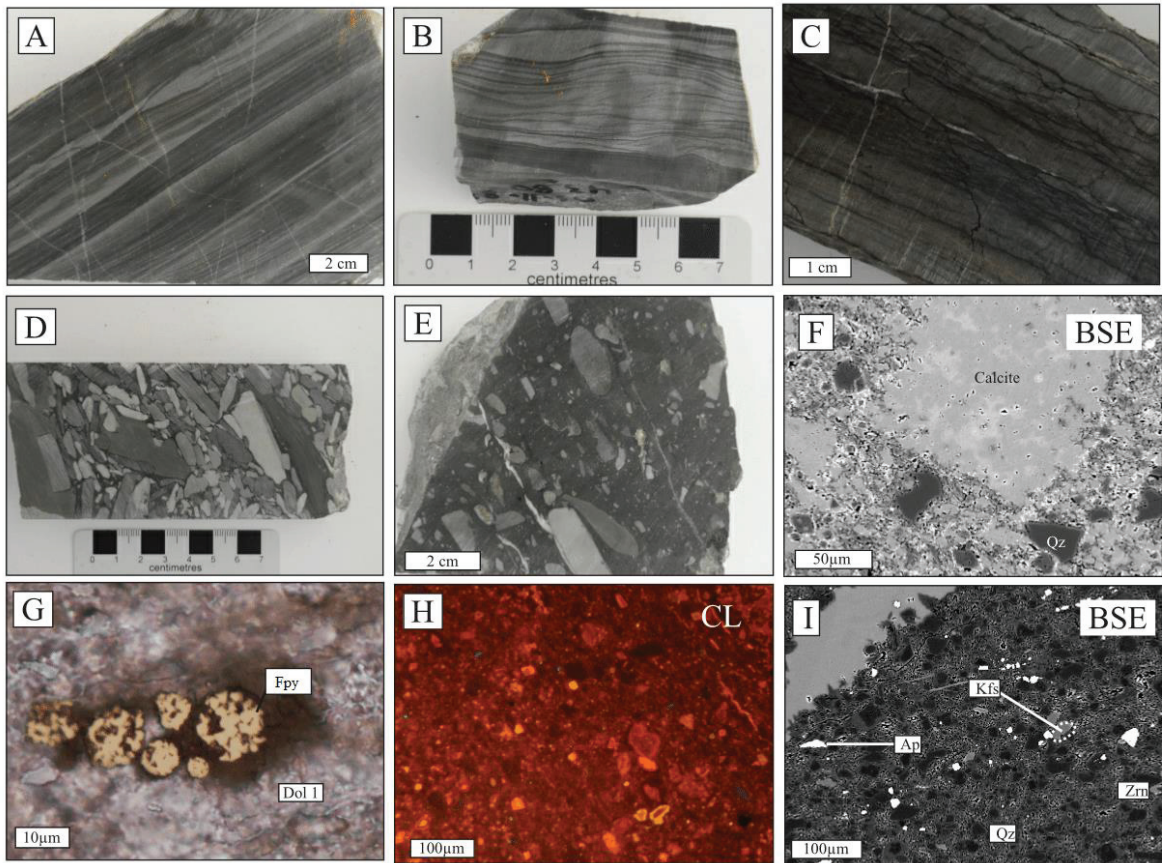


Figure 9. Typical host-rocks. A) OS-11-83.43.05m – Host rock. The alternating lighter and darker layers are laminated wackestone and lime mudstone, respectively. B) OS-11-83 43.80m - Laminated host rock with ripples. C) OS-11-52 5.55m - Limestone with dewatering structures. D) OS-11-80 131.00m - Imbricated rudstone. E) OS-11-83 140.82m - Diamictite with lime mudstone matrix and grains of limestone and dolostone. F) OS-12-120 43.37m - BSE image of wackestone with calcite matrix, calcite grains, and quartz clasts. G) OS-11-80 73.08m. Reflected light (RL) + PPL image of framboidal pyrite in a dolomite 1 matrix. H) OS-11-120 43.37m - CL image of lime mudstone. The dull brown material is the host limestone, brighter phases are diagenetic cements. I) OS-11-80 108.16m - BSE Image of wackestone with clasts of zircon, K-feldspar, apatite, and quartz grains in dolomite 1.

All of the host rocks mentioned above are relatively heterogeneous, as many calcite grains are rimmed by later carbonate phases (Fig. 9h), and many of the host rocks are partially dolomitized (Fig. 11b, 11c, 11d). The dull brown cathodoluminescence of the matrix and grains in Figure 9h are typical of the unaltered host rock, whereas the brighter CL components represent detrital grains or later carbonate phases. The drill holes in Osiris and Isis east have the most abundant unaltered host rock, although they are commonly interbedded with dolomitized units (Fig. 6 and 7). Isis hole OS-11-72 is completely dolomitized and does not have any unaltered host rocks (Fig. 5). Framboidal pyrite has been observed in two samples in Osiris; it occurs in matrix material of the host rocks as 3- to 18-diameter framboids. (Fpy; Fig. 9g).

The paragenetic sequence of events to affect these host rocks is shown in Figure 10.

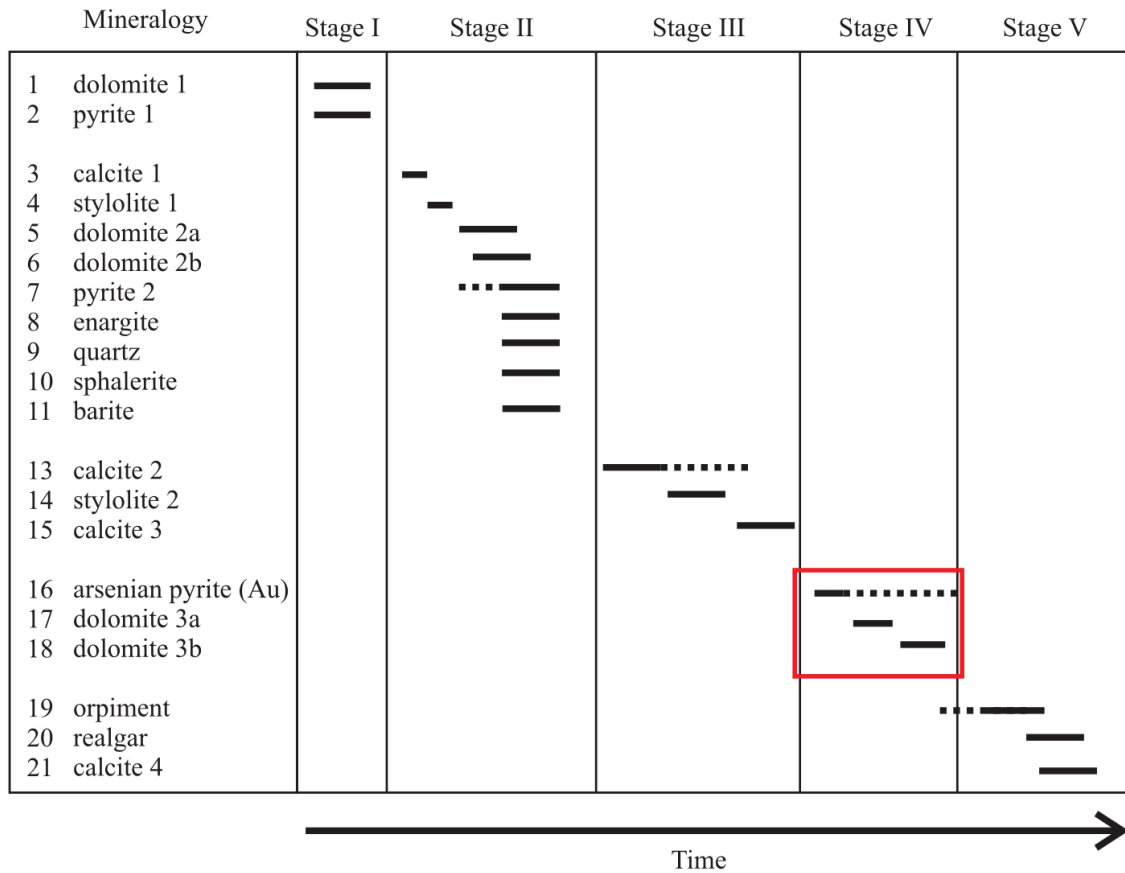


Figure 10. Paragenetic Sequence for the Osiris, Isis, and Isis East zones of the Eastern Nadaleen Trend. Solid lines indicate a high level of confidence in relative timing; dashed lines indicate uncertain temporal relationships.

Near-Surface Diagenesis Stage (Stage I)

Stage I is characterized by dolomite 1 and pyrite 1, which are interpreted to have developed in a near-surface diagenetic setting, i.e. within the first few meters of burial (Machel, 1999). Dolomite 1 can be pervasive, with some areas of dolomitization affecting up to 30 m of stratigraphy (Fig. 6, 7, and 8). In other parts of the stratigraphy the dolomitization is preferentially localized along lime mudstone and wackestone beds (Fig. 11c) and interbedded with these lithologies.

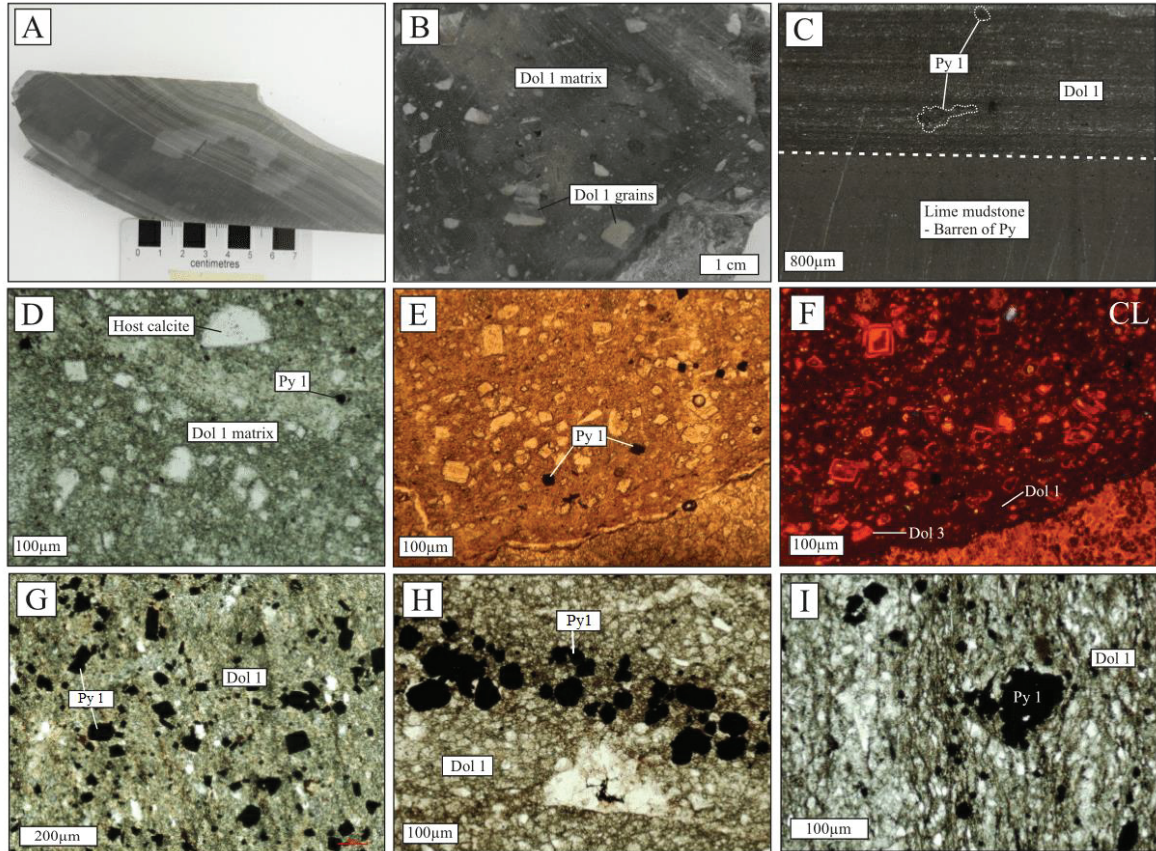


Figure 11. Stage I mineralization. A) OS-11-41 149.23m - Laminated dolostone composed of dolomite 1. Lighter layers are dolowackestone and darker layers are dolomudstone. B) OS-11-83 124.23m - Dolomitized diamictite. Both the matrix and the clasts are dolomitized. C) OS-11-80 73.08m. XPL image of a dolomitization front. There are larger volumes of pyrite 1 in dolomite 1 than the lime mudstone. D) OS-12-120 43.37m. PPL image of partially dolomitized wackestone. The matrix micrite has been dolomitized; the calcite grains have not. Pyrite 1 is purely in the dolomite 1. E) OS-11-83 123.84m - PPL image of dolostone comprising dolomite 1 and dolomite 3. F) OS-11-83 123.84m. Same field of view CL. The dull brown material is dolomite 1; the bright red material is dolomite 3. G) OS-11-85 184.66m - XPL image of subhedral pyrite 1 grains in dolomite 1. H) OS-11-80 149.35m PPL image of subhedral pyrite grains in dolomite 1. I) OS-11-80 114.54m - PPL image of subhedral pyrite 1.

There are some areas in which dolomite 1 has affected only the matrix micrite but not the calcite grains (Fig. 11d), and there are some areas in which dolomite 1 has replaced both the matrix and the grains (Fig. 11b). Rudstones and diamictites are commonly dolomitized as well. Dolomite 1 is fabric-retentive, and has the same sedimentary textures present in the host rocks (Fig. 11a, 11b). Dolomite 1 also has the same appearance as the host wackestone and lime mudstone in thin section (Fig. 11c); it occurs as grains or matrix which has dull CL response (Fig. 11d). In the drill holes of Osiris and Isis east, roughly 40% of the total dolomite is dolomite 1. Pyrite 1 occurs as subhedral crystals 5 to 30 μm in diameter (Py 1; Fig. 11h, 11i), and occurs within matrix material of dolomite 1 (Fig. 11c-i). Pyrite 1 is nearly

always associated with dolomite, and there are commonly significant volumes of pyrite in the dolomite compared to unaltered host rocks.

Base Metal Mineralization Stage (Stage II)

Stage II consists of calcite veining and stylolitization followed by a base metal mineralization event consisting of quartz, dolomite 2, pyrite 2, sphalerite, enargite, and barite. The base metal mineral assemblage is similar to those found in areas of MVT mineralization. Calcite 1 clearly cross-cuts both the host limestones and dolostones (Fig. 12a, 12b) and is post-dated by pressure solution seams and stylolites. These veins have a dull brown CL, similar to that of dolomite 1 and the calcite of the host limestone (Fig. 12a). Stylolites are sinuous, commonly form boundaries between lithologies, have amplitudes of 100 to 150 μm , and are commonly sutured (Fig. 12b). The presence of stylolites is indicative of shallow to intermediate diagenesis (Machel, 1999). These veins and stylolites are post-dated by the base metal event which comprises dolomite 2a and 2b, quartz veining/cements and base metal sulfides including pyrite and minor barite, sphalerite, and enargite (Cu_3AsS_4 ; Fig. 12). Dolomite 2 occurs as idiomorphic to xenomorphic sparry dolomite (Dol 2a) or as veins/veinlets (Dol 2b) which crosscut calcite 1 veinlets and dolomite 2a (Fig. 12b, 12h). Dolomite 2a has a xenomorphic to idiomorphic texture and in some cases occurs as local replacements of dolomite 1, retaining lamination and bedding textures of dolomite 1 (Fig. 12c). Dolomite 2b has 500 μm to 3 mm saddle-shaped crystals, which commonly have an associated porosity. Quartz commonly fills the pore spaces (Fig. 12g). Dolomite 2 has dull brown luminescence under cathodic light with local red/orange zoning (Fig. 12i), but can develop oscillatory zoning, with bright red and darker layers in the coarser saddle dolomites (Fig. 12i). Dolomite 2 is equally as pervasive as dolomite 1, commonly covering up to 30 m of stratigraphy in all drill holes of Osiris and Isis east (Fig. 6, 7). Roughly 90% of the gold-mineralized dolomitization fronts comprise dolomite 2 rather than dolomite 1. Pyrite 2 comprises euhedral to subhedral crystals that either occur as disseminated crystals (Fig. 12d) or as large stratabound clusters (Fig. 12c). Pyrite 2 is commonly intergrown with dolomite 2 and veinlets or anhedral crystals of quartz (Fig. 12d). Minor amounts of sphalerite (Fig. 12e), barite (Fig. 12f) and enargite occur as anhedral to subhedral grains and are commonly intergrown with pyrite 2 and dolomite 2.

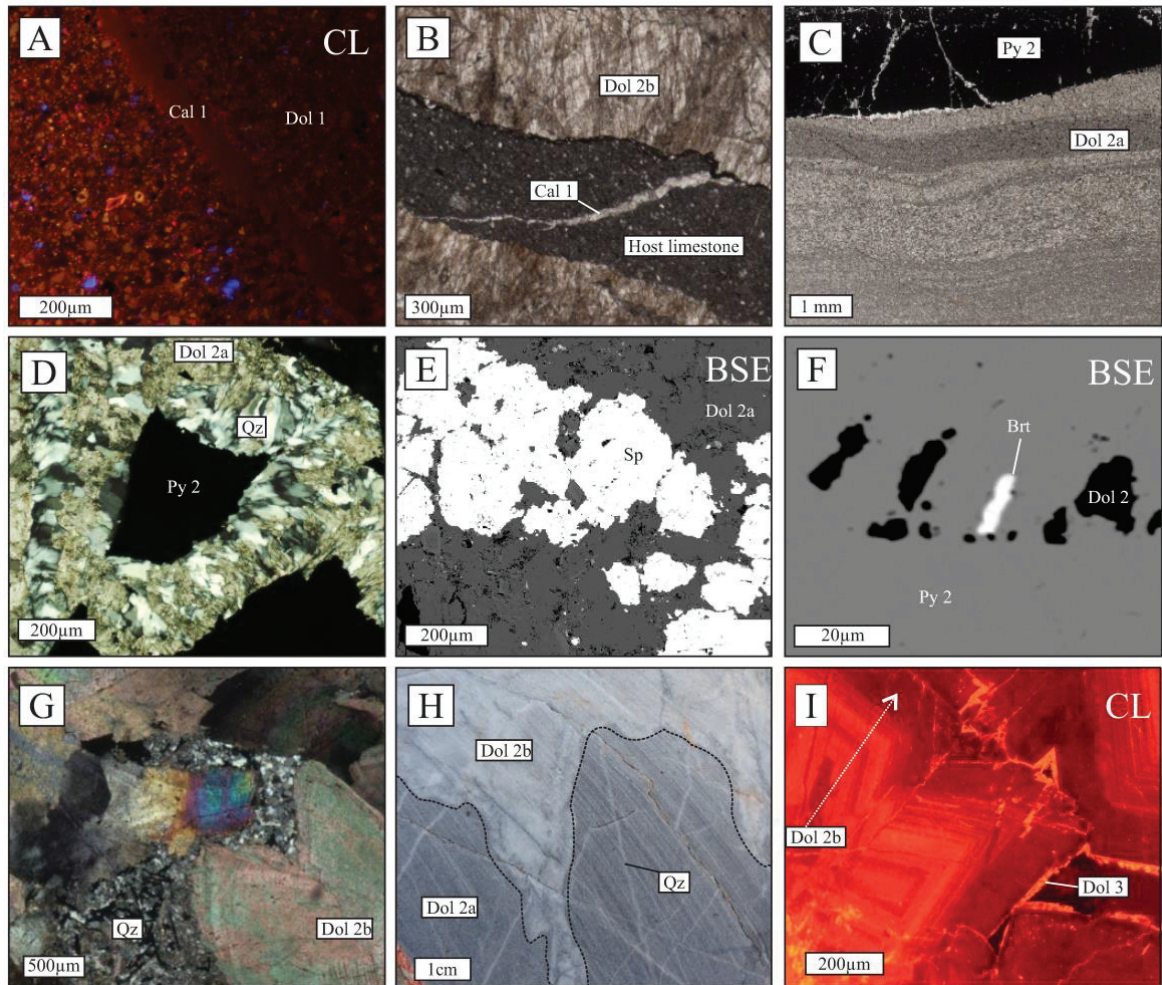


Figure 12. Stage II mineralization and features. A) OS-11-80 108.16m. CL image of a veinlet of calcite 1. B) OS-11-83 29.91m. PPL image of a calcite 2 veinlet crosscut by a vein of dolomite 2. C) OS-11-52 219.31m. XPL image of syngenetic base metal pyrite and dolomite 2. The pyrite is stratabound. D) OS-11-52 219.31m. XPL image of a pyrite 2 crystal partially dissolved by dolomite 2 and quartz. E) OS-11-72 219.73m. BSE image of syngenetic sphalerite and dolomite 2. F) OS-11-52 219.31m. BSE image of pyrite 2 dissolving dolomite 2 and barite. G) OS-12-120 104.75m. XPL image of dolomite 2 with saddle morphology. Quartz from the base metal stage fills the vugs. H) OS-12-120 101.44m. Rock comprising dolomite 2a and 2b veins. I) OS-12-120 115.26m. CL image of a zoned dolomite 2 crystal with pore spaces that accommodated crystal growth. The arrow indicates the direction from the crystal core to the outer layers; note the oscillatory zoning between bright and dark red. There are rims of later dolomite 3. grains in dolomite 1.

Intermediate Diagenesis Stage (Stage III)

Stage 3 comprises calcite 2 veining followed by a second phase stylolitization: these veins and stylolites are cross-cut by calcite 3 veins/veinlets. This stage of mineralization is interpreted to have occurred during intermediate diagenesis according to the classification of Machel (1999). Calcite 2 displays medium-intensity orange CL and commonly occurs as veinlets with twin lamellae (Fig. 13a, 13b). Calcite 2 can also occur as local cements associated with the veins (Fig. 13c). Stylolites are most commonly parallel to bedding and

are sinuous, with amplitudes of 50 to 500 μm (Fig. 13d). They are quite extensive, and are commonly interconnected, developing large networks and form boundaries between lithologies or different cement types (Fig. 13a, 13b, 13d). Calcite 3 displays bright orange CL and commonly occurs as veins/veinlets. It also occurs as local cements associated with the veins (Fig. 13e) and as partial replacement of dolomite 2 (Fig. 13f).

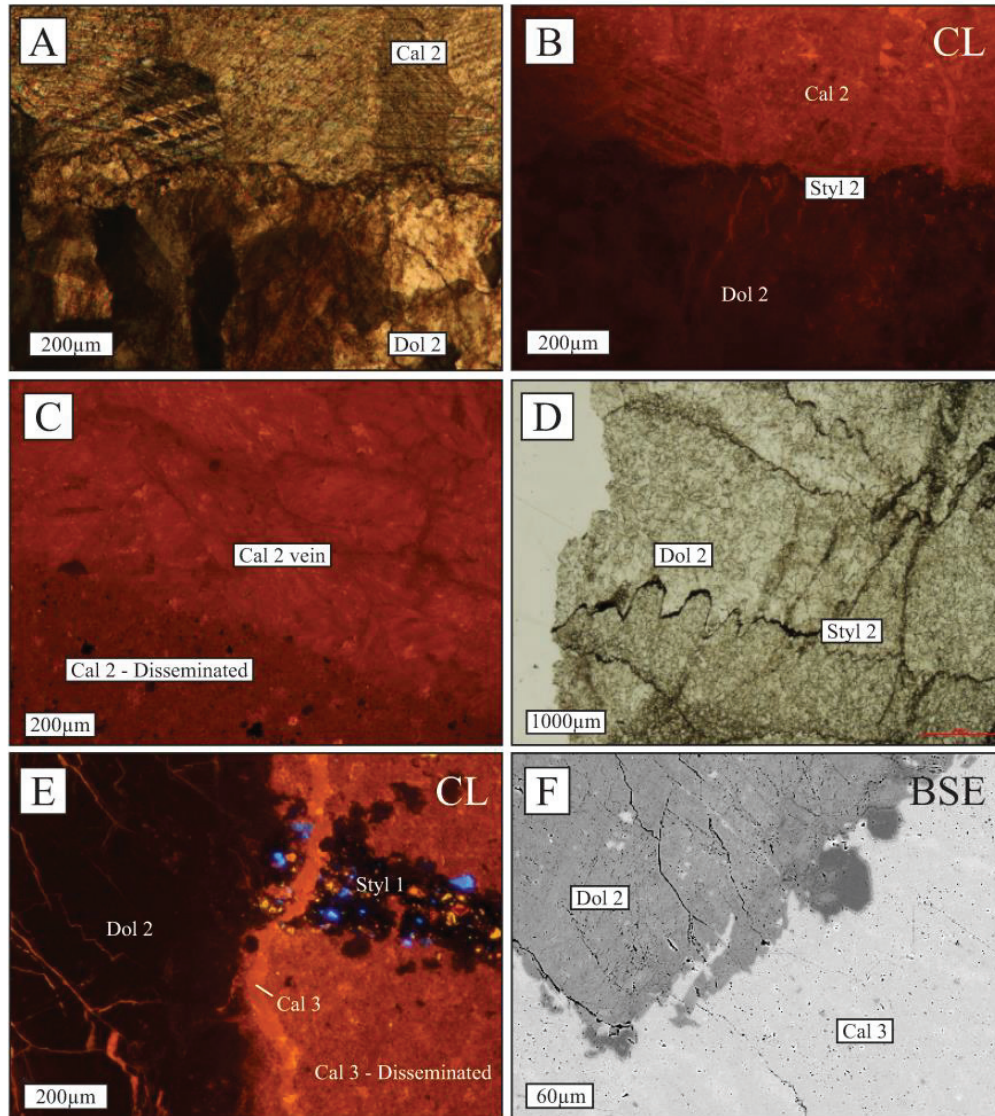


Figure 13. Stage 3 mineralization and features. A) OS-11-83 29.91m - XPL image of dolomite 2 and calcite 2. Note stylolite at contact. B) OS-11-83 29.91m – CL photo under the same field of view. C) OS-11-80 154.24m. Vein of calcite 2 and disseminated calcite 2. D) OS-11-83 52.50m - PPL image of stylolite in dolomite 2. E) OS-11-61 84.15m - CL image of stylolite crosscut by a dolomite 2 vein and a calcite 3 vein. Calcite 3 also occurs as disseminated material in the host rock. F) OS-11-52 6.96m - BSE image of dolomite 2 crosscut and partially replaced by calcite 3.

Ore Stage (Stage IV)

Stage IV is the ore stage, and is characterized by dolomite 3 and As-(Au)-bearing pyrite (Fig. 14).

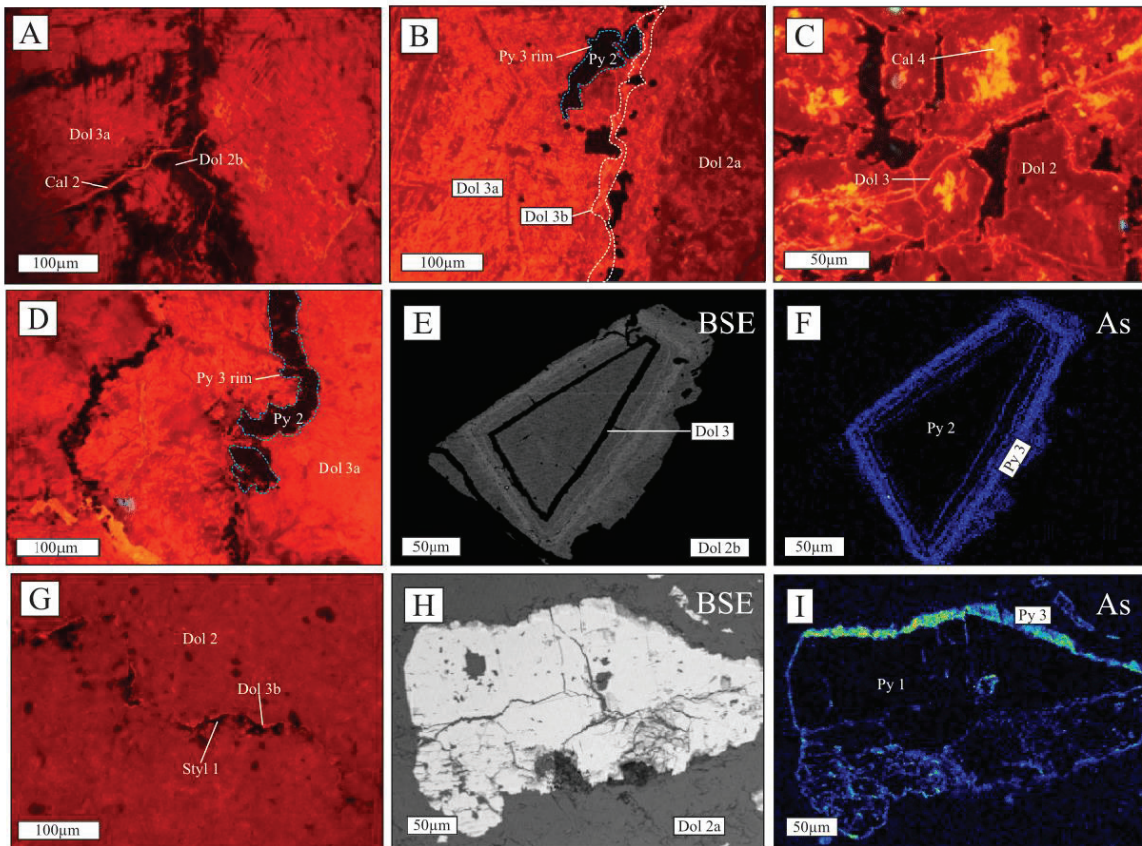


Figure 14. Stage IV minerals. A) OS-11-61 393.60m. CL image of dolomite 2b crystals partially replaced by dolomite 3a. B) OS-12-120 101.44m. CL image of dolomite 2 with later dolomite 3a and 3b. C) OS-11-80 176.03m. CL image of dolomite 2 with rims of dolomite 3. The yellow is a later phase of calcite which has partially replaced cores of crystals. D) OS-11-41 342.97m. E) OS-11-41 294.22m. BSE Image of dolomite 2 and pyrite 2 with a rim of pyrite 3. F) OS-11-41 294.22m. Arsenic map of the same pyrite crystal. Brighter colours indicate higher arsenic content. G) OS-11-80 210.57m. Stylolite in dolomite 2. A veinlet of dolomite 3b has formed along the stylolite. H) OS-11-41 294.22m. BSE image of pyrite 1 with a rim of pyrite 3. I) OS-11-41 294.22m. Arsenic map of the same pyrite crystal. Brighter colours indicate higher arsenic content.

Dolomite 3a is not identifiable in PPL or XPL microscopy, as it is difficult to distinguish from dolomite 2, but it has a distinctive bright red CL and occurs as replacements of dolomite 2 and dolomite 3b occurs as veinlets/rims which crosscut dolomite 3a (Fig. 14b). Dolomite 3a and 3b are commonly associated with stylolites, and dolomite 3b commonly occurs as veinlets within stylolites (Fig. 14a, 14g). Pyrite 3 occurs as rims on pre-existing

pyrite grains (Fig. 14c, 14d, 14e, 14f), as fracture-fills in pyrite, (Fig. 14f) and less often as individual anhedral crystals of arsenian pyrite (Fig. 20f). Arsenian pyrite rims and fracture-fills are usually between 2 and 10 μm thick, but are rarely up to 50 μm thick. Generally, the more fractured a crystal is, the more arsenian pyrite it contains, as can be seen Figure 13f. Pyrite 3 rims commonly occur on pyrite 2 in stylolites (Fig. 14b, 14d).

Post-Ore Stage (Stage V)

Stage V consists of post-ore stage minerals including realgar, orpiment, and a fourth generation of calcite. Orpiment and realgar are commonly found together, and both occur as amorphous patches and as veins/veinlets (Fig. 14a, 14b). Calcite 4 displays bright yellow CL and occurs as patches and as veinlets (Fig. 14d, 14f). Calcite 4 is commonly spatially associated with realgar, and also often partially replaces earlier dolomite phases (Fig. 14c). Whilst there is evidence of near-surface, early, and intermediate diagenesis, these carbonate rocks do not appear to have undergone deep diagenesis.

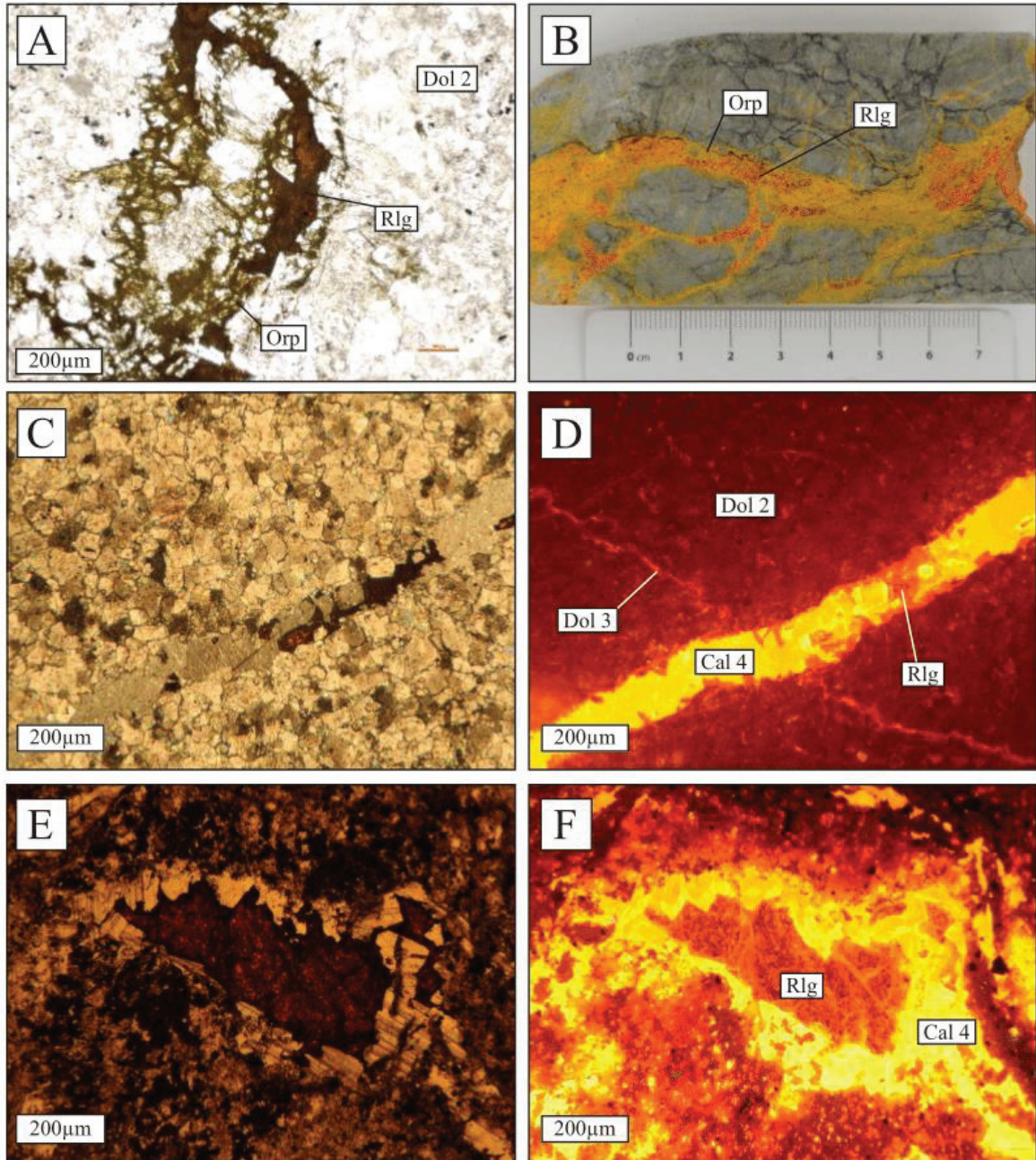


Figure 15. Stage V minerals. A) OS-11-61 116.55m - PPL image of a veinlet containing realgar and orpiment crosscutting dolomite 2 and quartz. B) OS-11-72 184.27m - Realgar/orpiment vein in dolostone. C) OS-11-41 293.18m – PPL image of a veinlet containing calcite 4 and realgar crosscutting dolomite 2. D) OS-11-41 293.18m – CL photo of the same image. Note the dolomite 3 veinlet. E) OS-12-120 122.68m – XPL image of an amorphous patch of realgar with rim of calcite 4. F) OS-12-120 122.68m – CL photo of the same image.

2.5.3 EMPA

Electron microprobe analysis was used to determine the major element geochemistry of the carbonate and sulfide phases. All EMPA data are listed in Appendix D.

Carbonate EMPA

The carbonates of the paragenetic stages outlined above have different major element compositions, particularly in their CaO, MgO, MnO and FeO contents. Some of the other components analyzed (BaO, SrO, NaO, ZnO) were below detection limit in most cases and were thus, not as helpful in characterization.

Host Rocks and Near-Surface Diagenesis Stage (Stage I)

Calcite grains of the lime mudstone and wackestone host rocks were analyzed by EMPA in two samples from Osiris and Isis East. The major element geochemistry of calcite grains in the host rock is commonly stoichiometric, with 54 to 55 wt. % CaO. This can vary depending on the concentration of MnO and FeO in the sample (Fig. 16a). The FeO concentration ranges from below detection limit (B.D.) to 1.22 wt. %; four of the seventeen calcite grains analyzed have FeO which is B.D. (see Appendix D). The MnO content generally increases with FeO content (Fig. 17a) and ranges from B.D. to 0.42 wt. %, and SrO ranges from B.D. to 0.54 wt. %. Roughly half of the samples have detectable quantities of MnO and SrO (see Appendix D).

Grains and matrix composed of dolomite 1 were analyzed by EMPA in two samples from different Osiris holes (Fig. 16b, 17b). The major element geochemistry of dolomite 1 is stoichiometric in a few samples (32 to 33 wt. % CaO and 19 to 20 wt. % MgO), but most samples have FeO concentrations of greater than 2 wt. % FeO (Fig. 18b). Dolomite 1 has 0.07 to 7.57 wt. % FeO and 0.01 to 0.39 wt. % MnO. Similar to the host rock calcite, the concentration of MnO generally increases with FeO content (Fig. 17b). There is one sample with anomalously high MnO content (Fig. 17b). This sample has the same general appearance as the rest of the samples, although the grain may have been partially affected by a later carbonate phase that was not identified.

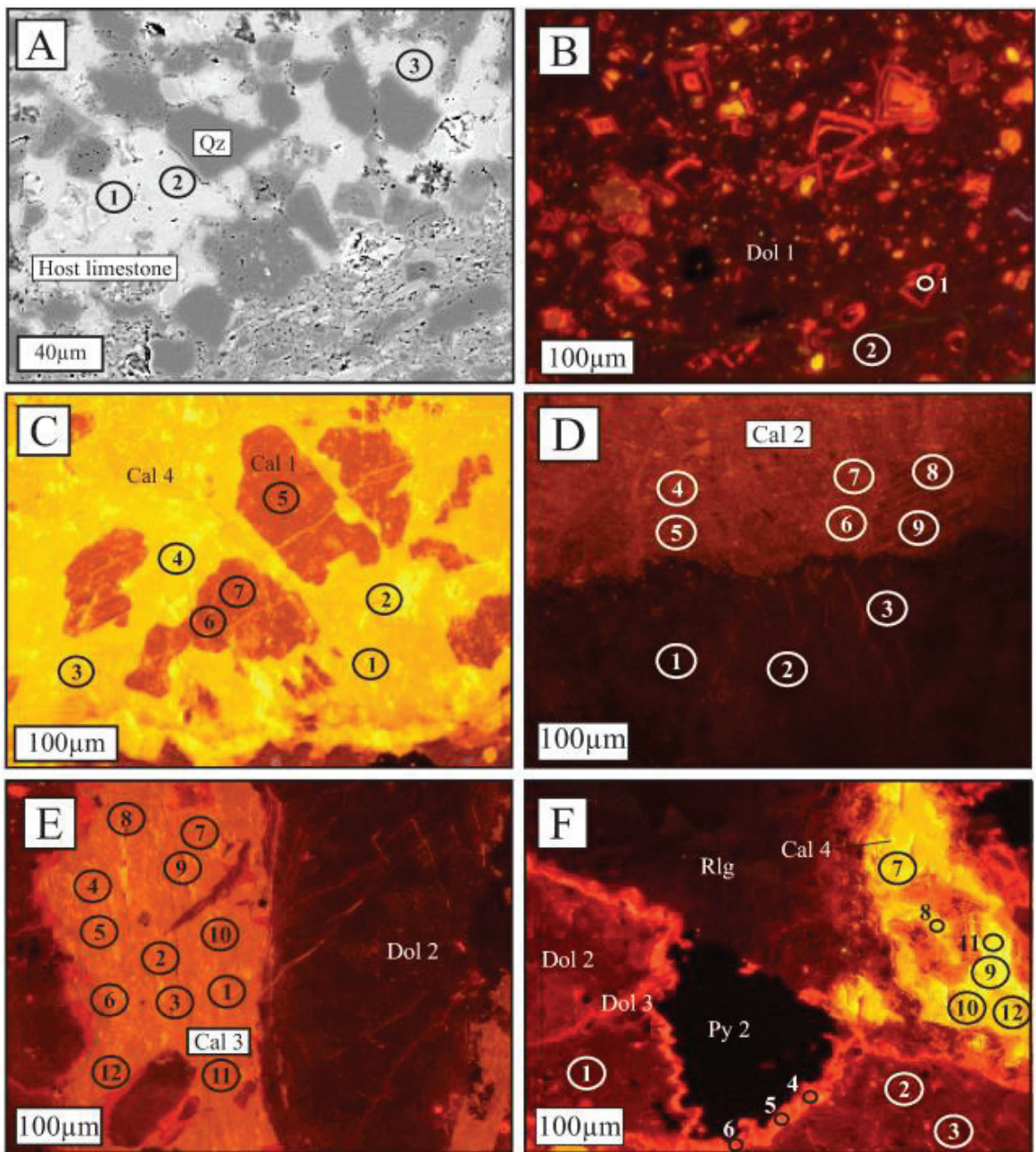


Figure 16. Locations of representative electron microprobe analyses of carbonates. Most analytical spot sizes are enlarged for ease of reference; actual size is 10 µm. Corresponding EMPA data are presented below. A) OS-11-80 73.08m. Calcite grains in wackestone host rock. B) OS-11-83 123.84m. Dolomite 1 (dull brown matrix and brown cores of clasts). C) OS-11-61 50.64m. Vein of calcite 1 partially replaced by calcite 4. D) OS-11-83 29.91m. Dolomite 2 in stylolite contact with calcite 2. E) OS-11-80 162.22m. Veinlet of calcite 3 crosscutting dolomite 2. F) OS-11-80 176.03m. Dolomite 2 with later veinlets of dolomite 3 and patch of calcite 4.

Spot	Phase	CaO	MgO	FeO	MnO	Spot	Phase	CaO	MgO	FeO	MnO
Host cal	A1	55.00	-	0.13	-	Cal 3	E4	56.19	-	0.11	0.02
Host cal	A2	55.26	-	0.09	-	Cal 3	E5	56.86	-	0.17	0.03
Host cal	A3	54.27	-	0.18	0.05	Cal 3	E6	56.72	-	0.05	0.04
Dol 1	B1	32.87	17.07	3.90	0.08	Cal 3	E7	56.94	17.07	-	-
Dol 1	B2	32.68	20.63	0.29	0.05	Cal 3	E8	56.49	20.63	-	0.01
Cal 1	C5	56.65	-	0.21	0.01	Cal 3	E9	56.28	-	0.10	-
Cal 1	C6	55.34	-	0.14	0.01	Cal 3	E10	56.52	-	0.10	0.01
Cal 1	C7	56.13	-	0.19	0.02	Cal 3	E11	56.81	-	-	0.01
Dol 2	D1	56.46	16.93	3.94	0.20	Cal 3	E12	56.57	16.93	-	-
Dol 2	D2	56.43	14.72	2.81	0.12	Dol 3	F4	56.60	14.72	0.14	0.32
Dol 2	D3	56.68	17.54	3.45	0.17	Dol 3	F5	30.57	17.54	0.16	0.53
Dol 2	F1	55.99	20.83	1.58	0.11	Dol 3	F6	30.38	20.83	0.11	0.87
Dol 2	F2	56.84	20.81	1.49	0.21	Cal 4	F7	30.29	20.81	0.02	0.60
Dol 2	F3	56.81	21.03	1.51	0.19	Cal 4	F8	31.63	21.03	-	0.59
Cal 2	D4	56.53	-	0.50	0.03	Cal 4	F9	32.03	-	-	0.76
Cal 2	D5	32.77	-	0.44	0.06	Cal 4	F10	31.75	-	-	0.47
Cal 2	D6	36.36	-	0.18	0.05	Cal 4	F11	55.45	-	-	0.63
Cal 2	D7	32.74	-	0.39	0.05	Cal 4	F12	55.85	-	-	0.88
Cal 2	D8	55.16	-	0.35	0.06	Cal 4	C1	55.70	-	-	0.24
Cal 3	E1	55.72	-	-	0.03	Cal 4	C2	55.83	-	0.01	0.11
Cal 3	E2	56.19	-	-	0.04	Cal 4	C3	55.62	-	0.25	0.25
Cal 3	E3	55.47	-	-	0.05	Cal 4	C4	54.92	-	0.02	0.07

Figure 16 cont'd. Corresponding EMPA data to Figure 16a. Values are in wt. % and a dash (-) denotes values below detection limit.

Base Metal Stage (Stage II)

Calcite 1 veinlets from Osiris and Isis East were analyzed in three different samples. Calcite 1 has a stoichiometric composition, with 55 to 56 wt. % CaO; this can vary depending on the concentration of MnO and FeO. The concentration of MnO ranges from B.D. to 0.12 wt. % and FeO concentration ranges from 0.09 to 0.96 wt. % (Fig. 16c; Fig 17c). Two of the nine calcite samples have MnO which is B.D (see Appendix D). The MnO and FeO content of samples varies regionally, with samples from different areas clustering in different parts of the Mn-Fe plot (Fig. 17c).

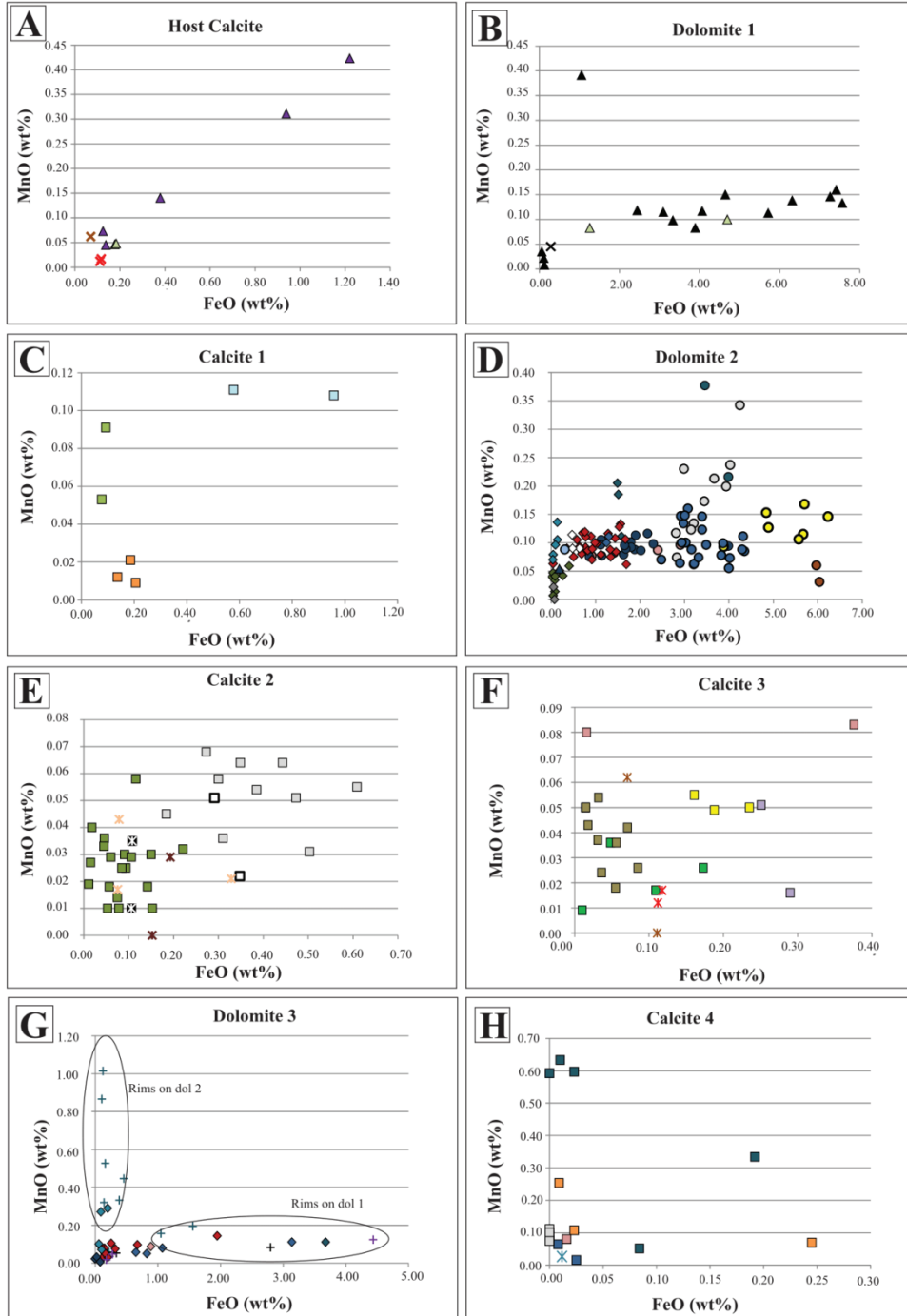
Dolomite 2a and 2b were analyzed heavily (163 data points total) in fifteen samples from Osiris and Isis East. Dolomite 2a and 2b were so heavily sampled because the crystals are commonly zoned. The major element geochemistry of dolomite 2 is typical of stoichiometric dolomite, with 20 to 22 wt. % MgO and 30 to 32 wt. % CaO (Fig. 16d, 16e, 16f). Dolomite 2 has MnO ranging from B.D. to 0.38 wt. %, and FeO content ranging from B.D. to 6.23 wt. % (Fig. 17d). Roughly 2/3 of the dolomite 2 data have detectable MnO, and nearly all data points have detectable FeO (see Appendix D). There is a weak positive correlation between MnO and FeO content in dolomite 2 (Fig. 17d). There is a spatial

variation in MnO and FeO concentrations, as different samples cluster in different parts of the plot. Overall, dolomite 2b (saddle morphology) has higher FeO and MnO content than dolomite 2a (sparry; Fig. 17d). Many dolomite 2 crystals are zoned (Fig. 12i); the more brightly cathodoluminescent zones have higher Mn and lower Fe, and the dull zones have higher Fe and lower Mn (Fig. 18). The outer rims of zoned dolomite 2 have duller CL.

Intermediate Diagenesis Stage (Stage III)

Five samples of calcite 2 veinlets and disseminated calcite were analyzed, and they have a composition typical of stoichiometric calcite, with 55 to 56 wt. % CaO. The concentration of MnO ranges from B.D. to 0.08 wt. % and the FeO content ranges from B.D. to 0.61 wt. % (Fig. 16d). Most calcite 2 analyzed has detectable quantities of MnO and FeO and there is a weak correlation between these two components (Fig. 17d; Appendix D). The composition of calcite 2 varies spatially, as different samples have different compositions (Fig. 17d).

Seven samples of calcite 3 veins/veinlets and disseminated calcite were analyzed, and they also have major element geochemistry typical of stoichiometric calcite, with 55 to 56 wt. % CaO (Fig. 16e). The minor element geochemistry is characterized by B.D. to 0.08 wt. % MnO, B.D. to 0.38 wt. % FeO (Fig. 17e), and B.D. to 0.50 wt. % SrO. Like calcite 2, calcite 3 has detectable quantities of MnO and FeO in nearly all samples (see Appendix D). Similar to calcite 2, different samples of calcite 3 plot in different parts of the geochemical plot (Fig. 17e).



Osiris			Isis East		Occurrence	
OS-11-41 67.75	OS-11-61 29.30	OS-11-80 154.24	OS-12-120 43.37	×	Matrix	
OS-11-41 206.98	OS-11-61 50.64	OS-11-80 162.22	OS-12-120 51.16	△	Carbonate Grain	
OS-11-41 267.68	OS-11-61 84.15	OS-11-80 176.03	OS-12-120 101.44	□	Calcite Vein	
OS-11-41 319.68	OS-11-61 92.45	OS-11-80 210.57	OS-12-120 104.75	×	Disseminated Calcite	
OS-11-41 341.42	OS-11-80 45.09	OS-11-83 14.14	OS-12-120 106.14	◇	Sparry dolomite (dol 2a, 3a)	
OS-11-41 342.97	OS-11-80 73.08	OS-11-83 29.91	OS-12-120 293.18	○	Saddle dolomite (dol 2b)	
OS-11-52 6.96	OS-11-80 108.16	OS-11-83 86.72	OS-12-120 138.05	+	Rim	
	OS-11-80 151.32	OS-11-83 123.84	OS-12-120 138.33			

Figure 17 (above). Plots of EMPA data for carbonates. Shapes of data points correspond to different mineral textures and are color-coded according to the sample number. Some data have been omitted because they have components that are below the detection limit. A) MnO vs. FeO for calcite of the host limestone. B) MnO vs. FeO for dolomite 1. C) MnO vs. FeO for calcite 1. D) MnO vs. FeO for dolomite 2. E) MnO vs. FeO for calcite 2. F) MnO vs. FeO for calcite 3. G) MnO vs. FeO for dolomite 3. The “+” points with higher Mn are from rims on dolomite 2; the “+” points with higher Fe are from dolomite 3 rims on dolomite 1. H) MnO vs. FeO for calcite 4.

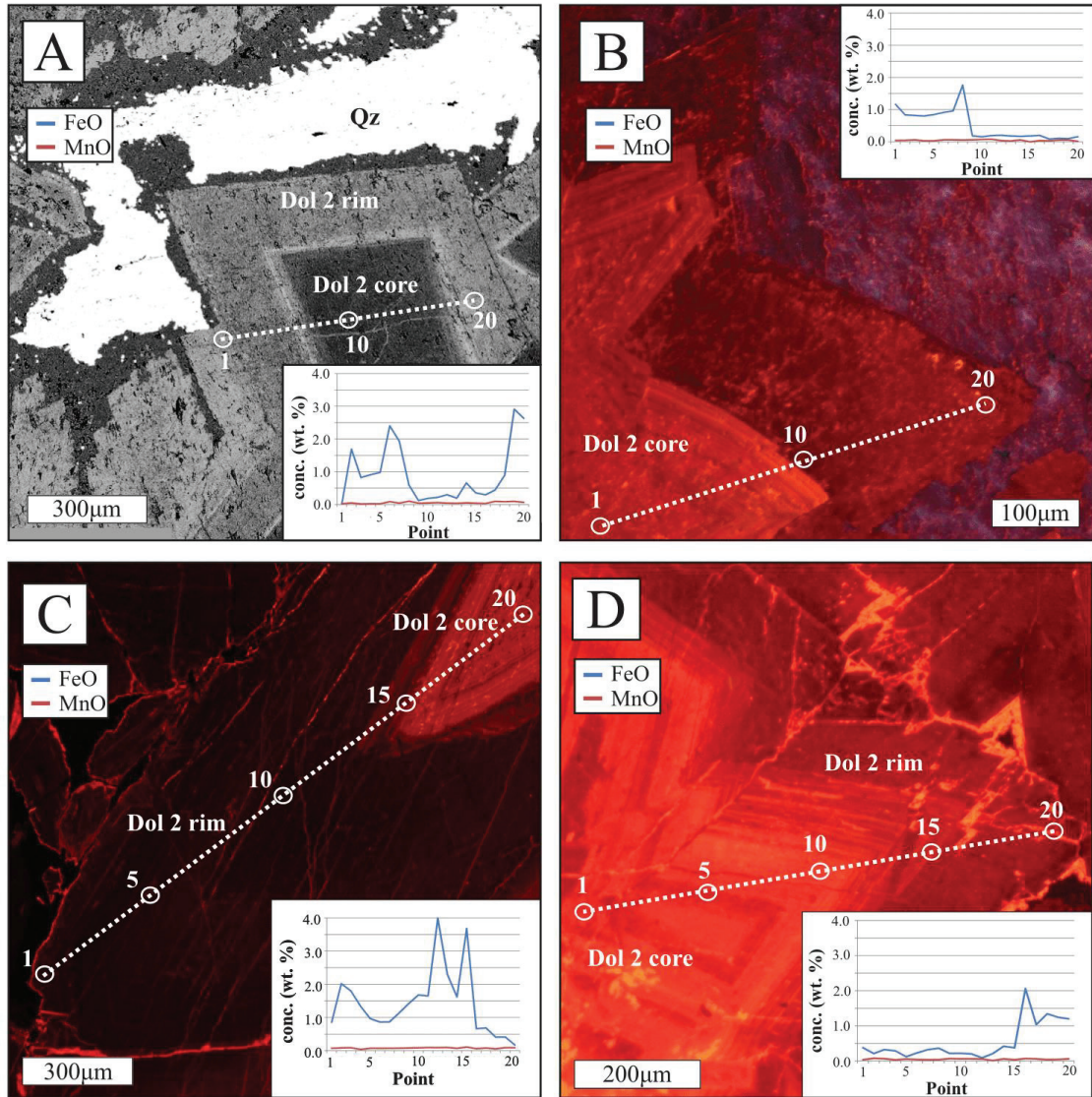


Figure 18. EMPA data of zoned dolomite 2 crystals (CL images). 20-point line analyses were conducted on the dolomite crystals; the transect of the line analysis is represented by a white dotted line. Graphs show MnO and FeO contents for each point of the line analysis. Note the inverse correlation between CL intensity and Fe content. Detection limits for MnO and FeO are 0.01 wt. %. A) OS-11-41 206.98m. BSE image. B) Also OS-11-41 206.98m. C) OS-12-120 104.75m. D) OS-12-120 115.26m.

Ore Stage (Stage IV)

Nine samples containing dolomite 3 were analyzed (133 data points total); some dolomite 3a and some dolomite 3b. Dolomite 3 typically has a stoichiometric composition, with 31 to 32 wt. % CaO and 20 to 21 wt. % MgO (Fig. 16f). The minor element geochemistry of dolomite 3 is characterized by B.D. to 1.01 wt. % MnO and B.D. to 4.44 wt. % FeO (Fig. 16f). Roughly half of the dolomite 3 data have detectable MnO and FeO. Samples with high MnO tend to have low FeO content, and samples with low MnO tend to have high FeO content (Fig. 17g). Dolomite 3 rims nucleating on dolomite 2 tend to have low FeO and high MnO (OS-11-80 176.03, Fig. 17g). Dolomite 3 rims nucleating on dolomite 1 grains have much lower MnO and variable FeO content (OS-11-83 123.84 and OS-12-120 43.37, Fig. 18g).

Post-Ore Stage (Stage V)

As previously noted, calcite 4 occurs as veins/veinlets or as amorphous patches which are commonly associated with realgar. Calcite 4 is the final carbonate phase in the paragenetic sequence, and has the highest average MnO content of all the carbonates in the Nadaleen Trend. Overall, the major element geochemistry of this phase of calcite is typical of stoichiometric calcite, with 55 to 56 wt. % CaO (Fig. 16c, 16f). This varies depending on the MnO concentration which can range from B.D. to 0.88 wt. %. FeO ranges from B.D. to 0.25 wt. % (Fig. 17h). Nearly all calcite 4 has detectable MnO, and roughly half of the calcite 4 data points have detectable FeO (see Appendix D).

Sulfide EMPA

Framboidal pyrite and the three later generations of pyrite were examined by EMPA, as were a few grains of sphalerite and realgar. Besides S and Fe, As was the most common element detected, and the most useful in characterizing the different generations of pyrite. Most of the other elements analyzed (Pb, Ni, Sb, Cu, Ag, Se, Zn, Cd, Si, Tl) were below the detection limit, but there are a few samples with significant Cu, Se, and Pb content. All EMPA data are presented in Appendix D. Most of the pyrite analyzed has a stoichiometric composition, although some, especially the ore stage pyrite, is arsenian pyrite, $\text{Fe}(\text{As,S})_2$ (0.1 to 10 wt. % As; Reich et al., 2005; Fig. 19). For the purpose of this thesis, “arsenian pyrite” will refer to pyrite with at least 0.1 wt. % As.

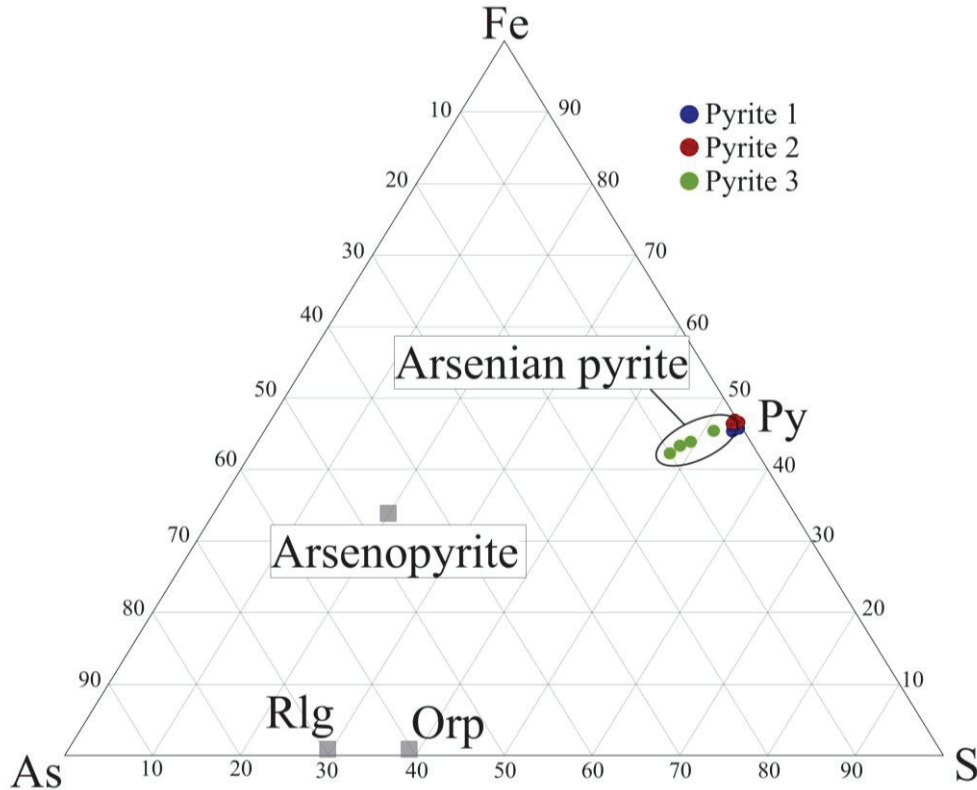


Figure 19. Ternary plot with compositions of the three generations of pyrite.

Host Rock and Near-Surface Diagenesis Stage (Stage I)

Two grains of framboidal pyrite and thirteen grains of pyrite 1 from Osiris hole OS-11-80 were analyzed (OS-11-80 contains the most abundant pyrite 1). These phases of pyrite both have a major element geochemistry typical of stoichiometric pyrite, with Fe and S concentrations of 45 to 46 wt. % and 52 to 53 wt. % S, respectively (Fig. 20a, 20b), varying slightly depending on As content. Some pyrite 1 has an arsenian pyrite composition, with 38 % of samples having As greater than 0.1 wt. % As (Fig. 21a, 21b). Some grains of pyrite 1 have significant amounts of Cu and Se, with Cu ranging from B.D. to 0.48 wt. % and Se ranging from B.D to 0.17 wt. %. Of the fourteen Stage I pyrite points analyzed, seven have detectable Ni, five have detectable Cu, and eleven have detectable Se (see Appendix D). Some of the pyrite 1 grains are zoned, with variable Fe, S, As, and Cu contents within the grain (Fig. 22a-f). Iron content generally increases with S content, and As content generally decreases with increasing S content. This is illustrated graphically (Fig. 21a, 21b) and with elemental maps (Fig. 22a-f).

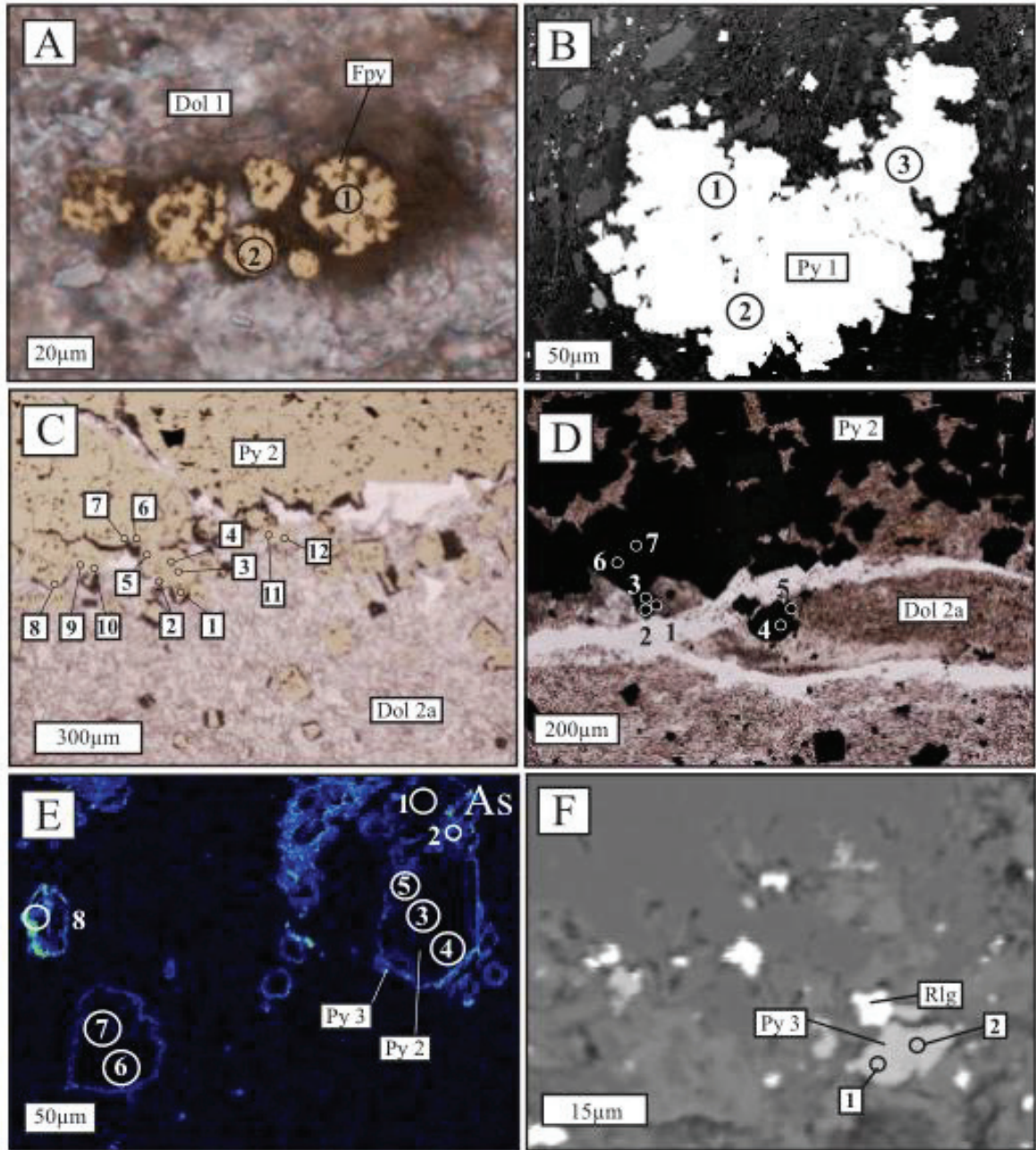


Figure 20. Locations of representative EMPA analyses of pyrite. Data are on next page. Analytical spot sizes are enlarged for ease of reference; actual size is $< 1 \mu\text{m}$. Values are in wt% and a dash (-) denotes values below detection limit. A) OS-11-80 73.08m. EMPA data from framboidal pyrite. B) OS-11-80 114.54m. EMPA data from pyrite 1. C) OS-11-52 219.31m. EMPA data from pyrite 2. D) OS-11-41 201.33m. EMPA data from pyrite 2. E) OS-11-41 294.22m. As map with EMPA data from pyrite 2 (dull blue) and pyrite 3 (bright blue). F) OS-11-61 401.20m. EMPA point on a small grain of pyrite 3.

Phase	Spot	S	Fe	As	Phase	Spot	S	Fe	As
Fpy	A1	52.62	45.90	-	Py 2	D1	53.52	47.03	-
Fpy	A2	52.83	46.17	0.05	Py 2	D2	53.70	46.95	-
Py 1	B1	52.35	46.45	0.09	Py 2	D3	53.23	46.61	0.03
Py 1	B2	53.05	46.72	0.07	Py 2	D4	53.38	46.99	-
Py 1	B3	51.74	45.86	0.13	Py 2	D5	53.06	46.75	-
Py 2	C1	53.35	45.41	-	Py 2	D6	53.27	46.75	0.03
Py 2	C2	53.45	45.76	-	Py 2	D7	53.53	47.27	-
Py 2	C3	53.24	46.00	-	Py 2	E1	53.47	46.58	-
Py 2	C4	53.42	46.23	0.03	Py 2	E3	54.65	46.87	-
Py 2	C5	53.17	45.82	-	Py 2	E4	54.01	46.62	-
Py 2	C6	53.58	46.30	-	Py 2	E5	53.80	46.49	0.05
Py 2	C7	53.39	46.27	0.05	Py 2	E6	53.35	46.47	-
Py 2	C8	53.46	46.24	-	Py 2	E7	53.82	46.46	-
Py 2	C9	53.52	45.90	-	Py 3	E2	53.45	46.49	0.23
Py 2	C10	53.47	46.26	0.03	Py 3	E8	53.19	46.17	0.59
Py 2	C11	53.51	45.66	0.03	Py 3	G1	48.55	43.20	6.69
Py 2	C12	53.45	46.38	-	Py 3	G2	47.87	42.81	8.09

Figure 20 cont'd. Corresponding EMPA data table to Figure 20a. Values are in wt% and a dash (-) denotes values below detection limit.

Base Metal Mineralization Stage (Stage II)

A large amount of data were collected on pyrite 2 (362 data points) in samples from Osiris, Isis, and Isis East. Pyrite 2 has a stoichiometric pyrite composition, with 46 to 47 wt. % Fe and 53 to 54 wt. % S, varying slightly depending on As content (Fig. 20c-e, 21c, 21d).

Arsenic content ranges from B.D to 0.59 wt. % As. For the most part, there is no Pb in any of the pyrite, with the exception of one analysis in which the Pb content is 0.32 wt. %; this came from a highly corroded crystal in a shear zone in Isis hole OS-11-72. In pyrite 2, Fe content generally increases with S content, and As content generally decreases with increasing Fe and S content (Fig. 21c, 21d, Fig. 22g-l). Sphalerite crystals were analyzed as well; Zn ranges from 64.18 to 66.29 wt. %, S ranges from 31.97 to 33.18 wt. %, and Fe ranges from 0.30 to 1.20 wt. % (Fig. 21e, 21f). There is a positive correlation between Zn and S content (Fig. 21e, 21f).

Ore Stage (Stage IV)

Pyrite 3 occurs as rims or as fracture-fills (Fig. 14f, 14i, 20e, 22f, 22i, 22l); and much less commonly as individual anhedral grains (Fig. 20f). Some pyrite 3 rims could be analyzed (12 data points were collected), whereas the individual grains were quite small and difficult to analyze. As a result, only two grains of pure pyrite 3 were analyzed (Fig. 20f). In grains where pyrite 3 occurs as rims or as fracture-fills, Fe ranges from 53 to 54 wt. % and S ranges from 46 to 47 wt. %. Arsenic content in these samples ranges from 0.09 to 3.27 wt. % As (Fig. 21h) and Cu is B.D. except for one Osiris sample (with 0.31 wt. % Cu), where pyrite 3 occurs on the rim of a grain of Cu-rich pyrite 1. In samples where pyrite 3 occurs as disseminated crystals, Fe ranges from 40 to 44 wt. %, S ranges from 46 to 48 wt. %, As ranges from 6.69 to 9.67 wt. % As, and Sb content ranges from 0.09 to 0.16 wt% (Fig. 21g, 21h). Overall, in pyrite 3, Fe content increases with S content, and As content decreases with increasing S content (Fig. 21g, 21h). The inverse relation that As has with Fe and S can be shown via qualitative elemental maps, in which the arsenian pyrite rims are relatively low in Fe and S (Fig. 22).

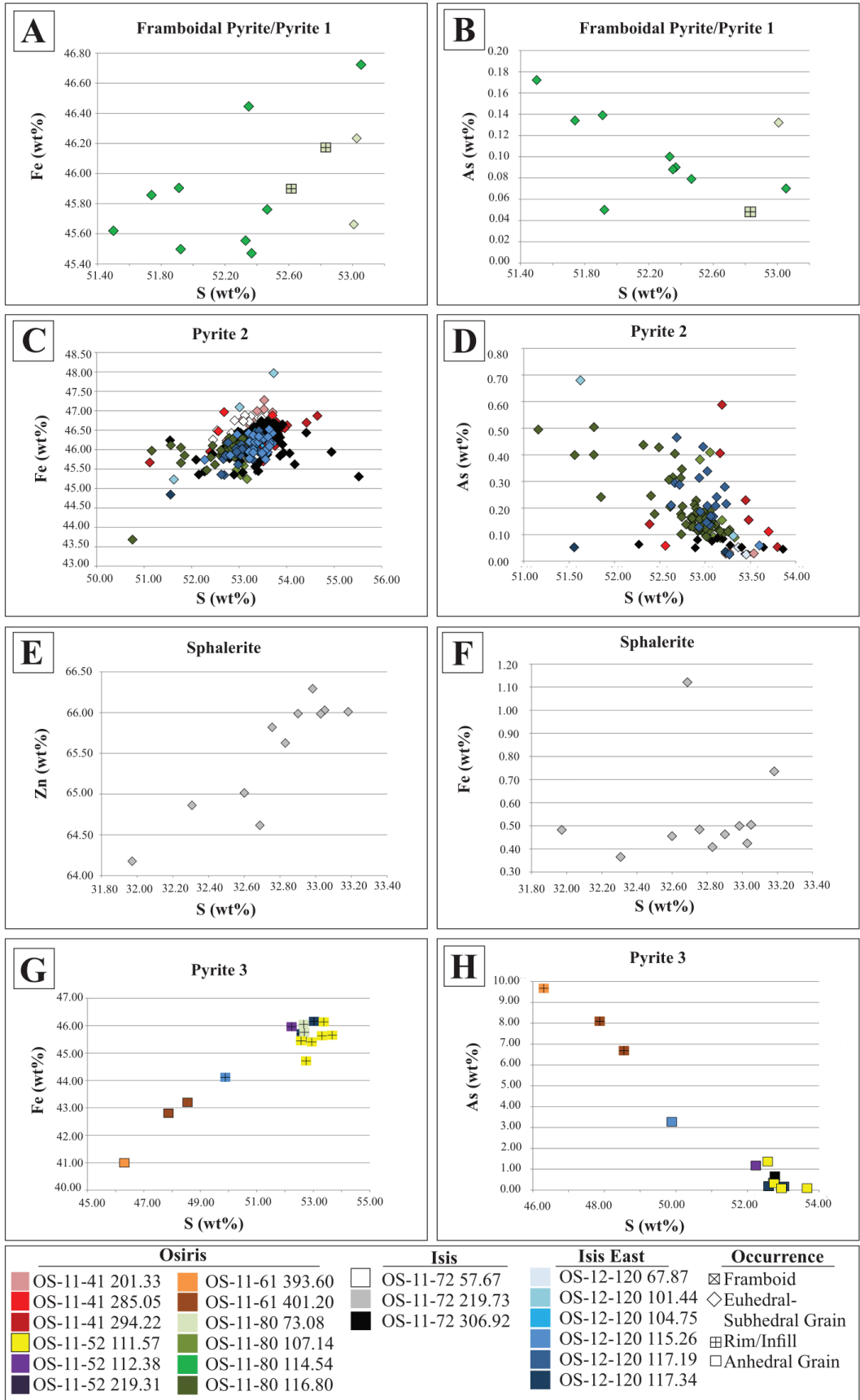


Figure 21 (above). Geochemical plots of EMPA major element data in sulfides. A) Fe vs. S in Fpy and pyrite 1. B) As vs. S in Fpy and pyrite 1. C) Fe vs. S in pyrite 2. D) As vs. S in pyrite 2. E) Zn vs. S in sphalerite. F) Fe vs. S in sphalerite. G) Fe vs. S in pyrite 3. H) As vs. S in pyrite 3.

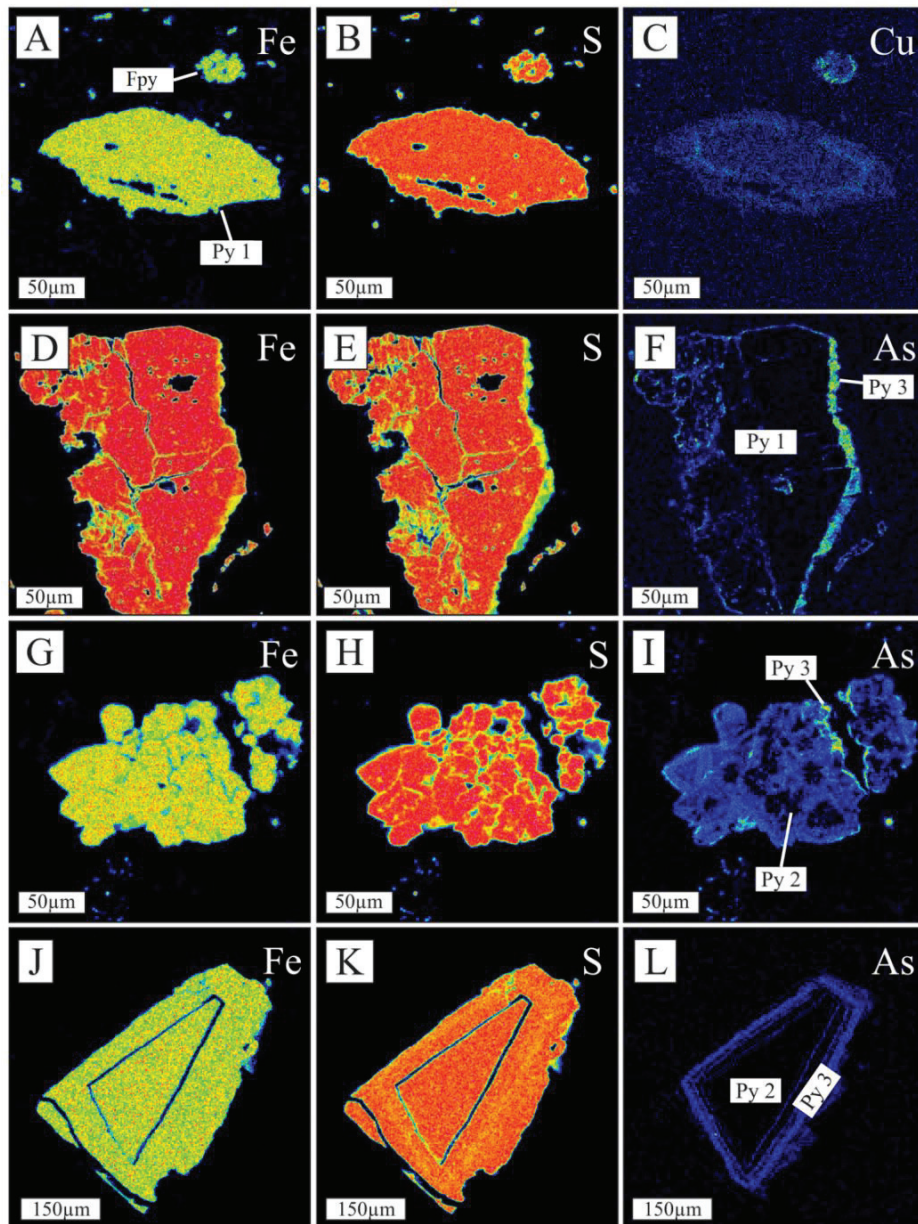


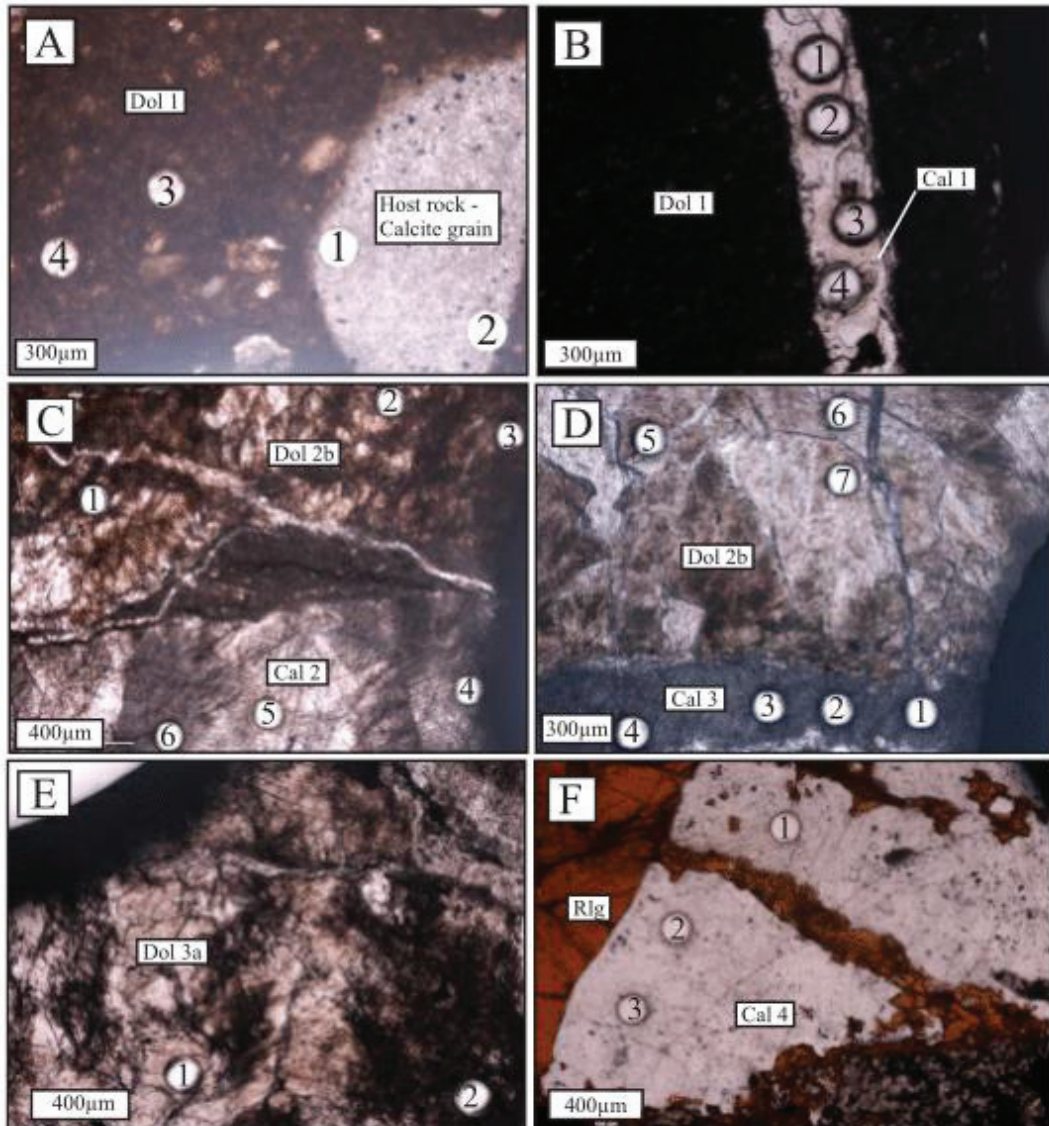
Figure 22. Qualitative EMPA elemental maps of pyrite grains. Warmer colors (red) indicate higher concentrations. Note the inverse relation between S + Fe and As. A) OS-11-80 114.54m. Fe map of grains of framboidal pyrite and pyrite 1. B) Same field of view - S map. C) Same field of view - Cu map. D) OS-11-41 294.22m. Fe map of pyrite 1 grain. E) Same field of view - S map. F) Same field of view - As map. Arsenian pyrite (pyrite 3) occurs as rims and fractures on pyrite 1. G) OS-11-52 112.38m. Fe map of pyrite 2 grain. H) Same field of view - S map. I) Same field of view - As map. Arsenian pyrite (pyrite 3) occurs as a rim on pyrite 2. J) OS-12-120 101.44m. Fe map of pyrite 2. K) Same field of view - S map. L) Same field of view - As map. Arsenian pyrite (pyrite 3) occurs as a rim on pyrite 2.

2.5.4 LA-ICP-MS

Laser ablation inductively coupled plasma mass spectrometry was used to determine the trace element composition of carbonate and sulfide phases. All LA-ICP-MS data are presented in Appendix E.

Carbonate LA-ICP-MS

The host rocks and all carbonate phases were analyzed by LA-ICP-MS to examine their trace element concentrations. Figure 23 presents LA-ICP-MS data on selected samples that display typical features of the host rocks or paragenetic phases. The remaining LA-ICP-MS data on these carbonates are presented in Appendix E. Forty-two elements were analyzed by LA-ICP-MS but Fe, Mn, Sr, Ba, Ti, V, Zn, Ti and As were the ones that were most commonly above detection limit.



Spot	Phase	Mn	Fe	Sr	Ba	Ti	ΣREY
A1	Host rock	61.80	2050.00	2338.00	X	13.00	11.96
A2	Host rock	54.90	3250.00	2346.00	X	7.70	12.851
A3	Dol 1	508.00	40640.00	452.00	464.00	5920.00	226.43
A4	Dol 1	455.00	38900.00	595.00	477.70	5200.00	239.30
B1	Cal 1	186.20	711.00	45.40	12.00	5.50	7.96
B2	Cal 1	191.60	721.00	49.20	7.20	2.70	15.34
B3	Cal 1	187.80	711.00	55.00	12.00	5.20	21.13
B4	Cal 1	208.40	756.00	46.40	13.00	5.70	9.26
C1	Dol 2	1151.00	88900.00	106.90	10.90	0.63	40.30
C2	Dol 2	1031.00	54690.00	109.20	11.56	0.43	44.74
C3	Dol 2	993.00	53750.00	149.20	20.56	0.77	28.23
D5	Dol 2	1041.00	32160.00	92.50	10.46	1.35	79.87
D6	Dol 2	857.00	30460.00	157.00	10.56	0.89	82.15
D7	Dol 2	936.00	29310.00	416.00	16.74	1.57	89.23
C4	Cal 2	246.00	2826.00	857.00	24.10	3.30	67.60
C5	Cal 2	230.30	3239.00	954.00	49.30	4.40	85.42
C6	Cal 2	227.60	3860.00	1026.00	14.30	0.34	105.94
D1	Cal 3	211.10	1764.00	601.00	24.40	2.84	6.05
D2	Cal 3	208.90	1653.00	385.30	4.13	-	2.23
D3	Cal 3	210.00	1770.00	399.90	3.79	-	2.81
D4	Cal 3	201.20	1758.00	480.00	9.97	-	4.71
E1	Dol 3	473.20	1541	43.91	3.19	1.18	15.51
E2	Dol 3	676.00	4397	139.60	30.50	2.76	29.60
F1	Cal 4	2560.00	500.00	26.20	0.53	-	1.26
F2	Cal 4	2400.00	71.00	23.56	0.38	-	15.60
F3	Cal 4	3740.00	390.00	32.00	2.20	-	28.05

Figure 23. Laser ablation craters and corresponding LA-ICP-MS data table. Values are in ppm. A dash (-) denotes data that were below detection limit; an “X” denotes data that were discarded due to interference or other factors. A) OS-12-120 43.37m. PPL image of dolomite 1 and a grain of the host limestone. B) OS-11-80 108.16m. PPL image of a veinlet of calcite 1 crosscutting dolomite 1. C) OS-11-83 29.91m. PPL image of a veinlet of calcite 2 crosscutting dolomite 2. D) OS-11-52 6.96m. PPL image of a veinlet of calcite 3 crosscutting dolomite 2. E) OS-11-41 342.97m. PPL image of dolomite 3, with darker areas more concentrated in trace elements. F) OS-11-80 176.03m. PPL image of calcite 4 mineralization along with realgar.

Host Rock and Near-Surface Diagenesis Stage (Stage I)

Five calcite grains of the host rock were analyzed from two samples in which calcite grains occur in a matrix of dolomite 1 (Fig. 23a). Calcite grains are enriched in Mn, Fe, Sr, Ba, and As, with Mn contents ranging from 54.90 to 915.00 ppm, Fe ranging from 1419.00 to 13260.00 ppm, Sr ranging from 287.00 to 2347.00 ppm, and As ranging from 4.30 to 69.00

ppm (Table 1; Fig. 24a). Barium was only detected in one analysis and had a value of 7.99 ppm. Calcite grains also contain significant amounts of rare earth elements and Y (REY) and minor concentrations of other elements (Ni, Pb, Zn, Cu, Mo, Co, Cd, Ti, Zr, Sb, Cr, V; Table 1; Fig. 23a). The dominant feature of the REY pattern is a medium rare earth element (MREE) enrichment (Fig. 26a). Ce/Ce* values were calculated for the calcite host rock, and the values range from 0.93 to 1.03. Plots of \sum REY vs. Ti indicates that there is not a strong positive correlation of REY with Ti (Fig. 27a).

Dolomite 1 was analyzed in two samples from Osiris and two from Isis East; a total of 60 data points were collected. Dolomite 1 generally has greater concentrations of Mn, Fe, Sr, Ba, and As than the host limestone (Table 1; Fig. 24b). Dolomite 1 contains 156.00 to 1381.00 ppm Mn, 9,000.00 to 151,00.00 ppm Fe, 234.00 to 1362.00 ppm Sr, 215.00 to 5010.00 ppm Ba, and 14.20 to 6540.00 ppm As. Dolomite 1 has greater trace element (Ni, Pb, Zn, Cu, Mo, Co, Cd, Ti, Zr, Sb, Cr, V) concentrations than the host rock (Table 1; Fig. 24b). In sample OS-11-80 73.08, the Mn, Fe, Sr, and Ba contents vary stratigraphically, with some laminae enriched in these elements and some depleted. Dolomite 1 is enriched in REY relative to the host rock and Ediacaran seawater (Table 1; Fig. 24). Broadly, there are two REY patterns present: OS-11-83 123.84 is enriched in light rare earth elements (LREE; La to Nd) compared to medium rare earth elements (Sm to Dy) and heavy rare earth elements and Y (HREE; Ho to Lu, and Y), and OS-11-80 73.08 has a flat pattern (Fig. 26b). There is a positive correlation between \sum REY and Ti for dolomite 1 for a number of samples; this suggests that these REY may come from a detrital source (Fig. 27b). Only the non-detrital data (the data which are not on the line of best fit) are presented in the REY plot of Figure 26 to represent the actual seawater REY composition.

Table 1. Selected LA-ICP-MS data for all paragenetic carbonate phases. Values are in ppm.
B.D. = Below detection limit. n = number of data

		Host Cal (n = 5)	Dol 1 (n = 60)	Cal 1 (n = 12)	Dol 2 (n = 37)	Cal 2 (n = 39)	Cal 3 (n = 21)	Dol 3 (n = 25)	Cal 4 (n = 16)
Sc	(min)	0.36	9.20	0.25	B.D.	B.D.	B.D.	B.D.	B.D.
	(mean)	3.29	36.87	0.94	0.18	0.36	0.06	0.41	B.D.
	(max)	8.41	131.00	2.31	1.09	1.28	0.11	1.30	B.D.
Ti	(min)	3.74	1830.00	2.70	B.D.	B.D.	B.D.	1.12	B.D.
	(mean)	9.74	14239.15	6.00	10.56	22.13	0.61	2.76	0.49
	(max)	18.9	61500	13.20	79.00	101.00	2.84	6.9	1.19
V	(min)	0.85	33.00	3.12	0.309	0.24	B.D.	0.56	B.D.
	(mean)	2.13	381.02	5.38	1.68	2.43	0.67	3.61	2.53
	(max)	3.19	1560.00	9.25	4.45	8.1	1.69	14.81	11.93
Cr	(min)	3.39	32	3.74	2.51	1.96	2.33	3.40	3.21
	(mean)	4.36	269.96	6.54	4.04	3.27	2.58	4.50	3.61
	(max)	6.32	950.00	11.75	11.78	6.03	2.87	10.13	3.92
Mn	(min)	54.90	156.00	186.20	309.20	67.70	100.70	104.50	139.50
	(mean)	399.18	663.35	223.68	780.66	111.95	232.71	877.26	1324.10
	(max)	915.00	1381.00	290.00	1706.00	246.50	427.00	2215.00	3740.00
Fe	(min)	1419.00	9000.00	711.00	356.00	136.40	156.20	1541.00	39.50
	(mean)	4771.80	64836.00	864.70	29174.00	1528.80	1417.20	7065.10	200.09
	(max)	13260.00	151000.00	1226.00	88900.00	9200.00	2206.00	22800.00	760.00
Co	(min)	0.29	1.57	B.D.	B.D.	B.D.	B.D.	B.D.	B.D.
	(mean)	2.17	12.02	0.02	0.76	0.38	0.07	0.14	0.04
	(max)	5.95	41.4	0.02	2.00	1.28	0.01	0.23	0.06
Ni	(min)	0.53	9.5	B.D.	B.D.	B.D.	0.12	0.14	B.D.
	(mean)	2.32	52.48	0.31	2.93	0.84	0.19	0.51	0.20
	(max)	4.03	170.00	0.36	6.82	4.7	0.49	3.02	0.26
Cu	(min)	1.83	8.9	0.18	B.D.	B.D.	B.D.	0.27	B.D.
	(mean)	12.85	109.99	1.47	1.29	1.26	1.54	1.43	1.68
	(max)	24.30	1540.00	3.40	4.7	6.6	7.90	10.10	4.40
Zn	(min)	1.37	12.7	B.D.	0.63	B.D.	B.D.	0.73	B.D.
	(mean)	2.67	58.43	0.46	4.72	0.65	0.20	2.01	0.17
	(max)	3.94	176.00	1.10	10.58	7.26	0.58	5.93	0.22
As	(min)	4.30	14.20	16.00	0.38	0.80	0.66	2.50	0.27
	(mean)	28.02	426.76	58.00	65.25	31.07	8.72	79.45	98.86
	(max)	69.00	6540.00	100.00	429.00	250.00	72.00	670.00	610.00
Rb	(min)	0.69	89.80	0.65	B.D.	B.D.	B.D.	B.D.	B.D.
	(mean)	0.73	609.36	1.23	0.73	1.70	0.19	0.08	0.12
	(max)	0.78	2630.00	2.10	4.9	7.10	1.06	0.41	0.43
Sr	(min)	0.73	234.00	29.9	53.47	85.2	87.00	43.91	23.56
	(mean)	1275.40	775.66	62.33	127.92	499.98	1292.20	71.46	104.13
	(max)	2346.00	1362.00	111.00	416.00	1026.00	4700.00	139.60	212.00
Zr	(min)	0.82	56.5	1.50	0.02	0.09	0.16	0.02	0.04
	(mean)	0.82	308.02	3.25	0.48	3.10	0.60	0.14	0.57
	(max)	0.98	1320.00	4.50	3.01	11.80	1.74	0.38	4.56
Mo	(min)	B.D.	0.20	B.D.	B.D.	B.D.	B.D.	B.D.	B.D.
	(mean)	0.75	0.92	B.D.	0.21	0.10	0.37	0.02	0.01
	(max)	0.2	5.50	B.D.	1.50	0.16	0.37	0.02	0.02
Ag	(min)	B.D.	B.D.	B.D.	B.D.	B.D.	B.D.	B.D.	B.D.
	(mean)	0.04	0.12	B.D.	0.03	B.D.	B.D.	0.05	B.D.
	(max)	0.04	0.17	B.D.	0.03	B.D.	B.D.	0.07	B.D.
Cd	(min)	B.D.	B.D.	B.D.	B.D.	B.D.	B.D.	B.D.	B.D.
	(mean)	0.06	0.42	B.D.	0.02	0.01	0.01	0.02	B.D.
	(max)	0.08	2.66	B.D.	0.03	0.02	0.02	0.03	B.D.
Sb	(min)	B.D.	B.D.	B.D.	B.D.	B.D.	B.D.	B.D.	B.D.
	(mean)	0.20	2.35	B.D.	0.33	0.016	0.06	23.68	0.42
	(max)	0.20	18.30	B.D.	1.24	0.016	0.09	178.00	1.22
Ba	(min)	7.9	215.00	3.80	1.25	5.6	3.79	3.19	0.38
	(mean)	7.9	1188.98	10.26	12.32	26.24	12.83	9.24	1.48
	(max)	7.9	5010.00	15.00	41.6	61.00	24.40	30.5	7.04
ΣREY	(min)	9.26	70.28	5.12	11.91	4.97	0.32	8.81	0.06
	(mean)	62.23	472.23	9.54	38.58	20.57	3.64	17.63	14.28
	(max)	191.61	1650.30	25.33	81.30	98.92	19.64	36.12	36.12
Pb	(min)	1.82	4.69	0.14	0.04	0.04	0.05	0.05	B.D.
	(mean)	3.06	19.55	0.32	0.39	0.88	0.16	0.30	0.16
	(max)	4.21	290.00	0.61	2.00	5.60	0.56	1.27	0.62

Base Metal Mineralization Stage (Stage II)

Several veinlets of calcite 1 from OS-11-80 108.16 were analyzed (12 data points total); a few of the spots are shown in Fig. 23b. This phase of calcite has 186.20 to 290.00 ppm Mn, 711.00 to 1226.00 ppm Fe, 29.90 to 111.00 ppm Sr, 3.80 to 15.00 ppm Ba, and 16.00 to 100.00 ppm As. Calcite 1 is depleted in REY and other elements compared to the host rock and dolomite 1 (Table 1; Fig. 24c). Calcite 1 is depleted in LREE and relatively enriched in MREE and HREE, with a positive Y anomaly (Fig. 26c).

Four samples of dolomite 2 (Dol 2a and 2b) from four drill holes were analyzed for a total of 37 data points (Table 1; Fig. 23c, 23d, 24d). Dolomite 2 has 149.10 to 11706.00 ppm Mn, 356.00 to 88,900.00 ppm Fe, 53.47 to 416.00 ppm Sr, 1.20 to 41.60 ppm Ba, and 0.38 to 416.00 ppm As. There are some areas of dolomite 2 which have “dirty” brown material (in PPL); it appears that there is higher Mn, Sr, Ba, Ti, and REY content in these zones (Fig. 23e). Overall, there is a relatively flat REY pattern (Fig. 26d). There is a weak positive correlation between Mn and Ba (Fig. 27d).

Intermediate Diagenesis (Stage III)

Calcite 2 cement and calcite 2 veins were examined with LA-ICP-MS in two samples (39 data points total; Fig. 23; Table 1). Overall, the trace element geochemistry of calcite 2 is characterized by 67.00 to 427.50 ppm Mn, 136.40 to 9,200.00 ppm Fe, 85.20 to 1026.00 ppm Sr, 5.60 to 61.00 ppm Ba, and 0.86 to 250.00 ppm As. There is small-scale variation in CL intensity in this phase and higher Mn and lower Fe is found in brighter CL zones. There are higher Sr and Ba contents in the cements than the veins. There are minor concentrations of most trace elements, and there are higher REY concentrations than calcite 1 (Table 1; Fig. 25a). Overall, the REY pattern shows decreasing concentrations from LREE to HREE, with a positive Eu anomaly (Fig. 26e).

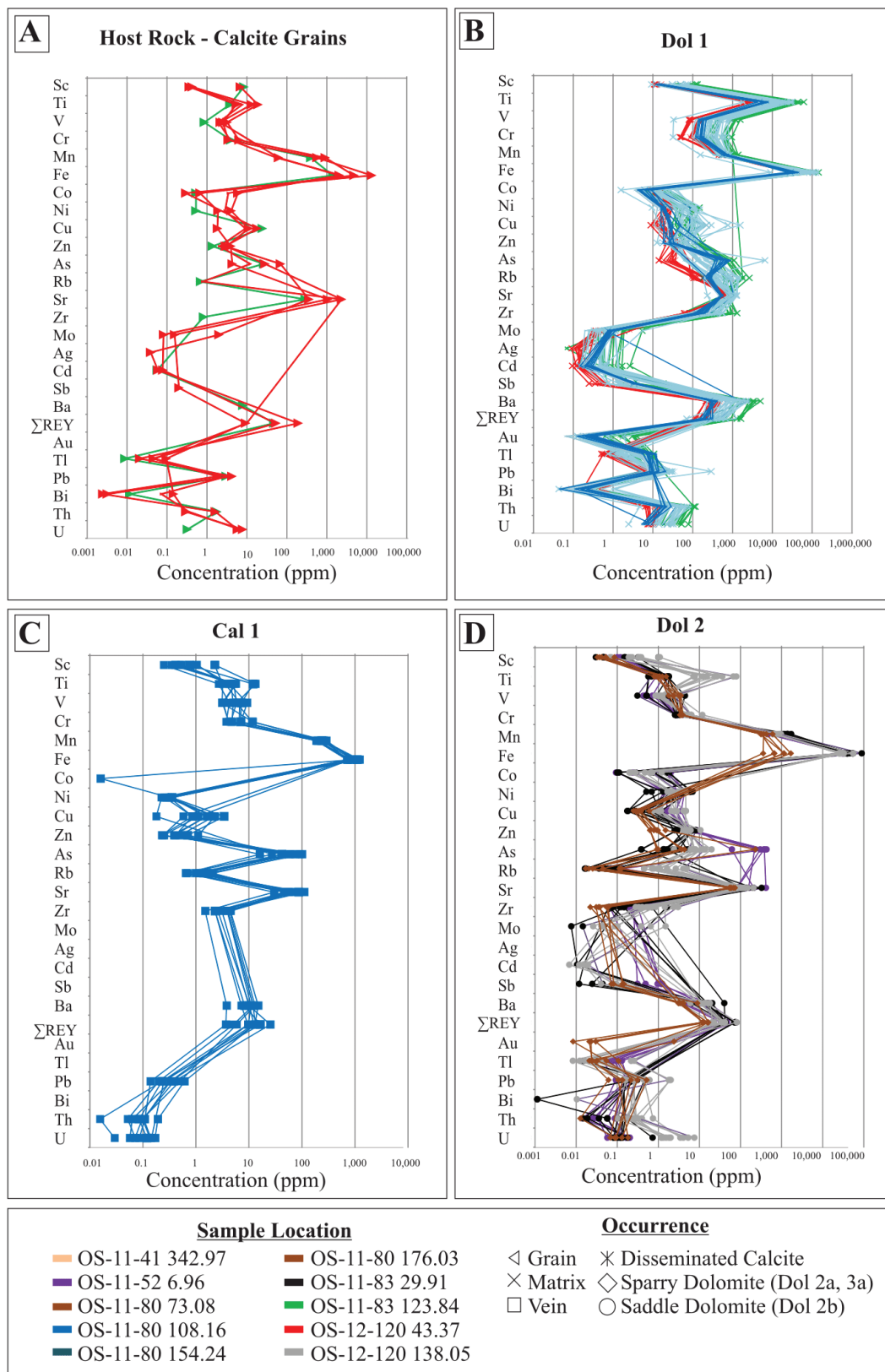


Fig. 24. Concentrations of various elements in carbonates. Each line represents an individual analysis (an ablation crater). A) Host rock. B) Dolomite 1. C) Calcite 1. D) Dolomite 2.

Two samples with calcite 3 veins were analyzed (21 data points total). The minor element and trace element geochemistry of calcite 3 is characterized by 100.70 to 427.00 ppm Mn, 156.20 to 2,206.00 ppm Fe, 87.00 to 4700.00 ppm Sr, 3.79 to 24.40 ppm Ba, and 0.66 to 72.00 ppm As. Overall, calcite 3 has similar trace element and REY concentrations to calcite 2 (Table 1; Fig. 25b). Calcite 3 also has a similar REY pattern to calcite 2, with LREE enrichment, HREE depletion, and a positive Eu anomaly (Fig. 26f). There is a negative correlation between Sr and Mn (Fig. 27f).

Ore Stage (Stage IV)

Two samples containing dolomite 3a were analyzed (25 data points total; Table 1; Fig. 25c). Dolomite 3a has 104.50 to 2,215.00 ppm Mn, 1,541.00 to 22,800.00 ppm Fe, 43.91 to 139.60 ppm Sr, 3.19 to 30.50 ppm Ba, and 2.50 to 670.00 ppm As. Dolomite 3a has similar base metal and REY concentrations to dolomite 2, but much less than dolomite 1 (Table 1; Fig. 25c). There is a relatively flat REY pattern, with a slight enrichment in HREE and a positive Y anomaly (Fig. 26g). There is a positive correlation between Sr and Ba (Fig. 27g).

Post-Ore Stage (Stage V)

Veinlets of calcite 4 were analyzed in two samples, OS-11-80 and OS-12-120. A total of 16 data points were analyzed. Calcite 4 has 139.50 to 3,740.00 ppm Mn, 39.05 to 760.00 ppm Fe, 23.56 to 212.00 ppm Sr, 0.37 to 7.04 ppm Ba, and 0.27 to 610.00 ppm As (Fig. 23f; 25d; Table 1). The areas with brighter CL tend to have higher Mn concentrations. Calcite 4 has low concentrations of base metals and REY. The REY pattern of calcite 4 is characterized by relative depletion in LREE, enrichment in HREE, and a positive Eu anomaly (Fig. 26h). There is a weak positive correlation between Ba and Mn (Fig. 27h).

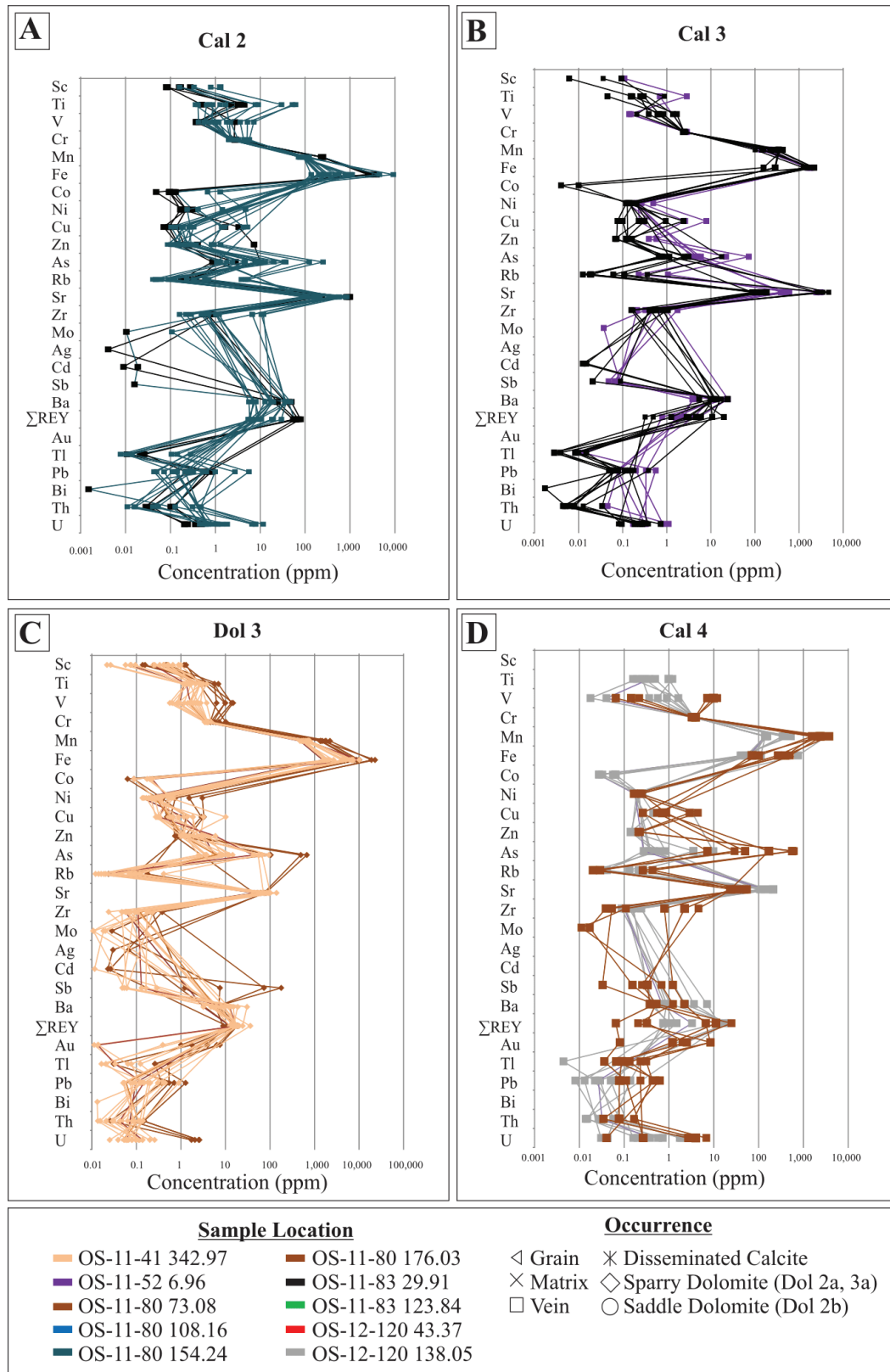


Figure 25. Concentrations of various elements in carbonates. Each line represents an individual analysis (a single ablation). A) Calcite 2. B) Calcite 3. C) Dolomite 3. D) Calcite 4.

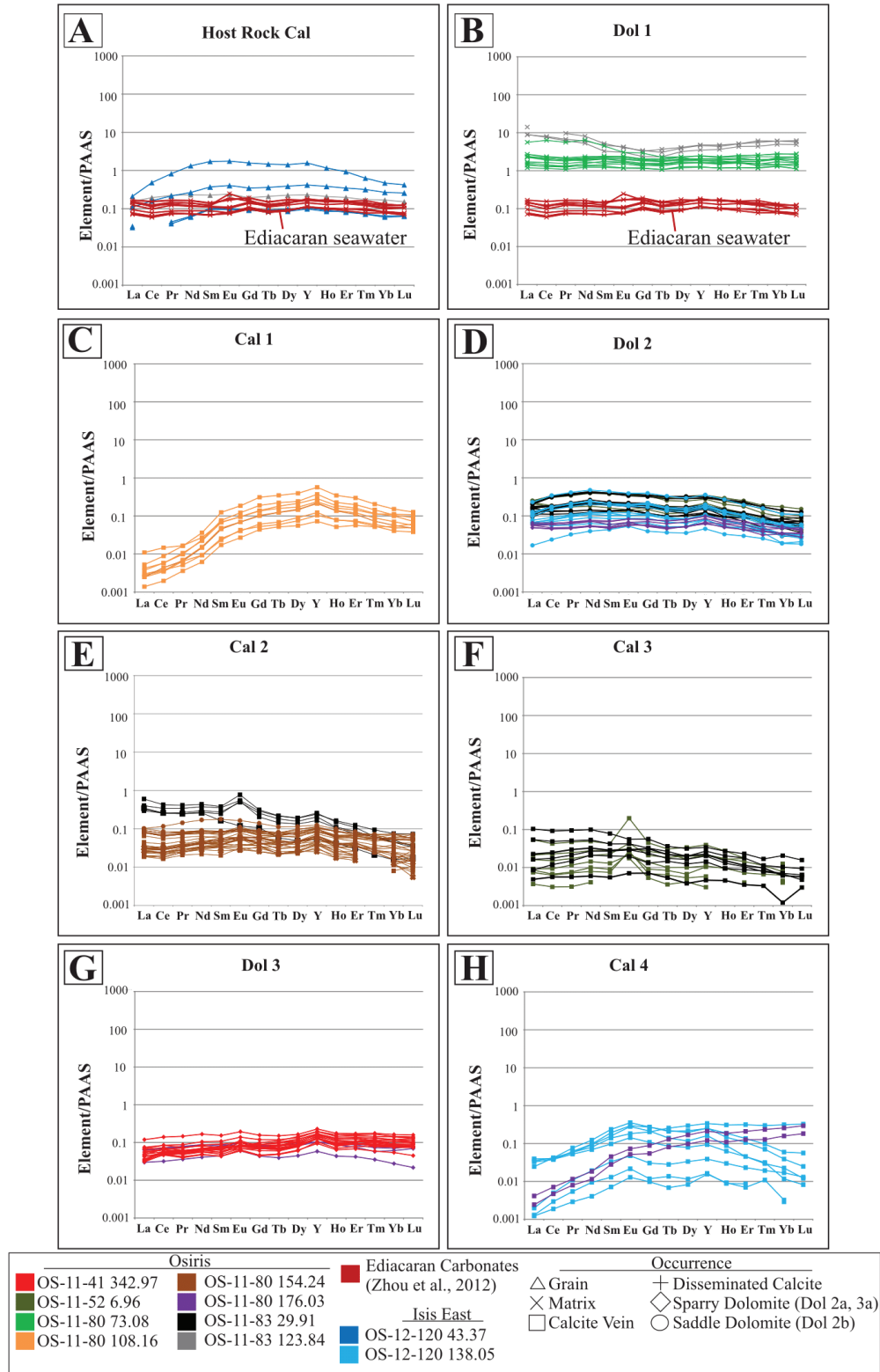


Figure 26 (above). REY concentrations of host rocks and paragenetic phases. Data are normalized to PAAS data from Pourmand et al. (2012). Each line represents an individual ablation. The Ediacaran seawater data in A) and B) are from Shuram excursion-age carbonates from Zhou et al. (2012). A) Calcite in host limestone. B) Dolomite 1. C) Calcite 1. D) Dolomite 2. E) Calcite 2. F) Calcite 3. G) Dolomite 3. H) Calcite 4.

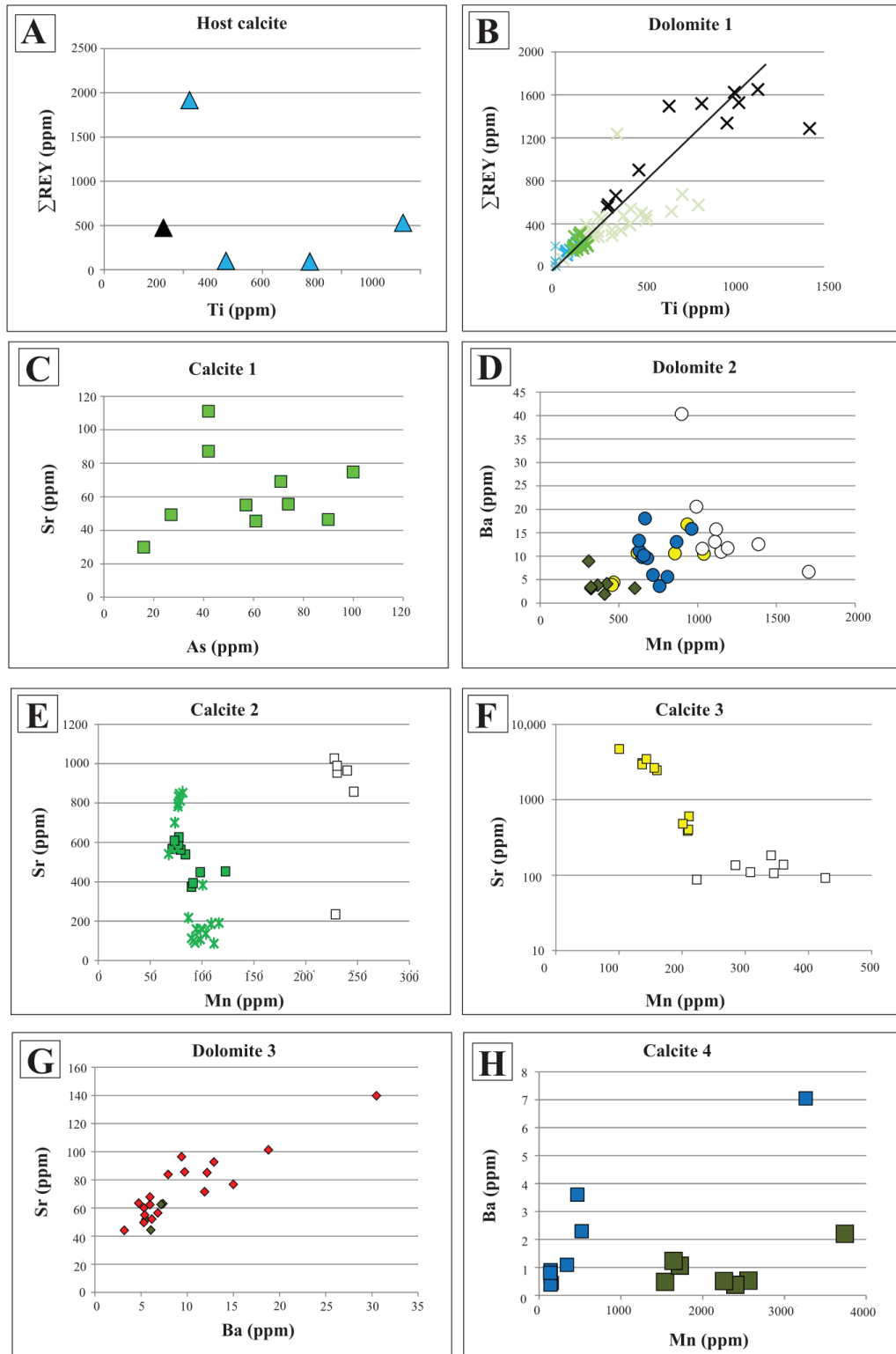
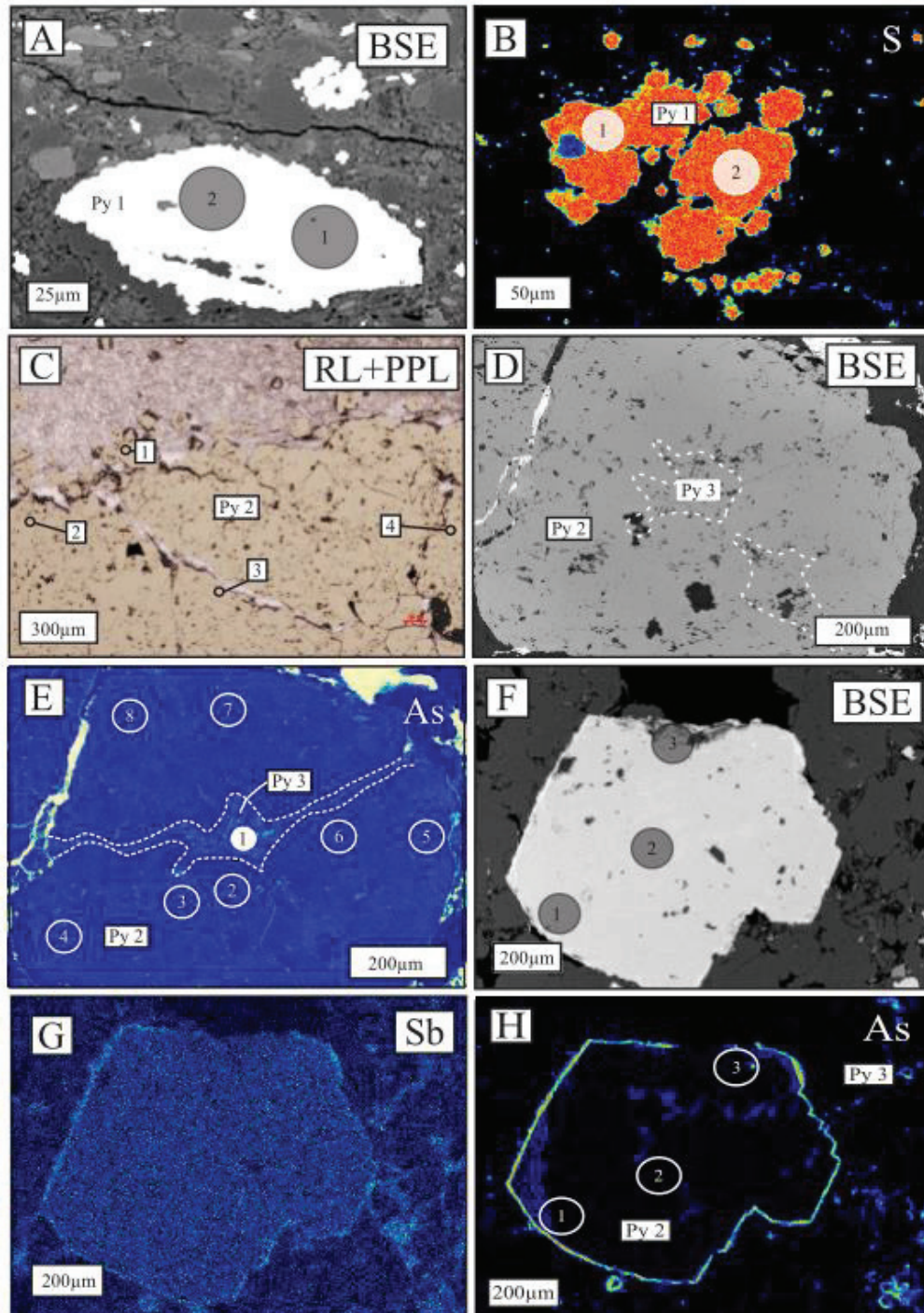


Figure 27. Geochemical plots of LA-ICP-MS data from host rock and different paragenetic phases of the Nadaleen carbonates. A) ΣREY vs. Ti for calcite of the host limestone. B) ΣREE vs. Ti for dolomite 1 with line of best fit. C) Sr vs. As in calcite 1. D) Ba vs. Mn in dolomite 2. E) Sr vs. Mn in calcite 2. F) Sr vs. Mn in calcite 3. G) Sr vs. Ba in dolomite 3. H) Ba vs. Mn in calcite 4.

Pyrite LA-ICP-MS

Pyrite 1, 2, and 3 were analyzed by LA-ICP-MS. Figure 28 shows locations of ablation craters with the corresponding data table. The most abundant and commonly detected trace elements in pyrite are As, Sb, Ni, Cu, and Zn. Table 2 presents the minimum, mean, and maximum concentrations of the rest of the elements for each phase of pyrite. Figure 29 shows plots of selected elements in the different paragenetic phases.



Spot	Phase	As	Sb	Au	Ni	Cu	Zn
A1	Py 1	14600.00	2050.00	0.61	420.00	3700.00	67.70
A2	Py 1	2230.00	16.10	1.00	940.00	2290.00	109.90
B1	Py 1	3230.00	9.20	1.27	1170.00	142.00	85.00
B2	Py 1	2350.00	7.10	0.89	1210.00	177.00	31.70
C1	Py 2	7300.00	17.30	0.02	310.00	53.00	2.10
C2	Py 2	47.00	3.54	0.05	18.60	2.50	1.17
C3	Py 2	49.00	4.59	0.07	20.10	1.33	0.79
C4	Py 2	134.00	5.02	0.02	18.10	3.10	1.59
D-E1	Py 3	4600.00	20.50	3.07	441.00	109.00	5.07
D-E2	Py 2	1681.00	8.33	0.03	227.00	25.30	7.01
D-E3	Py 2	2552.00	12.16	0.08	376.60	17.50	6.95
D-E4	Py 2	2530.00	27.42	0.28	828.00	1.23	6.86
D-E5	Py 2	3026.00	36.70	0.39	1465.00	4.69	6.48
D-E6	Py 2	1970.00	8.97	0.03	200.10	33.10	7.27
D-E7	Py 2	2250.00	12.40	0.77	225.30	4.21	6.01
D-E8	Py 2	3820.00	7.52	0.09	88.10	14.00	4.64
F-G-H1	Py 2	255,000.00	44.00	0.80	460.00	140.00	130.00
F-G-H2	Py 2	220,000.00	21.00	-	1900.00	136.00	120.00
F-G-H3	Py 3	650,000.00	200.00	15.00	1920.00	960.00	320.00

Figure 28. Laser ablation craters in pyrite and corresponding LA-ICP-MS data table. Values in ppm. A dash denotes data which were below detection limit. A) OS-11-80 114.54m. BSE image of a grain of pyrite 1. B) OS-11-80 114.54m. Sulfur map of several grains of pyrite 1. C) OS-11-52 219.31. RL + PPL image of a cluster of grains of pyrite 2. D) OS-11-120 116.80m. BSE image of a grain of pyrite 2 with small zones of pyrite 3. E) OS-11-120 116.80m. Arsenic map of the same grain shown in “E”. F) OS-11-52 112.38m. BSE image of a grain of pyrite 2 with a fracture. G) OS-11-52 112.38m. Antimony map of the same grain shown in “F” H) OS-11-52 112.38m. Arsenic map of the same grain shown in “F” showing a rim of arsenian pyrite.

Near-Surface Diagenesis Stage (Stage I)

Pyrite 1 grains were analyzed in two different thin sections from the same drill hole (OS-11-80). This generation of pyrite has 800.00 to 146,000 ppm As, Sb ranging from B.D. to 4,200.00 ppm, 420.00 to 3390.00 ppm Ni, Cu ranging from B.D. to 3,700 ppm, Zn ranging from B.D. to 1,210, and Au ranging from B.D. to 1.00 ppm. There is a lot of variation from grain to grain, and there is also a lot of variation within individual grains (Fig. 28a, 28b). There are certain elements which commonly occur together, i.e. V, Cr, Mn, Co, Ni, Pb, and Pb. In samples with low concentrations of these elements, Cu, Sb and As are commonly abundant. There is a weak positive correlation between Co and Ni (Fig. 29b).

Table 2. Selected LA-ICP-MS data for sulfides. Values are in ppm. B.D. = Below detection limit.

	Py 1 (n = 17)	Py 2 (n = 45)	Py 3 (n = 16)		Py 1 (n = 17)	Py 2 (n = 45)	Py 3 (n = 16)		
V	(min)	B.D.	B.D.	0.34	Ag	(min)	B.D.	B.D.	0.33
	(mean)	457.02	0.78	68.90		(mean)	5.34	0.72	13.57
	(max)	1810.00	5.40	500.00		(max)	12.00	4.49	74.00
Cr	(min)	2.30	B.D.	0.91	Cd	(min)	B.D.	B.D.	B.D.
	(mean)	204.97	54.37	438.13		(mean)	21.01	0.30	10.32
	(max)	620.00	1100.00	2400.00		(max)	150.00	1.60	53.000
Mn	(min)	19.00	B.D.	4.10	Sb	(min)	B.D.	B.D.	6.70
	(mean)	14431.62	13.83	1546.84		(mean)	13.70	8.06	405.41
	(max)	50500.00	201.00	11600.00		(max)	42.00	36.7	4000.00
Co	(min)	34.80	B.D.	4.00	Au	(min)	B.D.	B.D.	B.D.
	(mean)	504.87	29.90	201.71		(mean)	0.65	0.17	23.54
	(max)	1320.00	202.40	550.00		(max)	0.89	0.77	203.00
Ni	(min)	420.000	B.D.	200.00	Hg	(min)	B.D.	B.D.	6.10
	(mean)	1413.00	286.82	1271.06		(mean)	25.01	2.99	576.03
	(max)	3390.00	2290.00	2870.00		(max)	140.00	19.00	5800.00
Cu	(min)	B.D.	B.D.	27.00	Tl	(min)	B.D.	0.42	4.61
	(mean)	706.50	60.90	712.00		(mean)	7.24	14.35	695.77
	(max)	3700.00	560.00	3800.00		(max)	21.00	105.00	6600.00
Zn	(min)	B.D.	B.D.	5.07	Pb	(min)	36.00	0.038	22.00
	(mean)	409.77	11.36	178.28		(mean)	196.56	497.00	2074.78
	(max)	600.00	102.00	1300.00		(max)	500.00	4310.00	7600.00
Mo	(min)	B.D.	B.D.	9.00	Bi	(min)	B.D.	B.D.	0.05
	(mean)	119.55	76.57	151.10		(mean)	6.74	0.46	1.86
	(max)	232.00	444.00	280.00		(max)	16.00	3.8	6.80

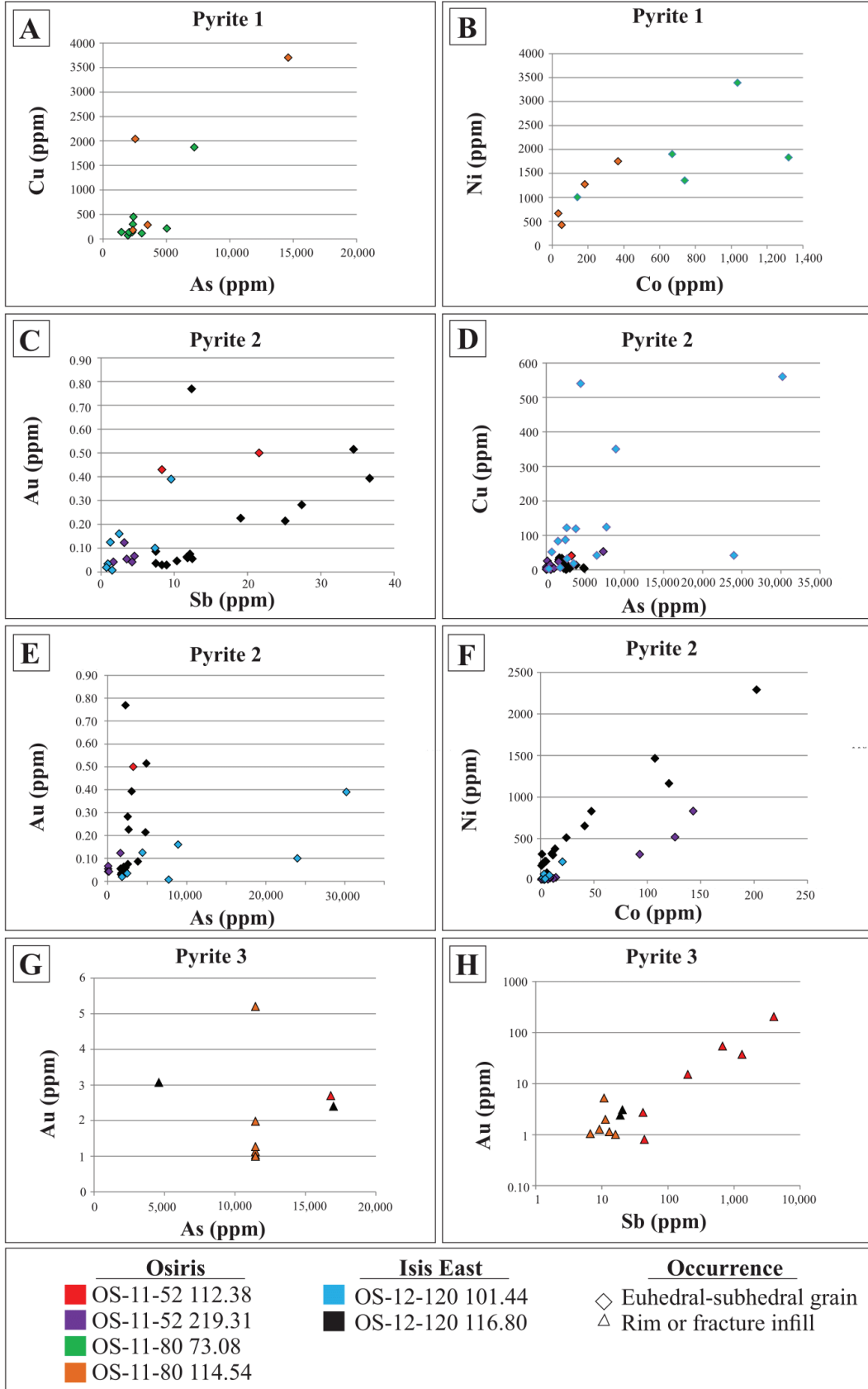


Figure 29 (above). Geochemical plots of LA-ICP-MS data from different generations of pyrite. A) Cu vs. As in pyrite 1. B) Ni vs. Co in pyrite 1. C) Au vs. Sb in pyrite 2. D) Cu vs. As in pyrite 2. E) Au vs. As in pyrite 2. F) Ni vs. Co in pyrite 2. G) Au vs. Zn in pyrite 3. H) Au vs. Sb in pyrite 2.

Base Metal Mineralization Stage (Stage II)

Pyrite 2 was analyzed in four different thin sections. This generation of pyrite has As ranging from B.D. to 3,000 ppm, Sb ranging from B.D. to 36.70 ppm, Ni ranging from B.D. to 2,290 ppm, Cu ranging from 0.53 to 560.00 ppm, Zn ranging from B.D. to 102.00 ppm, and Au from B.D. to 0.77 ppm. This generation of pyrite is depleted in elements such as V, Cr, Mn, Co, Cu, Zn, Pb, and Pb compared to pyrite 1 (Table 2). There are certain elements which commonly occur together, i.e. V + Cr + Mn + Ni, Cu + As, and Sb + Tl + Pb. There is a weak positive correlation between Ni and Co (Fig. 29f).

Ore Stage (Stage IV)

Rims and fracture-fills of pyrite 3 were analyzed in three different thin sections from drill hole intervals with high gold grade. This generation of pyrite has 2230.00 to 17,000 ppm As, 6.70 to 4,000.00 ppm Sb, 200.00 to 2,870.00 ppm Ni, 27.00 to 2,800.00 ppm Cu, 5.07 to 1,300.00 ppm Zn, and Au which ranges from B.D. to 203.00 ppm. In pyrite 3, there are a number of elements which commonly occur together: V, Cr, Mn, Sb, Hg, Pb, Bi, and Au. There is a positive correlation between Au and Sb (Fig. 29h).

2.5.5 C and O Isotopes – Bulk Analyses

30 carbonate samples were analyzed for bulk carbon and oxygen isotopic composition; this data is presented in Table 3. Samples were taken from different depths of different drill holes to examine spatial isotopic variation within paragenetic stages. Two or three different veins from a single sample were analyzed to test smaller-scale isotopic variation. Figure 30 presents a plot of $\delta^{18}\text{O}$ vs. $\delta^{13}\text{C}$ values. Since the Gametrail Formation of the Eastern Nadaleen Trend includes the Shuram $\delta^{13}\text{C}$ excursion, the data are compared to some other Shuram excursion-age carbonates globally.

Host Rocks and Near-Surface Diagenesis Stage (Stage I)

Only one sample each of the host rock and dolostone (dolomite 1) were analyzed due to difficulty in finding enough sample of unaltered limestones and dolostones. The host limestone sample was taken from Osiris hole OS-11-61, from a sample which consists mostly of micrite. This sample has a $\delta^{18}\text{O}$ value of 21.2‰ and a $\delta^{13}\text{C}$ value of -7.8‰, which is in the range of Shuram excursion-age seawater carbonates (Fig. 30).

Table 2. $\delta^{18}\text{O}$ and $\delta^{13}\text{C}$ values for carbonates.

Area	Hole: depth	Paragenetic phase	$\delta^{18}\text{O}_{\text{-VSMOW}}(\text{‰})$	$\delta^{13}\text{C}_{\text{-VPDB}}(\text{‰})$
Osiris	OS-11-61: 29.30	Host limestone	21.2	-7.8
Osiris	OS-11-83: 121.52	Dol 1	32.4	1.7
Osiris	OS-11-41: 341.42A	Dol 2a	21.7	-1.5
Osiris	OS-11-41: 341.42B	Dol 2a	22.1	-1.5
Osiris	OS-11-41: 341.42C	Dol 2a	22.9	-1.3
Osiris	OS-11-52: 6.96A	Dol 2b	21.4	-5.8
Osiris	OS-11-52: 6.96B	Dol 2b	21.3	-5.7
Osiris	OS-11-52: 6.96C	Dol 2b	20.8	-5.1
Osiris	OS-11-61: 84.15A	Dol 2b	21.5	-9.3
Osiris	OS-11-61: 84.15B	Dol 2b	21.3	-9.4
Osiris	OS-11-61: 84.15C	Dol 2b	21.7	-9.1
Isis east	OS-12-120: 14.07B-1	Dol 2b	22.0	3.0
Isis east	OS-12-120: 14.07B-2	Dol 2b	21.5	2.5
Isis east	OS-12-120: 138.33A	Dol 2b	21.6	-4.9
Isis east	OS-12-120: 138.33B	Dol 2b	21.7	-5.0
Isis east	OS-12-120: 138.33C	Dol 2b	21.3	-4.9
Isis east	OS-12-120: 51.16	Cal 2	17.3	-3.1
Osiris	OS-11-80: 154.24	Cal 2	21.4	-4.6
Osiris	OS-11-41: 267.58A	Cal 3	21.0	-4.5
Osiris	OS-11-41: 267.58B	Cal 3	24.2	-2.4
Osiris	OS-11-41: 267.58C	Cal 3	23.5	-2.7
Osiris	OS-11-61: 92.45	Cal 3	20.8	-6.7
Osiris	OS-11-80: 151.32A	Cal 3	21.1	-1.9
Osiris	OS-11-80: 151.32B	Cal 3	22.1	-2.1
Osiris	OS-11-80: 151.32	Cal 3	21.1	-1.9
Osiris	OS-11-80: 162.22	Cal 3	16.3	-1.0
Osiris	OS-11-41: 342.97	Dol 3a	22.7	-1.9
Isis east	OS-12-120: 138.33D	Dol 3a	22.0	-6.5
Isis east	OS-12-120: 138.33E	Dol 3a	21.6	-6.0
Isis east	OS-12-120: 138.33F	Dol 3a	22.0	-6.3
Osiris	OS-11-80: 45.09A	Cal 4	13.9	-0.7
Osiris	OS-11-80: 45.09B	Cal 4	15.2	-0.7
Osiris	OS-11-80: 45.09C	Cal 4	15.1	-0.6

The stage I dolostone sample was taken from Osiris hole OS-11-83 in a sample composed of mostly dolomicrite. This sample is highly enriched in ^{18}O ($\delta^{18}\text{O}$ value of 32.4‰) and ^{13}C ($\delta^{13}\text{C}$ value of 1.7‰) and lies outside of the range of Ediacaran seawater carbonates.

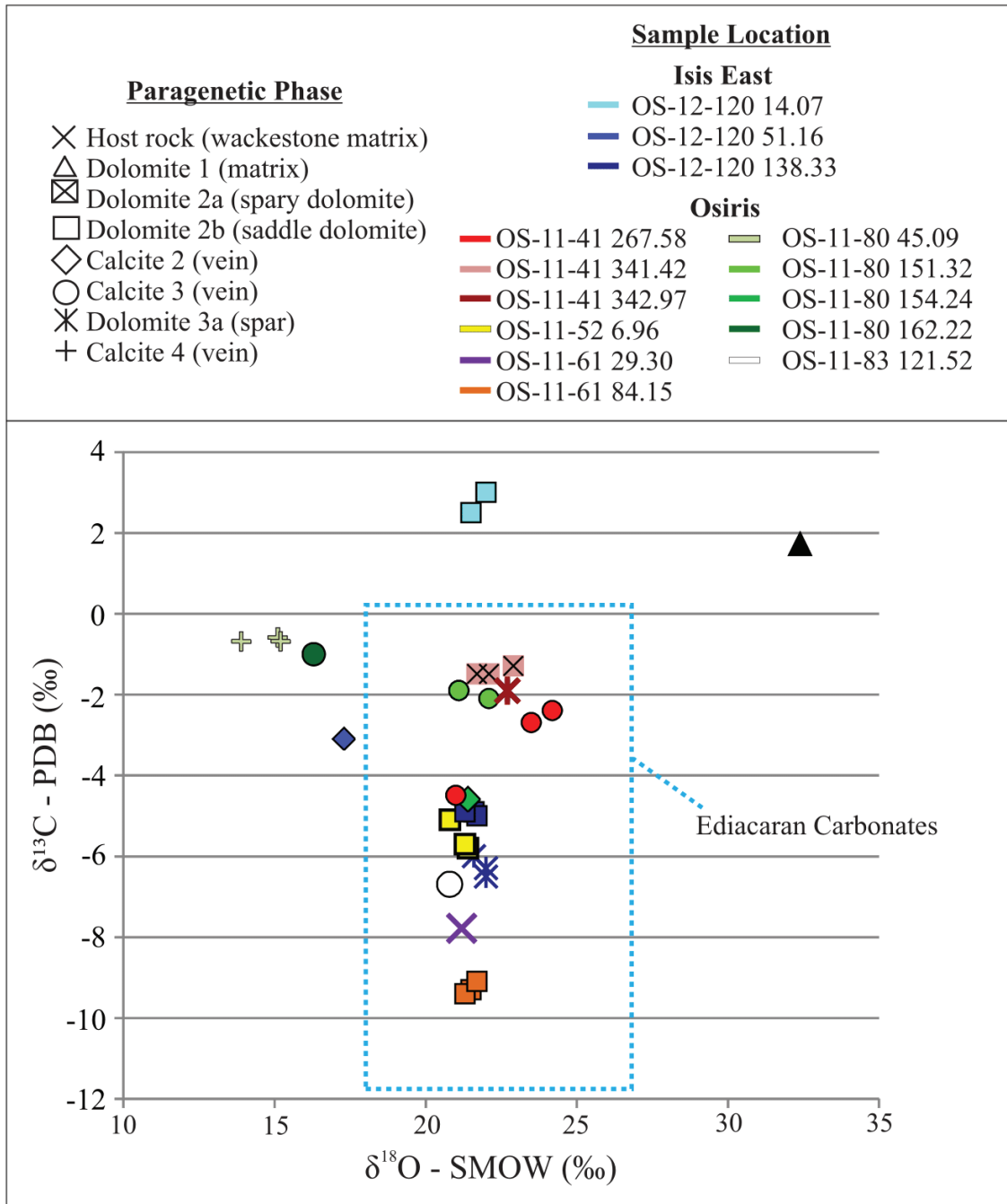


Figure 30. Plot of $\delta^{18}\text{O}$ vs. $\delta^{13}\text{C}$ values in carbonates from Osiris and Isis East. Range of Ediacaran carbonate data are from seawater Shuram excursion-age carbonates from Calver (2000); Jacobsen and Kaufman (1999); and MacDonald et al. (2013).

Base Metal Mineralization Stage (Stage II)

Dolomite 2 samples were examined from three drill holes in Osiris and one in Isis east. The dolomites of Stage II have fairly uniform oxygen isotopic composition ($\delta^{18}\text{O}$ values from 20.8 to 22.9 ‰) but have a large range in carbon isotopic values (from -9.4 to 3.0 ‰). The samples with the highest $\delta^{13}\text{C}$ values are the ones that are proximal to faults and decarbonated zones, and the samples with low $\delta^{13}\text{C}$ are from veins in unaltered host rock.

Intermediate Diagenesis Stage (Stage III)

Two samples of calcite 2 were analyzed from veins in OS-11-80 and OS-12-120. There is a moderate amount of variation between these two samples ($\delta^{13}\text{C}$ values of -3.1 to -4.6 ‰ and $\delta^{18}\text{O}$ values of 17.3 to 21.4 ‰; Fig. 30). The sample with a lower $\delta^{18}\text{O}$ value is a vein which has crosscut dolomite 1, whereas the sample with higher the highest $\delta^{18}\text{O}$ value is a vein in which calcite also occurs as a cement disseminated throughout the host rock. Eight samples of calcite 3 were collected from calcite veins in various locations throughout Osiris. There is a large amount of variation in oxygen isotopic composition and also in carbon, with $\delta^{18}\text{O}$ values ranging from 16.3 to 24.2 ‰ and $\delta^{13}\text{C}$ values ranging from -6.7 to -1.0 ‰. For calcite 3, the samples with low $\delta^{18}\text{O}$ values are calcite veins which have crosscut dolomite 2. The samples with high $\delta^{18}\text{O}$ values are calcite veins which have crosscut dolomite and calcite also occurs disseminated throughout the host rock (as is the case with calcite 2).

Ore Stage (Stage IV)

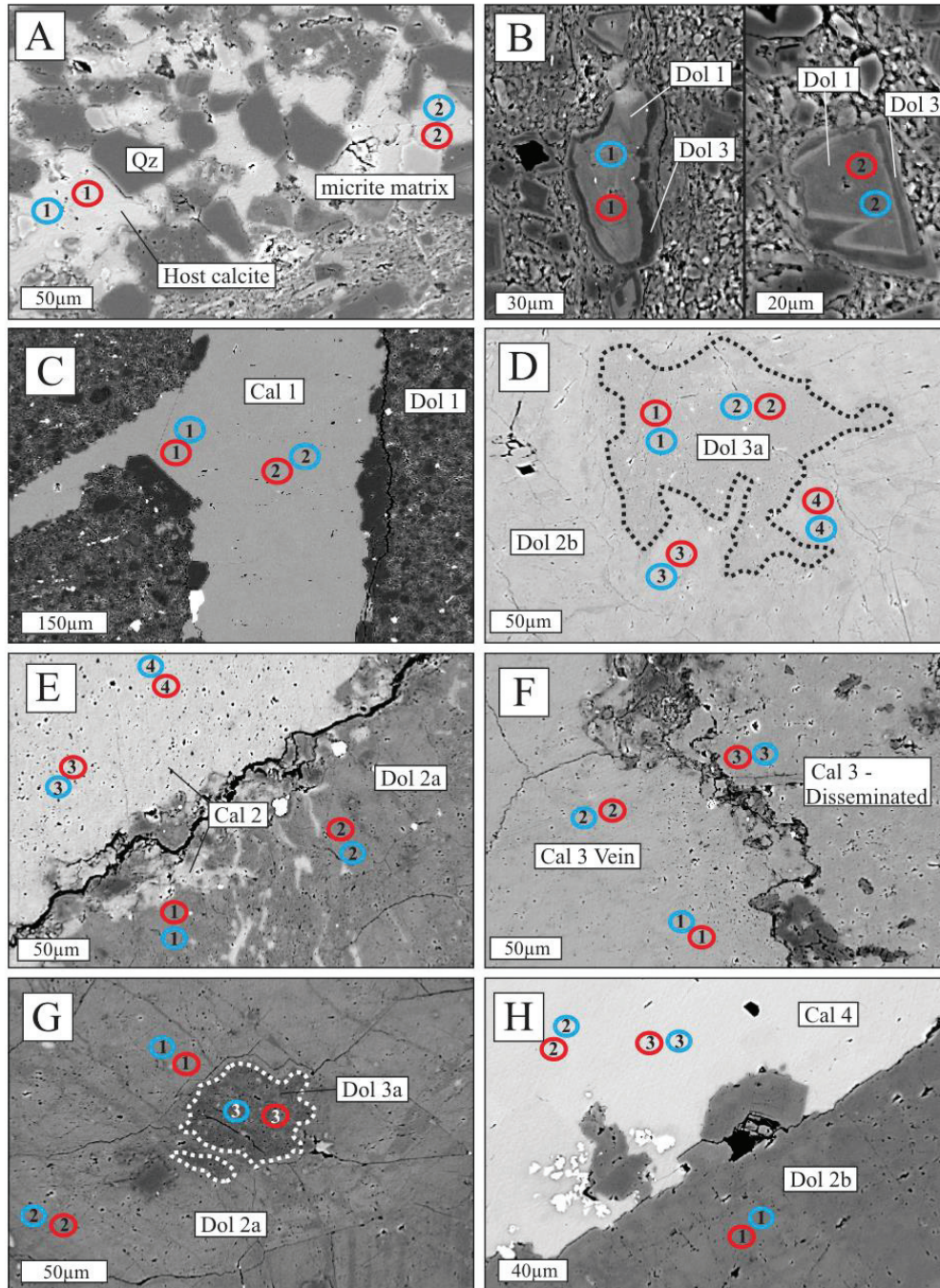
Dolomite 3a from two different samples was analyzed; one in Osiris and one in Isis east. The Isis East sample (138.33m) was analyzed in three different veins to test for small-scale variation. The Osiris sample has a $\delta^{18}\text{O}$ value of 22.7 ‰ and a $\delta^{13}\text{C}$ value of -1.9 ‰. The three veins in the same Isis east sample have a narrow range of values, with $\delta^{18}\text{O}$ values ranging from 22.0 to 21.6 ‰ and $\delta^{13}\text{C}$ values ranging from -6.0 to -6.5 ‰.

Post-Ore Stage (Stage V)

Three different calcite 4 veins from the same sample were analyzed for isotopic composition. The veins analyzed were a few centimeters wide. These post-ore stage calcite veins are depleted in ^{18}O , with $\delta^{18}\text{O}$ values of 13.9 to 15.1‰. These vein calcites have higher ^{13}C content than the other carbonate phases, with $\delta^{13}\text{C}$ values of -0.6 to -0.7‰. The veins in this sample are slightly heterogeneous (they display zoning in their CL signature).

2.5.6 C and O Isotopes - Secondary Ion Mass Spectrometry

The host rocks and all carbonate phases were analyzed in situ by SIMS to accurately examine small-scale isotopic variation in light of the sample heterogeneity. All SIMS data are presented in Appendix F. Figure 31 presents a selection of representative SIMS data from the host rocks as well as all of the carbonate phases. Figure 32 presents geochemical plots of SIMS data. EMPA data was collected adjacent to nearly all SIMS analytical plots; these data are shown in Figure 33.



Spot	Phase	$\delta^{13}\text{C}$ (PDB)	$\delta^{18}\text{O}$ (VSMOW)	Spot	Phase	$\delta^{13}\text{C}$ (PDB)	$\delta^{18}\text{O}$ (VSMOW)
A1	Host lime	-12.12	20.54	F1	Cal 3	-8.23	20.33
A2	Host lime	-12.32	20.60	F2	Cal 3	-7.27	20.32
B1	Dol 1	-5.38	27.81	F3	Cal 3	-8.04	18.73
B2	Dol 1	-4.90	30.91	G1	Dol 2	-7.10	25.38
C1	Cal 1	-0.02	10.18	G2	Dol 2	-8.15	25.07
C2	Cal 1	-1.11	10.21	G3	Dol 3	-8.85	20.19
D1	Dol 3	-3.84	19.95	H1	Dol 2	-5.48	19.61
D2	Dol 3	-3.92	20.10	H2	Cal 4	-5.00	17.37
D3	Dol 2	-7.44	23.44	H3	Cal 4	-6.21	19.33
D4	Dol 2	-6.29	23.35				
E1	Dol 2	-7.61	27.19				
E2	Dol 2	-7.64	27.63				
E3	Cal 2	-4.94	19.30				
E4	Cal 2	-4.08	20.92				

Figure 31. BSE images of locations of representative SIMS analyses of carbonates with associated data table. Most analytical spots are enlarged for ease of reference; actual size is 20 μm . Red spots are locations of $\delta^{13}\text{C}$ values and blue spots are locations of $\delta^{18}\text{O}$ values. Values are in ‰. A) OS-11-80 73.08m. Calcite grains in wackestone. B) OS-11-83 123.84m. Coated grains of dolomite 1. C) OS-11-80 108.16m. Vein of calcite 1 crosscutting dolomite 1. D) OS-11-41 342.97m. Dolomite 2 which is partially replaced by dolomite 3. E) OS-11-83 29.91m. Calcite 2 vein in contact with dolomite 2. Note that calcite 2 has also partially replaced dolomite 2. F) OS-11-52 6.96m. Calcite 3. On the right side of the stylolite is fine-grained calcite 3 and on the left side is a more coarse-grained calcite 3 vein. G) OS-12-120 138.05m. Dolomite 2 which is partially replaced by veins and patches of dolomite 3. H) OS-11-80 176.03m. Dolomite 2 in contact with a vein of calcite 4.

Host Rocks and Near-Surface Diagenesis Stage (Stage I)

Grains of calcite in wackestone of the host rock were analyzed by SIMS in three samples: OS-11-80 73.08, OS-11-83 123.84, and OS-12-120. The $\delta^{18}\text{O}$ values of calcite grains in the host rock range from 19.57 to 21.91 ‰ and $\delta^{13}\text{C}$ values range from -12.32 to -3.53 ‰. The samples with the lowest $\delta^{13}\text{C}$ values (-12.32 and -12.12 ‰) are from a laminated wackestone (Fig. 31a), whereas the samples with higher $\delta^{13}\text{C}$ values are from wackestone clasts in diamictite. The data fall in the range of Ediacaran seawater from Shuram excursion-age carbonates (Fig. 32). The $\delta^{18}\text{O}$ value generally increases with $\text{Ca}/(\text{Mg}+\text{Mn}+\text{Fe})$ (Fig. 33a).

Several grains of dolomite 1 were analyzed in OS-11-83 123.84 and OS-11-80 73.08; two of the analyzed grains are shown in Figure 31b. The $\delta^{18}\text{O}$ values of dolomite 1 range from 20.88 to 34.28 ‰ and the $\delta^{13}\text{C}$ values range from -8.66 to +3.15 ‰. Sample OS-11-83 123.84 was analyzed for both isotopes but OS-11-80 73.08 was only analyzed for carbon;

for this reason OS-11-80 73.08 is not plotted in Figure 32b. OS-11-80 73.08 has $\delta^{13}\text{C}$ values of -4.09, -8.16, and -8.66 ‰ (see Appendix F). There is a great deal of small-scale variation in dolomite 1, as dolomite grains separated by 100 μm can differ in $\delta^{18}\text{O}$ value by 3 ‰ and $\delta^{13}\text{C}$ value by 4 ‰. The data fall in the range of Ediacaran seawater in Figure 32. The $\delta^{18}\text{O}$ value generally increases with $\text{Ca}/(\text{Mg}+\text{Mn}+\text{Fe})$ (Fig. 33a).

Base Metal Mineralization Stage (Stage II)

Calcite 1 veins were analyzed in sample OS-11-80 108.16 in a vein that crosscuts dolomite (Fig. 31c). The $\delta^{18}\text{O}$ values in calcite 1 range from 10.07 to 10.34 ‰ and the $\delta^{13}\text{C}$ values range from -1.11 to -0.02 ‰. The vein analyzed has a uniform CL signature, indicating that it is relatively homogeneous (Fig. 12a).

Dolomite 2 samples were examined from Osiris samples OS-11-41 342.97, OS-11-52 6.96, OS-11-80 176.03, OS-11-83 29.91, and Isis East hole sample OS-12-120 138.05. The $\delta^{18}\text{O}$ values in dolomite 2 range from 19.17 to 25.65 ‰ and the $\delta^{13}\text{C}$ values range from -9.43 to -0.72 ‰. There is a great deal of small-scale variation in $\delta^{13}\text{C}$ values, with spots a few hundred μm apart having differences of up to 4 ‰. Sparry dolomite (dolomite 2a) generally has higher $\delta^{18}\text{O}$ values than saddle dolomite (dolomite 2b; Fig. 31d). There is no strong correlation between $\delta^{18}\text{O}$ value and FeO content (Fig. 33d).

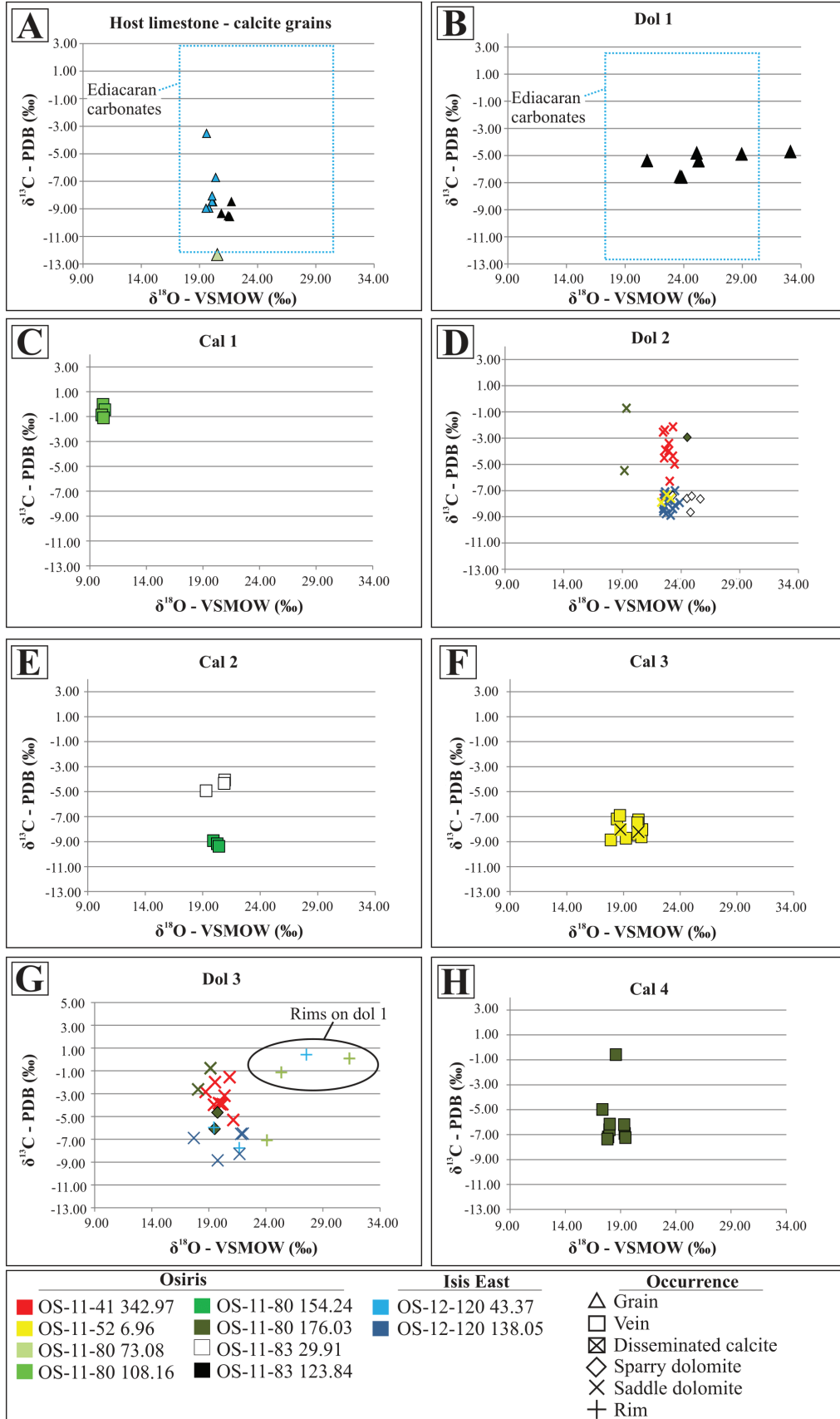


Figure 32 (above). Plots of $\delta^{18}\text{O}$ vs. $\delta^{13}\text{C}$ values from SIMS for host rocks and all paragenetic phases. Range of Ediacaran carbonate data are from Shuram Excursion-age seawater carbonates from Calver, (2000); Jacobsen and Kaufman, (1999); and MacDonald et al. (2013). A) Calcite grains from host rock with Ediacaran seawater isotopic composition. B) Dolomite 1. C) Calcite 1. D) Dolomite 2. E) Calcite 2. F) Calcite 3. G) Dolomite 3. H) Calcite 4.

Intermediate Diagenesis Stage (Stage III)

Several calcite 2 veins/veinlets from Osiris samples OS-11-80 154.24 and OS-11-83 29.91 were analyzed (Fig. 31e, 32e). The $\delta^{13}\text{C}$ values of calcite 2 range from -9.39 to -4.08 ‰ and the $\delta^{18}\text{O}$ values range from 19.30 to 20.92 ‰. The calcite veins with lower ^{13}C are relatively pure, with very few solid inclusions; the calcite veins with higher $\delta^{13}\text{C}$ are full of solid inclusions of an unknown phase, partially replacing the dolomite 2 that it crosscuts (Fig. 32e). The $\delta^{13}\text{C}$ values generally decrease with $\text{Ca}/(\text{Mg}+\text{Mn}+\text{Fe})$ (Fig. 33e).

Several calcite 3 veins/veinlets from Osiris sample OS-11-52 6.96 were analyzed. The $\delta^{13}\text{C}$ values in calcite 3 range from -8.74 to -6.91 ‰ and the $\delta^{18}\text{O}$ values range from 17.89 to 20.65 ‰. Besides occurring in veins, there is also disseminated calcite 3 (Fig. 31f). There are no major differences in isotopic composition between these two modes of occurrence (Fig. 32f). The $\delta^{13}\text{C}$ values generally increase with $\text{Ca}/(\text{Mg}+\text{Mn}+\text{Fe})$ (Fig. 33f).

Ore Stage (Stage IV)

Dolomite 3 occurs as sparry dolomite (Dol 3a; Fig. 31d, 31g) or as rims on pre-existing carbonates (Dol 3b; Fig. 31b). Dolomite 3 has $\delta^{13}\text{C}$ values ranging from -8.85 to +3.55 ‰ and $\delta^{18}\text{O}$ values ranging from 17.69 to 31.32 ‰. Overall, the highest $\delta^{13}\text{C}$ and $\delta^{18}\text{O}$ values are in dolomite 3b rims on dolomite 1 grains.

Post-Ore Stage (Stage V)

Calcite 4 veins from Osiris sample OS-11-80 176.03 were analyzed (Fig. 31h). Calcite 4 has $\delta^{13}\text{C}$ values ranging from -7.36 to +0.19 ‰ and $\delta^{18}\text{O}$ values ranging from 13.30 to 19.44 ‰. The areas with the highest $\delta^{13}\text{C}$ values and lowest $\delta^{18}\text{O}$ values are the areas where the calcite vein has tapered out.

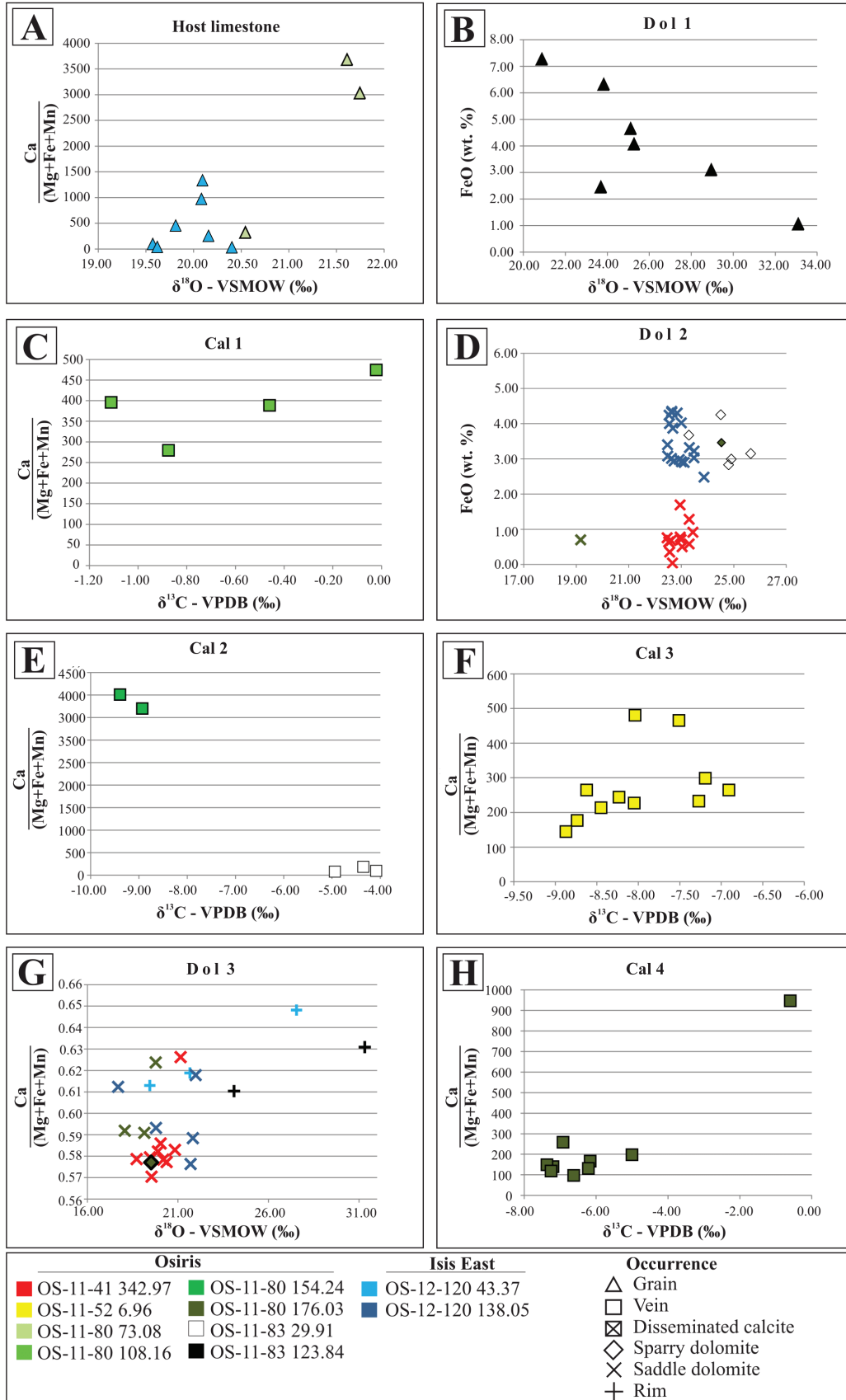


Figure 33 (above). Plots of SIMS data vs. EMPA data for host rocks and all paragenetic phases. Diamonds represent original SIMS data; “X”s represent Fe-corrected SIMS data in dolomite. Diamonds are color-coded to match their corresponding “X”. A) $\delta^{18}\text{O}$ values vs. $\text{Ca}/(\text{Mg}+\text{Mn}+\text{Fe})$ in host limestone. B) $\delta^{18}\text{O}$ values vs. FeO in Dolomite 1 with Neoproterozoic seawater isotopic composition. C) $\delta^{13}\text{C}$ values vs. $\text{Ca}/(\text{Mg}+\text{Mn}+\text{Fe})$ in calcite 1. D) $\delta^{18}\text{O}$ values vs. FeO in dolomite 2. E) $\delta^{13}\text{C}$ values vs. $\text{Ca}/(\text{Mg}+\text{Mn}+\text{Fe})$ in calcite 2. F) $\delta^{13}\text{C}$ values vs. $\text{Ca}/(\text{Mg}+\text{Mn}+\text{Fe})$ in calcite 3. G) $\delta^{18}\text{O}$ values vs. $\text{Ca}/(\text{Mg}+\text{Mn}+\text{Fe})$ in dolomite 3. H) $\delta^{13}\text{C}$ values vs. $\text{Ca}/(\text{Mg}+\text{Mn}+\text{Fe})$ in calcite 4.

2.5.7 Strontium isotopes

Host rocks and carbonates of Stages II, III, IV, and V were analyzed to determine their strontium isotopic composition. Samples from these paragenetic stages were examined in a variety of drill holes and depths. Stage I dolomite was not examined due to difficulty in finding unaltered samples. Isotopic data from these analyses are listed in Table 4.

Table 4. $^{87}\text{Sr}/^{86}\text{Sr}$ ratios for carbonates

Area	Hole: depth	Paragenetic phase, occurrence	$^{87}\text{Sr}/^{86}\text{Sr}$
Osiris	OS-11-61: 84.15	Host Rock, lime mudstone	0.709272
Osiris	OS-11-41: 67.75	Host Rock, lime mudstone	0.709000
Osiris	OS-11-80: 108.16	Cal 1, veinlet	0.716881
Isis east	OS-12-120: 51.16	Cal 1, veinlet	0.716776
Osiris	OS-11-41: 293.18	Dol 2a, sparry dolomite mosaic	0.711752
Osiris	OS-11-41: 341.42	Dol 2b, saddle dolomite mosaic	0.718077
Osiris	OS-11-61: 84.15	Dol 2a, sparry dolomite vein	0.713697
Osiris	OS-11-80: 210.57	Dol 2a, sparry dolomite mosaic	0.712544
Osiris	OS-11-83: 29.91D	Dol 2b, saddle dolomite vein	0.715096
Osiris	OS-11-83: 86.72	Dol 2b, saddle dolomite vein	0.714304
Isis east	OS-12-120: 101.44D	Dol 2b, saddle dolomite vein	0.715789
Osiris	OS-11-52: 6.96	Cal 2, vein	0.712538
Osiris	OS-11-61: 29.30	Cal 2, disseminated	0.711170
Osiris	OS-11-61: 92.45	Cal 2, vein	0.712093
Osiris	OS-11-80: 151.32	Cal 2, vein	0.721772
Osiris	OS-11-80: 154.24	Cal 2, disseminated	0.711975
Osiris	OS-11-83: 14.14	Cal 2, disseminated	0.711351
Osiris	OS-11-83: 29.91	Cal 2, vein	0.713423
Osiris	OS-11-41: 267.58	Cal 3, vein	0.718000
Osiris	OS-11-52: 6.96	Cal 3, vein	0.713354
Isis east	OS-12-120: 101.44	Dol 3a, partial replacement	0.714319
Isis east	OS-12-120: 106.14	Dol 3a, partial replacement	0.726592
Isis east	OS-12-120: 115.26	Dol 3a, partial replacement	0.713874
Isis east	OS-12-120: 138.33	Dol 3a, partial replacement	0.712827
Osiris	OS-11-41 319.68	Cal 4, vein	0.724579
Osiris	OS-11-80 45.09	Cal 4, vein	0.717939
Isis east	OS-12-120 138.05	Cal 4, vein	0.713710

Shuram excursion-age Ediacaran seawater Sr isotope ratios are also shown in Figure 34 for comparison and have a range in $^{87}\text{Sr}/^{86}\text{Sr}$ from 0.70859 to 0.70876 (Burns et al., 1994; Calver, 2000).

Host Rocks

Two samples of the host rock were analyzed, OS-11-61 84.15 and OS-11-41 67.75. They have $^{87}\text{Sr}/^{86}\text{Sr}$ ratios of 0.709272 and 0.709000, respectively, which are slightly higher than the Shuram-age seawater $^{87}\text{Sr}/^{86}\text{Sr}$ values (Burns et al., 1994; Calver, 2000).

Base Metal Mineralization Stage (Stage II)

Calcite 1 veins were examined from Osiris sample OS-11-80 108.16 and Isis East sample OS-12-120 51.16. They have very similar isotopic signatures (0.716881 and 0.716776, respectively). Seven samples of dolomite 2 were analyzed from different depths in the Osiris and Isis east drill holes; some of the analyses were from dolomite 2a and some from dolomite 2b. Strontium isotope compositions are quite variable in dolomite 2, with $^{87}\text{Sr}/^{86}\text{Sr}$ ratios ranging from 0.711752 to 0.718077. Saddle dolomite (dolomite 2b) generally has higher $^{87}\text{Sr}/^{86}\text{Sr}$ ratios than dolomite 2a (Fig. 34).

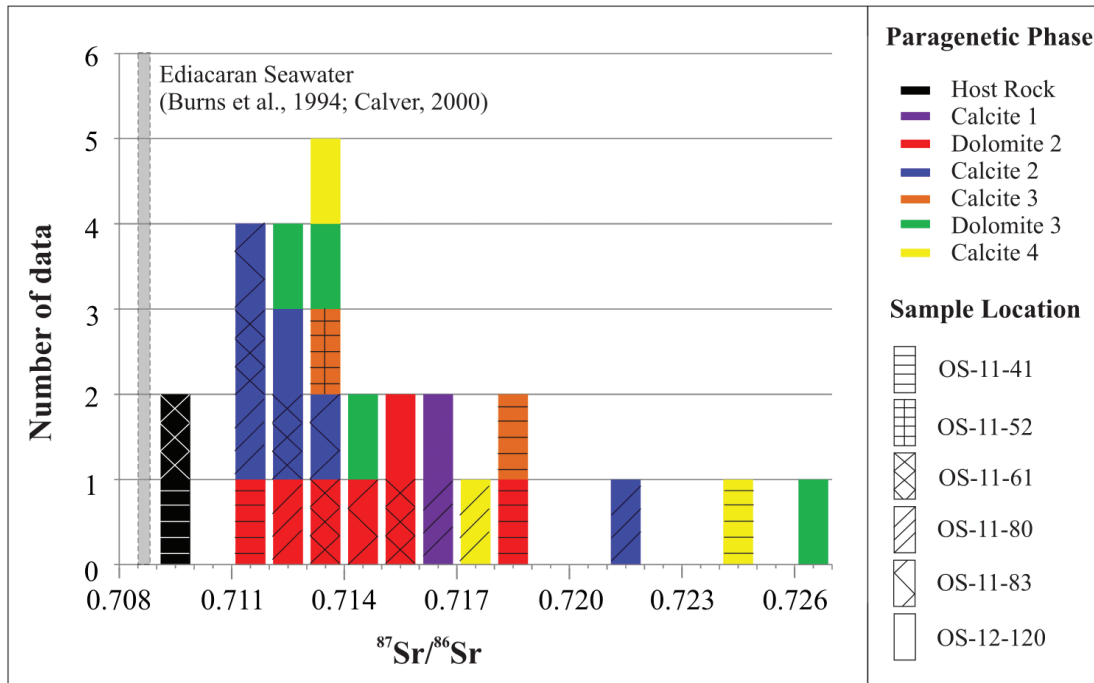


Figure 34. Plot of $^{87}\text{Sr}/^{86}\text{Sr}$ data vs. frequency. seawater $^{87}\text{Sr}/^{86}\text{Sr}$ values of marine limestone are from Burns et al. (1994) and Calver (2000).

Intermediate Diagenesis Stage (Stage III)

Seven calcite 2 veins were analyzed from four different drill holes. Five of these veins have $^{87}\text{Sr}/^{86}\text{Sr}$ ratios in the range of 0.711170 to 0.713423, and there is one outlier which has ratio of 0.721772. In calcite 2, the samples with the lowest $^{87}\text{Sr}/^{86}\text{Sr}$ ratios are the ones in which calcite occurs as disseminated calcite. Two veins of calcite 3 were analyzed from

two different drill holes in Osiris. Calcite 3 $^{87}\text{Sr}/^{86}\text{Sr}$ ratios range from 0.713354 to 0.718000.

Ore Stage (Stage IV)

Four samples of dolomite 3 were analyzed from four different samples within Isis east hole OS-12-120. Three of these samples have relatively similar isotopic signatures, with $^{87}\text{Sr}/^{86}\text{Sr}$ values of 0.712827, 0.713874 and 0.714319. There is one outlier with a value of 0.726592.

Post-Ore Stage (Stage V)

Three veins of calcite 4 from three different drill holes were examined. There is a large spread in the data, with values of 0.713710, and 0.717939, and 0.724579.

2.5.8 Sulfur Isotopes

Stage I and II pyrite grains were analyzed for $\delta^{34}\text{S}$ values. The results are presented in Table 5 and shown graphically in Figure 35. Pyrite 3 could not be analyzed because it occurs as very small rims. There are some grains of pyrite 1 and 2 which have pyrite 3 rims/fracture infills. These were analyzed, and they are likely to be at least partially representative of the pyrite 3 isotopic composition.

Table 5. All $\delta^{34}\text{S}$ values for Nadaleen Trend pyrite

Area	Hole: depth	Paragenetic phase	$\delta^{34}\text{S}_{\text{-CDT}}$ (‰)
Osiris	OS-11-41: 342.97	Py 1	24.9
Osiris	OS-11-41: 358.59	Py 1	17.2
Osiris	OS-11-83: 126.35	Py 1	16.8
Osiris	OS-11-41: 201.33	Py 2	11.6
Osiris	OS-11-52: 219.31	Py 2	21.4
Osiris	OS-11-61: 353.71	Py 2	19.4
Osiris	OS-11-61: 370.48	Py 2	12.4
Osiris	OS-11-61: 374.32	Py 2	15.9
Osiris	OS-11-61: 381.43	Py 2	12.6
Isis	OS-11-72: 71.10	Py 2	14.8
Isis	OS-11-72: 290.64	Py 2	7.2
Osiris	OS-11-80: 162.22	Py 2	27.4
Osiris	OS-11-80: 176.53	Py 2	23.6
Osiris	OS-11-83: 113.88	Py 2	21.0
Isis east	OS-12-120: 66.43	Py 2	14.3
Isis	OS-11-72: 41.83	Py 2/3	6.6
Isis	OS-11-72: 42.04	Py 2/3	5.7
Isis	OS-11-72: 52.93	Py 2/3	4.3
Isis	OS-11-72: 57.67	Py 2/3	4.2
Isis	OS-11-72: 154.69	Py 2/3	7.0
Isis	OS-11-72: 303.40	Py 2/3	6.4
Isis	OS-11-72: 306.92	Py 2/3	6.2
Isis east	OS-12-120: 116.80B	Py 1/3	-25.4
Isis east	OS-12-120: 117.34	Py 2/3	14.6

Near-Surface Diagenesis (Stage I)

Three samples of pyrite 1 were analyzed from two drill holes in the Osiris zone. The analyzed pyrite 1 samples were taken from pyrite which occurs in grains or matrix of dolomite 1. These pyrites have $\delta^{34}\text{S}$ values of 16.8, 17.2, and 24.9 ‰.

Base Metal Mineralization Stage (Stage II)

Twelve samples of pyrite 2 from Osiris, Isis, and Isis east were analyzed. There is a large amount of variation in this generation of pyrite, with $\delta^{34}\text{S}$ values ranging from 7.2 to 27.4 ‰.

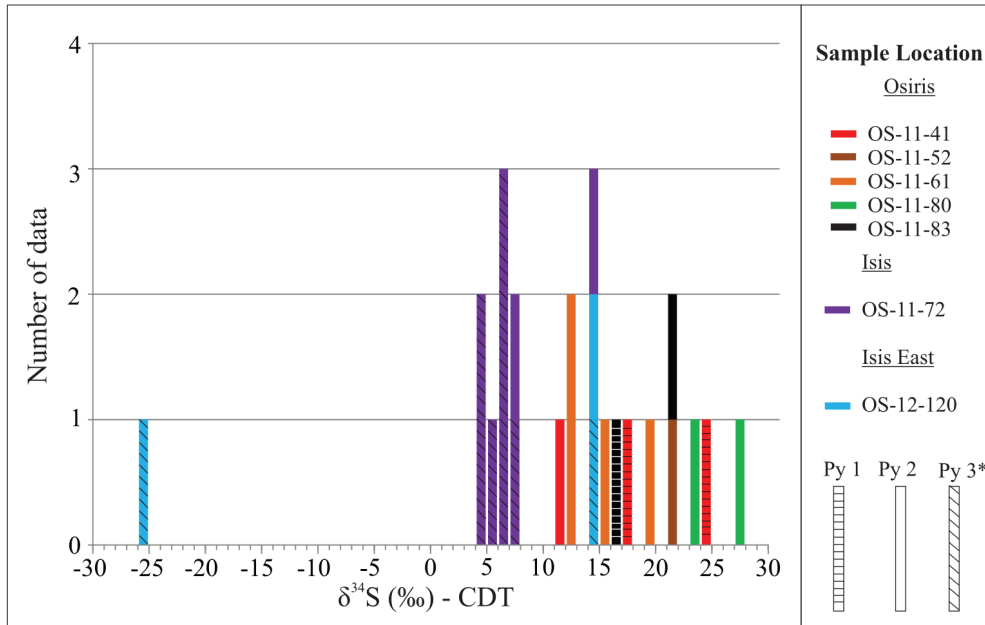


Figure 35. Plot of $\delta^{34}\text{S}$ values of pyrite 1, 2, and 3 vs. frequency. *Pyrite 3 samples are actually pyrite 1 or 2 which has been rimmed by pyrite 3. The isotopic composition likely reflects combination of two pyrite generations.

Ore-Stage (Stage IV)

Eight samples of pyrite 2 which are rimmed by pyrite 3 (or have pyrite 3 infills) were analyzed from different depths in drill holes of Isis and Isis east. One sample of pyrite 1 with a pyrite 3 rim from Isis East was analyzed. There is a large amount of variation in $\delta^{34}\text{S}$ values, with values ranging from -25.4 to 14.6 ‰. The extremely negative value of -25.4 ‰ is from an area where the gold grade is 11.05 g/T, which is much higher than the gold grades in the other samples (mostly less than 0.1 g/T). The samples from OS-11-72 all cluster in roughly the same part of the plot (Fig. 34).

2.6 Discussion

2.6.1 Host Rocks

The carbonate host rocks exposed at the surface of the Osiris and Isis East zones are interpreted to be part of the Ediacaran Gametrail Formation, whereas Isis drill hole OS-11-72 intersects the overlying Blueflower Formation (also Ediacaran, Fig. 3; Colpron et al., 2013). The Blueflower Formation is nearly all dolomite, is weakly mineralized and was not the focus of this thesis. The Gametrail Formation is part of the upper Windermere Supergroup and comprises a 60 to 320m thick succession of partially dolomitized limestones with debris-flow breccias (Narbonne and Aitken, 1993; Colpron et al., 2013). The presence of partially dolomitized wackestones and lime mudstones with poorly sorted diamictites in the Osiris and Isis East drill holes indicates that the full depth of these drill holes are in the Gametrail Formation. The composition of the carbonate units suggests that these rocks precipitated in a marine setting with minor influx of detrital components. The immaturity of the detritus (quartz, apatite, K-feldspar, zircon) indicates that these components did not travel a great distance before deposition. The presence of carbonate rip-up clasts in diamictites and rudstone suggests that these rocks formed in a carbonate slope setting, possibly as part of a passive margin setting as suggested by Narbonne and Aitken (1993).

The carbonates of the Gametrail Formation contain the globally-recognized ^{13}C excursion known as the Shuram excursion (MacDonald et al., 2013). The Shuram excursion represents a time interval (roughly 600 to 550 Ma) during which seawater carbonates were forming with $\delta^{13}\text{C}$ values of 0 to -12 ‰ (VPDB), among the lowest in Earth's history (MacDonald et al., 2013). The host rock carbonates analyzed in Osiris and Isis East in this study have similarly low $\delta^{13}\text{C}$ values (-3 to -13 ‰ VPDB), and are thus likely to have formed during the Shuram excursion. The $\delta^{18}\text{O}$ values of carbonates of the Shuram excursion range from 17.92 to 26.92 ‰ (Jacobsen and Kaufman, 1999; Halverson et al., 2007), which are comparable to the values of the Osiris and Isis East host rocks (19 to 23 ‰). The two host rock samples analyzed (from Osiris) have $^{87}\text{Sr}/^{86}\text{Sr}$ ratios of 0.709000 and 0.709272, which are on the upper end of the range of Ediacaran $^{87}\text{Sr}/^{86}\text{Sr}$ values (0.708 to 0.709; Jacobsen and Kaufman, 1999; Burns et al, 1994; Calver, 2000). As that there is negligible Sr fractionation during carbonate precipitation (Veizer, 1983), it can be assumed that these represent the actual Sr isotopic composition of Ediacaran seawater.

The Shuram excursion has been attributed to fluid-rock and fluid-fluid interactions (Derry, 2010) or the development of authigenic carbonate extending onto the continental shelf as part of a marine transgression (Schrag et al., 2013). Other authors believe that the Shuram excursion is the result of ocean stratification and oxidation of a large reservoir of dissolved organic carbon (DOC) sourced from anoxic seawater (Fike et al., 2006; Jiang et al., 2007; McFadden et al., 2008). This process coincides with the Ediacaran oxygenation

event, during which the oceans became partially oxygenated and stratified, with oxic shallow waters and deep waters which were anoxic, reducing, ferruginous, euxinic, or some combination of these features (Canfield, 2005; Shields-Zhou and Och, 2008; Fike et al., 2006; Fan et al., 2014; Wang et al., 2014).

The high Fe content of the calcite grains in the lime mudstone and wackestone of Nadaleen (up to 1.22 wt. % FeO) suggests that these rocks precipitated from ferruginous waters. The host rock calcite grains also contain significant amounts of MnO (mean = 0.15 wt. %), which is evidence of reducing (anoxic) conditions since reducing conditions are required for Mn and Fe to be incorporated into the calcite crystal structure as divalent ions (Hiatt and Pufahl, 2014). The dull brown CL signature of the host rock calcite is the result of the high Fe concentrations and lower Mn concentrations. It is widely accepted that Mn acts as a CL activator in carbonates whereas Fe acts as a CL inhibitor (Schulman et al., 1947; Budd et al., 2000).

The trace element chemistry of the rocks also places constraints of the genesis of the host carbonates. In order to assess whether the carbonate REY patterns reflect the character of the seawater rather than detrital input, the REYs were plotted against Ti, as Ti in sediments is nearly always detrital in origin (Tribovillard et al., 2006). The REY in the host rock do not correlate strongly with Ti (Fig. 26a), so they are unlikely to be detritally controlled, and rather reflect the character of the seawater. When precipitating from seawater, carbonates tend to attain a REY pattern that consists of LREE depletion, a positive La anomaly, a negative Ce anomaly, slight Gd enrichment, and a positive Y anomaly. This is a pattern that has been reported from rocks of all geologic ages; and has been referred to as a “typical” seawater REY pattern (Shields and Webb, 2004; Bolhar and Van Kranendonk, 2007; Frimmel, 2009). The overall REY concentration is slightly elevated compared to the Shuram excursion-age Ediacaran carbonates studied by Zhou et al. (2012; Fig. 26a). The data from the Osiris and Isis East host rocks do not have typical seawater REY patterns, but rather have MREE enrichment relative to LREE and HREE. The MREE enrichment can be attributed to the ferruginous character of Ediacaran seawater. In a seawater REY model by Haley et al. (2004), it is proposed that when Fe-oxides develop in the water column, they scavenge REY (especially MREE) and the Fe-oxides attain a MREE-enriched REY signature. When the Fe-oxides reach an anoxic environment (commonly within the sediments), they release their REY and the water becomes enriched in MREE. In Ediacaran seawater, it is likely that Fe-oxides developed in the upper, oxic waters. Once the Fe-oxides reached the deeper, anoxic waters, or were buried, Fe-oxides were reduced and released their REY, leaving the seawater or pore water enriched in MREE. The calcite of the Nadaleen host rocks may have inherited their MREE-enriched pattern via this process. The Osiris and Isis East samples also have a marked positive Ce anomaly. The cerium anomaly, Ce/Ce* can be used as a proxy for redox conditions. In a study by Wright et al. (1987), a Ce/Ce* value greater than 0.8 was interpreted to be indicative of anoxic

conditions, whereas Ce/Ce* values less than 0.8 were indicative of oxic conditions. Ce/Ce* values of calcite grains in the host rock range from 0.93 to 1.03. Positive Ce/Ce* values have also been reported in other Ediacaran rocks that are contemporaneous with the Shuram excursion (Zhou et al., 2012). Furthermore, the U/Th ratios in the host rocks are higher than 1.25, which also suggests an anoxic environment (Jones and Manning, 1994). The U/Th ratio in sample OS-11-83 123.84 is 0.18, but the U/Th ratios in OS-12-120 43.37 range from 3.58 to 26.54. This range may be attributed to varying redox conditions due to the stratification of the Ediacaran ocean.

Some framboidal pyrite may have been precipitated cogenetically with the host carbonates. In order for pyrite to form, H₂S and Fe are required; at low temperatures H₂S is normally produced through bacterial reduction of seawater sulfate (Raiswell and Berner, 1985). In H₂S-bearing fluids, the limiting reagent in pyrite development is the availability of Fe (Raiswell and Berner, 1985). Pyrite can be created syngenetically (in the water column) or diagenetically (in the sediments). In a classification by Wang et al. (2012), the setting of pyrite generation was inferred from the morphology and the size of the pyrite grains. The framboidal pyrite in Osiris and Isis East can be classified as type C, which refers to framboidal pyrite with mean diameters of 5.2 to 5.8 μm and max diameters of 13 to 19 μm. These are interpreted to have been created syngenetically or diagenetically with overlying waters which are dysoxic or euxinic. In a study of modern sediments, it was determined that pyrite framboids smaller than 10 microns typically form in euxinic water whereas framboids larger than 10 microns form in non-euxinic water (Wilkin et al., 1996); this study also shows that framboidal pyrite less than 10 μm in diameter generally precipitates from the water column (syngenetic). Most of the framboidal pyrite in Osiris is less than 10 microns in diameter, so it is probable that this pyrite precipitated syngenetically from euxinic water. There were no sulfur isotope studies carried out on framboidal pyrite because the grains were too small, but a study on Shuram excursion-age seawater sulfates indicate that seawater at this time had δ³⁴S values of 19 to 27 ‰ VCDT (Loyd et al., 2013).

2.6.2 Near-Surface Diagenesis Stage (Stage I)

Stage I comprises near-surface diagenetic events that took place within the first few meters of burial (Machel, 1999). Dolomite 1 and pyrite 1 were generated during this paragenetic stage as a result of interaction of the pore waters and the host rocks. The pore waters likely retained the reducing and/or ferruginous character of the seawater. Dolomite 1 occurs most commonly as matrix material rather than grains (Fig. 11d), suggesting there was porosity and permeability in the matrix. The micrite matrix of the host rocks (Fig. 9g, 9h) was probably dolomitized by the reaction of calcite with Mg-rich seawater in pore spaces (e.g. $2\text{CaCO}_3 + \text{Mg}^{2+} \rightarrow \text{CaMg}(\text{CO}_3)_2 + \text{Ca}^{2+}$; Hsu, 1967; Warren, 2000). Dolomite 1 has very high Fe content (up to 7.57 wt. % FeO), so it is likely that the pore waters were highly enriched in Fe. This supports growth in a reducing environment, since Fe must occur as a

reduced species (Fe^{2+}) in order to substitute into dolomite. The presence of Mn in dolomite (mean MnO = 0.10 wt. %) confirms this, since Mn can only substitute into dolomite in reducing conditions.

There is a correlation of REY with Ti which suggests that some of the REY analyzed is detrital in origin, especially in samples OS-120 43.37, OS-11-80 108.16, and partially in OS-11-83 123.84 (Fig. 26b). This may be the result of analyzing the carbonate matrix, which contains small grains of apatite or zircon (Fig. 9i), as these minerals typically have significant REY concentrations (Joosu et al., 2015; Hanchar and Westrenen, 2007). Sample OS-11-80 73.08 and some of the data from OS-11-83 123.84 do not fit on the Ti trend; these are thus the most likely to reflect the REY characteristics of the pore waters. Dolomite 1 is enriched in REY compared to the REY studied by Zhou et al. (2012), which are from dolomitic limestones in China that also formed in Ediacaran seawater during the Shuram excursion. This difference may be attributed to the depositional environment, as the carbonates in the Zhou et al. (2012) study are part of the Doushantuo Formation which has been interpreted to have developed in a lagoon setting separated from the open ocean (Jiang et al., 2011). Sample OS-11-83 123.84 has a LREE-enriched REY pattern and OS-11-80 73.08 has both a LREE-enriched and a flat REY pattern; the Ce/Ce* values of these samples range from 2.82 to 3.65. LREE enrichment and a highly positive Ce/Ce* value suggest dolomite 1 was derived from anoxic pore waters (Hood and Wallace, 2015; Frimmel, 2009). The flat REY patterns of OS-11-80 73.08 may be due to silicate contamination, as a flat REE pattern is commonly indicative of oxide or detrital silicate contamination (Nothdurft et al., 2004; Hood and Wallace, 2015).

The $\delta^{18}\text{O}$ values of dolomite 1 (from bulk isotope and SIMS analyses) range from 20.89 to 34.28 ‰. The dolomite 1 $\delta^{18}\text{O}$ values are higher than those of the host rock, which may be partially attributed to isotopic fractionation during dolomitization. Experimental data has suggested that at 25 °C, a limestone being converted to dolomite can be enriched in ^{18}O , with a 4 to 7 ‰ increase in $\delta^{18}\text{O}$ value (Land, 1980). This explanation accounts for all of the dolomite $\delta^{18}\text{O}$ values except the one very high value of 34.28 ‰. This value is from a dolomite grain that may be derived from a grain which originally was part of the Keele Formation, a unit with carbonate $\delta^{18}\text{O}$ values as high as 26 ‰ (Halverson et al. 2007). The $\delta^{13}\text{C}$ values of dolomite 1 (-8.66 to +3.15 ‰) have a wide range, which may reflect the composition of the limestone host rocks. For example, the host rock sample with the lowest $\delta^{13}\text{C}$ value in calcite grains (OS-11-80 73.08, -12.32 ‰) also has the lowest $\delta^{13}\text{C}$ value in dolomite grains (-8.66 ‰). Overall, dolomite 1 has higher $\delta^{13}\text{C}$ values than the host rock, so it is possible that dolomitization decreased the ^{13}C content in carbonates.

There are large volumes of pyrite which developed during near-surface diagenesis; this pyrite commonly occurs disseminated within dolomite 1 as euhedral-subhedral pyrite. The

euohedral-subohedral character of pyrite 1 indicates that it probably grew at a slower rate in the sub-surface than the framboidal pyrite (Butler and Rickard, 2000). Given the large volumes of pyrite, it is probable that dysoxic or anoxic, H₂S-rich waters were present in the pore spaces of the sediments. The $\delta^{34}\text{S}$ values of pyrite 1 reflect the isotopic composition of the pore water sulfate and BSR processes. At low temperatures in an open system (i.e. high seawater sulfate supply), sulfate reduction can result in a -40 ‰ change in $\delta^{34}\text{S}$ value as SO_4^{2-} is reduced to H₂S (Zhelezinskaia et al., 2014). In a closed system, where the rate of sulfate reduction is greater than the rate of sulfate supply, the magnitude of isotopic fractionation becomes smaller as sulfate becomes depleted from the seawater (Misra, 2000). The $\delta^{34}\text{S}$ values of pyrite 1 (16.8 to 24.9 ‰) are only slightly lower than the values of Ediacaran seawater (19 to 27 ‰, Loyd et al., 2013), so it is likely that pyrite was being created in an anoxic, closed system in which the rate of sulfate reduction was much higher than the rate of sulfate replenishment.

Pyrite 1 is enriched in many trace elements. Besides As, the elements occurring in the highest concentrations are Mn, Zn, Ni, Cu, and Co. The enrichment in these metals may be attributed to the anoxic character of Ediacaran seawater, since lack of oxidative scavenging may promote a high concentration of trace elements in oceans (Hood and Wallace, 2015). Ni can become enriched in pyrite under reducing conditions (Grosjean et al., 2004) and Zn may be incorporated through bacterial sulfate reduction (BSR) (Morse and Luther 1999).

2.6.3 Base Metal Mineralization Stage (Stage II)

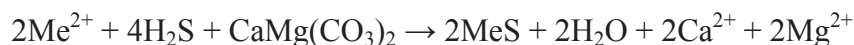
Stage II includes calcite 1 and stylolite 1 followed by a base metal mineralization assemblage comprising quartz, dolomite 2 and pyrite 2, and lesser amounts of barite, enargite, and sphalerite.

The first event of this stage is veining of calcite 1. Calcite 1 has a dull CL signature due to its high FeO content. The presence of Mn and Fe in the calcite 1 structure is evidence of reducing conditions. The $\delta^{18}\text{O}$ values of calcite 1 (10.07 to 10.34 ‰) are much lower than the host rock and its $\delta^{13}\text{C}$ values are slightly higher than the host rock, suggesting that the fluids did not fully equilibrate with the host rocks. The low $\delta^{18}\text{O}$ values suggest that the veins may have been derived from relatively hot fluids and/or meteoric water. This is supported by the REY pattern (Fig. 26c), which is very different from that of the host rock. The $^{87}\text{Sr}/^{86}\text{Sr}$ values of calcite 1 are also much higher than that of the host rock, indicating that the fluids acquired radiogenic Sr during their migration. The Little Dal Group underlying the Windermere Supergroup (Fig. 5) has dolostone $^{87}\text{Sr}/^{86}\text{Sr}$ values as high as 0.7303 (Wallace 2009; Halverson et al., 2007), so it is possible that radiogenic Sr was scavenged from this unit. A hydrothermal fluid that mobilizes Y and Ho from a host rock will retain the Y/Ho ratio of the host rock, and this ratio will decrease with increasing migration distance since Y fractionates from Ho in aqueous solutions (Bau, 1996; Tanaka

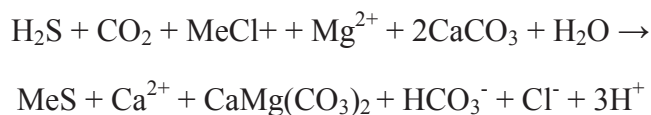
et al., 2008). The host limestones in Osiris samples OS-11-83 123.84 and OS-12-120 43.37 have an average Y/Ho ratio of 30.53, and the calcite 1 veinlets in Osiris sample OS-11-80 108.16 have an average Y/Ho ratio of 37.56. The high Y/Ho ratio of calcite 1 indicates that the fluid did not originate from the carbonate host rocks of the Nadaleen Trend, but may have originated from another source with a high Y/Ho ratio.

Calcite 1 is crosscut by stylolites, which require significant compaction in order to form. Stylolites generally begin to develop at depths of 600 to 1000 m as a result of pressure solution (Machel, 1999; Mountjoy et al., 1999). In a classification by Machel (1999), the lower limit of the shallow diagenesis realm is 600 to 1000 m, which is followed by intermediate diagenesis. This first generation of stylolites may have formed in the lower shallow diagenesis or upper intermediate diagenesis realm. Stylolites are very common, occurring in roughly 50% of the samples collected.

Dolomite 2 is highly pervasive, comprising roughly 50% of the dolomite in the Osiris and Isis East holes. Isis hole OS-11-72 is dolomitized for the full depth of the drill hole, and ~90% of it is dolomite 2. The pervasive nature of dolomite 2 suggests that there must have been significant porosity for hydrothermal fluids to dolomitize the rocks. This porosity could have been created through dissolution of dolomite 1 via the following reaction (Wilkinson et al., 2011), where “Me” represents Pb or Zn, explaining the presence of sphalerite:



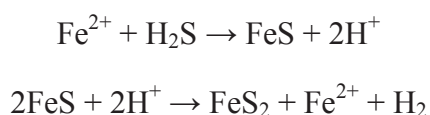
Dolomite 2 occurs either as fine- to coarse-sparry dolomite (dolomite 2a) or as coarse-grained crystalline dolomite (dolomite 2b). Some dolomite 2a mosaics have an idiotopic texture (planar crystal faces) whereas some have a xenotopic texture. It has been proposed that idiotopic dolomite is generated at temperatures of less than 50°C whereas xenotopic dolomite is generated at temperatures of greater than 50°C (Sibley and Gregg, 1987). The saddle morphology of dolomite 2b is evidence that these crystals grew in areas of porosity (Fig. 12i), and had the open space required for faceted growth. Following formation of dolomite 2, quartz infilled some of the remaining pore spaces (Fig. 12g). Saddle dolomite typically forms at temperatures of 60 to 150°C, and is thought to be a byproduct of chemical compaction and sulfate reduction, often related to hypersaline brines carrying base metals (Warren, 2000). Saddle dolomite has also been shown to coprecipitate with metal sulfides in MVT deposits at temperatures of 60 to 200°C (Hill, 1995):



Given the above constraints, the base metal stage (except for calcite 1) likely occurred at a temperature of ~100 to 150°C. Using a temperature of 100°C and an average dolomite 2

$\delta^{18}\text{O}$ value of 23.3 ‰, the calculated $\delta^{18}\text{O}$ value of the hydrothermal fluid is 4.8 ‰, using the fractionation factors of Böttcher (1994). The $\delta^{18}\text{O}$ and $\delta^{13}\text{C}$ values of dolomite 2 are comparable with the host rock and dolomite 1, indicating that the fluids that created dolomite 2 may have isotopically equilibrated with these rocks before precipitating dolomite. There is a larger range of $\delta^{13}\text{C}$ values in dolomite 2 than dolomite 1, with some spatial variation. This may be attributed to the local derivation of the isotopic signature from the host rock and dolomite 1. The Sr isotopic compositions of dolomite 2 are more radiogenic than the host rock so the fluids were probably not derived from seawater, but possibly from a fluid which interacted with ^{87}Sr -rich units. This radiogenic Sr may have been scavenged from the Little Dal Group (Halverson et al., 2007). Dolomite 2b (saddle) has higher $^{87}\text{Sr}/^{86}\text{Sr}$ values than dolomite 2a (sparry), indicating that they may have different Sr sources (Fig. 34). The Y/Ho ratios of dolomite range from 28.91 to 42.73, which are higher than the Y/Ho ratios of the host rocks (28.42 to 35.10) and dolomite 1 (28.04 to 30.80) suggesting that the dolomite 2 was not sourced from the host rocks or dolomite 1. As with dolomite 1, the high Mn and Fe content of dolomite 2 is evidence of reducing conditions. Some dolomite 2 is zoned, with varying amounts of Mn and Fe; the overall trend is an increase in Fe and a decrease in Mn from core to rim (Fig 18). When there is very little Fe content, the dolomite has bright red/orange CL, even in cases where MnO content is ~0.01 or B.D. The minimum Mn content in carbonates required to cause CL is 25 ppm (Budd et al., 2000); these very small Mn concentrations are probably causing CL in dolomite 2. The zoning in dolomite is evidence of changing redox conditions during diagenesis, as Mn and Fe are both sensitive to redox state. The average Ce anomaly in dolomite 2 is 1.01, indicating that the fluids are reduced.

As with dolomite 2, pyrite 2 is highly pervasive and occurs more commonly in dolomite 2a than dolomite 2b. Pyrite 2 is most commonly euhedral or subhedral, indicating that it developed slowly and that it was in equilibrium with the fluids that precipitated it (Ohmoto et al., 1997). There are also significant volumes of pyrite in stylolites (Fig. 14d), which may have been generated through a reaction of organic matter and Fe in the stylolites. Pyrite 2 has much lower metal concentrations than pyrite 1; this could be due to the fact that some of the metals were partitioned into other minerals such as sphalerite or barite. The co-existence of quartz, pyrite 2, and dolomite 2 in some samples suggests that these materials formed cogenetically (Fig. 12d). At temperatures greater than 110°C thermochemical sulfate reduction takes over as the dominant sulfate reduction process (Warren, 2000). Pyrite can be created through the following sequence of reactions (Ohmoto et al., 1997):



The reaction above and dolomitization reaction of Hill (1995) described above could have provided H^+ and given the fluids a low pH, explaining why some pyrite 2 is partially dissolved (Fig. 14h 28d). The $\delta^{34}S$ values of pyrite 2 range from 7.2 to 27.4 ‰ which are comparable to the isotopic composition of pyrite 1. It is thus probable that the sulfur in pyrite 2 ultimately came from seawater. There is one pyrite sample, OS-12-120 116.80, with a $\delta^{34}S$ value of -25.4 ‰; this sample is a mixture of pyrite 2 and 3 and also contains coeval barite. The low $\delta^{34}S$ value suggests that the S in this phase was generated by open system sulfate reduction and may be the result of remobilization of S from an earlier phase of pyrite.

Overall, the mineral assemblage present in this paragenetic stage is similar to those described from Mississippi Valley-Type Deposits (MVTs), a class of Pb-Zn ore deposits which form as a result of basinal migration of base metal-rich brines created through diagenetic processes in sedimentary basins (Anderson, 1975; Stoffell et al., 2008). There are no age constraints on Stage II mineralization in the Nadaleen Trend, but there is Cretaceous to Tertiary-age MVT mineralization in the Gayna River Deposit in the Northwest Territories in which Pb-Zn mineralization occurs in the Little Dal Group (Wallace, 2009). The ore-stage mineral assemblage in the Gayna River Deposit is similar to the base metal event of the Nadaleen Trend, comprising pyrite, quartz, dolomite and sphalerite. There is also Middle Paleozoic MVT ore mineralization in the northern Rocky Mountains of Yukon and Northwest Territories (Nelson et al., 2002).

2.6.4 Intermediate Diagenesis Stage (Stage III)

Stage III includes calcite 2, stylolite 2, and calcite 3, all of which formed in the “intermediate diagenesis” realm. In Machel (1999), “intermediate diagenesis” begins at 600 to 1000 m of burial depth and ends at 2000 to 3000 m, at which point deep diagenesis begins (Mountjoy et al., 1999). At intermediate burial, any empty pore spaces are not immediately replenished by overlying fluids. Here it is used to indicate a paragenetic stage which contains abundant calcite veining and stylolites.

In the intermediate diagenesis stage calcite 2 has high Mn and Fe concentrations, again suggesting reducing conditions. Calcite 2 has a brighter CL signature than the host rock or calcite 1; this can be attributed to a lower FeO/MnO ratio. The average Ce/Ce* value of calcite 2 is 0.88 and supports growth from reducing fluids. The average Y/Ho ratio of calcite 2 is 38.59, which is much higher than that of the host rock (30.53), suggesting that the fluids were not derived from the host rock. The REY patterns of calcite 2 in sample OS-11-80 154.24 are relatively flat, although the REY pattern of OS-11-83 29.91 has a pronounced positive Eu anomaly (Fig. 26e). A positive Eu anomaly is a common feature of reducing, acidic hydrothermal fluids (Frimmel, 2009). The acidic nature of these fluids may be related to the H^+ ions released during dolomitization and pyritization reactions that occurred in the base metal stage. The $^{87}Sr/^{86}Sr$ values of calcite 2 are higher than the host

rock, suggesting that the fluid scavenged radiogenic Sr from some other unit; possibly the Little Dal Group. The $^{87}\text{Sr}/^{86}\text{Sr}$ values of disseminated calcite 2 are lower than calcite 2 veins; this suggests that this phase may have partially inherited the isotopic signature of the host rock. Calcite 2 is crosscut by a second generation of stylolites. Stylolites are commonly generated as a result of intergranular pressure solution (Heap et al., 2014). They form through dissolution of carbonate material and the deposition of insoluble residue (Fig. 13d).

Calcite 3 has similar Fe and Mn contents, a positive Eu anomaly, an average C/Ce* value of 0.87, an average Y/Ho ratio of 33.40, and similar REY concentrations, suggesting these veins were derived from similar fluids to calcite 2. The $\delta^{18}\text{O}$ and $\delta^{13}\text{C}$ values of calcite 3 suggest that these fluids equilibrated with the host rocks. One sample of calcite 3 has a higher $^{87}\text{Sr}/^{86}\text{Sr}$ value (0.718000) and one lower (0.713354), but both are higher than seawater and host rock values, suggesting the fluids have interacted with some ^{87}Sr -rich rocks, such as the Little Dal Group.

2.6.5 Ore Stage (Stage IV)

Stage IV is the ore-bearing stage, which consists of Au-As-bearing pyrite (Pyrite 3) that was generated along with dolomite 3. Dolomite 3a formed as partial replacement and/or overprinting of dolomite 2, and is much more common than dolomite 3b. Dolomite 3b occurs as thin veinlets which commonly rim previous carbonate phases. Overall, dolomite 3 is not nearly as pervasive as dolomite 1 or 2; it is most commonly found in heavily stylolitized rocks associated with dolomite 2. The $\delta^{18}\text{O}$ values of dolomite 3 are on average lower than dolomite 2 and dolomite 1 (excluding three data points in which dolomite 3 occurs on grains of dolomite 1; Fig. 32g). It is likely that these three points have higher ^{18}O content because they inherited the isotopic signature of dolomite 1, indicating that the ore-stage fluids partially equilibrated with pre-existing carbonates. Other than these three high- ^{18}O data, the low $\delta^{18}\text{O}$ values of dolomite 3 suggest that the gold-bearing fluid was hotter than those that occurred earlier in the paragenesis. There are no temperature data available for this paragenetic phase, but the ore fluids in the Carlin District had temperatures of 180 to 240°C. Given that the $\delta^{18}\text{O}$ values of dolomite 3 range from 18.40 and 24.32 ‰, and assuming a temperature of 200°C, the calculated isotopic composition of the Nadaleen Trend ore fluids was between 7 and 13 ‰ (using the fractionation equations of Horita, 2014). This composition suggests the fluids could be derived from meteoric water or seawater which has partially equilibrated with the host-rocks, although a magmatic origin cannot be ruled out. The $^{87}\text{Sr}/^{86}\text{Sr}$ values of dolomite 3 range from 0.712827 to 0.726592, which are much higher than the values of the host rock (0.709000 and 0.709272). The high $^{87}\text{Sr}/^{86}\text{Sr}$ values of the ore stage dolomite suggest that these fluids came into contact with Rb-bearing units; possibly the Little Dal Group. The positive Eu anomaly and Ce/Ce* values in dolomite 3 are indicative of reducing, acidic hydrothermal fluids (Fig. 26g). If the

ore fluids were acidic, then they may have been responsible for decarbonatization of ferroan dolomite in the faults and shear zones.

The reduced nature of the fluids indicates that any sulfur in the system would likely exist as a sulfide species. The sulfur isotopic composition of pyrite 3 was not analyzed because the pyrite 3 rims are too small. Instead, pyrite 2 crystals which have been rimmed and partially replaced by pyrite 3 were analyzed (and are, therefore a mixture of pyrite 2 and 3). The $\delta^{34}\text{S}$ values of these pyrite 2/3 grains range from 4.2 to 14.6 ‰, and are slightly lower than pyrite 1 (16.8 to 24.9 ‰) and 2 (7.2 to 27.4 ‰) and likely formed from similar processes. The source of Fe in pyrite 3 may be ferroan dolomite (dolomite 1 and 2), as there is evidence of large volumes of decarbonatization near fault zones (Tucker, 2015). In a reducing fluid gold is likely transported as a $\text{Au}(\text{HS})_2^-$ complex (Emsbo et al. 2003; Cline and Hofstra, 2000; Benning and Seward, 1996; Pals et al., 2003). It has been suggested that there are reducing conditions present at the surface of arsenian pyrite, and that that a reduction reaction could be responsible for destabilization of gold-bearing hydrothermal fluids (Pokrovski et al., 2002). It has also been suggested that As-rich, Fe-deficient pyrite acts as a nucleation site for gold-rich pyrite (Deditius et al., 2014; Fleet and Mumin 1997; Reich et al. 2005). In the Nadaleen Trend, the pyrite grains with the highest Au-grade rims are most commonly As-rich, Fe-deficient grains of pyrite 1 or 2 (Fig. 28h), so this is a likely method of gold deposition. LA-ICP-MS data reveals that gold does occur in pyrite 3 but there are not consistently high gold concentrations in all As-rich rims. As indicated in Figure 29g, there is not a positive correlation between As and Au in pyrite 3. There is, however, a positive correlation between Au and Sb in pyrite 3 in sample OS-11-52 112.38 (Fig. 29h). This sample contains the only grain with a Sb-rich rim (Fig. 28g), and this sample is also one of the highest gold-grade samples. In pyrite, As can substitute for S, creating the $(\text{AsS})^{3-}$ anion which causes a charge imbalance as Fe^{2+} is no longer in balance with S^{2-} . The balance can be maintained by incorporation of Fe^{3+} , Au^{3+} , or Sb^{3+} (Cook and Chryssoulis, 1990). It is probable that As has substituted for S in the Nadaleen Trend from the negative correlation between these two elements (Fig. 21h) and Sb^{3+} has been incorporated into the pyrite lattice. Also, elemental maps of sulfur reveal As-rich rims on pyrite which are deficient in S (Fig. 22e, 22f). The lack of correlation between Au and As can be attributed to the $(\text{AsS})^{3-}$ anion being paired with Fe^{3+} or Sb^{3+} rather than Au^{3+} . In the As-rich rims of pyrite grains, it is evident that S has replaced much of the As (Fig. 22e, 22f), and it is also evident that the rims are deficient in Fe. This means that Fe^{3+} cations were not solely responsible for pairing with $(\text{AsS})^{3-}$ anions, and Sb^{3+} ions may have been substituted in.

2.6.6 Post-Ore Stage (Stage V)

Stage V is the post-ore stage, and comprises calcite 4, realgar, and orpiment. Calcite 4 has $\delta^{18}\text{O}$ values of 13.9 to 19.44 ‰, which are on average lower than the values of the host rocks (19.57 to 21.91 ‰). The data suggest calcite 4 was derived from a hot fluid which

partially equilibrated with the host rocks. The $\delta^{13}\text{C}$ values of calcite 4 range from -7.36 to -0.59 ‰, which are in the range of the host rock carbon isotopic values. Three samples from three drill holes were analyzed for Sr isotopic composition, and they all have different $^{87}\text{Sr}/^{86}\text{Sr}$ values (0.713710, 0.717939, and 0.724579). This may be attributed to fluids taking different migration paths and acquiring different amounts of radiogenic Sr. Calcite 4 is depleted in trace elements compared to all previous paragenetic carbonate phases (Fig. 25d), indicating that all metals may have been exhausted by this point. Realgar and orpiment occur as veins and amorphous patches, mostly associated with areas of gold mineralization.

2.6.7 Controls on hydrothermal fluid flow

On a regional scale, hydrothermal fluids were most strongly controlled by structural features such as faults and folds (Palmer, 2014; Tucker, 2015). Reverse faults acted as aquitards, channeling fluids updip into the sedimentary rocks of the Nadaleen Trend. These fluids were then concentrated into the hinges of SSW-plunging anticlines (Palmer, 2014). This study on the Osiris, Isis, and Isis East zones suggests that fluid flow away from fault zones was strongly controlled by permeability associated with hydrothermal dolomitization and stylolitization.

Large volumes of dolomite 2b (saddle dolomite) occur in veins or as cements, and these saddle dolomite crystals are associated with the generation of porosity and/or permeability (Fig. 36a, 36b, 36c). In thin section view, it is not possible to view the interconnectivity of these pore spaces, but some of the heavily saddle-dolomitized samples consist of up to ~15 % pore space in 2 dimensions, suggesting that these rocks may have been highly permeable. The pore spaces have been partially infilled by calcite, quartz, dolomite 3, pyrite 3, although in some cases they are not filled at all (Fig. 36a, c). The abundance of rims and fracture-fills of dolomite 3 is evidence that fluids were effective in migrating through these saddle dolomitized zones (Fig. 36c, 14c). Both generations of stylolites are commonly filled with veinlets of dolomite 3 (Fig. 36d), indicating that stylolites also acted as conduits for hydrothermal fluids. This supports the theory that zones of porosity can develop within and on the flanks of stylolites (Van Geet et al., 2000; Carozzi and Bergen, 1987). Pyrite 3 rims occur most commonly on pyrite 2 or pyrite 1 crystals which are adjacent to saddle dolomite or stylolites.

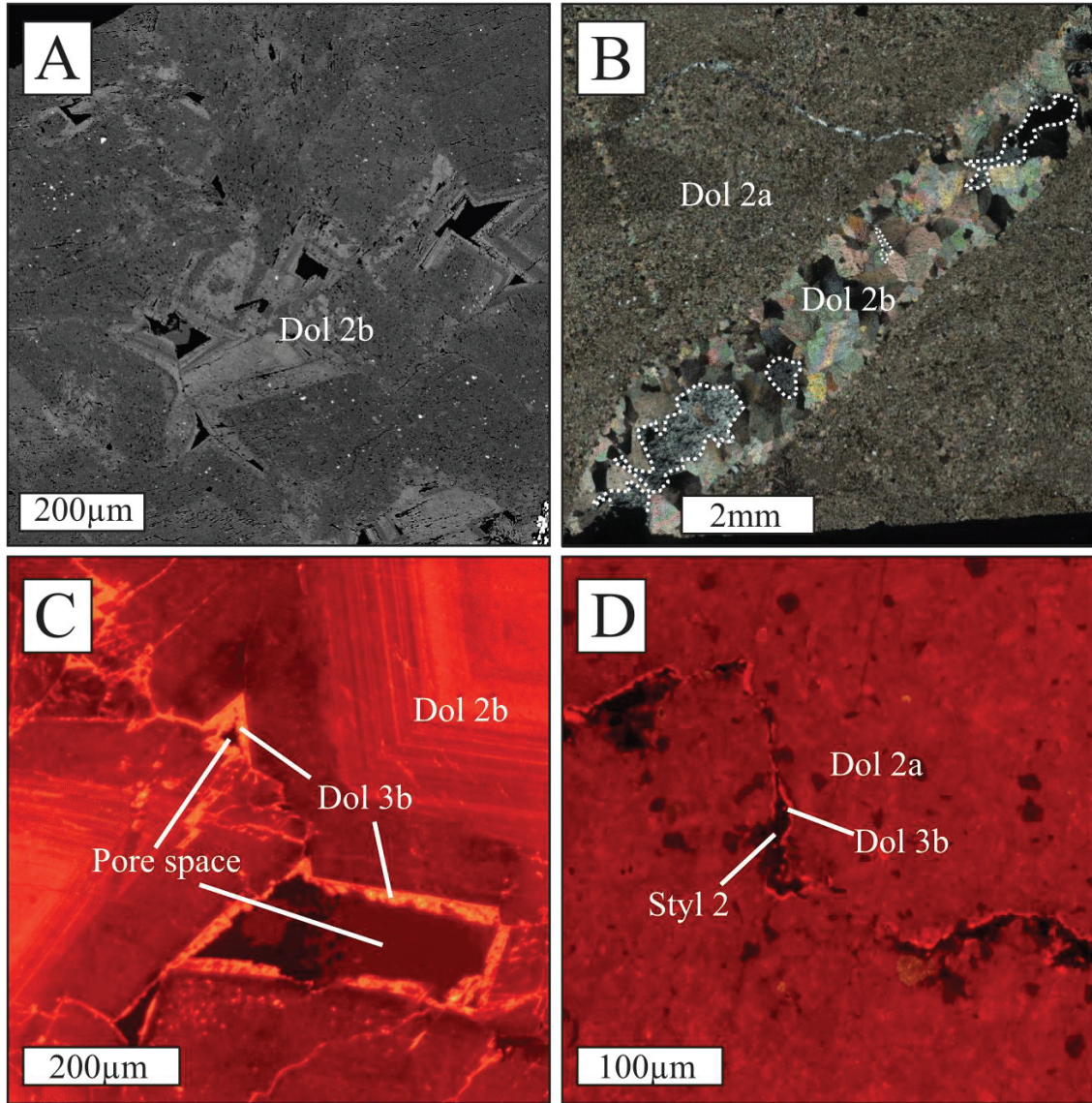


Figure 36. A) OS-11-41 342.97m. Dolomite 2b mosaic; black material is empty pore space. Red arrow indicates implied hydrothermal fluid migration path. B) OS-11-41 206.98m. Vein of dolomite 2b crosscutting dolomite 2a; dolomite 2b has substantially higher porosity and permeability. Pore spaces have been partially infilled by quartz. C) OS-12-120 115.26m. Dolomite 2b with associated pore space. Dolomite 3b has partially infilled pore space, showing evidence that ore stage fluids travelled through pore space. D) OS-11-80 210.57m. Stylolite crosscutting dolomite 2a. Presence of dolomite 3b veinlet in stylolite is evidence that ore stage fluids travelled through stylolites.

2.6.8 Deposit model and controls on gold mineralization

The wackestones, lime mudstones, diamictites, rudstones, and framboidal pyrite of the Osiris and Isis East zones were deposited in the Ediacaran period during the Shuram ^{13}C excursion (600 to 550 Ma), a time during which carbonates were forming with $\delta^{13}\text{C}$ values of -3 to -13 ‰. Ediacaran oceans were stratified, with an oxic layer overlying an anoxic, reducing, euxinic, ferruginous layer. The host rocks were enriched in Fe, Mn, Sr, and MREE. During near-surface diagenesis (Stage I), rocks were dolomitized and significant volumes of pyrite were created with enrichments in As, Mn, Zn, Ni, Cu, and Co as well and low concentrations of gold (Fig. 37).

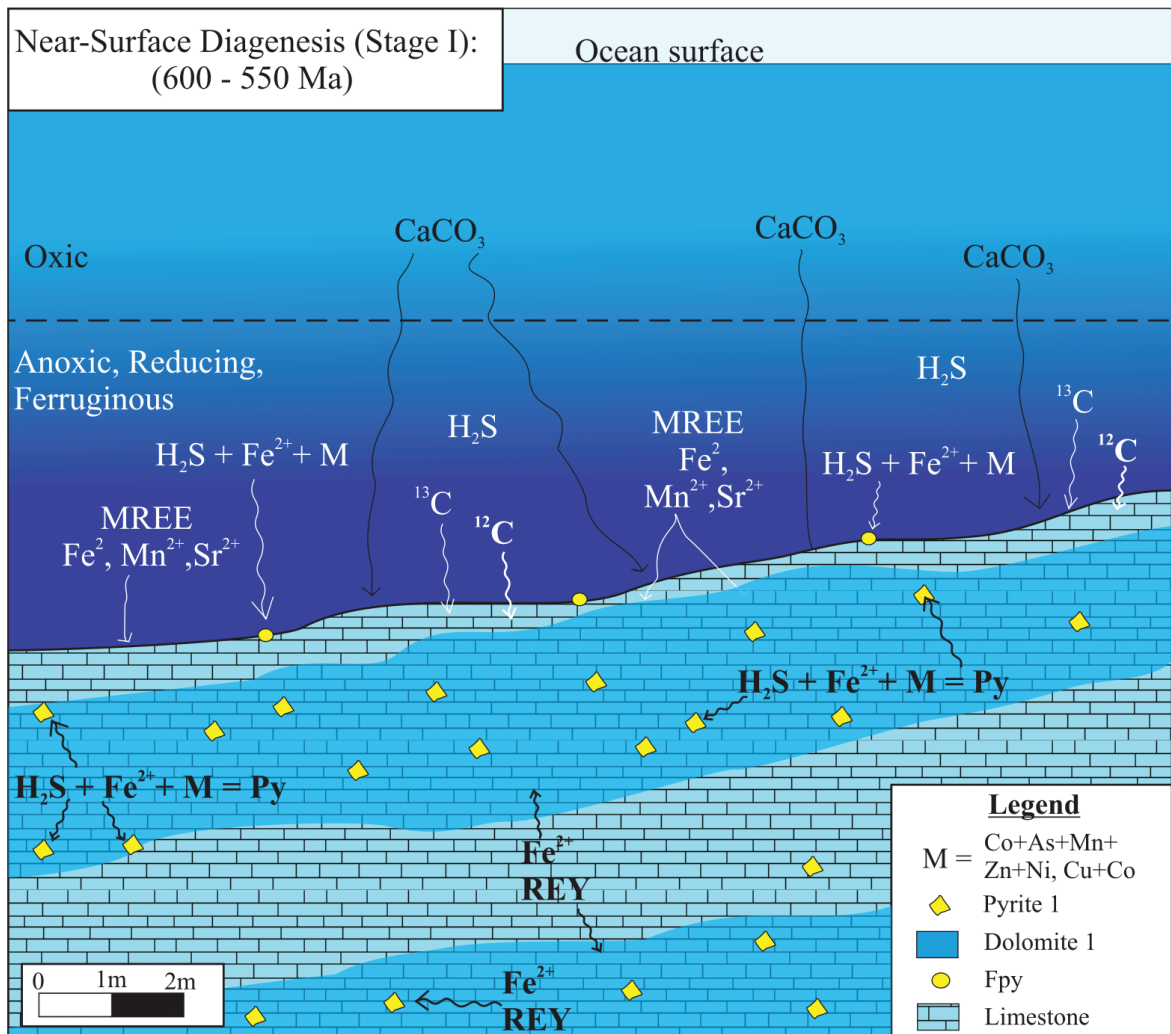


Figure 37. Schematic model for host rocks deposition and near-surface diagenesis (Stage I) of the Osiris and Isis zones. Bold text denotes greater magnitude of input. For example, greater concentrations of ^{12}C were input to the host rocks than ^{13}C .

After shallow to intermediate diagenesis and burial, a phase of hot hydrothermal fluids deposited calcite 1 and subsequently compaction formed the first phase of stylolites. An MVT-style base metal mineralizing event occurred, creating large quantities of pyrite, dolomite, and quartz, as well as minor amounts of sphalerite, barite, and enargite (Fig. 38). Porosity was created during this stage, through dissolution of dolomite 1 and the host rock. This pore space accommodated the growth of saddle dolomite, and the remaining pore spaces were partially filled by quartz and other paragenetic phases or remained empty. The age of Stage II mineralization is unknown.

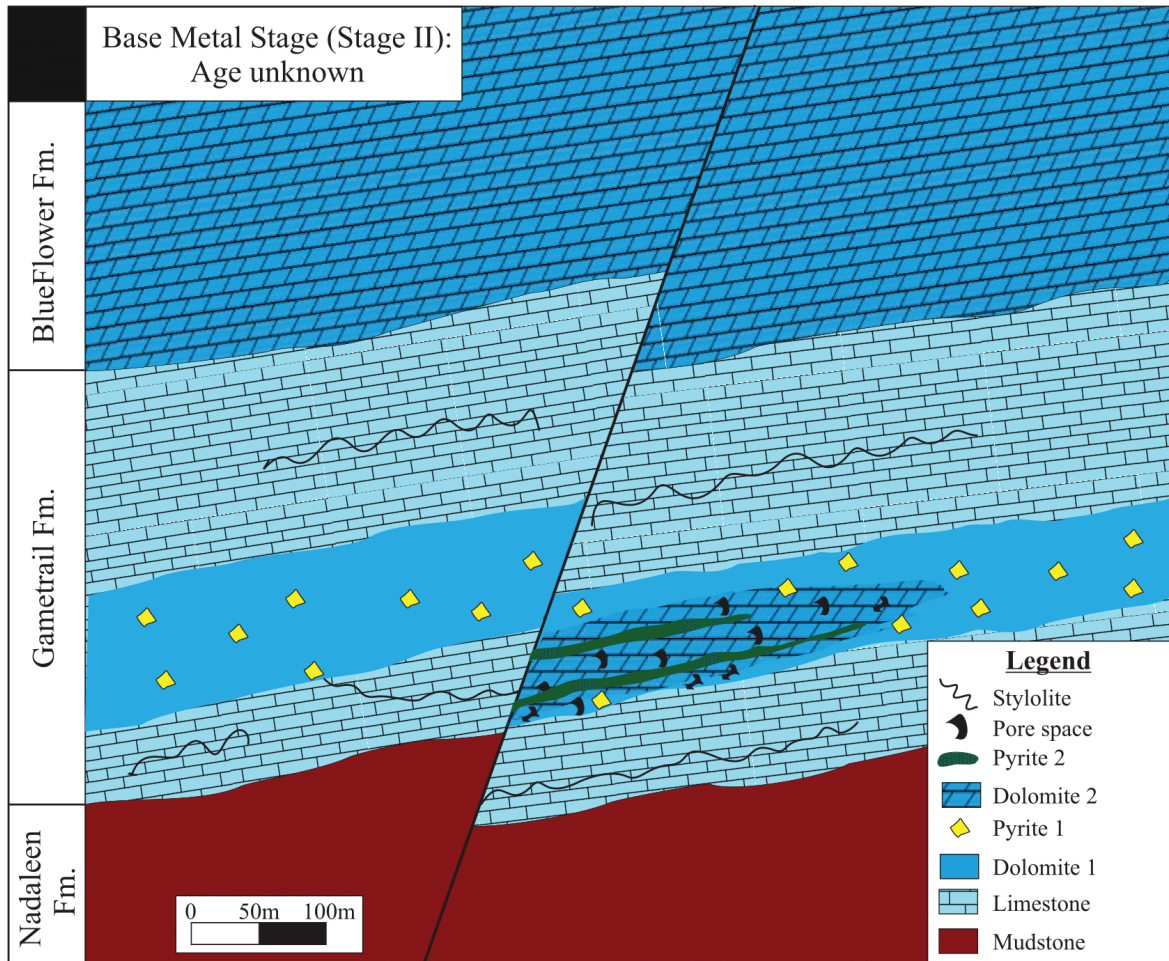


Figure 38. Schematic model for Stage II mineralization. Acidic, reducing fluids dissolved dolomite 1, creating porosity. Dolomite 2 was deposited and filled in the pore spaces. Some pore space remained unfilled following generation of dolomite 2.

Next, veins of calcite and a second generation of stylolites developed. This was followed by the ore precipitation of a third generation of dolomite and a gold-bearing third generation of pyrite. Ore fluids travelled vertically along faults, and significant quantities of gold were deposited in decarbonatized, silicified, argillized fault zones (Tucker, 2015). Decarbonatization of ferroan dolomite occurred in these zones and Fe was released into the

ore fluids. Fluids were only moderately buoyant and thus migrated laterally into the unaltered rocks. Ore fluids preferentially migrated through dolomite rather than limestone, due to the enhanced porosity and permeability associated with dolomite 2b (saddle dolomite; Fig. 39). However, in some cases ore fluids also used stylolites as conduits and mineralization occurred in limestone. Once $\text{Au}(\text{HS})_2^-$ -bearing ore fluids encountered As-rich, Fe-deficient pyrite, they underwent a sulfidation reaction and deposited a thin rim of gold-bearing arsenian pyrite on the pre-existing pyrite. Nearly all of the pyrite in the Nadaleen Trend occurs in dolostone rather than limestone, as dolostone contains more pyrite and provided a permeability pathway for the fluids. The ore stage has been constrained to have occurred between 74 and 42 Ma (Tucker, 2015).

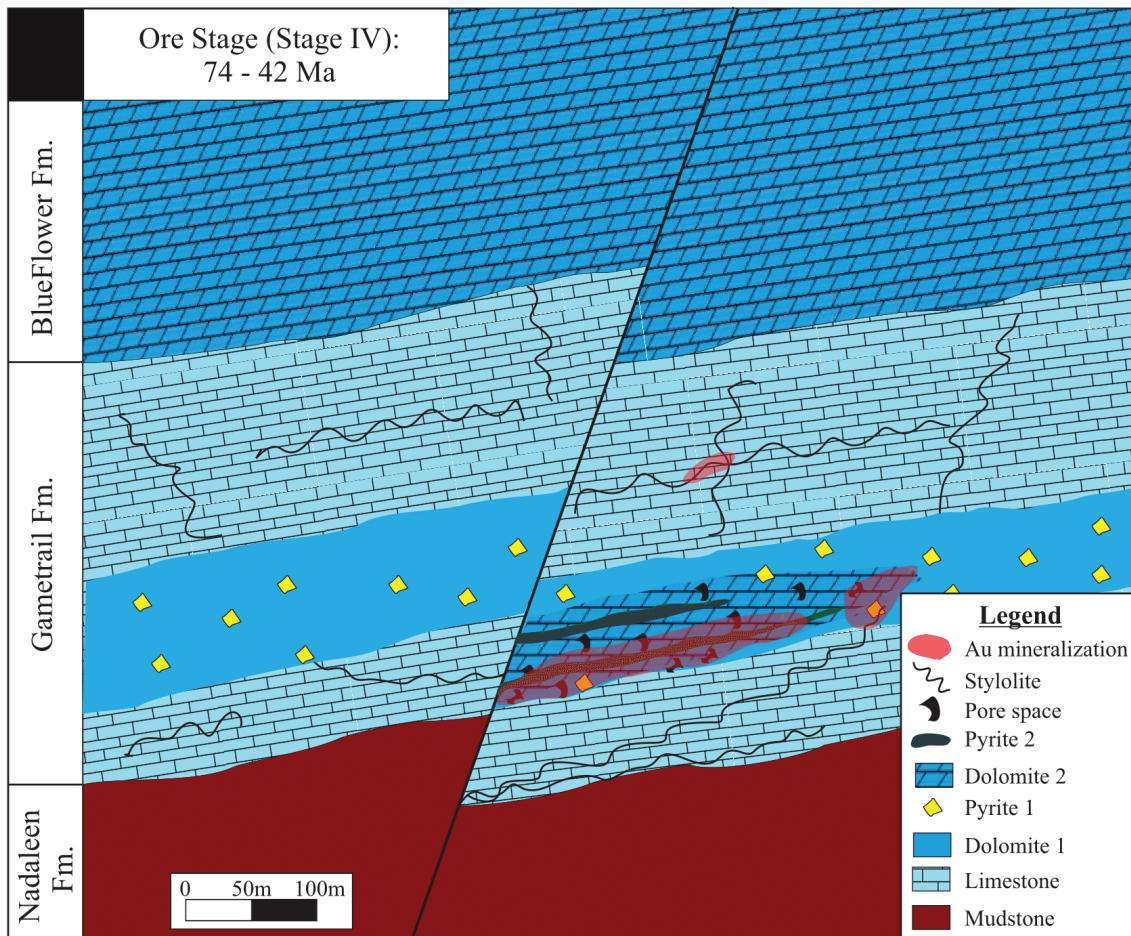


Figure 39. Schematic model for ore stage. gold-bearing fluids travelled vertically along faults and then laterally out into the hydrothermal dolomite due to the permeability associated with dolomite 2. When gold-bearing fluids encountered As-rich, Fe-deficient pyrite, they precipitated gold-bearing arsenian pyrite rims.

A post-ore stage of realgar, orpiment, and calcite veining occurred next. Most metals (including gold) were exhausted after the ore stage, and thus very low metal concentrations are present in the calcite of the post-ore stage.

2.6.9 Comparison with Carlin-type Gold Deposits

Carlin-type gold deposits are characterized by gold mineralization hosted in silty carbonate rocks in which gold-rich fluid migration was controlled by regional thrust faults. There are a number of features of CTGDs that are used to distinguish these deposits from other types of ore deposits. Cline et al. (2005) outlined these features in several of Nevada's CTGDs, and they are listed in Table 6. The Nadaleen Trend is compared to these CTGDs using the present study as well as Gleeson (2012), Palmer (2014), and Tucker (2015).

Table 6. Features of Nevada Carlin-Type Gold Deposits and the Nadaleen Trend

Deposit Features	N Carlin Trend	Central Carlin Trend	S Carlin Trend	Battle Mtn-Eureka Trend	Getchell Trend	Jerritt Canyon	Alligator Ridge	Nadaleen Trend
Pre-Eocene structural and stratigraphic architecture	XX	XX	XX	XX	XX	XX	XX	XX
Underlain by Archean or thinned and mixed Paleoproterozoic and Archean transitional crust	XX	XX	XX	XX	XX	XX	XX	?
Underlain by thick Neoproterozoic to Early Cambrian rift-related clastic rocks	X	X	X	X	X	X	X	X
Location east of or near continental margin	XX	XX	XX	XX	XX	XX	XX	X
Proximal to regional thrust fault	XX	XX	XX	XX	XX	XX	-	XX
Proximal to reactivated rift structures	X	X	X	X	X	X	?	-
High-angle structures control ore	XX	XX	XX	XX	XX	XX	XX	XX
Low-angle structures control ore	XX	XX	-	XX	XX	XX	-	-
Rheologic contrast around older stock controls ore	XX	XX	-	XX	XX	-	-	X
C- and pyrite-rich silty limestone or limey siltstone host rocks	XX	XX	XX	XX	XX	XX	XX	XX
Proximal coeval igneous rocks	X	X	X	X	-	X	-	X
Characteristic alteration present	XX	XX	XX	XX	XX	XX	XX	XX
Characteristic ore and late ore minerals present	XX	XX	XX	XX	XX	XX	XX	XX
Au in arsenian trace element-rich pyrite or marcasite	XX	XX	XX	XX	XX	XX	XX	XX
Deep magmatic ± metamorphic source identified for He, Pb, Nd, ±Sr	X	nd	nd	nd	XX	nd	nd	?
Magmatic ± metamorphic water identified in ore fluid	X	-	-	-	XX	-	-	?
Meteoric water identified in ore fluid	XX	XX	nd	nd	-	XX	nd	?
Magmatic ore S source identified	X	-	-	-	X	-	-	?
Sedimentary ore S source identified	XX	XX	XX	XX	-	XX	XX	?
Postore oxidation	XX	XX	XX	XX	XX	XX	XX	X

XX = important deposit feature, X = observed feature, - = not present, nd = no data, ? = unknown

One of the most notable differences between the Nadaleen Trend and Nevada's CTGDs is the age of the host rocks; the Carlin District host rocks are Paleozoic in age whereas the Nadaleen Trend host rocks are Ediacaran in age. Aside from the age of deposition, the host rocks and geological setting of the two deposits are similar. The host rocks of the Nadaleen

Trend are carbonates and mudstones which formed in a carbonate slope of a passive margin or intracratonic basin, and the Carlin District host rocks are silty carbonates which formed on a continental slope on the western margin of Laurentia (Cline et al., 2005).

Table 7. Maximum concentrations (in ppm) of selected trace elements in various paragenetic stages of the Nadaleen Trend (this study) and the Northern Carlin District (Large et al., 2009).
n.a. = not analyzed

	Early Diagenetic Pyrite - Nadaleen	Early Diagenetic Pyrite - N. Carlin	Base metal stage Pyrite - Nadaleen	Ore stage Pyrite - Nadaleen	Ore stage Pyrite - N. Carlin
Ag	12.00	620	4.49	74.00	1,000
V	1,810.00	4542	5.40	500.00	60
Ni	3,390.00	9601	2,290.00	2,870.00	100
Zn	600.00	3409	102.00	1,300.00	30
Mo	232.00	2657	444.00	280.00	150
Se	n.a.	3992	n.a.	n.a.	220
Mn	50,500.00	3000	201.00	11,600.00	60
As	2,900.00	73835	5,900.00	96,700.00	100,000
Au	0.89	1858	0.77	203.00	2,000

The mineral assemblage present in the base metal stage paragenetic stage is similar to MVTs, a class of Pb-Zn ore deposits which are generated through basinal migration of base metal-rich brines created through diagenetic processes in sedimentary basins (Anderson, 1975). A base metal mineralization stage is not an important aspect of most CTGDs (Cline et al. 2005), which differentiates the Nadaleen Trend from most CTGDs.

In the Carlin District it is theorized that rift-related structures were re-activated in the Eocene, accommodating the migration of gold-bearing fluids upward into the carbonate host rocks. The fluids were then channeled along thrust faults before depositing gold in the carbonate host rocks. There is no evidence of a re-activated rift structure in the Nadaleen Trend, but there are high-angle regional thrust faults that channeled ore fluids into the carbonate host rocks (Palmer, 2014). The age constraints of the Nadaleen Trend and Carlin District gold mineralization are different; the Nadaleen Trend mineralization occurred 74 – 42 Ma (Tucker, 2015) and the Carlin District mineralization occurred 42 to 36 Ma (Cline et al., 2005). The source of gold-bearing fluids in CTGDs is debated, with many authors having suggested a metamorphic/magmatic source (Muntean et al., 2011; Cline and Hofstra, 2000) and others having suggested a sedimentary source (Ilchik and Barton, 1997). The source of the Nadaleen Trend ore fluids is unknown, as the fluids have isotopically equilibrated with the host rocks, making it difficult to trace their origin.

Seawater is a likely source, although a magmatic origin cannot be ruled out, as there are dykes in the Nadaleen which range in age from 74 to 53 Ma (Tucker, 2015). These dykes are volumetrically minor though and there are no other major magmatic events recognized in the Rackla Belt between 74 and 42 Ma. The characteristic ore-stage alteration features of CTGDs (decarbonatization, silicification, argillization) are also present in some fault zones of the Nadaleen Trend, especially in the Conrad zone (Tucker, 2015). Trace element-rich arsenian pyrite is the host for Au in the Nadaleen Trend (Fig. 28d - 28h), as is the case with CTGDs. In the Carlin District, it is suggested that the Fe in the ore-stage pyrite was derived from dissolution of ferroan dolomite (Stenger et al., 1998). Decarbonatization of ferroan dolomite could be important in the Nadaleen Trend as there are large volumes of decarbonatized material near fault zones in parts of Osiris and Isis East. It has been suggested that trace element-rich (Ag, V, Ni, Zn, Mo, Se, Mn) Au-As-bearing pyrite may be the source of Au and As in ore-stage pyrite in CTGDs (Large et al., 2009). They proposed that during the deposition of black shales at the seafloor, pyrite is enriched in Au along with As, Ni, Zn, Ag, Mo, V, and Se, and that Au eventually becomes mobilized and is incorporated into ore-stage fluids. The near-surface diagenetic pyrite in the Nadaleen Trend also has significant concentrations of these metals, so it is possible that this early diagenetic enrichment is an important control for the ore stage (Table 2, Table 7). However, the concentrations of these metals in pyrite 1 are not as high as those in the early diagenetic pyrite of the Carlin District, perhaps due to the lack of large volumes of shale in the Gametrail Formation. Given the high concentrations of As and moderate concentrations of Au in pyrite 1 and 2 (Table 7), these are possible sources of ore-stage Au and As.

The post-ore stage of the Nadaleen Trend comprises realgar, orpiment, and fourth generation of calcite, which is similar to the post-ore mineral assemblage in CTGDs which typically involve orpiment, fluorite, realgar, calcite, and Fe-oxides (Cline et al., 2005). Given the above features, it seems suitable to classify the Nadaleen Trend as a Carlin-type gold deposit.

Chapter 3 - Conclusions

The Nadaleen Trend in central Yukon hosts the first Carlin-type gold mineralization to be discovered in Canada. The Osiris, Isis, and Isis East zones of the Eastern Nadaleen Trend were studied in order to examine diagenetic controls on hydrothermal fluid flow and gold mineralization. Prior to this study, company geologists and consultants determined that gold mineralization occurs in fault zones, but it was also observed that there is significant gold mineralization away from faults. This study reveals that away from the faults, gold mineralization is focused at hydrothermal dolomitization fronts in the Osiris and Isis East zones; minimal gold mineralization is found in the Isis zone, as it does not contain any dolomitization fronts. Hand sample descriptions, petrographic analyses, CL petrography, EMPA, and LA-ICP-MS were used to characterize the host rocks and all carbonate and pyrite paragenetic phases by their major, minor, and trace element composition. Bulk stable isotope analyses of carbon, oxygen, strontium, and sulfur as well as high-precision SIMS analyses of carbon and oxygen were used to gain an understanding of the possible sources of hydrothermal fluids.

These host rocks are lime mudstones, wackestones, rudstones, and diamictites which were deposited on a passive margin or intracratonal basin and are part of the Gametrail Formation of the Windermere Supergroup. The Isis zone is interpreted to be part of the overlying Blueflower Formation. They formed during the Ediacaran oxygenation event, a time during which the oceans became stratified with oxic water overlying euxinic, ferruginous, reducing water. These rocks are enriched in Mn, Fe, Sr, MREE, and have high Ce/Ce* values due to the euxinic and ferruginous character of the bottom seawater. Small amounts of framboidal pyrite were generated at the seafloor along with the carbonates. During near-surface diagenesis, large quantities of ferroan dolomite (dolomite 1) and pyrite (pyrite 1) were generated; the latter of which became highly enriched in trace metals including small amounts of gold. Enrichment in trace elements can be attributed to the anoxic character of diagenetic pore waters, as lack of oxygen prevented oxidative scavenging of metals.

During shallow/intermediate diagenesis, calcite veins formed with high Mn and Fe concentrations and high Ce/Ce* values, indicative of derivation from acidic, reducing hydrothermal fluids. A first generation of stylolites occurred after calcite veining. An MVT-style base metal mineralization event then occurred which produced large volumes of dolomite, pyrite, quartz, and minor amounts of sphalerite, barite, and enargite. Cathodoluminescent zoning in dolomite 2 suggests fluctuating redox conditions. This second dolomitization event created vast amounts of saddle dolomite-associated porosity, some of which was infilled by quartz/calcite and some of which remained unfilled. During intermediate diagenesis, 2 phases of calcite veining (calcite 2 and 3) and a second generation of stylolitization occurred. From the positive Eu anomalies, high Ce/Ce*

values, and high Mn and Fe content, it is suggested that calcite 2 and 3 were both derived from reducing, acidic fluids.

The ore stage occurred between 74 and 42 Ma and produced a third generation of dolomite as well as As-(Au)-bearing pyrite (pyrite 3). Much of the gold was deposited in steeply-dipping fault zones, but fluids also migrated laterally into the carbonates of the Gametrail Formation. Permeability associated with base metal-stage saddle dolomite and stylolites accommodated the lateral migration of these fluids. When the fluids encountered Fe-deficient, As-rich grains of pyrite 1 or 2, a sulfidation reaction occurred, resulting in deposition of gold-bearing arsenian pyrite rims on these pyrite grains. Limestones are generally not mineralized because they contain only rare pyrite. A post-ore stage comprising realgar, orpiment, and a fourth generation of calcite occurred next. The overall trace element concentration of calcite 4 is lower than all of the other carbonate phases, indicating that most metals had been exhausted by this point in the paragenesis.

The carbonate host rocks have $\delta^{18}\text{O}$ values typical of Ediacaran seawater carbonates, and the $\delta^{13}\text{C}$ values are very low because they formed during the Shuram ^{13}C excursion. The $\delta^{18}\text{O}$ values of all carbonate paragenetic phases except for calcite 1 are similar to the host rock, suggesting that the hydrothermal fluids isotopically equilibrated with the host rocks in most locations. As a result, the source of the fluids is unknown. Calcite 1 has $\delta^{18}\text{O}$ values lower than the other paragenetic phases, indicating that it may have been derived from hotter fluids. The estimated temperature of the base metal stage hydrothermal fluid is 100°C and the calculated $\delta^{18}\text{O}$ value is 4 to 5 ‰. The estimated temperature of the ore-stage fluid is 200°C and the calculated $\delta^{18}\text{O}$ value of the fluids is 7 to 13 ‰. The $\delta^{13}\text{C}$ values of all carbonate paragenetic phases are in the range of the host rocks, therefore it is suggested that the carbon isotopic composition of these phases is locally derived from the host rocks.

The $^{87}\text{Sr}/^{86}\text{Sr}$ values of the host rocks are similar to other Shuram-age carbonates, and the $^{87}\text{Sr}/^{86}\text{Sr}$ values of all carbonate paragenetic phases are all relatively high. This indicates that the hydrothermal fluids scavenged radiogenic Sr from a deeper unit during their migration, possibly the Little Dal Group. The $\delta^{34}\text{S}$ values of pyrite 1 are similar to the range of Shuram excursion-age seawater sulfate values, suggesting that it was generated in a system which was closed to sulfate (euxinic conditions). The $\delta^{34}\text{S}$ values of pyrite 2 are similar to those of pyrite 1, suggesting that it precipitated from seawater-derived sulfur. The $\delta^{34}\text{S}$ values of pyrite 3 were analyzed with low precision due to the small size of the pyrite 3 rims; similar values to pyrite 2 suggests that pyrite 3 was derived from an anoxic fluid system that was closed to sulfate.

The Nadaleen Trend meets most of the criteria for classification as a Carlin-type gold deposit. It is characterized by carbonate-hosted gold mineralization with regional thrust faults acting as feeder structures for gold-bearing fluids. Much of the mineralization is focused in decarbonatized, argillized, silicified fault zones, although significant mineralization is located at hydrothermal dolomitization fronts due to the permeability associated with saddle dolomite.

3.1 Implications for Exploration

In the Nadaleen Trend there are high gold grades associated with faulting, decarbonatization, argillization, and silicification, as described by Tucker (2015) and also in the hinges of anticlines as described by Palmer (2014). This study reveals that significant gold mineralization is also concentrated at dolomitization fronts. The highest gold grades in this study are in drill holes of Osiris and Isis East, whereas Isis is poorly mineralized due to lack of dolomitization fronts or pyrite. Two of the highest-grade intervals in this study are the depths of 106.07 to 121.31m in Osiris hole OS-11-52 in which the average gold grade is 3.53 g/T and the depths of 106.07 to 133.50m in Isis East hole OS-12-120 in which the average gold grade is 6.37 g/T. These highly mineralized intervals are spatially associated with dolomitization fronts, and are not proximal to any faults or CTGD-style alteration. Further gold mineralization could potentially be discovered by stratigraphically interpolating between drill holes and following the dolomitization fronts. It is recommended not to search in totally dolomitized areas such as Isis, but to focus on areas of the Gametrail Formation with alternating beds of limestone and hydrothermal dolostone.

Works Cited

- Acosta-Gongora, P., and Gleeson, S.A., 2011, Petrographic and Scanning Electron Microscope Study of Ore Samples from Osiris, Nadaleen Trend, Yukon. Prepared for ATAC Resources, Internal Report.
- Aitken, J. D., 1989, Uppermost Proterozoic Formations in Central Mackenzie Mountains, Northwest Territories. Geological Survey of Canada Bulletin.
- Anderson, G.M., 1975, Precipitation of Mississippi Valley-Type Ores. *Economic Geology*, v. 70, p. 937–942.
- Arehart, G. B., Chakurian, A. M., and Tretbar, D.R., 2003, Evaluation of Radioisotope Dating of Carlin-Type Deposits in the Great Basin, Western North America, and Implications for Deposit Genesis. *Economic Geology*, v. 98, p. 235–48.
- Arehart, G. B., Chryssoulis, S.L., and Kesler, S.E., 1993, Gold and Arsenic in Iron Sulfides from Sediment-Hosted Disseminated Gold Deposits: Implications for Depositional Processes. *Economic Geology*, v. 88, p. 171–85.
- Armstrong, R.L., 1988, Mesozoic and Early Cenozoic Magmatic Evolution of the Canadian Cordillera. In *Processes in Continental Lithospheric Deformation*. Geological Society of America Special Paper 218, p. 55–91.
- ATAC Resources Ltd. 2011a, ATAC Resources Drills 26.12 Metres of 6.08 g/T Gold at Osiris Zone. Isis East Discovery Hole Intersects 38.10 Metres of 3.33 g/T Gold. Retrieved from http://www.atacresources.com/s/NewsReleases.asp?ReportID=488465&_Type=News-Releases&_Title=ATAC-Resources-Drills-26.12-Metres-of-6.08-gt-Gold-at-Osiris-Zone.-Isis-Eas...
- . 2011b, ATAC Resources Announces Initial Resource Estimates for its Tiger Gold Deposit, Yukon. October 20, 2011. Retrieved from <http://www.atacresources.com/news/news-releases/atac-resources-announces-initial-resource-estimate-for-its-tiger-gold-deposit-yukon>
- . 2012a, ATAC Resources Ltd. Intersects 42.93 M of 18.44 g/T Gold at Its Rackla Gold Project, Yukon. August 21, 2012. Retrieved from <http://www.atacresources.com/news/news-releases/atac-resources-ltd-intersects-42-93-m-of-18-44-g-t-gold-at-its-rackla-gold-project-yukon>
- . 2012b. ATAC Resources Ltd . Announces 2012 Exploration and Drilling Plans for Its Rackla Gold Project, Yukon. March 1, 2012. Retrieved from <http://www.atacresources.com/news/news-releases/atac-resources-ltd-announces-2012-exploration-and-drilling-plans-for-its-rackla-gold-project-yukon>

- . 2013. ATAC Resources Ltd. Drills 16.76 M of 6.76 G/t Gold at Sunrise Rackla Gold Project, Yukon. Sept 10, 2013. Retrieved from <http://www.atacresources.com/news/news-releases/atac-resources-ltd-drills-16-76-m-of-6-76-g-t-gold-at-sunrise-rackla-gold-project-yukon>
- . 2014. ATAC Advances Carlin-Type Gold Targets in the Anubis Area , Rackla Gold Project - Yukon. October 28, 2014. Retrieved from <http://www.atacresources.com/news/news-releases/atac-advances-carlin-type-gold-targets-in-the-anubis-area-rackla-gold-project-yukon>
- Bakken, B. M., 1990, Gold Mineralization, Wall-Rock Alteration and the Geochemical Evolution of the Hydrothermal System in the Main Ore Body, Carlin Mine, Nevada: PhD Thesis. Stanford University.
- Barker, S. L.L., Hickey, K.A., Cline, J.S. Dipple, G.M., Kilburn, M.R., Vaughan, J.R., and Longo, A.A., 2009. Uncloaking invisible gold: use of nanosims to evaluate gold⁰, trace elements, and sulfur isotopes in pyrite from Carlin-type gold deposits. *Economic Geology*, v.104, p. 897–904.
- Bau, M., 1996, Controls on the Fractionation of Isovalent Trace Elements in Magmatic and Aqueous Systems: Evidence from Y/Ho, Zr/Hf, and Lanthanide Tetrad Effect. *Contrib Mineral Petrol*, v. 123, p. 323–33.
- Bell, R.T., and Jefferson, C.W., 1987, A Hypothesis for an Australian– Canadian Connection in the Late Proterozoic and the Birth of the Pacific Ocean. In: *Proceedings of Pacific Rim Congress '87*, Parkville, Victoria, Australia. The Australasian Institute of Mining and Metallurgy, Carlton, Victo, 39–50.
- Benning, L. G., and Seward, T.M., 1996, Hydrosulfide Complexing of Au(I) in Hydrothermal Solutions from 150°–400°C and 500–1500 Bar. *Geochimica et Cosmochimica Acta*, v. 60 (11), p. 1849–1871.
- Bolhar, R., and Van Kranendonk, M.J., 2007, A Non-Marine Depositional Setting for the Northern Fortescue Group, Pilbara Craton, Inferred from Trace Element Geochemistry of Stromatolitic Carbonates. *Precambrian Research*, v. 155, p. 229–250.
- Böttcher, M.E. 1994, ¹³C/¹²C and ¹⁸O/¹⁶O Fractionation during Synthesis of BaMg(CO₃)₂ and PbMg(CO₃)₂. Abstracts of the 16th IMA Meeting, p. 53.
- Budd, D. A., Hammes, U., and Ward, B.W., 2000, Cathodoluminescence in Calcite Cements: New Insights on Pb and Zn Sensitizing, Mn Activation, and Fe Quenching at Low Trace-Element Concentrations. *Journal of Sedimentary Research*, v. 70 (1), p. 217-226.

- Burns, S.J., Haudenschild, U., and Matter, A., 1994, The Strontium Isotopic Composition of Carbonates from the Late Precambrian (560-540 Ma) Huqf Group of Oman. *Chemical Geology*, v. 111, p. 269–282.
- Butler, I. B., and Rickard, D.T., 2000, Framboidal Pyrite Formation via the Oxidation of Iron(II) Monosulfide by Hydrogen Sulphide. *Geochimica et Cosmochimica Acta*, v. 64 (15), p. 2665–2672.
- Calver, C.R. 2000, Isotope Stratigraphy of the Ediacarian (Neoproterozoic III) of the Adelaide Rift Complex, Australia, and the Overprint of Water Column Stratification. *Precambrian Research*, v. 100, p. 121–150.
- Canfield, D.E. 2005, The Early History of Atmospheric Oxygen: Homage to Robert M. Garrels. *Annu. Rev. Earth Planet. Sci.*, v. 33, p. 1–36.
- Carozzi, A. V., and Von Bergen, D., 1987, Stylolitic Porosity in Carbonates: A Critical Factor for Deep Hydrocarbon Production. *Journal of Petroleum Geology*, v. 10 (3), p. 267–82.
- Cline, J.S., Hofstra, A.H., Muntean, J.L., Tosdal, R.M., and Hickey, K.A., 2005, Carlin-Type Gold Deposits in Nevada: Critical Geologic Characteristics and Viable Models. *Economic Geology 100th Anniversary Volume*, p. 451–84.
- Cline, J. S., and Hofstra, A.H., 2000, Ore-Fluid Evolution at the Getchell Carlin-Type Gold Deposit, Nevada, USA. *European Journal of Mineralogy*, v. 12, p. 195–212.
- Colpron, M., Logan, J.M., and Mortensen, J.K., 2002, U-Pb Zircon Age Constraint for Late Neoproterozoic Rifting and Initiation of the Lower Paleozoic Passive Margin of Western Laurentia. *Canadian Journal of Earth Sciences*, v. 39 (2), p. 133–43.
- Colpron, M., Moynihan, D. Israel, S. and Abbott, G., 2013, Bedrock Geology of the Rackla Belt (106D / 1 and 106C / 1-4), Southern Nadaleen Map Area: Structural Inheritance along the Rackla Belt.
- . 2013. Bedrock Geology of the Rackla Belt (106D / 1 and 106C/1-4), Southern Nadaleen Map Area. Yukon Geological Survey: Poster (#3) presented at 2013 AME BC Mineral Exploration Roundup Conference. Vancouver, B.C. January 28 - 31, 2013.
- Coney, P.J., Jones, D.L., and Monger, J.W.H., 1980, Cordilleran Suspect Terranes. *Nature*, v. 288, p. 329–33.
- Cook, N. J., and Chryssoulis, S.L., 1990, Concentrations of ‘Invisible Gold’ in the Common Sulfides. *Canadian Mineralogist*, v. 28, p. 1–16.

- Dalziel, I.W.D. 1991, Pacific Margins of Laurentia and East Antarctica – Australia as a Conjugate Rift Pair: Evidence and Implications for an Eocambrian Supercontinent. *Geology*, v. 19, p. 598–601.
- Deditius, A. P., Reich, M. Kesler, S.E., Utsunomiya, S., Chryssoulis, S.L., Walshe, J., and Ewing, R.C., 2014. The Coupled Geochemistry of Au and As in Pyrite from Hydrothermal Ore Deposits. *Geochimica et Cosmochimica Acta*, v. 140, p. 644–670.
- Derry, L.A., 2010. A Burial Diagenesis Origin for the Ediacaran Shuram–Wonoka Carbon Isotope Anomaly. *Earth and Planetary Science Letters*, v. 294 (1-2), p. 152–62.
- Eisenbacher, G.H. 1981. Sedimentary Tectonics and Glacial Record in the Windermere Supergroup, Mackenzie Mountains, North-Western Canada. *Geological Survey of Canada Paper*, 80-27, 40 P.
- Emsbo, P., Hofstra, A.H., Lauha, E.A., Griffin, G.L. and Hutchinson, R.W., 2003, Origin of High-Grade Gold Ore, Source of Ore Fluid Components, and Genesis of the Meikle and Neighboring Carlin-Type Deposits, Northern Carlin Trend, Nevada. *Economic Geology*, v. 98 (2), p. 1069–1105.
- Fan, H., Zhu, X., Wen, H., Yan, B., Li, J., and Feng, ., 2014, Oxygenation of Ediacaran Ocean Recorded by Iron Isotopes. *Geochimica et Cosmochimica Acta*, v. 140, p. 80–94.
- Fayek, M., Harrison, M. T., Grove, M., McKeegan, K.D., Coath, C.D., and Boles, J.R., 2001. In Situ Stable Isotopic Evidence for Protracted and Complex Carbonate Cementation in a Petroleum Reservoir, North Coles Levee, San Joaquin Basin, California, U.S.A. *Journal of Sedimentary Research*, v. 71 (3), p. 444–458.
- Fike, D.A., Grotzinger, J.P., Pratt, L.M., and Summons, R.E., 2006, Oxidation of the Ediacaran Ocean. *Nature*, v. 444, p. 744–747.
- Fleet, M. E., and Mumin, A.H., 1997, Gold-Bearing Arsenian Pyrite and Marcasite and Arsenopyrite from Carlin Trend Gold Deposits and Laboratory Synthesis. *American Mineralogist*, v. 82, p. 182–193.
- Frimmel, H. E., 2009, Trace Element Distribution in Neoproterozoic Carbonates as Palaeoenvironmental Indicator. *Chemical Geology*, v. 258 (3-4), p. 338–53.
- Gleeson, S. A., 2012, The Relationship between Cementation History and Mineralization at the Osiris Gold Deposit, Nadaleen Trend, Yukon. Prepared for ATAC Resources, Internal Report.
- Gregg, J.M., Sibley, D.F., 1984, Epigenetic Dolomitization and the origin of xenotopic dolomite texture. *Jour. Sed. Petrology*, v. 54, p. 908–931.

- Grosjean, E., Adam, P., Connan, J., and Albrecht, P., 2004, Effects of Weathering on Nickel and Vanadyl Porphyryns of a Lower Toarcian Shale of the Paris Basin. *Geochimica et Cosmochimica Acta*, v. 68, p. 789–804.
- Haley, B. A., Klinkhammer, G.P., and McManus, J., 2004, Rare Earth Elements in Pore Waters of Marine Sediments. *Geochimica et Cosmochimica Acta*, v. 68 (6), p. 1265–1279.
- Halverson, G. P., Dudás, F. Ö., Maloof, A.C., and Bowring, S.A., 2007, Evolution of the $^{87}\text{Sr}/^{86}\text{Sr}$ Composition of Neoproterozoic Seawater. *Palaeogeography, Palaeoclimatology, Palaeoecology*, v. 256 (3-4), p. 103–29.
- Hanchar, J. M., and Van Westrenen, W., 2007, In: *Zircon – Melt Systems*, p. 37–42.
- Hiatt, E.E., and Pufahl, P.K., 2014, Cathodoluminescence of carbonate rocks: a review of applications for understanding diagenesis, reservoir quality, and pore system evolution. In: *CL Petrography of Carbonate Rocks*.
- Hickey, K. A., Ahmed, A.D., Barker, S.L.L., and Leonardson, R., 2014a, Fault-Controlled Lateral Fluid Flow Underneath and Into a Carlin-Type Gold Deposit : Isotopic and Geochemical Footprints. *Society of Economic Geologists*, v. 109, p. 1431–1460.
- Hickey, K. A., Barker, S.L.L., Dipple, G.M., Arehart, G.B., and Donelick, R.A., 2014b, The Brevity of Hydrothermal Fluid Flow Revealed by Thermal Halos around Giant Gold Deposits: Implications for Carlin-Type Gold Systems. *Society of Economic Geologists*, v. 109, p. 1461–87.
- Hill, C.A., 1995, H₂S-Related Porosity and Sulfuric Acid Oil-Field Karst. In: Budd, D.A., Saller, A.H., Harris, P.M. (eds), *Unconformities and Porosity in Carbonate Strata*. AAPG Mem. v. 63, 301–6.
- Hofstra, A. H., Leventhal, J.S., Northrop, H.R., Landis, G.P., Rye, R., Birak, D.J., and Dahl, A.R., 1991, Genesis of Sediment-Hosted Disseminated Gold Deposits by Fluid Mixing and Sulfidization: Chemical-Reaction-Path Modeling of Ore-Depositional Processes Documented in the Jerritt Canyon District, Nevada. *Geology*, v. 19, p. 36–40.
- Hofstra, A., Snee, L.W., Rye, R.O., Folger, H.W., Phinisey, J.D., Loranger, J., Dahl, A.R., Naeser, C.W., Stein, H.J., and Lewchuk, M., 1999, Age Constraints on Jerritt Canyon and Other Carlin-Type Gold Deposits in the Western United States - Relationship to Mid-Tertiary Extension and Magmatism. *Economic Geology*, v. 94, p. 769–802.
- Hood, A. V., and Wallace, M.W., 2015, Extreme Ocean Anoxia during the Late Cryogenian Recorded in Reefal Carbonates of Southern Australia. *Precambrian Research*, v. 261, p. 96–111.

- Horita, J. 2014, Oxygen and Carbon Isotope Fractionation in the System dolomite–water–CO₂ to Elevated Temperatures. *Geochimica et Cosmochimica Acta*, v. 129, p. 111–124.
- Hsu, K.J. 1967, Chemistry of Dolomite Formation. *Elsevier Dev. Sediment*, v. 9b, p. 169–191.
- Ilchik, R.P., and Barton, M.D., 1997, An Amagmatic Origin of Carlin-Type Gold Deposits. *Economic Geology*, v. 92, p. 269–288.
- Jacobsen, S. B., and Kaufman, A.J., 1999, The Sr, C and O Isotopic Evolution of Neoproterozoic Seawater. *Chemical Geology*, v. 161 (1-3), p. 37–57.
- Jiang, G.Q., Kaufman, A.J., Christie-Blick, N. Zhang, S.H., and Wu, H.C., 2007, Carbon Isotope Variability across the Ediacaran Yangtze Platform in Southern China: Implications for a Large Surface-to Deep Ocean Delta C-13 Gradient. *Earth and Planetary Science Letters*, v. 261, p. 303–20.
- Jiang, G., Shi, X., Zhang, S., Wang, Y., and Xiao, S., 2011, Stratigraphy and Paleogeography of the Ediacaran Doushantuo Formation (ca. 635–551Ma) in South China. *Gondwana Research*, v. 19 (4), p. 831–849.
- Jones, B., and Manning, D.A.C., 1994, Comparison of geochemical indices used for the interpretation of palaeoredox conditions in ancient mudstones. *Chemical Geology*, v. 114, p. 111–129.
- Joosu, L., Lepland, A., Kirsimäe, K., Romashkin, A.E., Roberts, N.M.W., Martin, A.P., and Črne, A.E., 2015, The REE-Composition and Petrography of Apatite in 2Ga Zaonega Formation, Russia: The Environmental Setting for Phosphogenesis. *Chemical Geology*, v. 395, p. 88–107.
- Ketner, K. B., 1977, Late Paleozoic Orogeny and Sedimentation, Southern California, Nevada, Idaho, and Montana. In: *Paleozoic Paleogeography of the Western United States: Pacific Section*, Society of Economic Paleontologists and Mineralogists, Pacific Coast Paleogeography Symposium, edited by J.H. Stewart, C.H. Stevens, and A.E. Fritsche, p. 363–369.
- Kuehn, C.A., and Rose, A.W., 1992, Geology and Geochemistry of Wall-Rock Alteration at the Carlin Gold Deposit, Nevada. *Economic Geology*, v. 87, p. 1697–1721.
- Land, L.S. 1980, The isotopic and trace element geochemistry of dolomite: the state of the art. *Society of Economic Paleontologists Special Publication no. 28*, p.87-110
- Li, Z.X., Zhang, L., and Powell, C., 1995, South China in Rodinia: Part of the Missing Link between Australia – East Antarctica and Laurentia?, *Geology*, v. 23, p. 407–410.

- Loyd, S. J., Marengo, P.J., Hagadorn, J.W., Lyons, T.W., Kaufman, A.J., Sour-Tovar, F., and Corsetti, F.A., 2013, Local $\delta^{34}\text{S}$ Variability in ~580 Ma Carbonates of Northwestern Mexico and the Neoproterozoic Marine Sulfate Reservoir. *Precambrian Research*, v. 224, p. 551–569.
- Macdonald, F.A., Strauss, J.V., Sperling, E.A., Halverson, G.P., Narbonne, G.M., Johnston, D.T., Kunzmann, M., Schrag, D.P., and Higgins, J.A., 2013, The Stratigraphic Relationship between the Shuram Carbon Isotope Excursion, the Oxygenation of Neoproterozoic Oceans, and the First Appearance of the Ediacara Biota and Bilaterian Trace Fossils in Northwestern Canada June Beds. *Chemical Geology*, v. 362, p. 250–72.
- Machel, H. G., 1999, Effects of Groundwater Flow on Mineral Diagenesis, with Emphasis on Carbonate Aquifers. *Hydrogeology Journal*, v.7, p. 94–107.
- Mair, J. L., Hart, C.J.R., and Stephens, J.R., 2006, Deformation History of the Northwestern Selwyn Basin, Yukon, Canada: Implications for Orogen Evolution and Mid-Cretaceous Magmatism. *Geological Society of America Bulletin* 118 (3-4), p. 304–323.
- McFadden, K.A., Huang, J., Chu, X., Jiang, G., Kaufman, A.J., Zhou, C., Yuan, X., and Xiao, S., 2008, Pulsed Oxidation and Biological Evolution in the Ediacaran Doushantuo Formation. *Proceedings of the National Academy of Science*, v. 105 (9), p. 3197–3202.
- Misra, K.C. 2000. *Understanding Mineral Deposits*, p. 158-160.
- Monger, J.W.H., Price, R.A., and Templeman-Kluit, D.J., 1982, Tectonic Accretion and the Origin of the Two Major Metamorphic and Plutonic Belts in the Canadian Cordillera. *Geology*, v. 10, p. 70–75.
- Moores, E.M., 1991. Southwest U.S. – East Antarctic (SWEAT) Connection: A Hypothesis. *Geology*, v. 19, p. 425–28.
- Morse, J.W., and Luther, G.W., 1999, Chemical Influences on Trace Metal-Sulfide Interactions in Anoxic Sediments. *Geochimica et Cosmochimica Acta*, v. 63, p. 3373–3378.
- Mountjoy, E.W., Machel, H.G., Green, D., and Duggan, J., 1999, Devonian Matrix Dolomites and Deep Burial Carbonate Cements: A Comparison between the Rimbey-Meadowbrook Reef Trend and the Deep Basin of West-Central Alberta. v. 47 (4), p. 487–509.

- Moynihan, D., Colpron, M., Israel, S. and Abbott, G., 2014, Geology of the Eastern Rackla Belt, East-Central Yukon. Yukon Geological Survey: Poster presented at 2014 AME BC Mineral Exploration Roundup Conference. Vancouver, B.C. January 27 - 30, 2014.
- Muntean, J. L., Cline, J.S., Simon, A.C., and Longo, A.A., 2011, Magmatic–hydrothermal Origin of Nevada’s Carlin-Type Gold Deposits. *Nature Geoscience*, v. 4 (2), p. 122–127.
- Narbonne, G. M., and Aitken, J.D., 1993, Neoproterozoic of the Mackenzie Mountains, Northwestern Canada. *Precambrian Research*, v. 73, p. 101–121.
- Nelson, J., Paradis, S., Christensen, J. and Gabites, J., 2002, Canadian Cordilleran mississippi valley-type deposits; a case for Devonian-Mississippi back-arc hydrothermal origin. *Econ. Geol.*, v. 97, p. 1013–1036.
- Norris, D.K., and Dyke, L.D., 1997, Proterozoic. In *The Geology, Mineral, and Hydrocarbon Potential of Northern Yukon Territory and Northwestern District of Mackenzie*. Edited by D.K. Norris. Geological Survey of Canada Bulletin 422, Chap. 4, p. 65–84.
- Nothdurft, L. D., Webb, G.E., and Kamber, B.S., 2004, Rare Earth Element Geochemistry of Late Devonian Reefal Carbonates, Canning Basin, Western Australia: Confirmation of a Seawater REE Proxy in Ancient Limestones. *Geochimica et Cosmochimica Acta*, v. 68 (2), p. 263–283.
- Ohmoto, H., and Goldhaber, M.B., 1997, Sulfur and Carbon Isotopes. In: *Geochemistry of Hydrothermal Ore Deposits*, p. 517–600.
- Palmer, J. C., 2014, Structural Geology and Geochemistry of Sedimentary Rock-Hosted Gold in the Eastern Nadaleen Trend, Yukon Territory, Canada.
- Pals, D.W., Spry, P.G., and Chryssoulis, S.L., 2003, Invisible Gold and Tellurium in Arsenic-Rich Pyrite from the Emperor Gold Deposit, Fiji: Implications for Gold Distribution and Deposition. *Economic Geology*, v. 98, p. 479–493.
- Perkins, W.T., and Pearce, N.G.J., 1995, Mineral Microanalysis by Laserprobe Inductively Coupled Plasma Mass Spectrometry. Chapman & Hall, London, p. 291–325.
- Pigage, L.C., Sack, P.J., Torgerson, D., and Deklerk, R., 2014, Yukon Hardrock Mining, Development, and Exploration Overview 2013. MacFarlane, K.E. Nordling, M.G. (Eds.), *Yukon Mines and Exploration and Geology Overview 2013*, p. 21–47.
- Pokrovski, G.S., Kara, S., and Roux, J., 2002, Stability and Solubility of Arsenopyrite, FeAsS, in Crustal Fluids. *Geochimica et Cosmochimica Acta*, v. 66, p. 2361–2378.

- Pourmand, A., Dauphas, N., and Ireland, T.J., 2012, A Novel Extraction Chromatography and MC-ICP-MS Technique for Rapid Analysis of REE , Sc and Y: Revising CI-Chondrite and Post-Archean Australian Shale (PAAS) Abundances. *Chemical Geology*, v. 291.p. 38–54.
- Powell, C. McA., McElhinny, M.W., Li, Z.X., Meert, J.G., and Park, J.K., 1993, Paleomagnetic Constraints on Timing of the Neoproterozoic Breakup of Rodinia and the Cambrian Formation of Gondwana. *Geology*, v. 21, p. 889–892.
- Price, J. G., and Meeuwig, R.O., 2004, Overview: In Nevada Bureau of Mines and Geology Special Publication MI-2003: The Nevada Mineral Industry 2003. Nevada Bureau of Mines and Geology Special Publication MI-2003. 78 p.
- Radtke, A. S., Rye, R.O., and Dickson, F.W., 1980, Geology and Stable Isotope Studies of the Carlin Gold Deposit, Nevada. *Society of Economic Geologists*, v. 75, p. 641–72.
- Rainbird, R.H., Jefferson, C.W., and Young, G.M., 1996, The Early Neoproterozoic Sedimentary Succession B of Northwestern Laurentia: Correlations and Paleogeographic Significance. *Geological Society of America Bulletin* 108, p. 454–470.
- Raiswell, R., and Berner, R.A., 1985. Pyrite Formation in Euxinic and Semi-Euxinic Settings. *American Journal of Science*, v. 285, p. 710- 724.
- Reich, M., Kesler, S.E., Utsunomiya, S., Palenik, C.S., Chryssoulis, S.L., and Ewing, R.C., 2005, Solubility of Gold in Arsenian Pyrite. *Geochimica et Cosmochimica Acta*, v. 69 (11), p. 2781–2796.
- Roberts, R.J., Hotz, P.E., Gilluly, J., and Ferguson, H.G., 1958, Paleozoic Rocks of North-Central Nevada. *American Association of Petroleum Geologists Bulletin* 42, p. 2813–2857.
- Ross, G.M., Bloch, J.D., and Krouse, H.R., 1995, Neoproterozoic Strata of the Southern Canadian Cordillera and the Isotopic Evolution of Seawater Sulphate. *Precambrian Research*, v. 73, p. 71–99.
- Schrag, D. P., Higgins, J.A., MacDonald, F.A., and Johnston, D.T., 2013, Authigenic Carbonate and the History of the Global Carbon Cycle. *Science*, v. 39, p. 540–543.
- Schulman, J.H., Evans, L.W., Ginther, R.J., and Murata, K.J., 1947. The Sensitized Luminescence of Manganese-Activated Calcite. *Journal of Applied Physics*, v. 18, p. 732-739.
- Scott, R.J., Meffre, S., Woodhead, J. E., Sarah, G., Berry, R.F., and Emsbo, P., 2009, Development of Framboidal Pyrite During Diagenesis , Low-Grade Regional

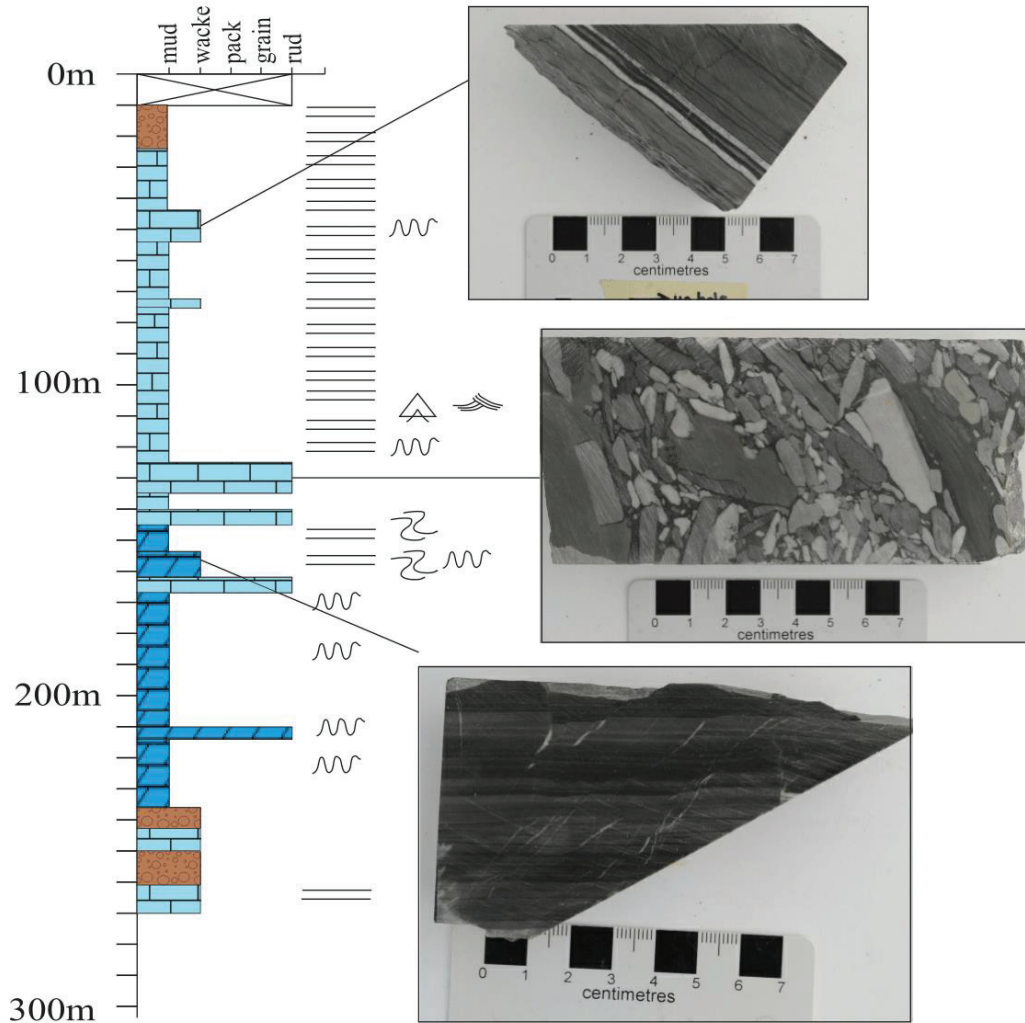
- Metamorphism, and Hydrothermal Alteration. *Economic Geology*, v. 104, p. 1143–1168.
- Sears, J.W., and Price, R.A., 2000, New Look at the Siberian Connection: No SWEAT. *Geology* v. 28, p. 423–426.
- Shields, G.A., and Webb, G.E., 2004, Has the REE Composition of Seawater Changed over Geological Time? *Chemical Geology*, v. 204, p. 103–107.
- Shields-Zhou, G., and Och, L., 2008, The Case for a Neoproterozoic Oxygenation Event: Geochemical Evidence and Biological Consequences. *GSA Today*, v. 21, p. 4–11.
- Sibley, D.F., and Gregg, J.M., 1987, Classification of Dolomite Rock Textures. *Journal of Sedimentary Petrology*, v. 57, p. 967–975.
- Stenger, D. P., Kesler, S.E., Peltonen, D.R., and Tapper, C.J., 1998, Deposition of Gold in Carlin-Type Deposits: The Role of Sulfidation and Decarbonation at Twin Creeks, Nevada. *Economic Geology*, v. 93, p. 201-215
- Stoffell, B, Appold, M.S., Wilkinson, J.J., McClean, N.A., and Jeffries, T.E., 2008, Geochemistry and Evolution of Mississippi Valley-Type Mineralizing Brines from the Tri-State and Northern Arkansas Districts Determined by LA-ICP-MS Microanalysis of Fluid Inclusions. *Society of Economic Geologists*, v. 103, p. 1411–1135.
- Tahata, M., Ueno, Y., Ishikawa, T., Sawaki, Y., Murakami, K., Han, J., Shu, D., 2013, Carbon and Oxygen Isotope Chemostratigraphies of the Yangtze Platform , South China: Decoding Temperature and Environmental Changes through the Ediacaran. *Gondwana Research*, v. 23 (1), p. 333–353.
- Tanaka, K., Takahashi, Y., and Shimizu, H., 2008, Local Structure of Y and Ho in Calcite and Its Relevance to Y Fractionation from Ho in Partitioning between Calcite and Aqueous Solution, v. 248, p. 104–113.
- Theodore, T. G., Berger, V.I., Singer, D.A., Harris, A.G., and Stevens, C.H., 2004, Synthrusting Deposition of the Pennsylvanian and Permian Strathearn Formation , Northern Carlin Trend, Nevada. *Sedimentary Geology*, v. 165, p. 1–28.
- Thorkelson, D. J., Abbott, J.G., Mortensen, J.K., Creaser, R.A., Villeneuve, M.E., Mcnicoll, V.I., and Layer, P.W., 2005, Early and Middle Proterozoic Evolution of Yukon , *Canadian Journal of Earth Sciences*, v. 42, p. 1045–1071.
- Tretbar, D. R., Arehart, G.B., and Christensen, J.N., 2000, Dating Gold Deposition in a Carlin-Type Gold Deposit Using Rb/Sr Methods on the Mineral Galkhaite. *Geology*, v. 28 (10), p. 947–950.

- Tribovillard, N., Algeo, T.J., Lyons, T., and Riboulleau, A., 2006, Trace Metals as Paleoredox and Paleoproductivity Proxies: An Update. *Chemical Geology*, v. 232 (1-2), p. 12–32.
- Tucker, M. J., Hart, C.J.R., and Carne, R.C., 2013, Geology, Alteration, and Mineralization of the Carlin-Type Conrad Zone, Yukon. In: *Yukon Exploration and Geology 2012*. K.E. MacFarlane, M.G. Nordling, and P.J. Sack (eds), Yukon Geological Survey, p. 163–78.
- Tucker, M. J. 2015, *Geology, Mineralization and Geochronology of the Conrad Zone Carlin-Type Gold Deposit, East-Central Yukon Territory, Canada*.
- Van Geet, M., Swennen, R., and Wevers, M., 2000, Quantitative Analysis of Reservoir Rocks by Microfocus X-Ray Computerised Tomography. *Sedimentary Geology*, v. 132 (1-2), p. 25–36.
- Veizer, J. 1983, Trace Elements and Isotopes in Sedimentary Carbonates. *Rev. Mineral. Geochem*, v. 11, p. 265–299.
- Wallace, S. 2009, *University of Alberta The Genesis of the Gayna River Carbonate-Hosted Zn-Pb Deposit by Master of Science Department of Earth and Atmospheric Sciences*.
- Wang, L., Shi, X., and Jiang, G., 2012, Pyrite Morphology and Redox Fluctuations Recorded in the Ediacaran Doushantuo Formation. *Palaeogeography, Palaeoclimatology, Palaeoecology* v. 333-334, p. 218–27.
- Wang, W., Zhou, C., Guan, C., Yuan, X., Chen, Z., and Wan, B., 2014, An Integrated carbon, oxygen, and strontium isotopic studies of the Lanthian Formation in South China with implications for the Shuram anomaly. *Chemical Geology* v. 373, p. 10–26.
- Warren, J. 2000, Dolomite: Occurrence, Evolution and Economically Important Associations. *Earth-Science Reviews*, v. 52 (1-3), p. 1–81.
- Wells, J. D., and Mullens, T.E., 1973, Gold-Bearing Arsenian Pyrite Determined by Microprobe Analysis, Cortez and Carlin Gold Mines, *Economic Geology*, v. 68, p. 187–201.
- Wilkin, R. T., Barnes, H.L., and Brantley, S.L., 1996, The Size Distribution of Framboidal Pyrite in Modern Sediments: An Indicator of Redox Conditions, v. 60 (20), p. 3897–3912.
- Wilkinson, J.J., Crowther, H.L., and Coles, B.J., 2011, Chemical Mass Transfer during Hydrothermal Alteration of Carbonates: Controls of Seafloor Subsidence, Sedimentation and Zn–Pb Mineralization in the Irish Carboniferous. *Chemical Geology*, v. 289 (1-2), p. 55–75.

- Windgate, M.T.D., and Giddings, J.W., 2000, Age and Paleomagnetism of the Mundine Well Dyke Swarm, Western Australia: Implications for an Australia–Laurentia Connection at 750 Ma. *Precambrian Research*, v. 100, p. 335–357.
- Wright, J., Schrader, H., and Holser, W.T., 1987, Paleoredox variations in ancient oceans recorded by rare earth elements in fossil apatite. *Geochim Cosmochim Acta*, v. 51, p. 631–644.
- Zhelezinskaia, I., Kaufman, A.J., Farquhar, J., and Cliff, J., 2014, Large Sulfur Isotope Fractionations Associated with Neoproterozoic Microbial Sulfate Reduction. *Science*, v. 346, p. 742–744.
- Zhou, C., Jiang, S., Xiao, S., Chen, Z., and Yuan, X. 2012. Rare Earth Elements and Carbon Isotope Geochemistry of the Doushantuo Formation in South China : Implication for Middle Ediacaran Shallow Marine Redox Conditions, v. 57 (16), p. 1998–2006.

Appendix A – Extra Stratigraphic Logs

OS-11-80 (Osiris)



Legend	
	Limestone
	Early Diagenetic Dolostone
	Hydrothermal Dolostone
	Diamictite
	Intraclasts
	Soft-sediment deformation
	Ripples
	Grading
	Parallel Lamination
	Stylolites
	Cross-bedding

Appendix B – EMPA operating conditions

Table 8. EMPA operating conditions for WDS analyses.

Date	Analyte	Spot diameter (μm)	Accelerating voltage (kV)	Probe current (nA)	Peak scan time (sec)	Background scan time (sec)
12/12/2013	Carbonates	10	15	10.1	50 ^A	100 ^B
13/12/2013	Carbonates	10	15	10.1	50 ^C	100 ^D
22/1/2014	Sulfides	1	15	50.0	30	60
23/1/2014	Sulfides	1	15	50.0	30	60
27/3/2014	Carbonates	10	15	10.1	15	30
31/3/2014	Sulfides	1	15	30.4 ^E	30	60
1/4/2014	Sulfides	1	15	30.4 ^F	30	60
29/8/2014	Sulfides	1	15	30.3 ^G	15 ^H	30 ^I
2/12/2014	Carbonates	10	15	10.1	15	30
5/2/2015	Carbonates	10	15	10.1	15	30

^A Scan times ranged from 15 to 100 s

^B Scan times ranged from 30 to 100 s

^C Scan times ranged from 15 to 100 s

^D Scan times ranged from 30 to 100 s

^E Prb. current ranged from 30.4 to 30.5 nA

^F Prb. current ranged from 30.4 to 30.5 nA

^G Prb. current ranged from 30.1 to 30.5 nA

^H Scan times ranged from 15 to 15 s

^I Scan times ranged from 20 to 30 s

Appendix C – Whole-rock Geochemistry Au grades

Drill Hole	Depth Interval (m)		Au grade (g/T)	Drill Hole	Depth Interval (m)		Au grade (g/T)
OS -11-041	0	to 3.05	0.09	OS -11-041	156.97	to 160.02	0.01
OS -11-041	3.05	to 6.1	0.03	OS -11-041	160.02	to 163.07	0.05
OS -11-041	6.1	to 9.14	0.02	OS -11-041	163.07	to 166.12	0.03
OS -11-041	9.14	to 12.19	0.01	OS -11-041	166.12	to 169.16	0.02
OS -11-041	12.19	to 15.24	-	OS -11-041	169.16	to 172.21	-
OS -11-041	15.24	to 18.29	-	OS -11-041	172.21	to 175.26	-
OS -11-041	18.29	to 21.34	-	OS -11-041	175.26	to 178.31	-
OS -11-041	21.34	to 24.38	0.01	OS -11-041	178.31	to 181.36	-
OS -11-041	24.38	to 27.43	-	OS -11-041	181.36	to 184.4	-
OS -11-041	27.43	to 30.48	-	OS -11-041	184.4	to 187.45	-
OS -11-041	30.48	to 33.53	-	OS -11-041	187.45	to 190.5	-
OS -11-041	33.53	to 36.58	-	OS -11-041	190.5	to 192.9	-
OS -11-041	36.58	to 39.62	-	OS -11-041	192.9	to 193.85	0.01
OS -11-041	39.62	to 42.67	-	OS -11-041	193.85	to 194.59	0.47
OS -11-041	42.67	to 45.72	-	OS -11-041	194.59	to 196.28	0.09
OS -11-041	45.72	to 48.77	-	OS -11-041	196.28	to 197.45	0.31
OS -11-041	48.77	to 51.82	-	OS -11-041	197.45	to 198.8	0.45
OS -11-041	51.82	to 54.86	-	OS -11-041	198.8	to 199.75	0.01
OS -11-041	54.86	to 57.91	-	OS -11-041	199.75	to 200.65	-
OS -11-041	57.91	to 60.96	-	OS -11-041	200.65	to 202.69	-
OS -11-041	60.96	to 64.01	0.03	OS -11-041	202.69	to 205.74	-
OS -11-041	64.01	to 67.06	-	OS -11-041	205.74	to 208.79	-
OS -11-041	67.06	to 70.1	-	OS -11-041	208.79	to 211.84	-
OS -11-041	70.1	to 73.15	-	OS -11-041	211.84	to 214.88	-
OS -11-041	73.15	to 76.2	-	OS -11-041	214.88	to 217.93	-
OS -11-041	76.2	to 79.25	0.01	OS -11-041	217.93	to 220.98	-
OS -11-041	79.25	to 82.3	-	OS -11-041	220.98	to 224.03	-
OS -11-041	82.3	to 85.34	-	OS -11-041	224.03	to 227.08	-
OS -11-041	85.34	to 88.39	-	OS -11-041	227.08	to 230.12	-
OS -11-041	88.39	to 91.44	-	OS -11-041	230.12	to 233.17	0.01
OS -11-041	91.44	to 94.49	0.01	OS -11-041	233.17	to 236.22	-
OS -11-041	94.49	to 97.54	-	OS -11-041	236.22	to 239.27	-
OS -11-041	97.54	to 100.58	-	OS -11-041	239.27	to 242.32	-
OS -11-041	100.6	to 103.63	0.01	OS -11-041	242.32	to 245.36	-
OS -11-041	103.6	to 106.68	-	OS -11-041	245.36	to 248.41	-
OS -11-041	106.7	to 109.73	-	OS -11-041	248.41	to 251.46	-
OS -11-041	109.7	to 112.78	-	OS -11-041	251.46	to 254.51	-
OS -11-041	112.8	to 115.82	-	OS -11-041	254.51	to 257.56	-
OS -11-041	115.8	to 118.87	-	OS -11-041	257.56	to 260.6	-
OS -11-041	118.9	to 121.92	-	OS -11-041	260.6	to 263.65	0.02
OS -11-041	121.9	to 124.97	-	OS -11-041	263.65	to 266.7	-
OS -11-041	125	to 128.02	-	OS -11-041	266.7	to 269.75	-
OS -11-041	128	to 129.59	-	OS -11-041	269.75	to 272.8	-
OS -11-041	129.6	to 132.59	-	OS -11-041	272.8	to 275.84	-
OS -11-041	132.6	to 135.64	-	OS -11-041	275.84	to 278.89	-
OS -11-041	135.6	to 138.68	0.01	OS -11-041	278.89	to 280.5	0.04
OS -11-041	138.7	to 141.73	0.01	OS -11-041	280.5	to 281.55	1.01
OS -11-041	141.7	to 144.78	0.01	OS -11-041	281.55	to 283	0.4
OS -11-041	144.8	to 147.83	-	OS -11-041	283	to 284.99	0.81
OS -11-041	147.8	to 150.88	-	OS -11-041	284.99	to 288.09	0.73
OS -11-041	150.9	to 153.92	0.01	OS -11-041	288.09	to 291.08	1.32
OS -11-041	153.9	to 156.97	-	OS -11-041	291.08	to 294.13	0.99

Drill Hole	Depth Interval (m)	Au grade (g/T)	Drill Hole	Depth Interval (m)	Au grade (g/T)
OS -11-041	294.1 to 297.18	0.55	OS -11-052	84.73 to 87.78	-
OS -11-041	297.2 to 300.23	0.44	OS -11-052	87.78 to 90.83	-
OS -11-041	300.2 to 303.28	0.08	OS -11-052	90.83 to 93.88	-
OS -11-041	303.3 to 306.32	0.05	OS -11-052	93.88 to 96.93	-
OS -11-041	306.3 to 309.37	0.01	OS -11-052	96.93 to 99.97	-
OS -11-041	309.4 to 312.42	0.03	OS -11-052	99.97 to 103.02	-
OS -11-041	312.4 to 315.47	0.02	OS -11-052	103.02 to 106.07	0.01
OS -11-041	315.5 to 318.52	0.02	OS -11-052	106.07 to 109.12	1.99
OS -11-041	318.5 to 321.56	0.04	OS -11-052	109.12 to 111.15	2.29
OS -11-041	321.6 to 324.61	0.05	OS -11-052	111.15 to 112.17	5.11
OS -11-041	324.6 to 327.66	0.07	OS -11-052	112.17 to 113.69	8.46
OS -11-041	327.7 to 330.71	0.01	OS -11-052	113.69 to 115.21	4.23
OS -11-041	330.7 to 333.76	0.04	OS -11-052	115.21 to 117.28	4.96
OS -11-041	333.8 to 336.8	-	OS -11-052	117.28 to 118.26	1.54
OS -11-041	336.8 to 339.85	-	OS -11-052	118.26 to 119.79	1.15
OS -11-041	339.9 to 342.9	-	OS -11-052	119.79 to 121.31	2.01
OS -11-041	342.9 to 345.95	-	OS -11-052	121.31 to 123.5	0.21
OS -11-041	346 to 349	0.02	OS -11-052	123.5 to 125.88	0.03
OS -11-041	349 to 352.04	0.02	OS -11-052	125.88 to 128.4	0.05
OS -11-041	352 to 355.09	-	OS -11-052	128.4 to 129.65	4.36
OS -11-041	355.1 to 358.14	-	OS -11-052	129.65 to 131.98	1.34
OS -11-041	358.1 to 361.19	-	OS -11-052	131.98 to 134.2	0.58
OS -11-041	361.2 to 364.24	-	OS -11-052	134.2 to 136.55	0.6
OS -11-041	364.2 to 367.28	-	OS -11-052	136.55 to 138.07	0.4
OS -11-052	0 to 2.44	0.31	OS -11-052	138.07 to 139.6	0.23
OS -11-052	2.44 to 5.49	0.01	OS -11-052	139.6 to 141.12	0.2
OS -11-052	5.49 to 8.33	0.01	OS -11-052	141.12 to 142.65	0.85
OS -11-052	8.33 to 11.58	0.02	OS -11-052	142.65 to 144.17	1.01
OS -11-052	11.58 to 14.63	-	OS -11-052	144.17 to 145.69	1.41
OS -11-052	14.63 to 17.68	0.04	OS -11-052	145.69 to 147.22	1.53
OS -11-052	17.68 to 20.73	0.01	OS -11-052	147.22 to 150.27	0.48
OS -11-052	20.73 to 23.77	-	OS -11-052	150.27 to 153.31	0.41
OS -11-052	23.77 to 26.82	-	OS -11-052	153.31 to 156.36	0.14
OS -11-052	26.82 to 29.87	-	OS -11-052	156.36 to 159.41	0.1
OS -11-052	29.87 to 32.92	-	OS -11-052	159.41 to 162.46	0.06
OS -11-052	32.92 to 35.97	-	OS -11-052	162.46 to 165.51	0.12
OS -11-052	35.97 to 39.01	-	OS -11-052	165.51 to 168.55	0.07
OS -11-052	39.01 to 42.06	-	OS -11-052	168.55 to 171.6	0.14
OS -11-052	42.06 to 45.11	-	OS -11-052	171.6 to 174.65	0.04
OS -11-052	45.11 to 48.16	-	OS -11-052	174.65 to 177.7	0.04
OS -11-052	48.16 to 51.21	-	OS -11-052	177.7 to 179	-
OS -11-052	51.21 to 54.25	0.01	OS -11-052	179 to 181	0.01
OS -11-052	54.25 to 57.3	-	OS -11-052	181 to 182.81	-
OS -11-052	57.3 to 60.35	0.01	OS -11-052	182.81 to 184.65	0.01
OS -11-052	60.35 to 63.4	-	OS -11-052	184.65 to 186.84	-
OS -11-052	63.4 to 66.45	-	OS -11-052	186.84 to 189.89	0.01
OS -11-052	66.45 to 69.49	0.01	OS -11-052	189.89 to 192.94	-
OS -11-052	69.49 to 72.54	-	OS -11-052	192.94 to 195.99	0.01
OS -11-052	72.54 to 75.59	-	OS -11-052	195.99 to 199.03	-
OS -11-052	75.59 to 78.64	-	OS -11-052	199.03 to 202.08	-
OS -11-052	78.64 to 81.69	-	OS -11-052	202.08 to 205.13	0.02
OS -11-052	81.69 to 84.73	-	OS -11-052	205.13 to 208.18	0.01

Drill Hole	Depth Interval (m)	Au grade (g/T)	Drill Hole	Depth Interval (m)	Au grade (g/T)
OS -11-052	208.2 to 211.23	0.01	OS -11-061	81.69 to 84.93	-
OS -11-052	211.2 to 214.27	0.01	OS -11-061	84.93 to 87.78	0.03
OS -11-052	214.3 to 217.32	0.01	OS -11-061	87.78 to 90.83	-
OS -11-052	217.3 to 220.37	-	OS -11-061	90.83 to 93.88	-
OS -11-052	220.4 to 223.42	0.01	OS -11-061	93.88 to 95.4	-
OS -11-052	223.4 to 224.2	-	OS -11-061	95.4 to 96.93	-
OS -11-052	224.2 to 226.47	0.08	OS -11-061	96.93 to 98.45	-
OS -11-052	226.5 to 229.51	0.46	OS -11-061	98.45 to 101.5	-
OS -11-052	229.5 to 230.99	0.43	OS -11-061	101.5 to 104.55	0.02
OS -11-052	231 to 232.56	1.33	OS -11-061	104.55 to 107.59	0.01
OS -11-052	232.6 to 235.61	0.7	OS -11-061	107.59 to 110.64	0.01
OS -11-052	235.6 to 238.66	0.05	OS -11-061	110.64 to 113.69	0.01
OS -11-052	238.7 to 241.71	0.01	OS -11-061	113.69 to 116.3	0.01
OS -11-052	241.7 to 244.75	0.01	OS -11-061	116.3 to 117.85	0.32
OS -11-052	244.8 to 247.8	0.01	OS -11-061	117.85 to 119.79	0.01
OS -11-052	247.8 to 250.85	0.02	OS -11-061	119.79 to 122.83	0.01
OS -11-052	250.9 to 253.9	0.02	OS -11-061	122.83 to 125.88	0.01
OS -11-052	253.9 to 256.95	-	OS -11-061	125.88 to 128.93	-
OS -11-052	257 to 260	-	OS -11-061	128.93 to 131.98	-
OS -11-052	260 to 263.04	-	OS -11-061	131.98 to 135.03	0.01
OS -11-052	263 to 266.09	-	OS -11-061	135.03 to 138.07	0.01
OS -11-052	266.1 to 269.14	-	OS -11-061	138.07 to 141.12	-
OS -11-052	269.1 to 272.19	-	OS -11-061	141.12 to 142.65	-
OS -11-061	1.7 to 3.96	0.32	OS -11-061	142.65 to 145.69	0.01
OS -11-061	3.96 to 5.49	3.58	OS -11-061	145.69 to 148.74	0.01
OS -11-061	5.49 to 7.01	7.15	OS -11-061	148.74 to 151.79	0.01
OS -11-061	7.01 to 8.53	3.9	OS -11-061	151.79 to 154.84	-
OS -11-061	8.53 to 11.58	1.6	OS -11-061	154.84 to 156.1	0.01
OS -11-061	11.58 to 13.11	4.83	OS -11-061	156.1 to 157.89	-
OS -11-061	13.11 to 16.15	0.78	OS -11-061	157.89 to 160.93	0.01
OS -11-061	16.15 to 19.2	0.88	OS -11-061	160.93 to 163.98	0.01
OS -11-061	19.2 to 21.15	2.63	OS -11-061	163.98 to 167.03	0.01
OS -11-061	21.15 to 23.77	5.9	OS -11-061	167.03 to 170.08	-
OS -11-061	23.77 to 26.82	1.01	OS -11-061	170.08 to 173.13	0.02
OS -11-061	26.82 to 29.87	0.01	OS -11-061	173.13 to 176.17	0.01
OS -11-061	29.87 to 32.92	0.03	OS -11-061	176.17 to 179.22	-
OS -11-061	32.92 to 35.97	0.01	OS -11-061	179.22 to 182.27	0.02
OS -11-061	35.97 to 39.01	-	OS -11-061	182.27 to 185.32	-
OS -11-061	39.01 to 42.06	-	OS -11-061	185.32 to 188.36	-
OS -11-061	42.06 to 45.11	-	OS -11-061	188.36 to 191.41	-
OS -11-061	45.11 to 48.16	-	OS -11-061	191.41 to 194.46	-
OS -11-061	48.16 to 51.21	0.01	OS -11-061	194.46 to 197.51	-
OS -11-061	51.21 to 54.25	-	OS -11-061	197.51 to 200.56	-
OS -11-061	54.25 to 57.3	0.01	OS -11-061	200.56 to 203.61	-
OS -11-061	57.3 to 60.35	0.01	OS -11-061	203.61 to 206.65	-
OS -11-061	60.35 to 63.4	0.02	OS -11-061	206.65 to 209.7	-
OS -11-061	63.4 to 66.45	-	OS -11-061	209.7 to 212.75	-
OS -11-061	66.45 to 69.49	0.01	OS -11-061	212.75 to 215.8	-
OS -11-061	69.49 to 72.54	-	OS -11-061	215.8 to 218.85	-
OS -11-061	72.54 to 75.59	-	OS -11-061	218.85 to 221.89	0.01
OS -11-061	75.59 to 78.64	0.01	OS -11-061	221.89 to 224.94	0.01
OS -11-061	78.64 to 81.69	-	OS -11-061	224.94 to 227.99	0.01

Drill Hole	Depth Interval (m)	Au grade (g/T)	Drill Hole	Depth Interval (m)	Au grade (g/T)
OS -11-061	228 to 231.04	0.01	OS -11-061	372.85 to 374.29	0.04
OS -11-061	231 to 234.09	0.01	OS -11-061	374.29 to 376.05	0.11
OS -11-061	234.1 to 237.13	-	OS -11-061	376.05 to 377.34	0.45
OS -11-061	237.1 to 240.18	0.01	OS -11-061	377.34 to 378.45	0.45
OS -11-061	240.2 to 243.23	-	OS -11-061	378.45 to 380.39	0.7
OS -11-061	243.2 to 246.28	-	OS -11-061	380.39 to 383.44	0.08
OS -11-061	246.3 to 249.33	-	OS -11-061	383.44 to 386.49	0.02
OS -11-061	249.3 to 252.37	-	OS -11-061	386.49 to 389.53	0.05
OS -11-061	252.4 to 255.42	-	OS -11-061	389.53 to 390.98	0.19
OS -11-061	255.4 to 258.47	-	OS -11-061	390.98 to 392.58	2.76
OS -11-061	258.5 to 261.52	-	OS -11-061	392.58 to 393.52	7.8
OS -11-061	261.5 to 264.57	-	OS -11-061	393.52 to 395.63	4.55
OS -11-061	264.6 to 267.61	0.01	OS -11-061	395.63 to 398.68	0.28
OS -11-061	267.6 to 270.66	-	OS -11-061	398.68 to 401.73	1.83
OS -11-061	270.7 to 273.71	-	OS -11-061	401.73 to 404.77	1.32
OS -11-061	273.7 to 276.76	0.01	OS -11-061	404.77 to 407.82	0.63
OS -11-061	276.8 to 279.81	-	OS -11-061	407.82 to 410.87	0.07
OS -11-061	279.8 to 281.75	0.01	OS -11-061	410.87 to 413.92	0.09
OS -11-061	281.8 to 283.5	0.02	OS -11-061	413.92 to 416.97	0.03
OS -11-061	283.5 to 284.4	0.03	OS -11-061	416.97 to 420.01	-
OS -11-061	284.4 to 285.9	0.05	OS -11-061	420.01 to 423.06	-
OS -11-061	285.9 to 288.95	0.05	OS -11-061	423.06 to 426.11	-
OS -11-061	289 to 292	0.55	OS -11-061	426.11 to 429.16	0.11
OS -11-061	292 to 293.15	1.4	OS -11-061	429.16 to 432.21	0.02
OS -11-061	293.2 to 294.8	1.74	OS -11-061	432.21 to 435.25	0.01
OS -11-061	294.8 to 296.3	0.1	OS -11-061	435.25 to 438.3	-
OS -11-061	296.3 to 298.09	0.04	OS -11-061	438.3 to 441.35	-
OS -11-061	298.1 to 301.19	0.02	OS -11-061	441.35 to 444.4	-
OS -11-061	301.2 to 304.19	0.01	OS -11-061	444.4 to 447.45	-
OS -11-061	304.2 to 307.24	0.01	OS -11-061	447.45 to 450.49	-
OS -11-061	307.2 to 310.29	0.01	OS -11-061	450.49 to 453.54	0.03
OS -11-061	310.3 to 313.33	0.01	OS -11-061	453.54 to 456.59	-
OS -11-061	313.3 to 316.38	0.02	OS -11-061	456.59 to 459.64	-
OS -11-061	316.4 to 319.43	0.02	OS -11-061	459.64 to 462.69	-
OS -11-061	319.4 to 322.48	0.03	OS -11-072	8.53 to 11.58	0.01
OS -11-061	322.5 to 325.53	0.02	OS -11-072	11.58 to 12.8	0.06
OS -11-061	325.5 to 328.57	0.03	OS -11-072	12.8 to 14.63	0.03
OS -11-061	328.6 to 331.62	0.02	OS -11-072	14.63 to 17.68	0.04
OS -11-061	331.6 to 334.67	0.01	OS -11-072	17.68 to 20.73	0.01
OS -11-061	334.7 to 337.72	0.02	OS -11-072	20.73 to 23.77	0.09
OS -11-061	337.7 to 340.77	0.04	OS -11-072	23.77 to 26.82	0.06
OS -11-061	340.8 to 343.81	0.02	OS -11-072	26.82 to 29.87	0.17
OS -11-061	343.8 to 346.86	0.01	OS -11-072	29.87 to 32.92	0.05
OS -11-061	346.9 to 349.91	0.04	OS -11-072	32.92 to 35.97	0.18
OS -11-061	349.9 to 352.96	0.15	OS -11-072	35.97 to 39.01	0.02
OS -11-061	353 to 356.01	0.32	OS -11-072	39.01 to 42.06	0.1
OS -11-061	356 to 359.05	0.03	OS -11-072	42.06 to 45.11	0.01
OS -11-061	359.1 to 362.1	0.06	OS -11-072	45.11 to 48.16	0.04
OS -11-061	362.1 to 365.15	0.17	OS -11-072	48.16 to 51.21	0.06
OS -11-061	365.2 to 368.2	0.03	OS -11-072	51.21 to 54.25	0.18
OS -11-061	368.2 to 370.95	0.03	OS -11-072	54.25 to 57.3	0.17
OS -11-061	371 to 372.85	0.07	OS -11-072	57.3 to 60.35	0.33

Drill Hole	Depth Interval (m)	Au grade (g/T)	Drill Hole	Depth Interval (m)	Au grade (g/T)
OS -11-072	60.35 to 63.4	0.09	OS -11-072	202.08 to 205.13	0.41
OS -11-072	63.4 to 66.45	0.02	OS -11-072	205.13 to 208.18	0.04
OS -11-072	66.45 to 69.49	0.01	OS -11-072	208.18 to 211.23	0.04
OS -11-072	69.49 to 72.54	0.1	OS -11-072	211.23 to 214.27	0.07
OS -11-072	72.54 to 75.59	0.04	OS -11-072	214.27 to 217.32	0.06
OS -11-072	75.59 to 78.64	0.01	OS -11-072	217.32 to 220.37	0.1
OS -11-072	78.64 to 81.69	0.01	OS -11-072	220.37 to 223.42	0.25
OS -11-072	81.69 to 84.73	0.04	OS -11-072	223.42 to 226.47	0.04
OS -11-072	84.73 to 87.78	0.02	OS -11-072	226.47 to 229.51	0.04
OS -11-072	87.78 to 90.83	0.01	OS -11-072	229.51 to 232.56	0.05
OS -11-072	90.83 to 93.88	0.03	OS -11-072	232.56 to 235.61	0.02
OS -11-072	93.88 to 96.93	0.04	OS -11-072	235.61 to 238.66	0.02
OS -11-072	96.93 to 99.97	-	OS -11-072	238.66 to 241.7	-
OS -11-072	99.97 to 103.02	-	OS -11-072	241.7 to 244.75	0.01
OS -11-072	103 to 106.07	-	OS -11-072	244.75 to 247.8	0.14
OS -11-072	106.1 to 107.59	-	OS -11-072	247.8 to 250.45	0.06
OS -11-072	107.6 to 110.64	-	OS -11-072	250.45 to 252	1.6
OS -11-072	110.6 to 113.69	-	OS -11-072	252 to 253.89	1.41
OS -11-072	113.7 to 116.74	-	OS -11-072	253.89 to 256.94	0.12
OS -11-072	116.7 to 119.79	-	OS -11-072	256.94 to 259.99	0.05
OS -11-072	119.8 to 122.83	0.15	OS -11-072	259.99 to 263.04	0.14
OS -11-072	122.8 to 125.88	0.05	OS -11-072	263.04 to 266.09	0.17
OS -11-072	125.9 to 128.93	0.09	OS -11-072	266.09 to 269.13	0.2
OS -11-072	128.9 to 131.98	0.35	OS -11-072	269.13 to 272.19	0.15
OS -11-072	132 to 133.5	0.04	OS -11-072	272.19 to 275.23	0.19
OS -11-072	133.5 to 135.24	0.08	OS -11-072	275.23 to 278.28	0.13
OS -11-072	135.2 to 138.07	0.22	OS -11-072	278.28 to 281.33	0.04
OS -11-072	138.1 to 141.12	-	OS -11-072	281.33 to 284.38	0.1
OS -11-072	141.1 to 144.17	-	OS -11-072	284.38 to 287.43	0.01
OS -11-072	144.2 to 147.22	-	OS -11-072	287.43 to 290.47	0.05
OS -11-072	147.2 to 148.31	-	OS -11-072	290.47 to 293.52	0.15
OS -11-072	148.3 to 150.26	-	OS -11-072	293.52 to 296.57	-
OS -11-072	150.3 to 153.31	-	OS -11-072	296.57 to 299.61	0.06
OS -11-072	153.3 to 156.36	-	OS -11-072	299.61 to 302.67	0.11
OS -11-072	156.4 to 157.32	-	OS -11-072	302.67 to 305.71	0.03
OS -11-072	157.3 to 159.41	0.25	OS -11-072	305.71 to 308.76	0.32
OS -11-072	159.4 to 162.46	0.01	OS -11-072	308.76 to 311.81	0.03
OS -11-072	162.5 to 165.51	0.06	OS -11-072	311.81 to 314.86	0.12
OS -11-072	165.5 to 168.55	0.12	OS -11-072	314.86 to 317.91	0.03
OS -11-072	168.6 to 171.6	0.05	OS -11-072	317.91 to 320.95	0.06
OS -11-072	171.6 to 174.65	0.03	OS -11-072	320.95 to 324	0.08
OS -11-072	174.7 to 177.7	0.06	OS -11-072	324 to 327.05	0.06
OS -11-072	177.7 to 180.75	0.07	OS -11-072	327.05 to 330.1	-
OS -11-072	180.8 to 183.79	0.05	OS -11-072	330.1 to 333.15	-
OS -11-072	183.8 to 186.84	0.3	OS -11-072	333.15 to 336.19	-
OS -11-072	186.8 to 189.89	0.45	OS -11-072	336.19 to 339.24	-
OS -11-072	189.9 to 191.33	0.06	OS -11-072	339.24 to 342.29	0.01
OS -11-072	191.3 to 194	1.18	OS -11-072	342.29 to 345.34	0.01
OS -11-072	194 to 195.99	0.94	OS -11-072	345.34 to 346.97	-
OS -11-072	196 to 198.51	0.89	OS -11-080	1.32 to 3.05	0.12
OS -11-072	198.5 to 200	0.31	OS -11-080	3.05 to 6.1	0.11
OS -11-072	200 to 202.08	0.14	OS -11-080	6.1 to 9.14	0.01

Drill Hole	Depth Interval (m)		Au grade (g/T)	Drill Hole	Depth Interval (m)		Au grade (g/T)
OS -11-080	9.14	to 12.19	0.02	OS -11-080	152.4	to 155.45	-
OS -11-080	12.19	to 15.24	0.03	OS -11-080	155.45	to 158.5	-
OS -11-080	15.24	to 18.29	0.22	OS -11-080	158.5	to 161.54	-
OS -11-080	18.29	to 21.34	0.57	OS -11-080	161.54	to 164.59	-
OS -11-080	21.34	to 24.39	0.81	OS -11-080	164.59	to 165.47	-
OS -11-080	24.39	to 26.47	0.63	OS -11-080	99.06	to 100.58	-
OS -11-080	26.47	to 28.96	0.12	OS -11-080	165.47	to 167.64	-
OS -11-080	28.96	to 32	0.26	OS -11-080	167.64	to 170.69	-
OS -11-080	32	to 33.53	13.8	OS -11-080	170.69	to 173.74	-
OS -11-080	33.53	to 35.05	11.25	OS -11-080	173.74	to 175.75	-
OS -11-080	35.05	to 36.58	16.55	OS -11-080	175.75	to 176.78	0.07
OS -11-080	36.58	to 37.7	18.55	OS -11-080	176.78	to 179.83	0.02
OS -11-080	37.7	to 39.62	2.22	OS -11-080	179.83	to 182.88	0.01
OS -11-080	39.62	to 42.67	2.57	OS -11-080	182.88	to 185.93	0.13
OS -11-080	42.67	to 44.2	1.01	OS -11-080	185.93	to 187.72	0.08
OS -11-080	44.2	to 47.24	0.32	OS -11-080	187.72	to 190.5	0.01
OS -11-080	47.24	to 50.29	0.02	OS -11-080	190.5	to 193.55	0.02
OS -11-080	50.29	to 53.34	0.01	OS -11-080	193.55	to 195.07	0.01
OS -11-080	53.34	to 56.39	0.15	OS -11-080	195.07	to 198.12	0.01
OS -11-080	56.39	to 59.44	0.17	OS -11-080	198.12	to 201.17	0.01
OS -11-080	59.44	to 62.48	0.01	OS -11-080	201.17	to 204.21	0.01
OS -11-080	62.48	to 65.53	-	OS -11-080	204.21	to 207.26	0.03
OS -11-080	65.53	to 68.58	-	OS -11-080	207.26	to 210.3	0.01
OS -11-080	68.58	to 71.63	-	OS -11-080	210.31	to 213.36	0.02
OS -11-080	71.63	to 74.68	0.28	OS -11-080	213.36	to 216.41	0.01
OS -11-080	74.68	to 77.72	-	OS -11-080	216.41	to 219.46	0.03
OS -11-080	77.72	to 80.77	-	OS -11-080	219.46	to 222.5	0.02
OS -11-080	80.77	to 83.82	-	OS -11-080	222.5	to 225.55	0.03
OS -11-080	83.82	to 86.87	-	OS -11-080	225.55	to 226.9	0.13
OS -11-080	86.87	to 89.92	-	OS -11-080	226.9	to 228.6	-
OS -11-080	89.92	to 92.96	-	OS -11-080	228.6	to 231.65	0.37
OS -11-080	92.96	to 96.01	-	OS -11-080	231.65	to 234.7	0.65
OS -11-080	96.01	to 99.06	-	OS -11-080	234.7	to 237.74	0.03
OS -11-080	100.6	to 103.63	-	OS -11-080	237.74	to 240.8	-
OS -11-080	103.6	to 106.68	-	OS -11-080	240.8	to 243.84	-
OS -11-080	106.7	to 109.73	0.02	OS -11-083	6.52	to 8.53	0.02
OS -11-080	109.7	to 112.78	0.43	OS -11-083	8.53	to 11.58	0.06
OS -11-080	112.8	to 115.82	0.54	OS -11-083	11.58	to 14.63	0.07
OS -11-080	115.8	to 118.87	-	OS -11-083	14.63	to 17.68	0.07
OS -11-080	118.9	to 121.92	-	OS -11-083	17.68	to 20.73	0.01
OS -11-080	121.9	to 123.44	-	OS -11-083	20.73	to 23.77	0.01
OS -11-080	123.4	to 126.49	-	OS -11-083	23.77	to 26.82	-
OS -11-080	126.5	to 129.54	-	OS -11-083	26.82	to 29.87	-
OS -11-080	129.5	to 132.59	-	OS -11-083	29.87	to 32.92	-
OS -11-080	132.6	to 135.64	-	OS -11-083	32.92	to 35.97	-
OS -11-080	135.6	to 138.68	-	OS -11-083	35.97	to 39.01	0.04
OS -11-080	138.7	to 141.73	-	OS -11-083	39.01	to 42.06	5.73
OS -11-080	141.7	to 144.78	0.01	OS -11-083	42.06	to 45.11	1.56
OS -11-080	144.8	to 146.3	0.04	OS -11-083	45.11	to 46.85	1.1
OS -11-080	146.3	to 147.85	-	OS -11-083	46.85	to 48.2	7.57
OS -11-080	147.9	to 149.35	-	OS -11-083	48.2	to 49.68	0.13
OS -11-080	149.4	to 152.4	0.03	OS -11-083	49.68	to 52.73	0.11

Drill Hole	Depth Interval (m)	Au grade (g/T)	Drill Hole	Depth Interval (m)	Au grade (g/T)
OS -11-083	52.73 to 55.78	0.14	OS -12-120	39.01 to 42.06	-
OS -11-083	55.78 to 58.83	0.31	OS -12-120	42.06 to 43.59	-
OS -11-083	58.83 to 61.87	0.29	OS -12-120	43.69 to 46.63	-
OS -11-083	61.87 to 64.92	0.12	OS -12-120	46.63 to 49.68	-
OS -11-083	64.92 to 67.97	1.28	OS -12-120	49.68 to 52.73	-
OS -11-083	67.97 to 71.02	0.02	OS -12-120	52.73 to 55.78	-
OS -11-083	71.02 to 74.07	0.01	OS -12-120	55.78 to 58.83	-
OS -11-083	74.07 to 77.11	0.07	OS -12-120	58.83 to 61.87	-
OS -11-083	77.11 to 80.16	0.02	OS -12-120	61.87 to 64.92	-
OS -11-083	80.16 to 83.21	0.02	OS -12-120	64.92 to 67.97	-
OS -11-083	83.21 to 86.26	0.01	OS -12-120	67.97 to 71.02	-
OS -11-083	86.26 to 89.31	0.01	OS -12-120	71.02 to 74.07	-
OS -11-083	89.31 to 92.35	0.01	OS -12-120	74.07 to 77.11	-
OS -11-083	92.35 to 95.4	0.06	OS -12-120	77.11 to 80.16	0.01
OS -11-083	95.4 to 98.45	0.02	OS -12-120	80.16 to 81.69	0.03
OS -11-083	98.45 to 101.5	0.41	OS -12-120	81.69 to 84.73	0.04
OS -11-083	101.5 to 104.55	1.85	OS -12-120	84.73 to 86.26	0.11
OS -11-083	104.6 to 107.59	0.73	OS -12-120	86.26 to 89.31	0.1
OS -11-083	107.6 to 110.64	0.04	OS -12-120	89.31 to 91.5	0.09
OS -11-083	110.6 to 113.69	0.02	OS -12-120	91.5 to 93.49	0.41
OS -11-083	113.7 to 115.21	0.04	OS -12-120	93.49 to 95.56	0.36
OS -11-083	115.2 to 118.26	0.02	OS -12-120	95.56 to 98.45	0.13
OS -11-083	118.3 to 121.31	0.01	OS -12-120	98.45 to 101.5	0.16
OS -11-083	121.3 to 124.36	0.02	OS -12-120	101.5 to 104.55	0.05
OS -11-083	124.4 to 127.41	-	OS -12-120	104.55 to 106.07	0.26
OS -11-083	127.4 to 130.45	-	OS -12-120	106.07 to 109.12	1.35
OS -11-083	130.5 to 133.5	0.04	OS -12-120	109.12 to 112.17	1.99
OS -11-083	133.5 to 136.55	0.01	OS -12-120	112.17 to 114.88	8.21
OS -11-083	136.6 to 139.6	0.01	OS -12-120	114.88 to 116.83	11.05
OS -11-083	139.6 to 142.65	-	OS -12-120	116.83 to 119.79	2.17
OS -11-083	142.7 to 145.69	0.01	OS -12-120	119.79 to 121.85	2.78
OS -11-083	145.7 to 148.74	-	OS -12-120	121.85 to 123.83	5.16
OS -11-083	148.7 to 150.27	-	OS -12-120	123.83 to 125.63	6.42
OS -11-083	150.3 to 151.79	-	OS -12-120	125.63 to 127.41	7.76
OS -11-083	151.8 to 154	-	OS -12-120	127.41 to 130.45	21.7
OS -11-083	154 to 156.36	-	OS -12-120	130.45 to 133.50	1.49
OS -11-083	156.4 to 159.41	-	OS -12-120	133.50 to 136.55	0.02
OS -11-083	159.4 to 162.46	-	OS -12-120	136.55 to 139.60	0.03
OS -11-083	162.5 to 163.98	-	OS -12-120	139.60 to 142.65	0.01
OS -12-120	6.10 to 8.53	-	OS -12-120	142.65 to 145.69	0.01
OS -12-120	8.53 to 11.58	0.03	OS -12-120	145.69 to 148.74	-
OS -12-120	11.58 to 14.63	-	OS -12-120	148.74 to 151.79	-
OS -12-120	14.63 to 17.68	-	OS -12-120	151.79 to 154.83	0.01
OS -12-120	17.68 to 20.73	-	OS -12-120	154.83 to 157.88	-
OS -12-120	20.73 to 23.77	-	OS -12-120	157.88 to 160.93	-
OS -12-120	23.77 to 26.82	0.04	OS -12-120	160.93 to 163.98	-
OS -12-120	26.82 to 29.87	-	OS -12-120	163.98 to 167.03	-
OS -12-120	29.87 to 31.07	0.01	OS -12-120	167.03 to 170.08	-
OS -12-120	31.07 to 32.92	-	OS -12-120	170.08 to 173.13	-
OS -12-120	32.92 to 35.97	-	OS -12-120	173.13 to 176.17	0.02
OS -12-120	35.97 to 36.90	-	OS -12-120	176.17 to 179.22	-
OS -12-120	36.90 to 39.01	-	OS -12-120	179.22 to 180.75	-
			OS -12-120	180.75 to 182.30	-

Appendix D – EMPA Data

EMPA data of calcite and dolomite (wt%). Detection limits (in wt%) are reported below each element symbol in bold. Data below detection limit are indicated by (-)

Sample ID	Phase	Occurrence	BaO	MgO	CaO	SrO	MnO	Na ₂ O	ZnO	FeO	Total
(OS-11-80 154.24) grid 1-1	Calcite 2	Veinlet	0.04	0.3	0.2	0.02	0.01	0.01	0.39	0.01	57.08
Osiris: Grid 1-2 18cc_vein	Calcite 2	Veinlet	-	-	56.97	-	0.04	0.01	-	0.02	57.08
Osiris: Grid 1-3 18cc_vein	Calcite 2	Veinlet	-	-	56.56	0.03	0.02	0.03	-	0.06	56.74
Osiris: Grid 2-1 18cc_vein	Calcite 2	Veinlet	-	-	56.20	0.04	0.01	0.01	-	0.15	56.41
Osiris: Grid 2-2 18cc_vein	Calcite 2	Veinlet	-	-	56.34	0.06	0.04	-	-	0.05	56.51
Osiris: Grid 2-3 18cc_vein	Calcite 2	Veinlet	0.10	-	56.44	0.03	0.03	0.00	-	0.09	56.69
Osiris: Grid 3-1 18cc_vein	Calcite 2	Veinlet	-	-	56.39	-	0.06	0.03	-	0.12	56.61
Osiris: Grid 3-2 18cc_vein	Calcite 2	Veinlet	0.04	-	56.44	-	0.03	0.03	-	0.22	56.78
Osiris: Grid 3-3 18cc_vein	Calcite 2	Veinlet	-	-	55.99	-	-	-	-	0.12	56.12
Osiris: Grid 3-3 18cc_vein	Calcite 2	Veinlet	-	-	56.61	0.03	0.03	-	-	0.11	56.77
Osiris: Grid 3-3 18cc_vein	Calcite 2	Veinlet	-	-	58.07	0.02	0.03	0.02	-	0.06	58.22
Osiris: Grid 1-1 18cc_vein	Calcite 2	Veinlet	0.06	-	56.76	-	0.02	-	-	0.01	56.85
Osiris: Grid 1-2 18cc_vein	Calcite 2	Veinlet	-	-	55.76	-	0.03	0.01	-	0.02	55.83
Osiris: Grid 1-3 18cc_vein	Calcite 2	Veinlet	0.04	-	56.58	-	0.03	0.02	-	0.05	56.73
Osiris: Grid 2-1 18cc_vein	Calcite 2	Veinlet	-	-	55.99	0.07	0.03	0.02	-	0.09	56.25
Osiris: Grid 2-2 18cc_vein	Calcite 2	Veinlet	-	-	56.55	0.02	0.01	-	-	0.08	56.67
Osiris: Grid 2-3 18cc_vein	Calcite 2	Veinlet	0.04	-	56.11	-	0.01	0.04	-	0.05	56.26
Osiris: Grid 3-1 18cc_vein	Calcite 2	Veinlet	-	-	56.15	-	0.01	0.02	-	0.08	56.31
Osiris: Grid 3-2 18cc_vein	Calcite 2	Veinlet	-	-	56.38	0.02	0.03	0.03	-	0.15	56.61
Osiris: Grid 3-3 18cc_vein	Calcite 2	Veinlet	-	-	56.16	0.02	0.02	0.03	-	0.14	56.37
Osiris: 14cc_blob_1 (176.03)	Calcite 4	Veinlet	-	-	56.34	-	0.03	0.01	-	0.09	56.51
Osiris: 14cc_blob_2	Calcite 4	Veinlet	-	-	55.45	-	0.60	0.02	-	0.02	56.09
Osiris: 14cc_blob_3B	Calcite 4	Veinlet	-	-	55.85	-	0.59	0.01	-	0.00	56.45
Osiris: 14cc_blob_4	Calcite 4	Veinlet	-	-	55.70	0.02	0.76	-	-	-	56.50
Osiris: 14cc_blob_5	Calcite 4	Veinlet	-	-	55.83	-	0.47	0.01	-	-	56.33
Osiris: 14cc_blob_6	Calcite 4	Veinlet	-	-	55.62	-	0.63	0.03	-	0.01	56.32
Osiris: 3_cal_bright_1 (50.64)	Calcite 4	Veinlet	-	-	54.92	-	0.88	0.02	-	-	55.82
Osiris: 3_cal_bright_2 (50.64)	Calcite 4	Veinlet	-	-	56.65	-	0.24	0.03	-	-	56.93
Osiris: 3_cal_bright_3 (50.64)	Calcite 4	Veinlet	-	-	56.13	0.08	0.07	0.03	-	0.25	56.56
Osiris: 3_cal_bright_4 (50.64)	Calcite 4	Veinlet	-	-	56.46	-	0.11	0.01	-	0.02	56.64
	Calcite 4	Veinlet	-	-	55.34	-	0.25	-	-	0.01	55.62

Sample ID	Phase	Occurrence	BaO	MgO	CaO	SrO	MnO	Na ₂ O	ZnO	FeO	Total
Osiris: 3_cal_dull_5 (50.64)	Calcite 1	Veinlet	0.04	0.3	0.2	0.02	0.01	0.01	0.39	0.01	56.71
Osiris: 3_cal_dull_6 (50.64)	Calcite 1	Veinlet	0.06	-	56.43	0.03	0.01	0.02	-	0.21	56.94
Osiris: 3_cal_dull_7 (50.64)	Calcite 1	Veinlet	-	-	56.68	0.04	0.01	0.00	-	0.14	56.77
Osiris: 13_cal_vein_1 (162.22)	Calcite 3	Veinlet	-	-	56.53	-	0.02	0.02	-	0.19	56.94
Osiris: 13_cal_vein_2 (162.22)	Calcite 3	Veinlet	-	-	56.86	-	0.03	0.02	-	-	56.79
Osiris: 13_cal_vein_3 (162.22)	Calcite 3	Veinlet	-	-	56.72	-	0.04	0.01	-	-	57.03
Osiris: 13_cal_vein_4 (162.22)	Calcite 3	Veinlet	-	-	56.94	-	0.05	0.02	-	-	56.63
Osiris: 13_cal_vein_5 (162.22)	Calcite 3	Veinlet	-	-	56.49	-	0.02	0.00	-	0.11	56.49
Osiris: 13_cal_vein_6 (162.22)	Calcite 3	Veinlet	-	-	56.28	-	0.03	0.02	-	0.17	56.63
Osiris: 13_cal_vein_7 (162.22)	Calcite 3	Veinlet	-	-	56.52	-	0.04	-	-	0.05	56.85
Osiris: 13_cal_vein_8 (162.22)	Calcite 3	Veinlet	-	-	56.81	-	0.04	-	-	-	56.65
Osiris: 13_cal_vein_9 (162.22)	Calcite 3	Veinlet	-	-	56.57	-	0.05	0.01	-	0.01	56.08
Osiris: 13_cal_vein_10 (162.22)	Calcite 3	Veinlet	-	-	55.99	-	0.05	-	-	0.01	56.90
Osiris: 13_cal_vein_11 (162.22)	Calcite 3	Veinlet	-	-	56.84	-	0.01	0.01	-	0.01	56.84
Osiris: 13_cal_vein_12 (162.22)	Calcite 3	Veinlet	-	-	56.81	-	0.02	0.01	-	-	56.68
Osiris: 17_cal_vn_1 (151.32)	Calcite 3	Veinlet	-	-	56.60	-	0.04	-	-	-	57.20
Osiris: 17_cal_vn_2 (151.32)	Calcite 3	Veinlet	-	-	57.11	-	0.04	0.01	-	0.03	56.81
Osiris: 17_cal_vn_3 (151.32)	Calcite 3	Veinlet	-	-	56.68	-	0.03	0.02	-	0.09	56.59
Osiris: 17_cal_vn_4 (151.32)	Calcite 3	Veinlet	-	-	56.44	-	0.04	-	-	0.07	55.22
Osiris: 17_cal_vn_5 (151.32)	Calcite 3	Veinlet	-	-	54.52	-	0.40	0.02	-	0.07	57.20
Osiris: 17_cal_vn_6 (151.32)	Calcite 3	Veinlet	-	-	57.13	-	0.03	0.03	-	-	56.79
Osiris: 17_cal_bx_1 V	Calcite 3	Veinlet	0.04	-	56.64	-	0.05	0.02	-	0.03	56.84
Osiris: 17_cal_bx_2 (151.32)	Calcite 3	Veinlet	-	-	56.77	-	0.02	-	-	0.04	57.29
Osiris: 17_cal_bx_3 (151.32)	Calcite 3	Veinlet	-	-	57.21	-	0.05	0.01	-	0.02	57.37
Osiris: 17_cal_bx_4 (151.32)	Calcite 3	Veinlet	-	-	57.30	-	0.04	-	-	0.02	57.20
Osiris: 17_cal_bx_5 (151.32)	Calcite 3	Veinlet	-	-	57.11	-	0.02	-	-	0.06	61.31
Osiris: 22_cal_twn_vn_1 (29.91)	Calcite 2	Veinlet	0.05	-	61.14	-	0.04	0.01	-	0.06	55.69
Osiris: 22_cal_twn_vn_2 (29.91)	Calcite 2	Veinlet	-	-	55.16	-	0.03	-	-	0.50	56.25
Osiris: 22_cal_twn_vn_3 (29.91)	Calcite 2	Veinlet	-	-	55.72	-	0.06	0.01	-	0.44	56.45
Osiris: 22_cal_twn_vn_4 (29.91)	Calcite 2	Veinlet	-	-	56.19	-	0.05	0.03	-	0.18	55.94
Osiris: 22_cal_twn_vn_5 (29.91)	Calcite 2	Veinlet	-	-	55.47	-	0.05	0.03	-	0.39	56.62
Osiris: 22_cal_twn_vn_6 (29.91)	Calcite 2	Veinlet	-	-	56.19	-	0.06	-	-	0.35	55.37
			-	1.36	51.64	-	0.08	0.01	-	2.27	

Sample ID	Phase	Occurrence	BaO	MgO	CaO	SrO	MnO	Na ₂ O	ZnO	FeO	Total
Osiris: 22_cal_vt_1 (29.91)	Calcite 2	Veinlet	0.04	0.3	0.2	0.02	0.01	0.01	0.39	0.01	55.93
Osiris: 22_cal_vt_2 (29.91)	Calcite 2	Veinlet	-	-	55.55	-	0.04	-	-	0.31	55.93
Osiris: 22_cal_vt_3 (29.91)	Calcite 2	Veinlet	-	-	55.86	-	0.06	-	-	0.30	56.23
Osiris: 14dol_dark_1 (176.03)	Dolomite 2	cement	0.04	20.83	30.57	-	0.11	0.01	-	1.58	53.14
Osiris: 14dol_dark_2 (176.03)	Dolomite 2	cement	-	20.81	30.38	-	0.21	-	-	1.49	52.89
Osiris: 14dol_dark_3 (176.03)	Dolomite 2	cement	-	21.03	30.29	-	0.19	-	-	1.51	53.02
Osiris: 14dol_bright_1 (176.03)	Dolomite 3	rim	-	20.66	31.63	-	0.32	-	-	0.14	52.75
Osiris: 14dol_bright_2 (176.03)	Dolomite 3	rim	-	20.00	32.03	-	0.53	0.02	-	0.16	52.78
Osiris: 14dol_bright_3 (176.03)	Dolomite 3	rim	0.04	20.19	31.75	-	0.87	0.04	-	0.11	53.00
Osiris: 15_dol_crs_1 (210.57)	Dolomite 2	cement	-	21.99	31.33	0.02	0.04	0.04	-	0.02	53.44
Osiris: 15_dol_crs_2 (210.57)	Dolomite 2	cement	-	21.60	31.29	-	0.06	-	-	0.40	53.35
Osiris: 15_dol_crs_3B (210.57)	Dolomite 2	cement	-	22.08	31.13	-	0.05	0.02	-	0.04	53.31
Osiris: 15_dol_fn_1 (210.57)	Dolomite 2	cement	-	21.84	31.38	0.02	0.01	0.00	-	0.08	53.36
Osiris: 15_dol_fn_2 (210.57)	Dolomite 2	cement	-	21.66	30.94	0.02	0.01	0.04	-	0.05	52.73
Osiris: 15_dol_fn_3 (210.57)	Dolomite 2	cement	-	21.45	31.45	-	0.03	0.01	-	0.08	53.04
Osiris: 17_dol_xtal_1 (210.57)	Dolomite 2	cement	-	19.58	33.89	-	0.05	0.02	-	0.19	53.74
Osiris: 17_dol_xtal_2 (210.57)	Dolomite 2	cement	0.04	20.01	32.92	-	0.04	0.03	-	0.09	53.13
Osiris: 17_dol_xtal_3 (210.57)	Dolomite 2	cement	-	19.53	33.05	-	0.04	0.03	-	0.26	52.92
Osiris: 22_dol_vn_1 (29.91)	Dolomite 2	cement	-	16.93	32.77	-	0.20	0.01	-	3.94	53.85
Osiris: 22_dol_vn_2 (29.91)	Dolomite 2	veinlet	-	14.72	36.36	-	0.12	0.03	-	2.81	54.04
Osiris: 22_dol_vn_3 (29.91)	Dolomite 2	veinlet	-	17.54	32.74	-	0.17	-	-	3.45	53.90
Osiris: 27_dolo_gn_1 (123.84)	Dolomite 1	cement	-	20.25	33.53	-	0.01	0.03	-	0.13	53.94
Osiris: 27_dolo_gn_2 (123.84)	Dolomite 1	cement	-	20.32	33.33	-	0.04	0.03	-	0.07	53.80
Osiris: 27_dolo_gn_3 (123.84)	Dolomite 1	cement	-	20.09	33.57	-	0.02	0.06	-	0.11	53.86
Osiris: 27_dolo_gn_4 (123.84)	Dolomite 3	rim	-	18.07	30.38	-	0.08	0.02	-	2.80	51.35
Osiris: 27_dolo_gn_5 (123.84)	Dolomite 3	rim	-	20.04	33.19	-	0.04	0.01	-	0.23	53.51
Osiris: 27_dolo_gn_6 (123.84)	Dolomite 3	rim	-	19.85	33.50	-	0.06	0.03	-	0.20	53.63
Osiris: 27_dolo_gn_7 (123.84)	Dolomite 1	cement	-	17.07	32.87	-	0.08	-	-	3.90	53.94
Osiris: 27_dolo_gn_9_(53_54)B (12: Dolomite 1	Dolomite 1	cement	-	20.63	32.68	-	0.05	0.03	-	0.29	53.70

Sample ID	Phase	Occurrence	BaO	MgO	CaO	SrO	MnO	Na ₂ O	ZnO	FeO	Total
Osiris: OS-11-41 Line 1 342_97_a1_dol	Dol 3	Rim of dolomite crystal	NA	0.4	0.05	NA	0.08	0.05	NA	0.85	
Osiris: OS-11-41 Line 2 342_97_a1_dol	Dol 3	Rim of dolomite crystal	NA	19.35	30.11	NA	-	0.05	NA	3.10	52.69
Osiris: OS-11-41 Line 3 342_97_a1_dol	Dol 3	Rim of dolomite crystal	NA	20.69	30.21	NA	0.14	-	NA	1.95	53.03
Osiris: OS-11-41 Line 4 342_97_a1_dol	Dol 3	Rim of dolomite crystal	NA	21.76	30.90	NA	-	-	NA	-	52.92
Osiris: OS-11-41 Line 5 342_97_a1_dol	Dol 3	Rim of dolomite crystal	NA	21.39	31.07	NA	-	-	NA	-	52.87
Osiris: OS-11-41 Line 6 342_97_a1_dol	Dol 3	Center of dolomite crystal	NA	22.08	31.01	NA	-	-	NA	-	53.23
Osiris: OS-11-41 Line 7 342_97_a1_dol	Dol 2	Center of dolomite crystal	NA	21.27	31.09	NA	0.11	-	NA	-	52.68
Osiris: OS-11-41 Line 8 342_97_a1_dol	Dol 2	Center of dolomite crystal	NA	21.40	30.13	NA	0.09	0.05	NA	-	52.42
Osiris: OS-11-41 Line 9 342_97_a1_dol	Dol 2	Center of dolomite crystal	NA	21.41	29.94	NA	0.09	0.05	NA	0.77	52.27
Osiris: OS-11-41 Line 10 342_97_a1_dol	Dol 2	Center of dolomite crystal	NA	21.35	29.91	NA	0.11	-	NA	0.90	52.28
Osiris: OS-11-41 342_97_Line_1a	Dol 2	Center of dolomite crystal	NA	21.70	29.92	NA	0.10	-	NA	1.03	52.78
Osiris: OS-11-41 342_97_Line_2a	Dol 2	Rim of dolomite crystal	NA	20.78	30.73	NA	0.08	-	NA	1.34	52.96
Osiris: OS-11-41 342_97_Line_3a	Dol 3	Rim of dolomite crystal	NA	22.09	30.87	NA	-	-	NA	-	53.27
Osiris: OS-11-41 342_97_Line_4a	Dol 3	Rim of dolomite crystal	NA	21.90	31.25	NA	-	-	NA	-	53.26
Osiris: OS-11-41 342_97_Line_5a	Dol 3	Rim of dolomite crystal	NA	22.18	31.39	NA	-	-	NA	-	53.66
Osiris: OS-11-41 342_97_Line_6a	Dol 3	Center of dolomite crystal	NA	22.02	30.91	NA	-	-	NA	-	53.24
Osiris: OS-11-41 342_97_Line_7a	Dol 3	Center of dolomite crystal	NA	21.84	30.77	NA	0.08	-	NA	-	52.90
Osiris: OS-11-41 342_97_Line_8a	Dol 3	Center of dolomite crystal	NA	21.66	30.78	NA	-	-	NA	-	52.85
Osiris: OS-11-41 342_97_Line_9a	Dol 3	Center of dolomite crystal	NA	21.70	31.21	NA	-	-	NA	-	52.99
Osiris: OS-11-41 342_97_Line_10a	Dol 3	Center of dolomite crystal	NA	21.72	31.20	NA	-	-	NA	-	53.02
Osiris: OS-11-41 342_97_Line_11a	Dol 3	Center of dolomite crystal	NA	21.67	31.52	NA	-	-	NA	-	53.27
Osiris: OS-11-41 342_97_Line_11a	Dol 3	Center of dolomite crystal	NA	21.45	32.06	NA	-	-	NA	-	53.63
Osiris: OS-11-41 Line 1 342_97area2b	Dol 2	Center of dolomite crystal	NA	21.47	31.91	NA	-	-	NA	-	53.46
Osiris: OS-11-41 Line 2 342_97area2b	Dol 2	Rim of dolomite crystal	NA	21.15	30.34	NA	0.08	-	NA	1.12	52.72
Osiris: OS-11-41 Line 3 342_97area2b	Dol 2	Rim of dolomite crystal	NA	20.74	30.33	NA	0.11	-	NA	1.44	52.62
Osiris: OS-11-41 Line 4 342_97area2b	Dol 3	Rim of dolomite crystal	NA	21.63	31.47	NA	-	-	NA	-	53.21
Osiris: OS-11-41 Line 5 342_97area2b	Dol 3	Rim of dolomite crystal	NA	22.00	30.59	NA	-	-	NA	-	52.77
Osiris: OS-11-41 Line 6 342_97area2b	Dol 3	Rim of dolomite crystal	NA	21.87	30.89	NA	-	-	NA	-	52.88
Osiris: OS-11-41 Line 7 342_97area2b	Dol 3	Center of dolomite crystal	NA	21.75	30.68	NA	0.08	-	NA	0.32	52.85
Osiris: OS-11-41 Line 8 342_97area2b	Dol 3	Center of dolomite crystal	NA	22.01	30.44	NA	-	-	NA	-	52.81
Osiris: OS-11-41 Line 9 342_97area2b	Dol 3	Center of dolomite crystal	NA	22.08	31.25	NA	-	-	NA	-	53.42
Osiris: OS-11-41 Line 10 342_97area2b	Dol 3	Center of dolomite crystal	NA	21.72	31.15	NA	-	-	NA	-	52.94
Osiris: OS-11-41 Line 1 206_98_area1	Dol 2	Center of dolomite crystal	NA	21.92	31.02	NA	-	0.05	NA	-	53.06
Osiris: OS-11-41 Line 2 206_98_area1	Dol 2	Rim of dolomite crystal	NA	20.47	30.17	NA	-	-	NA	1.84	52.56
Osiris: OS-11-41 Line 3 206_98_area1	Dol 2	Rim of dolomite crystal	NA	20.82	30.06	NA	-	-	NA	1.28	52.23
Osiris: OS-11-41 Line 4 206_98_area1	Dol 2	Rim of dolomite crystal	NA	19.35	32.51	NA	-	-	NA	0.86	52.80
Osiris: OS-11-41 Line 4 206_98_area1	Dol 2	Rim of dolomite crystal	NA	20.69	30.91	NA	-	-	NA	0.94	52.58

Sample ID	Phase	Occurrence	BaO	MgO	CaO	SrO	MnO	Na ₂ O	ZnO	FeO	Total
Osiris: OS-11-41 Line 5 206_98_areal	Dol 2	Rim of dolomite crystal	NA	0.4	0.05	NA	0.08	0.05	NA	0.85	
Osiris: OS-11-41 Line 6 206_98_areal	Dol 2	Center of dolomite crystal	NA	21.07	30.64	NA	-	-	NA	0.88	52.64
Osiris: OS-11-41 Line 7 206_98_areal	Dol 2	Center of dolomite crystal	NA	21.25	30.47	NA	-	-	NA	0.84	52.61
Osiris: OS-11-41 Line 8 206_98_areal	Dol 2	Center of dolomite crystal	NA	20.73	30.70	NA	0.08	-	NA	0.91	52.45
Osiris: OS-11-41 Line 9 206_98_areal	Dol 2	Center of dolomite crystal	NA	20.55	30.87	NA	-	-	NA	0.87	52.37
Osiris: OS-11-41 Line 10 206_98_areal	Dol 2	Center of dolomite crystal	NA	20.84	31.06	NA	-	-	NA	0.89	52.85
Osiris: OS-11-41 Line 11 206_98_areal	Dol 2	Center of dolomite crystal	NA	20.10	31.53	NA	-	-	NA	-	52.48
Osiris: OS-11-41 Line 12 206_98_areal	Dol 2	Center of dolomite crystal	NA	20.44	31.43	NA	-	-	NA	-	52.74
Osiris: OS-11-41 Line 13 206_98_areal	Dol 3	Center of dolomite crystal	NA	20.65	31.28	NA	-	-	NA	-	52.83
Osiris: OS-11-41 Line 14 206_98_areal	Dol 3	Center of dolomite crystal	NA	20.44	31.47	NA	-	-	NA	0.90	52.89
Osiris: OS-11-41 Line 15 206_98_areal	Dol 3	Center of dolomite crystal	NA	20.42	31.28	NA	-	-	NA	0.98	52.76
Osiris: OS-11-41 Line 16 206_98_areal	Dol 3	Center of dolomite crystal	NA	20.22	31.20	NA	-	-	NA	1.54	53.01
Osiris: OS-11-41 Line 17 206_98_areal	Dol 3	Center of dolomite crystal	NA	22.11	30.68	NA	-	-	NA	-	52.99
Osiris: OS-11-41 Line 18 206_98_areal	Dol 3	Center of dolomite crystal	NA	21.80	30.54	NA	-	-	NA	-	52.61
Osiris: OS-11-41 Line 19 206_98_areal	Dol 3	Center of dolomite crystal	NA	21.93	30.53	NA	-	-	NA	-	52.79
Osiris: OS-11-41 Line 20 206_98_areal	Dol 3	Center of dolomite crystal	NA	21.86	30.80	NA	-	-	NA	-	52.83
Osiris: OS-11-41 Line 1 206_98_areala	Dol 2	Rim of dolomite crystal	NA	21.17	31.50	NA	-	-	NA	-	52.83
Osiris: OS-11-41 Line 2 206_98_areala	Dol 2	Rim of dolomite crystal	NA	21.13	30.32	NA	-	-	NA	1.16	52.68
Osiris: OS-11-41 Line 3 206_98_areala	Dol 2	Rim of dolomite crystal	NA	21.67	30.30	NA	-	-	NA	-	52.86
Osiris: OS-11-41 Line 4 206_98_areala	Dol 2	Rim of dolomite crystal	NA	21.26	30.74	NA	-	-	NA	-	52.89
Osiris: OS-11-41 Line 5 206_98_areala	Dol 2	Rim of dolomite crystal	NA	20.72	31.30	NA	-	-	NA	-	52.85
Osiris: OS-11-41 Line 6 206_98_areala	Dol 2	Rim of dolomite crystal	NA	20.38	31.43	NA	-	-	NA	-	52.71
Osiris: OS-11-41 Line 7 206_98_areala	Dol 2	Rim of dolomite crystal	NA	20.48	31.41	NA	-	-	NA	0.91	52.90
Osiris: OS-11-41 Line 8 206_98_areala	Dol 2	Rim of dolomite crystal	NA	20.21	31.52	NA	-	-	NA	0.96	52.77
Osiris: OS-11-41 Line 9 206_98_areala	Dol 2	Rim of dolomite crystal	NA	20.46	30.53	NA	-	-	NA	1.76	52.83
Osiris: OS-11-41 Line 10 206_98_areala	Dol 2	Rim of dolomite crystal	NA	22.07	30.65	NA	-	-	NA	-	53.00
Osiris: OS-11-41 Line 11 206_98_areala	Dol 2	Rim of dolomite crystal	NA	22.60	30.67	NA	-	-	NA	-	53.50
Osiris: OS-11-41 Line 12 206_98_areala	Dol 2	Center of dolomite crystal	NA	21.83	31.05	NA	-	-	NA	-	53.17
Osiris: OS-11-41 Line 13 206_98_areala	Dol 2	Center of dolomite crystal	NA	22.12	30.93	NA	-	-	NA	-	53.31
Osiris: OS-11-41 Line 14 206_98_areala	Dol 2	Center of dolomite crystal	NA	22.16	30.73	NA	-	-	NA	-	53.12
Osiris: OS-11-41 Line 15 206_98_areala	Dol 2	Center of dolomite crystal	NA	21.97	31.15	NA	-	-	NA	-	53.36
Osiris: OS-11-41 Line 16 206_98_areala	Dol 2	Center of dolomite crystal	NA	22.08	30.62	NA	-	-	NA	-	52.90
Osiris: OS-11-41 Line 17 206_98_areala	Dol 2	Center of dolomite crystal	NA	22.04	30.65	NA	-	-	NA	-	52.93
Osiris: OS-11-41 Line 18 206_98_areala	Dol 2	Center of dolomite crystal	NA	21.99	30.96	NA	-	-	NA	-	53.07
Osiris: OS-11-41 Line 19 206_98_areala	Dol 2	Center of dolomite crystal	NA	22.03	30.99	NA	-	-	NA	-	53.21
Osiris: OS-11-41 Line 20 206_98_areala	Dol 2	Center of dolomite crystal	NA	22.05	31.12	NA	-	-	NA	-	53.33
Osiris: OS-11-41 Line 20 206_98_areala	Dol 2	Center of dolomite crystal	NA	22.06	30.71	NA	-	-	NA	-	52.98

Sample ID	Phase	Occurrence	BaO	MgO	CaO	SrO	MnO	Na ₂ O	ZnO	FeO	Total
Osiris: OS-11-41 Line 2 206_98_area2_dol	Dol 2	Rim of dolomite crystal	NA	0.4	0.05	NA	0.08	0.05	NA	0.85	53.22
Osiris: OS-11-41 Line 3 206_98_area2_dol	Dol 2	Rim of dolomite crystal	NA	20.63	31.24	NA	-	-	NA	1.69	52.73
Osiris: OS-11-41 Line 4 206_98_area2_dol	Dol 2	Rim of dolomite crystal	NA	20.93	31.42	NA	-	-	NA	0.91	53.31
Osiris: OS-11-41 Line 5 206_98_area2_dol	Dol 2	Rim of dolomite crystal	NA	21.18	31.06	NA	-	-	NA	0.98	53.28
Osiris: OS-11-41 Line 6 206_98_area2_dol	Dol 2	Center of dolomite crystal	NA	20.24	30.71	NA	0.09	-	NA	2.40	53.47
Osiris: OS-11-41 Line 7 206_98_area2_dol	Dol 2	Center of dolomite crystal	NA	20.10	31.25	NA	-	-	NA	1.93	53.34
Osiris: OS-11-41 Line 8 206_98_area2_dol	Dol 2	Center of dolomite crystal	NA	21.37	30.78	NA	0.10	-	NA	-	52.86
Osiris: OS-11-41 Line 9 206_98_area2_dol	Dol 2	Center of dolomite crystal	NA	22.51	30.69	NA	-	-	NA	-	53.38
Osiris: OS-11-41 Line 10 206_98_area2_dol	Dol 2	Center of dolomite crystal	NA	22.27	30.81	NA	-	-	NA	-	53.33
Osiris: OS-11-41 Line 11 206_98_area2_dol	Dol 2	Center of dolomite crystal	NA	22.55	30.59	NA	-	-	NA	-	53.45
Osiris: OS-11-41 Line 12 206_98_area2_dol	Dol 2	Center of dolomite crystal	NA	22.21	30.61	NA	-	-	NA	-	53.19
Osiris: OS-11-41 Line 13 206_98_area2_dol	Dol 2	Center of dolomite crystal	NA	22.38	30.49	NA	-	-	NA	-	53.13
Osiris: OS-11-41 Line 14 206_98_area2_dol	Dol 2	Center of dolomite crystal	NA	22.31	30.27	NA	-	-	NA	-	53.30
Osiris: OS-11-41 Line 15 206_98_area2_dol	Dol 2	Center of dolomite crystal	NA	22.56	30.49	NA	-	-	NA	-	53.44
Osiris: OS-11-41 Line 16 206_98_area2_dol	Dol 2	Center of dolomite crystal	NA	22.41	30.41	NA	-	-	NA	-	53.16
Osiris: OS-11-41 Line 17 206_98_area2_dol	Dol 2	Rim of dolomite crystal	NA	22.04	30.60	NA	0.10	-	NA	-	53.19
Osiris: OS-11-41 Line 18 206_98_area2_dol	Dol 2	Rim of dolomite crystal	NA	21.41	30.84	NA	0.09	-	NA	0.89	53.26
Osiris: OS-11-41 Line 19 206_98_area2_dol	Dol 2	Rim of dolomite crystal	NA	19.56	30.91	NA	0.10	-	NA	2.91	53.51
Osiris: OS-11-41 Line 20 206_98_area2_dol	Dol 2	Rim of dolomite crystal	NA	19.72	30.92	NA	-	-	NA	2.63	53.35
Isis east: OS-12-120 Line 1 104_75_area2	Dol 3	Rim of dolomite crystal	NA	20.74	30.98	NA	-	-	NA	-	52.41
Isis east: OS-12-120 Line 2 104_75_area2	Dol 3	Rim of dolomite crystal	NA	21.17	30.56	NA	-	-	NA	-	52.40
Isis east: OS-12-120 Line 3 104_75_area2	Dol 3	Rim of dolomite crystal	NA	20.98	30.18	NA	-	-	NA	0.95	52.19
Isis east: OS-12-120 Line 4 104_75_area2	Dol 3	Rim of dolomite crystal	NA	21.24	30.20	NA	-	-	NA	1.43	52.98
Isis east: OS-12-120 Line 5 104_75_area2	Dol 2	Rim of dolomite crystal	NA	20.41	30.46	NA	-	-	NA	2.19	53.13
Isis east: OS-12-120 Line 6 104_75_area2	Dol 2	Center of dolomite crystal	NA	20.36	30.12	NA	0.12	-	NA	2.17	52.77
Isis east: OS-12-120 Line 7 104_75_area2	Dol 2	Center of dolomite crystal	NA	20.54	30.39	NA	0.11	-	NA	1.90	52.98
Isis east: OS-12-120 Line 8 104_75_area2	Dol 2	Center of dolomite crystal	NA	20.41	30.64	NA	0.08	-	NA	1.63	52.77
Isis east: OS-12-120 Line 9 104_75_area2	Dol 2	Center of dolomite crystal	NA	20.59	30.31	NA	-	-	NA	1.38	52.39
Isis east: OS-12-120 Line 10 104_75_area2	Dol 2	Center of dolomite crystal	NA	19.96	31.49	NA	-	-	NA	1.74	53.26
Isis east: OS-12-120 Line 11 104_75_area2	Dol 2	Center of dolomite crystal	NA	20.98	30.16	NA	0.09	-	NA	1.88	53.15
Isis east: OS-12-120 Line 12 104_75_area2	Dol 2	Center of dolomite crystal	NA	20.94	29.98	NA	0.10	-	NA	1.79	52.84
Isis east: OS-12-120 Line 13 104_75_area2	Dol 2	Center of dolomite crystal	NA	21.15	30.19	NA	-	-	NA	1.18	52.62
Isis east: OS-12-120 Line 14 104_75_area2	Dol 2	Center of dolomite crystal	NA	21.02	30.58	NA	-	-	NA	1.01	52.68
Isis east: OS-12-120 Line 15 104_75_area2	Dol 2	Center of dolomite crystal	NA	18.04	34.72	NA	-	-	NA	-	53.63
Isis east: OS-12-120 Line 16 104_75_area2	Dol 2	Center of dolomite crystal	NA	21.13	30.55	NA	-	-	NA	0.89	52.64
Isis east: OS-12-120 Line 17 104_75_area2	Dol 2	Center of dolomite crystal	NA	20.96	30.77	NA	-	-	NA	0.85	52.63

Sample ID	Phase	Occurrence	BaO	MgO	CaO	SrO	MnO	Na ₂ O	ZnO	FeO	Total
Isis east: OS-12-120 Line 18 104_75_area2	Dol 2	Center of dolomite crystal	NA	0.4	0.05	NA	0.08	0.05	NA	0.85	
Isis east: OS-12-120 Line 19 104_75_area2	Dol 2	Center of dolomite crystal	NA	21.48	30.29	NA	-	-	NA	1.01	52.88
Isis east: OS-12-120 Line 20 104_75_area2	Dol 2	Center of dolomite crystal	NA	21.59	30.28	NA	0.11	-	NA	1.13	53.11
Isis east: OS-12-120 Line 1 104_75_area3	Dol 2	Rim of dolomite crystal	NA	20.76	30.88	NA	0.10	-	NA	1.12	52.87
Isis east: OS-12-120 Line 2 104_75_area3	Dol 2	Rim of dolomite crystal	NA	20.60	31.07	NA	-	-	NA	0.86	52.61
Isis east: OS-12-120 Line 3 104_75_area3	Dol 2	Rim of dolomite crystal	NA	20.62	30.36	NA	0.09	-	NA	2.02	53.09
Isis east: OS-12-120 Line 4 104_75_area3	Dol 2	Rim of dolomite crystal	NA	20.63	30.06	NA	0.09	-	NA	1.80	52.60
Isis east: OS-12-120 Line 5 104_75_area3	Dol 2	Rim of dolomite crystal	NA	21.20	30.34	NA	-	-	NA	1.34	52.96
Isis east: OS-12-120 Line 6 104_75_area3	Dol 2	Rim of dolomite crystal	NA	19.72	32.50	NA	-	-	NA	0.97	53.28
Isis east: OS-12-120 Line 7 104_75_area3	Dol 2	Center of dolomite crystal	NA	19.92	31.69	NA	0.08	-	NA	0.86	52.56
Isis east: OS-12-120 Line 8 104_75_area3	Dol 2	Center of dolomite crystal	NA	20.79	30.49	NA	-	-	NA	0.87	52.23
Isis east: OS-12-120 Line 9 104_75_area3	Dol 2	Center of dolomite crystal	NA	20.85	30.59	NA	0.08	-	NA	1.14	52.68
Isis east: OS-12-120 Line 10 104_75_area3	Dol 2	Center of dolomite crystal	NA	20.47	30.51	NA	0.08	-	NA	1.42	52.50
Isis east: OS-12-120 Line 11 104_75_area3	Dol 2	Center of dolomite crystal	NA	19.39	31.45	NA	0.09	-	NA	1.68	52.62
Isis east: OS-12-120 Line 12 104_75_area3	Dol 2	Center of dolomite crystal	NA	20.56	30.44	NA	0.10	-	NA	1.65	52.78
Isis east: OS-12-120 Line 13 104_75_area3	Dol 2	Center of dolomite crystal	NA	19.52	30.12	NA	0.09	-	NA	3.99	53.76
Isis east: OS-12-120 Line 14 104_75_area3	Dol 2	Center of dolomite crystal	NA	20.11	30.39	NA	0.10	-	NA	2.30	52.90
Isis east: OS-12-120 Line 15 104_75_area3	Dol 2	Center of dolomite crystal	NA	20.69	30.14	NA	-	-	NA	1.62	52.52
Isis east: OS-12-120 Line 16 104_75_area3	Dol 2	Center of dolomite crystal	NA	19.70	29.91	NA	0.11	-	NA	3.68	53.41
Isis east: OS-12-120 Line 17 104_75_area3	Dol 2	Center of dolomite crystal	NA	21.58	30.08	NA	-	-	NA	-	52.43
Isis east: OS-12-120 Line 18 104_75_area3	Dol 2	Center of dolomite crystal	NA	21.74	30.39	NA	0.08	-	NA	-	52.90
Isis east: OS-12-120 Line 19 104_75_area3	Dol 2	Center of dolomite crystal	NA	21.90	30.59	NA	-	-	NA	-	52.97
Isis east: OS-12-120 Line 20 104_75_area3	Dol 2	Center of dolomite crystal	NA	21.76	30.50	NA	0.09	-	NA	-	52.81
Isis east: OS-12-120 Line 1 115_26_area1	Dol 2	Center of dolomite crystal	NA	22.43	30.64	NA	0.09	-	NA	-	53.33
Isis east: OS-12-120 Line 2 115_26_area1	Dol 2	Rim of dolomite crystal	NA	20.22	32.26	NA	-	-	NA	-	52.89
Isis east: OS-12-120 Line 3 115_26_area1	Dol 2	Rim of dolomite crystal	NA	21.51	31.61	NA	0.08	-	NA	-	53.43
Isis east: OS-12-120 Line 4 115_26_area1	Dol 2	Rim of dolomite crystal	NA	21.54	30.74	NA	-	-	NA	-	52.70
Isis east: OS-12-120 Line 5 115_26_area1	Dol 2	Center of dolomite crystal	NA	21.30	31.52	NA	-	-	NA	-	53.17
Isis east: OS-12-120 Line 6 115_26_area1	Dol 2	Center of dolomite crystal	NA	20.77	32.24	NA	-	-	NA	-	53.21
Isis east: OS-12-120 Line 7 115_26_area1	Dol 2	Center of dolomite crystal	NA	20.96	31.73	NA	-	-	NA	-	52.98
Isis east: OS-12-120 Line 8 115_26_area1	Dol 2	Center of dolomite crystal	NA	20.83	31.67	NA	-	-	NA	-	52.86
Isis east: OS-12-120 Line 9 115_26_area1	Dol 2	Center of dolomite crystal	NA	20.47	32.04	NA	-	-	NA	-	52.92
Isis east: OS-12-120 Line 10 115_26_area1	Dol 2	Center of dolomite crystal	NA	21.33	31.73	NA	-	-	NA	-	53.37
Isis east: OS-12-120 Line 11 115_26_area1	Dol 2	Center of dolomite crystal	NA	21.71	31.01	NA	-	-	NA	-	53.01
Isis east: OS-12-120 Line 12 115_26_area1	Dol 2	Center of dolomite crystal	NA	21.62	30.96	NA	-	-	NA	-	52.86
Isis east: OS-12-120 Line 13 115_26_area1	Dol 2	Center of dolomite crystal	NA	21.66	31.51	NA	-	-	NA	-	53.36
Isis east: OS-12-120 Line 13 115_26_area1	Dol 2	Center of dolomite crystal	NA	21.64	31.04	NA	-	-	NA	-	52.90

Sample ID	Phase	Occurrence	BaO	MgO	CaO	SrO	MnO	Na ₂ O	ZnO	FeO	Total
Isis east: OS-12-120 Line 14 1115_26_areal	Dol 2	Center of dolomite crystal	NA	0.4	0.05	NA	0.08	0.05	NA	0.85	53.06
Isis east: OS-12-120 Line 15 1115_26_areal	Dol 2	Center of dolomite crystal	NA	21.48	31.07	NA	-	-	NA	-	52.74
Isis east: OS-12-120 Line 16 1115_26_areal	Dol 2	Center of dolomite crystal	NA	21.46	30.87	NA	-	-	NA	-	52.88
Isis east: OS-12-120 Line 17 1115_26_areal	Dol 2	Center of dolomite crystal	NA	20.47	30.25	NA	-	-	NA	2.06	52.72
Isis east: OS-12-120 Line 18 1115_26_areal	Dol 2	Rim of dolomite crystal	NA	21.03	30.58	NA	-	-	NA	1.34	52.80
Isis east: OS-12-120 Line 19 1115_26_areal	Dol 2	Rim of dolomite crystal	NA	20.79	30.63	NA	-	-	NA	1.24	52.62
Isis east: OS-12-120 Line 20 1115_26_areal	Dol 2	Rim of dolomite crystal	NA	21.08	30.25	NA	-	-	NA	1.20	52.81
Osiris: OS-11-41 342_97_dol_1	Dol 3	Rim of dolomite crystal	NA	20.54	30.98	NA	-	-	NA	0.15	53.15
Osiris: OS-11-41 342_97_dol_2	Dol 3	Rim of dolomite crystal	NA	21.93	30.96	NA	0.08	-	NA	0.10	53.31
Osiris: OS-11-41 342_97_dol_3	Dol 3	Center of dolomite crystal	NA	21.77	31.35	NA	-	-	NA	0.07	53.28
Osiris: OS-11-41 342_97_dol_4	Dol 2	Center of dolomite crystal	NA	21.83	31.32	NA	-	-	NA	0.82	52.46
Osiris: OS-11-41 342_97_dol_5	Dol 2	Center of dolomite crystal	NA	21.53	30.00	NA	0.09	-	NA	0.93	52.73
Osiris: OS-11-41 342_97_dol_6	Dol 2	Center of dolomite crystal	NA	21.03	30.64	NA	0.09	0.05	NA	0.99	52.67
Osiris: OS-11-41 342_97_dol_7	Dol 2	Center of dolomite crystal	NA	21.39	30.16	NA	0.10	-	NA	1.67	41.15
Osiris: OS-11-41 342_97_cal_1	Cal 4	Calcite veinlet	NA	16.57	22.75	NA	-	-	NA	0.05	56.15
Osiris: OS-11-41 342_97_cal_2	Cal 4	Calcite veinlet	NA	-	55.75	NA	-	-	NA	0.01	56.37
Osiris: OS-11-41 342_97_cal_3	Cal 4	Calcite veinlet	NA	-	55.96	NA	-	-	NA	0.00	56.30
Osiris: OS-11-41 342_97_cal_4	Cal 4	Calcite veinlet	NA	-	56.08	NA	-	-	NA	0.01	56.37
Osiris: OS-11-41 342_97_dol_8	Dol 2	Calcite veinlet	NA	20.96	30.60	NA	0.13	-	NA	1.56	53.27
Osiris: OS-11-41 342_97_dol_9	Dol 2	Calcite veinlet	NA	20.88	30.61	NA	0.08	-	NA	1.46	53.03
Osiris: OS-11-41 342_97_dol_10	Dol 2	Calcite veinlet	NA	21.04	30.60	NA	0.09	-	NA	1.33	53.08
Osiris: OS-11-41 342_97_dol_11	Dol 3	Calcite veinlet	NA	22.09	31.26	NA	-	-	NA	0.20	53.60
Osiris: OS-11-41 342_97_dol_12	Dol 3	Calcite veinlet	NA	21.61	30.98	NA	-	-	NA	0.43	53.12
Osiris: OS-11-41 342_97_dol_13	Dol 3	Calcite veinlet	NA	22.01	31.33	NA	-	-	NA	0.04	53.42
Sample ID	Phase	Occurrence	BaO	MgO	CaO	SrO	MnO	Na₂O	ZnO	FeO	Total
Osiris 103A1dol2_1	Dol 2	Zoned dolomite crystal	0.20	0.4	0.05	0.09	0.08	0.05	0.11	0.85	52.54
Osiris 103A1dol2_2	Dol 2	Zoned dolomite crystal	-	21.21	30.89	-	0.09	-	-	0.35	52.32
Osiris 103A1dol2_3	Dol 2	Zoned dolomite crystal	-	21.29	30.34	-	0.11	-	-	0.58	52.02
Osiris 103A1dol2_4	Dol 2	Zoned dolomite crystal	-	21.27	29.99	-	0.08	-	-	0.68	52.48
Osiris 103A1dol2_5	Dol 2	Zoned dolomite crystal	-	21.79	30.11	-	0.08	-	-	0.50	52.31
Osiris 103A1dol3_1 moved	Dol 2	Zoned dolomite crystal	-	21.48	30.00	-	0.12	-	-	0.71	52.80
Osiris 103A1dol3_2	Dol 3	Zoned dolomite crystal	-	21.95	30.74	-	0.06	-	-	0.04	52.77
Osiris 103A1dol3_3	Dol 3	Zoned dolomite crystal	-	21.95	30.46	-	0.11	-	-	0.26	52.51
Osiris 103A1dol3_4	Dol 3	Zoned dolomite crystal	-	21.62	30.71	-	0.09	-	-	0.09	52.77
Osiris 103A2dol2_1	Dol 2	Zoned dolomite crystal	-	21.95	30.71	-	0.02	-	-	0.09	52.77
Osiris 103A2dol2_2	Dol 2	Zoned dolomite crystal	-	21.52	29.94	-	0.09	-	-	0.64	52.20
Osiris 103A2dol2_3	Dol 2	Zoned dolomite crystal	-	21.45	29.85	-	0.11	-	-	0.78	52.18
Osiris 103A2dol2_3	Dol 2	Zoned dolomite crystal	-	21.43	29.90	-	0.12	-	-	0.76	52.21

Sample ID	Phase	Occurrence	BaO	MgO	CaO	SrO	MnO	Na ₂ O	ZnO	FeO	Total
Osiris 103A2dol3_1	Dol 3	Zoned dolomite crystal	0.20	21.98	30.45	0.09	0.08	0.05	0.11	0.85	52.60
Osiris 103A2dol3_2	Dol 3	Zoned dolomite crystal	-	21.70	29.71	-	0.10	-	-	0.68	52.18
Osiris 103A2dol3_3	Dol 3	Zoned dolomite crystal	-	22.13	30.61	-	0.05	-	-	0.16	52.95
Osiris 103B1dol2_1C	Dol 2	Rim of dolomite crystal	-	20.73	29.91	-	0.13	-	-	1.53	52.30
Osiris 103B1dol2_1O	Dol 2	Rim of dolomite crystal	-	20.25	30.26	-	0.12	-	-	1.28	51.90
Osiris 103B1dol3_1	Dol 3	Center of dolomite crystal	-	21.69	30.65	-	0.02	-	-	-	52.36
Osiris 103B2dol2_1	Dol 2	Rim of dolomite crystal	-	20.83	29.39	-	0.06	-	-	1.69	51.97
Osiris 103B2dol3_1	Dol 3	Center of dolomite crystal	-	21.69	30.60	-	0.03	-	-	0.20	52.52
Osiris 103B3dol2_1	Dol 2	Rim of dolomite crystal	-	21.22	30.04	-	0.07	-	-	0.92	52.25
Osiris 103B3dol3_1	Dol 3	Center of dolomite crystal	-	22.04	30.31	-	0.05	-	-	0.16	52.56
Osiris 104A1dol1_3 (cal)	Host lime	Allochem	-	-	53.77	-	-	-	-	0.13	53.90
104A1dol1_unk (cal)	Host lime	Allochem	-	-	54.71	-	0.05	-	-	0.18	54.93
Osiris 104A2dol1_3	Dol 1	Allochem	-	14.29	27.32	-	0.10	0.18	-	4.70	46.59
Osiris 104A2dol1_4 (cal)	Host lime	Allochem	-	-	54.29	-	-	-	-	0.11	54.41
Osiris 104B3calh_1	Host lime	Allochem	-	-	55.00	-	-	-	-	0.13	55.13
Osiris 104B3calh_1a	Host lime	Allochem	-	-	55.26	-	-	-	-	0.09	55.35
Osiris 104B3calh_3	Host lime	Allochem	-	-	54.27	0.11	0.05	-	-	0.18	54.61
Osiris 104B3calh_3a	Dol 1	Allochem	-	19.15	31.60	-	0.08	-	-	1.26	52.10
Osiris 105A1dol2_1 moved	Dol 3	Veinlet	-	20.75	30.63	-	0.45	0.05	-	0.46	52.33
Osiris 105A1dol2_2 moved	Dol 3	Veinlet	-	20.86	30.43	-	1.01	-	-	0.13	52.43
Osiris 105A1cal4_2	Cal 4	Veinlet	-	-	55.34	-	0.05	-	-	-	55.39
Osiris 105A1cal4_3	Cal 4	Veinlet	-	-	55.55	-	0.05	-	-	-	55.60
Osiris 105A2dol2_1	Dol 2	Center of dolomite crystal	-	17.52	31.35	-	0.38	-	-	3.46	52.71
Osiris 105A2dol3_1O	Dol 3	Rim	-	20.84	30.96	-	0.33	0.04	-	-	52.17
Osiris 105A2dol3_1C	Dol 3	Rim	-	20.44	30.75	-	0.33	0.06	-	0.39	51.96
Osiris 105A3dol2_1	Dol 2	Veinlet	-	17.77	31.07	-	0.22	-	-	3.99	53.04
Osiris 105A3dol3_2	Dol 3	Veinlet	-	20.73	30.27	-	0.16	-	-	1.05	52.21
Osiris 105A3dol3_3	Dol 3	Veinlet	-	19.33	31.47	-	0.20	-	-	-	50.99
Osiris 105B1dol2_1	Dol 2	Zoned dolomite crystal	-	21.61	30.36	-	0.17	-	-	-	52.14
Osiris 105B1dol3_1	Dol 3	Zoned dolomite crystal	-	21.89	30.17	-	0.06	-	-	0.22	52.34
Osiris 105B1cal4_1	Cal 4	Zoned dolomite crystal	-	-	55.58	-	0.37	-	-	-	55.95
Osiris 105B1cal4_2	Cal 4	Zoned dolomite crystal	-	-	55.20	-	0.33	-	-	0.19	55.72
Osiris 105B1cal4_3	Cal 4	Zoned dolomite crystal	-	-	55.70	-	0.35	-	-	-	56.05
Osiris 105B1cal4_4	Cal 4	Zoned dolomite crystal	-	-	55.85	-	0.31	-	-	-	56.16
Osiris 105B2_cal4_1	Cal 4	Zoned dolomite crystal	-	-	56.21	-	0.20	-	-	-	56.41
Osiris 105B2_cal4_2	Cal 4	Zoned dolomite crystal	-	-	55.61	-	0.44	-	-	-	56.05

Sample ID	Phase	Occurrence	BaO	MgO	CaO	SrO	MnO	Na ₂ O	ZnO	FeO	Total
Osiris 105B2_cal4_3	Cal 4	Zoned dolomite crystal	0.20	-	55.63	0.09	0.39	0.05	0.11	-	56.02
Osiris 105B2_cal4_3	Cal 4	Zoned dolomite crystal	-	-	56.03	-	0.26	-	-	-	56.29
Osiris 105B2_dol2_1	Dol 2	Zoned dolomite crystal	-	21.52	29.84	-	0.08	-	-	0.70	52.14
Osiris 105B2_dol3_1	Dol 3	Zoned dolomite crystal	-	21.90	30.62	-	0.04	-	-	-	52.56
Osiris 106A1dol1_1	Dol 1	Allochem	-	18.75	31.82	-	0.39	0.07	-	1.06	52.09
Osiris 106A2dol1_3	Dol 1	Rim on coated grain	-	17.20	32.58	-	0.10	-	-	3.34	53.22
Osiris 106A2dol1_1	Dol 1	Allochem	-	17.95	29.67	-	0.12	-	-	3.10	50.84
Osiris 106A3dol1_1	Dol 1	Allochem	-	17.24	31.55	-	0.12	-	-	4.07	52.97
Osiris 106A3dol3_1	Dol 3	Rim on coated grain	-	19.60	33.65	-	-	-	-	0.09	53.34
Osiris 106A3dol3_2	Dol 3	Rim on coated grain	-	19.36	32.99	-	0.05	0.06	-	0.15	52.61
Osiris 106A3cal1_1	Host lime	Allochem	-	-	55.81	0.38	-	-	-	-	56.19
Osiris 106A3cal1_2	Host lime	Allochem	-	-	55.79	-	-	-	-	-	55.79
Osiris 106B1dol1_1	Host lime	Allochem	-	16.43	31.61	-	0.15	-	-	4.65	52.84
Osiris 106B1dol3_1	Dol 3	Rim on coated grain	-	20.22	32.20	-	0.05	-	-	0.34	52.82
Osiris 106B1dol1_2	Dol 1	Allochem	-	15.93	30.41	-	0.13	-	-	7.57	54.04
Osiris 106B2dol1_1	Dol 1	Allochem	-	17.97	29.32	-	0.14	-	-	6.32	53.75
Osiris 106B2dol1_3	Dol 1	Allochem	-	15.01	31.28	-	0.15	0.04	-	7.27	53.74
Osiris 106B3dol1_2	Dol 1	Allochem	-	18.06	31.83	-	0.12	-	-	2.45	52.46
Osiris 106B3dol1_3O	Dol 1	Allochem	-	17.49	28.93	-	0.11	-	-	5.72	52.25
Osiris 106B3dol1_3C	Dol 1	Allochem	-	15.41	30.80	-	0.16	-	-	7.42	53.79
Isis east 107A2_calh_1	Host lime	Allochem	-	-	54.75	0.54	0.07	-	-	0.13	55.49
Isis east 107A2_calh_2	Host lime	Allochem	-	-	54.99	0.51	-	-	-	-	55.49
Isis east 107A4_calh_1	Host lime	Allochem	-	-	55.29	0.23	-	0.09	-	0.08	55.68
Isis east 107A4_calh_2	Host lime	Allochem	-	-	54.72	-	0.14	-	-	0.38	55.24
Isis east 107A4_calh_3	Host lime	Allochem	-	-	53.42	-	0.31	-	-	0.94	54.67
Isis east 107Bdol3_3	Dol 3	Rim on coated grain	-	19.20	32.38	-	-	-	-	0.75	52.33
Isis east 107Bdol3_4	Dol 3	Rim on coated grain	-	19.88	32.98	-	0.02	0.04	-	0.18	53.10
Isis east 107Bdol3_5	Dol 3	Rim on coated grain	-	20.31	32.38	-	-	-	-	0.14	52.83
Isis east 107Bdol3_6	Dol 3	Rim on coated grain	-	16.57	30.98	-	0.12	0.07	-	4.44	52.19
Isis east 107C1_calh_1	Host lime	Allochem	-	-	52.58	-	0.42	0.04	-	1.22	54.26
Isis east 107C1_calh_2	Host lime	Allochem	-	-	54.90	0.12	-	-	-	-	55.02
Isis east 107C1_calh_3	Host lime	Allochem	-	-	54.36	0.14	0.05	0.05	-	0.14	54.73
Isis east 107C2_dol3_3	Dol 3	Rim on coated grain	-	18.34	34.03	-	-	-	-	0.14	52.51
Isis east 107C2_dol4	Dol 3	Rim on coated grain	-	21.99	29.98	-	0.05	0.10	-	0.28	52.40
Osiris 108A1cal3_1	Cal 3	veinlet	-	-	54.17	0.29	-	-	-	0.15	54.61
Osiris 108A1cal3_2	Cal 3	veinlet	-	-	54.59	0.39	-	-	-	0.17	55.15

Sample ID	Phase	Occurrence	BaO	MgO	CaO	SiO	MnO	Na ₂ O	ZnO	FeO	Total
Osiris 108A1dol2_3	Dol2	Center of dolomite crystal	0.20	0.4	0.05	0.09	0.08	0.05	0.11	0.85	52.53
Osiris 108A1dol2_2	Dol2	Center of dolomite crystal		17.25	28.90	-	0.15	-	-	6.23	52.36
Osiris 108A1dol2_4	Dol2	Center of dolomite crystal		18.61	29.78	-	0.09	-	-	3.88	52.59
Osiris 108A1dol2_1	Dol2	Center of dolomite crystal		17.26	29.55	-	0.12	-	-	5.67	53.05
Osiris 108A2dol2_1	Dol2	Center of dolomite crystal		17.82	29.56	-	0.11	-	-	4.89	53.00
Osiris 108A2dol2_2	Dol2	Center of dolomite crystal		17.98	30.00	-	0.13	-	-	4.84	52.99
Osiris 108A2dol2_3	Dol2	Center of dolomite crystal		18.38	29.62	-	0.15	-	-	5.70	52.97
Osiris 108A2dol2_1	Dol2	Center of dolomite crystal		17.53	29.53	-	0.17	0.05	-	0.24	54.99
Osiris 108A2cal3_1	Cal3	veinlet		-	54.70	-	0.05	-	-	0.31	55.17
Osiris 108A2cal3_2	Cal3	veinlet		-	54.86	-	-	-	-	0.19	55.70
Osiris 108B1cal3_1	Cal3	veinlet		-	54.98	0.42	0.05	0.06	-	0.19	55.83
Osiris 108B1cal3_2	Cal3	veinlet		-	55.19	0.35	-	0.11	-	0.21	55.50
Osiris 108B1cal3_3	Cal3	veinlet		-	54.74	0.42	-	0.13	-	0.19	55.55
Osiris 108B3cal3_1	Cal3	veinlet		-	54.87	0.50	-	-	-	0.16	55.07
Osiris 108B3cal3_2	Cal3	veinlet		-	54.51	0.34	0.06	-	-	0.09	54.49
Osiris 108B3cal3_3	Cal3	veinlet		-	54.27	0.14	-	-	-	0.11	54.85
Osiris 108B3cal3_4	Cal3	veinlet		-	54.62	0.12	-	-	-	0.10	55.78
Osiris 109Acal1_1	Cal1	veinlet		-	55.69	-	-	-	-	0.12	55.84
Osiris 109Acal1_2	Cal1	veinlet		-	55.73	-	-	-	-	0.09	56.05
Osiris 109Acal1_3	Cal1	veinlet		-	55.79	-	0.09	0.08	-	0.08	56.02
Osiris 109Acal1_4	Cal1	veinlet		-	55.84	-	0.05	0.05	-	-	56.08
Osiris 110Acal2_1	Cal2	veinlet		-	56.08	-	-	-	-	-	56.04
Osiris 110Acal2_2	Cal2	veinlet		-	56.04	-	-	-	-	-	56.44
Osiris 110Acal2_3	Cal2	veinlet		-	56.43	-	0.01	-	-	-	55.34
Osiris 111A1cal2_1	Cal2	veinlet		-	54.68	-	0.06	-	-	0.61	55.07
Osiris 111A1cal2_2	Cal2	veinlet		-	54.55	-	0.05	-	-	0.47	55.26
Osiris 111A1cal2_3	Cal2	veinlet		-	54.94	-	-	0.08	-	0.24	55.26
Osiris 111A1dol2_1	Dol2	Center of dolomite crystal		16.60	31.65	-	0.21	0.04	-	3.67	52.17
Osiris 111A1dol2_2	Dol2	Center of dolomite crystal		16.41	29.93	-	0.34	0.06	-	4.25	50.99
Osiris 111A1dol2_3	Dol2	Center of dolomite crystal		17.59	32.23	-	0.13	0.04	-	3.21	53.21
Osiris 111A1dol2_4	Dol2	Center of dolomite crystal		16.30	32.55	-	0.24	0.05	-	4.03	53.16
Osiris 111A1dol2_5	Dol2	Center of dolomite crystal		17.39	32.31	-	0.12	-	-	3.15	52.97
Osiris 111A2dol2_1	Dol2	Center of dolomite crystal		17.65	32.33	-	0.07	0.05	-	2.83	52.93
Osiris 111A2dol2_2	Dol2	Center of dolomite crystal		17.24	32.62	-	0.23	-	-	2.99	53.08
Isis east 112A1dol2_1	Dol2	Zoned dolomite crystal		18.56	30.46	-	0.10	-	-	3.49	52.61
Isis east 112A1dol2_2	Dol2	Zoned dolomite crystal		19.03	30.68	-	0.10	-	-	3.03	52.84
Isis east 112A1dol2_3	Dol2	Zoned dolomite crystal		18.34	30.99	-	0.06	-	-	3.21	52.60

Sample ID	Phase	Occurrence	BaO	MgO	CaO	SrO	MnO	Na ₂ O	ZnO	FeO	Total
Isis east 112A1do12_4	Dol 2	Zoned dolomite crystal	0.20	0.4	0.05	0.09	0.08	0.05	0.11	0.85	52.97
Isis east 112A1do12_5	Dol 2	Zoned dolomite crystal	-	19.28	30.65	-	0.10	-	-	2.94	53.03
Isis east 112A1do13_1 moved	Dol 2	Zoned dolomite crystal	-	18.38	31.41	-	0.16	-	-	3.08	53.40
Isis east 112A2do12_1	Dol 2	Zoned dolomite crystal	-	17.32	31.84	-	-	-	-	4.24	53.20
Isis east 112A2do12_2	Dol 2	Zoned dolomite crystal	-	16.83	31.94	-	0.11	-	-	4.32	51.95
Isis east 112A2do12_3	Dol 2	Zoned dolomite crystal	-	19.08	29.91	-	0.06	-	-	2.90	53.12
Isis east 112A2do13_1	Dol 3	Zoned dolomite crystal	-	18.91	30.92	-	0.06	-	-	3.22	52.98
Isis east 112A2do13_2	Dol 3	Zoned dolomite crystal	-	19.26	30.47	-	0.11	-	-	3.14	53.01
Isis east 112A3do13_1 moved	Dol 2	Zoned dolomite crystal	-	20.72	31.19	-	-	-	-	1.10	52.99
Isis east 112A3do13_2C moved	Dol 2	Zoned dolomite crystal	-	16.92	31.53	-	0.09	0.10	-	4.35	52.74
Isis east 112A3do13_2O	Dol 3	Zoned dolomite crystal	-	18.09	31.15	-	-	0.04	-	3.46	51.41
Isis east 112A3do12_1	Dol 2	Zoned dolomite crystal	-	20.24	30.46	-	0.06	-	-	0.65	53.31
Isis east 112A3do12_2	Dol 2	Zoned dolomite crystal	-	18.33	31.46	-	0.12	-	-	3.40	53.24
Isis east 112A3do12_3	Dol 2	Zoned dolomite crystal	-	17.59	31.59	-	0.06	-	-	4.00	53.04
Isis east 112A5do12_1	Dol 2	Zoned dolomite crystal	-	18.31	31.48	-	0.09	-	-	2.98	53.14
Isis east 112A5do12_2	Dol 2	Zoned dolomite crystal	-	18.31	31.72	-	0.13	-	-	2.92	53.22
Isis east 112A5do12_3	Dol 2	Zoned dolomite crystal	-	19.20	30.95	-	0.15	-	-	3.83	53.80
Isis east 112B2do13_1	Dol 3	Zoned dolomite crystal	-	18.69	31.2	-	0.08	-	-	0.50	53.21
Isis east 112B2do13_2	Dol 3	Zoned dolomite crystal	-	19.28	33.43	-	-	-	-	1.07	52.79
Isis east 112B2do13_3 moved	Dol 2	Zoned dolomite crystal	-	19.34	32.3	-	0.08	-	-	3.32	52.95
Isis east 112B2do12_1	Dol 2	Zoned dolomite crystal	-	17.86	31.7	-	0.07	-	-	3.87	53.58
Isis east 112B2do12_2	Dol 2	Zoned dolomite crystal	-	17.77	31.84	-	0.10	-	-	3.01	53.24
Isis east 112B2do12_3	Dol 2	Zoned dolomite crystal	-	18.66	31.54	-	0.15	-	-	4.02	53.27
Isis east 112B3do12_1	Dol 2	Zoned dolomite crystal	-	17.53	31.62	-	0.07	-	-	4.30	53.16
Isis east 112B3do12_2	Dol 2	Zoned dolomite crystal	-	17.27	31.61	-	0.09	-	-	3.40	52.57
Isis east 112B3do12_3	Dol 3	Zoned dolomite crystal	-	18.64	30.97	-	0.15	-	-	2.48	52.72
Isis east 112B3do13_1	Dol 3	Zoned dolomite crystal	-	19.75	30.27	-	0.07	-	-	0.32	52.89
Isis east 112B3do13_2	Dol 3	Zoned dolomite crystal	-	19.81	32.53	-	0.06	-	-	1.12	52.48
Isis east 112B3do13_3	Dol 3	Zoned dolomite crystal	-	19.39	32.38	-	-	-	-	0.83	52.48
Isis east 112B3do13_3	Dol 3	Zoned dolomite crystal	-	19.39	32.21	-	0.05	-	-	0.83	52.48

Sample ID	Phase	Occurrence	BaO	MgO	CaO	SrO	MnO	Na ₂ O	ZnO	FeO	Total
Isis East 51_16_cal1	Cal 1	Veinlet	NA	0.4	0.05	0.07	0.08	NA	NA	0.85	55.30
Isis East 51_16_cal2	Cal 1	Veinlet	NA	0.00	54.05	0.18	0.11	NA	NA	0.96	56.27
Osiris 84_15_dol1	Dol 2	Center of dolomite crystal	NA	0.00	55.58	-	0.11	NA	NA	0.58	53.44
Osiris 84_15_dol2	Dol 2	Center of dolomite crystal	NA	17.30	30.04	-	0.03	NA	NA	6.04	53.66
Osiris 84_15_cal1	Host rock	Micrite	NA	0.00	55.12	0.14	0.00	NA	NA	0.11	55.38
Osiris 84_15_cal2	Host rock	Micrite	NA	0.00	55.98	0.16	0.06	NA	NA	0.07	56.27

Sample ID	Phase	Occurrence	BaO	MgO	CaO	SrO	MnO	Na ₂ O	ZnO	FeO	Total
Osiris 67_75_cal1	Host rock	Micrite	NA	0.4	0.05	0.07	0.08	NA	NA	0.85	
Osiris 67_75_cal2	Host rock	Micrite	NA	0.00	55.65	-	0.02	NA	NA	0.12	55.83
Isis East 138_05_cal1	Cal 4	Veinlet	NA	0.12	55.66	-	0.01	NA	NA	0.11	55.95
Isis East 138_05_cal2	Cal 4	Veinlet	NA	0.00	56.60	-	0.02	NA	NA	0.03	56.65
Osiris 14_14_cal1	Cal 2	Veinlet	NA	0.00	56.26	-	0.06	NA	NA	0.01	56.35
Osiris 14_14_cal2	Cal 2	Veinlet	NA	0.00	55.45	0.12	0.05	NA	NA	0.29	55.91
Osiris 14_14_cal3	Cal 2	Micrite	NA	0.00	55.35	0.10	0.02	NA	NA	0.35	55.82
Osiris 14_14_cal4	Cal 2	Micrite	NA	0.00	55.28	0.08	0.01	NA	NA	0.11	55.47
Osiris 341_42_dol1	Dol 2	Center of dolomite crystal	NA	0.00	55.08	0.09	0.04	NA	NA	0.11	55.31
Osiris 341_42_dol2	Dol 2	Center of dolomite crystal	NA	20.90	30.37	-	0.09	NA	NA	0.64	52.02
Osiris 341_42_dol3	Dol 2	Center of dolomite crystal	NA	20.96	30.44	-	0.09	NA	NA	0.48	52.01
Isis East 138_33-dol1	Dol 2	Center of dolomite crystal	NA	21.24	30.58	-	0.11	NA	NA	0.47	52.40
Isis East 138_33-dol2	Dol 3	Center of dolomite crystal	NA	18.81	33.66	-	0.02	NA	NA	0.00	52.53
Isis East 138_33-dol3	Dol 3	Center of dolomite crystal	NA	19.31	32.91	-	0.03	NA	NA	0.03	52.29
Isis East 138_33-dol4	Dol 2	Center of dolomite crystal	NA	18.32	34.21	-	0.05	NA	NA	0.18	52.81
Isis East 293_18_dol1	Dol 3	Center of dolomite crystal	NA	18.88	33.56	-	0.01	NA	NA	0.08	52.55
Isis East 293_18_dol2	Dol 2	Fine crystal	NA	20.40	29.93	-	0.10	NA	NA	1.25	51.69
Isis East 101_44A_dol1	Dol 2	Fine crystal	NA	20.03	30.02	-	0.11	NA	NA	1.30	51.51
Isis East 101_44A_dol2	Dol 3	Center of dolomite crystal	NA	21.42	31.12	-	0.10	NA	NA	0.06	52.73
Isis East 101_44A_dol3	Dol 2	Center of dolomite crystal	NA	21.58	30.51	-	0.09	NA	NA	0.31	52.49
Isis East 106_14A_dol1	Dol 3	Center of dolomite crystal	NA	21.29	30.75	-	0.07	NA	NA	0.10	52.21
Isis East 106_14A_dol2	Dol 3	Center of dolomite crystal	NA	20.73	30.09	-	0.27	NA	NA	0.09	51.18
Isis East 106_14A_dol3	Dol 2	Center of dolomite crystal	NA	21.21	30.92	-	0.08	NA	NA	0.04	52.25
Isis East 106_14A_dol4	Dol 2	Center of dolomite crystal	NA	20.81	30.48	-	0.11	NA	NA	0.14	49.33
Isis East 106_14A_dol5	Dol 2	Center of dolomite crystal	NA	20.99	31.35	-	0.07	NA	NA	0.09	51.48
Isis East 106_14A_dol6	Dol 2	Center of dolomite crystal	NA	21.21	30.82	-	0.14	NA	NA	0.14	52.33
Isis East 106_14A_dol7	Dol 3	Center of dolomite crystal	NA	19.91	28.82	-	0.29	NA	NA	0.20	49.23
Osiris 45_09_cal1	Cal 4	Calcite overgrowth on dol xtal	NA	0.12	55.85	-	0.03	NA	NA	0.01	56.01
Osiris 45_09_cal2	Cal 4	Vein	NA	0.00	55.87	-	0.09	NA	NA	0.00	55.96
Osiris 45_09_cal3	Cal 4	Vein	NA	0.00	56.04	-	0.08	NA	NA	0.00	56.13
Osiris 45_09_cal4	Cal 4	Vein	NA	0.00	56.12	-	0.11	NA	NA	0.00	56.24
Osiris 45_09_cal5	Cal 4	Vein	NA	0.00	56.37	-	0.10	NA	NA	0.00	56.50
Osiris 86.72_dol1	Cal 4	Vein	NA	0.00	56.05	-	0.07	NA	NA	0.00	56.15
Osiris 86.72_dol2	Dol 2	Fine crystal	NA	21.16	30.95	-	0.00	NA	NA	0.08	52.20
Osiris 29_30_cal1	Dol 2	Fine crystal	NA	20.70	30.61	-	0.02	NA	NA	0.05	51.38
Osiris 29_30_cal2	Cal 2	Micrite	NA	0.10	56.06	0.10	0.02	NA	NA	0.08	56.35
Osiris 29_30_cal3	Cal 2	Micrite	NA	0.00	55.57	0.09	0.04	NA	NA	0.08	55.78
Osiris 92_45_cal1	Cal 2	Micrite	NA	0.00	55.42	0.12	0.02	NA	NA	0.33	55.89
Osiris 267_58_cal1	Cal 2	Veinlet	NA	0.00	55.90	0.38	0.03	NA	NA	0.19	56.50
Osiris 267_58_cal2	Cal 3	Veinlet	NA	0.00	56.35	0.16	0.00	NA	NA	0.15	56.66
Osiris 319_68_cal1	Cal 3	Veinlet	NA	0.10	55.48	0.09	0.02	NA	NA	0.29	55.98
Osiris 319_68_cal2	Cal 4	Veinlet	NA	0.21	55.18	0.12	0.05	NA	NA	0.25	55.82
Osiris 319_68_cal3	Cal 3	Veinlet	NA	0.00	55.75	-	0.08	NA	NA	0.02	55.87
			NA	21.29	30.93	-	0.08	NA	NA	0.38	52.68

EMPA data from of pyrite (wt%) from the Osiris and Isis East zones. Detection limits are reported below element symbols.
Data below detection limit are indicated by (-)

Sample ID	Occurrence	S 0.39	Fe 0.85	Pb 0.08	As 0.03	Ni 0.03	Sb 0.03	Cu 0.09	Ag 0.04	Total
Osiris: 52_219_31_py_1	base metal pyrite - core	53.35	45.41	-	-	-	-	-	-	98.83
Osiris: 52_219_31_py_2	base metal pyrite - core	53.45	45.76	-	-	-	-	-	-	99.28
Osiris: 52_219_31_py_3	base metal pyrite - core	53.24	46.00	-	-	-	-	-	-	99.31
Osiris: 52_219_31_py_4	base metal pyrite - core	53.42	46.23	-	0.03	-	-	-	-	99.75
Osiris: 52_219_31_py_5	base metal pyrite - core	53.17	45.82	-	-	-	-	-	-	99.06
Osiris: 52_219_31_py_6	base metal pyrite - core	53.58	46.30	-	-	-	-	-	-	99.92
Osiris: 52_219_31_py_7	base metal pyrite - core	53.39	46.27	-	0.05	-	-	-	-	99.78
Osiris: 52_219_31_py_8	base metal pyrite - core	53.46	46.24	-	-	-	-	-	-	99.81
Osiris: 52_219_31_py_9	base metal pyrite - core	53.52	45.90	-	-	-	-	-	-	99.48
Osiris: 52_219_31_py_10	base metal pyrite - core	53.47	46.26	-	0.03	-	-	-	-	99.84
Osiris: 52_219_31_py_11	base metal pyrite - core	53.51	45.66	-	0.03	-	-	-	-	99.24
Osiris: 52_219_31_py_12	base metal pyrite - core	53.45	46.38	-	-	-	-	-	-	99.92
Osiris: 120_67_87_py_1	base metal pyrite - rim	53.41	46.65	-	-	-	-	-	-	100.13
Isis East: 120_67_87_py_2	base metal pyrite - rim	53.45	46.38	-	-	-	-	-	-	99.90
Isis East: 120_67_87_py_3	base metal pyrite - rim	53.46	46.44	-	0.03	-	-	-	-	99.96
Isis East: 120_67_87_py_4	base metal pyrite - rim	53.37	47.00	-	0.05	-	-	-	-	100.49
Isis East: 120_67_87_py_5	base metal pyrite - rim	53.42	46.20	-	-	-	-	-	-	99.72
Isis East: 120_67_87_py_6	base metal pyrite - rim	53.27	46.23	-	0.03	-	-	-	-	99.55
Isis East: 120_67_87_py_7	base metal pyrite - rim	53.51	46.55	-	-	-	-	-	-	100.15
Isis East: 120_67_87_py_8	base metal pyrite - rim	53.34	46.44	-	-	-	-	-	-	99.86
Isis East: 120_67_87_py_9	base metal pyrite - core	53.58	46.00	-	-	-	-	-	-	99.64
Isis East: 120_67_87_py_10	base metal pyrite - rim	53.16	46.09	-	-	-	-	-	-	99.31
Isis East: 120_67_87_py_11	base metal pyrite - core	53.51	46.74	-	-	-	-	-	-	100.34
Isis East: 120_67_87_py_12	base metal pyrite - core	53.28	46.03	-	-	-	-	-	-	99.43
Osiris: 41_201_33_py_1	base metal pyrite - core	53.52	47.03	-	-	-	-	-	-	100.60
Osiris: 41_201_33_py_2	base metal pyrite - core	53.70	46.95	-	-	-	-	-	-	100.73
Osiris: 41_201_33_py_3	base metal pyrite - core	53.23	46.61	-	0.03	-	-	-	-	99.93
Osiris: 41_201_33_py_4	base metal pyrite - core	53.38	46.99	-	-	-	-	-	-	100.48
Osiris: 41_201_33_py_5	base metal pyrite - core	53.06	46.75	-	-	-	-	-	-	99.88
Osiris: 41_201_33_py_6	base metal pyrite - core	53.27	46.75	-	0.03	-	-	-	-	100.13
Osiris: 41_201_33_py_7	base metal pyrite - core	53.53	47.27	-	-	-	-	-	-	100.88
Osiris: 41_201_33_py_8	base metal pyrite - core	52.74	46.23	-	-	-	-	-	-	99.01
Osiris: 41_201_33_py_9	base metal pyrite - core	53.54	45.95	-	0.03	-	-	-	-	99.59
Osiris: 80_107_14_py_1	base metal pyrite - core	53.03	45.34	-	0.09	-	-	-	-	98.54
Osiris: 80_107_14_py_2	base metal pyrite - rim	53.19	45.78	-	0.15	-	-	-	-	99.28
Osiris: 80_107_14_py_3	base metal pyrite - rim	52.98	45.99	-	0.11	-	-	-	-	99.15
Osiris: 80_107_14_py_4	base metal pyrite - rim	53.15	45.97	-	0.12	-	-	-	-	99.33
Osiris: 80_107_14_py_5	base metal pyrite - core	53.17	45.24	-	0.09	-	-	-	-	98.57
Osiris: 80_107_14_py_6	base metal pyrite - core	53.33	46.21	-	0.09	-	-	-	-	99.69
Osiris: 80_107_14_py_7	base metal pyrite - core	53.10	45.58	-	0.09	-	-	-	-	98.83
Osiris: 80_107_14_py_8	base metal pyrite - rim	52.94	45.47	-	0.38	-	-	-	-	98.93
Osiris: 80_107_14_py_9	base metal pyrite - rim	53.06	45.66	-	0.41	-	-	-	-	99.21
Osiris: 80_107_14_py_10	base metal pyrite - rim	53.27	46.48	-	0.11	-	-	-	-	99.95
Isis East: 120_117_34_sul_2	ore-stage pyrite - rim	52.59	45.70	-	0.18	-	-	-	-	98.60
Isis East: 120_117_34_sul_8	base metal pyrite - core	51.56	44.84	-	0.05	-	-	-	-	96.51
Isis East: 120_117_34_sul_9	base metal pyrite - core	53.23	46.10	-	0.04	-	-	-	-	99.47
Isis East: 120_117_34_sul_10	base metal pyrite - core	53.02	46.16	-	0.17	-	-	-	-	99.51
Isis east: 120_117_34_sul_2	ore-stage pyrite - amorphou	52.59	45.70	-	0.18	-	-	-	-	98.60
Isis east: 120_117_34_sul_9	base metal pyrite - core	53.23	46.10	-	0.04	-	-	-	-	99.47
Isis east: 120_117_34_sul_10	ore-stage pyrite - amorphou	53.02	46.16	-	0.17	-	-	-	-	99.51
Isis east: 120_117_34_sul_11	realgar veinlet	30.54	-	-	67.93	-	0.05	-	-	98.67
Isis east: 120_117_34_sul_12	realgar	30.51	-	-	72.27	-	-	-	0.04	102.92
Isis east: 120_117_34_sul_14	realgar	27.14	-	-	72.23	-	-	-	-	99.54
Isis east: 120_117_34_sul_15	realgar	31.80	-	-	71.10	-	-	-	-	102.98
Isis east: 120_117_34_sul_16	realgar	31.12	-	-	71.24	-	0.04	-	-	102.56
Isis east: 120_117_34_sul_18	realgar	32.13	-	-	71.79	-	-	-	-	103.98

EMPA data from from of pyrite (wt%) from the Osiris and Isis East zones. Detection limits are reported below element symbols. Data below detection limit are indicated by (-)

Sample ID	Occurrence	Se 0.01	Zn 0.04	Cd 0.14	Mn 0.02	Hg 0.11	Ge 0.01	Co 0.01	Total
Osiris: 52_219_31_py_1	base metal pyrite - core	0.01	-	-	-	-	-	-	98.83
Osiris: 52_219_31_py_2	base metal pyrite - core	0.03	-	-	-	-	-	-	99.28
Osiris: 52_219_31_py_3	base metal pyrite - core	0.03	-	-	-	-	-	0.01	99.31
Osiris: 52_219_31_py_4	base metal pyrite - core	0.02	-	-	-	-	-	0.02	99.75
Osiris: 52_219_31_py_5	base metal pyrite - core	0.02	-	-	-	-	0.01	-	99.06
Osiris: 52_219_31_py_6	base metal pyrite - core	0.02	-	-	-	-	-	-	99.92
Osiris: 52_219_31_py_7	base metal pyrite - core	0.02	-	-	-	-	-	0.02	99.78
Osiris: 52_219_31_py_8	base metal pyrite - core	0.02	-	-	-	-	-	-	99.81
Osiris: 52_219_31_py_9	base metal pyrite - core	0.02	-	-	-	-	-	-	99.48
Osiris: 52_219_31_py_10	base metal pyrite - core	0.02	-	-	0.02	-	-	-	99.84
Osiris: 52_219_31_py_11	base metal pyrite - core	0.02	-	-	-	-	-	0.01	99.24
Osiris: 52_219_31_py_12	base metal pyrite - core	0.01	-	-	-	-	-	0.02	99.92
Osiris: 120_67_87_py_1	base metal pyrite - rim	0.02	-	-	-	-	-	0.02	100.13
Isis East: 120_67_87_py_2	base metal pyrite - rim	0.02	-	-	-	-	-	-	99.90
Isis East: 120_67_87_py_3	base metal pyrite - rim	0.01	-	-	-	-	-	-	99.96
Isis East: 120_67_87_py_4	base metal pyrite - rim	0.03	-	-	0.02	-	-	0.01	100.49
Isis East: 120_67_87_py_5	base metal pyrite - rim	0.03	-	-	-	-	-	0.01	99.72
Isis East: 120_67_87_py_6	base metal pyrite - rim	0.01	-	-	-	-	-	0.02	99.55
Isis East: 120_67_87_py_7	base metal pyrite - rim	0.01	-	-	-	-	0.01	0.02	100.15
Isis East: 120_67_87_py_8	base metal pyrite - rim	0.01	-	-	-	-	-	-	99.86
Isis East: 120_67_87_py_9	base metal pyrite - core	0.01	-	-	-	-	0.01	0.01	99.64
Isis East: 120_67_87_py_10	base metal pyrite - rim	0.02	-	-	-	-	-	-	99.31
Isis East: 120_67_87_py_11	base metal pyrite - core	0.02	-	-	0.02	-	-	0.02	100.34
Isis East: 120_67_87_py_12	base metal pyrite - core	0.02	-	-	0.03	-	-	-	99.43
Osiris: 41_201_33_py_1	base metal pyrite - core	0.02	-	-	-	-	-	0.01	100.60
Osiris: 41_201_33_py_2	base metal pyrite - core	-	-	-	-	-	-	-	100.73
Osiris: 41_201_33_py_3	base metal pyrite - core	0.02	-	-	-	-	-	0.02	99.93
Osiris: 41_201_33_py_4	base metal pyrite - core	0.03	-	-	0.02	-	-	-	100.48
Osiris: 41_201_33_py_5	base metal pyrite - core	0.03	-	-	-	-	-	0.01	99.88
Osiris: 41_201_33_py_6	base metal pyrite - core	0.01	-	-	0.02	-	-	0.01	100.13
Osiris: 41_201_33_py_7	base metal pyrite - core	0.01	-	-	-	-	-	-	100.88
Osiris: 41_201_33_py_8	base metal pyrite - core	0.02	-	-	-	-	-	-	99.01
Osiris: 41_201_33_py_9	base metal pyrite - core	0.02	-	-	-	-	-	0.01	99.59
Osiris: 80_107_14_py_1	base metal pyrite - core	0.02	-	-	-	-	-	-	98.54
Osiris: 80_107_14_py_2	base metal pyrite - rim	0.03	-	-	0.02	-	-	0.01	99.28
Osiris: 80_107_14_py_3	base metal pyrite - rim	0.02	-	-	-	-	-	-	99.15
Osiris: 80_107_14_py_4	base metal pyrite - rim	0.03	-	-	-	-	-	0.01	99.33
Osiris: 80_107_14_py_5	base metal pyrite - core	0.03	-	-	-	-	-	-	98.57
Osiris: 80_107_14_py_6	base metal pyrite - core	0.01	-	-	0.02	-	-	-	99.69
Osiris: 80_107_14_py_7	base metal pyrite - core	0.02	-	-	-	-	-	-	98.83
Osiris: 80_107_14_py_8	base metal pyrite - rim	0.04	-	-	0.06	-	0.01	-	98.93
Osiris: 80_107_14_py_9	base metal pyrite - rim	0.03	-	-	-	-	-	-	99.21
Osiris: 80_107_14_py_10	base metal pyrite - rim	0.01	-	-	-	-	-	0.01	99.95
Isis East: 120_117_34_sul_2	ore-stage pyrite - rim	0.02	-	-	0.04	-	-	-	98.60
Isis East: 120_117_34_sul_8	base metal pyrite - core	0.03	-	-	-	-	-	0.02	96.51
Isis East: 120_117_34_sul_9	base metal pyrite - core	0.02	-	-	-	-	0.01	0.01	99.47
Isis East: 120_117_34_sul_10	base metal pyrite - core	0.02	-	-	-	-	-	0.01	99.51
Isis east: 120_117_34_sul_2	ore-stage pyrite - amorphot	0.02	-	-	0.04	-	-	-	98.60
Isis east: 120_117_34_sul_9	base metal pyrite - core	0.02	-	-	-	-	0.01	0.01	99.47
Isis east: 120_117_34_sul_10	ore-stage pyrite - amorphot	0.02	-	-	-	-	-	0.01	99.51
Isis east: 120_117_34_sul_11	realgar veinlet	0.03	-	-	0.02	-	-	0.03	98.67
Isis east: 120_117_34_sul_12	realgar	-	-	-	-	-	-	0.04	102.92
Isis east: 120_117_34_sul_14	realgar	0.06	-	-	-	-	-	0.04	99.54
Isis east: 120_117_34_sul_15	realgar	0.02	-	-	-	-	-	0.03	102.98
Isis east: 120_117_34_sul_16	realgar	-	-	-	0.03	-	-	0.03	102.56
Isis east: 120_117_34_sul_18	realgar	0.01	-	-	-	-	-	0.03	103.98

Sample ID	Occurrence	S	Fe	Pb	As	Ni	Sb	Cu	Ag	Total
		0.39	0.85	0.08	0.03	0.03	0.03	0.09	0.04	
Isis: 72_219_73_sul_2	Sphalerite	32.60	0.46	-	-	-	-	-	-	98.25
Isis: 72_219_73_sul_3	Sphalerite	32.31	0.37	-	0.04	-	-	-	-	97.83
Isis: 72_219_73_sul_4	Sphalerite	33.05	0.50	-	-	-	-	-	-	99.85
Isis: 72_219_73_sul_6	Sphalerite	32.90	0.46	-	0.03	-	-	-	-	99.58
Isis: 72_219_73_sul_7	Sphalerite	33.03	0.42	-	0.04	-	-	-	-	99.64
Isis: 72_219_73_sul_8	Sphalerite	32.98	0.50	-	-	-	-	-	-	99.98
Isis: 72_219_73_sul_9	Sphalerite	33.18	0.74	-	0.03	-	-	-	-	100.20
Isis: 72_219_73_sul_10	Sphalerite	32.76	0.48	-	0.07	-	-	-	-	100.08
Isis: 72_219_73_sul_11	Sphalerite	31.97	0.48	-	0.04	-	-	-	-	97.30
Isis: 72_219_73_sul_12	Sphalerite	32.69	1.12	-	0.08	-	-	-	-	99.46
Isis: 72_219_73_sul_13	Sphalerite	32.83	0.41	-	-	-	-	-	0.04	99.47
Osiris: 61_401_20_sul_8	ore-stage pyrite - amorphou	48.55	43.20	-	6.69	-	0.16	-	-	98.67
Osiris: 61_401_20_sul_9	ore-stage pyrite - amorphou	47.87	42.81	-	8.09	-	0.15	-	-	99.01
Osiris: 61_393_60_sul_1	realgar	31.48	-	-	70.20	-	0.08	-	-	101.90
Osiris: 61_393_60_sul_4	realgar	37.33	14.18	-	46.56	-	0.16	-	0.05	98.42
Osiris: OS-11-61 393.60	ore-stage pyrite - amorphou	46.31	40.99	-	9.67	-	0.09	-	-	97.16

Sample ID	Occurrence	S	Fe	Pb	As	Ni	Sb	Cu	Total
		0.26	0.05	0.15	0.05	0.07	0.09	0.09	
Osiris: 73_08 pyrite_1	ore-stage pyrite - rim	52.69	45.76	-	0.29	-	-	0.31	99.12
Osiris: 73_08 pyrite_2	early burial pyrite - core	53.03	46.23	-	-	-	-	-	99.42
Osiris: 73_08 sphalerite_1	detrital sphalerite	33.34	1.15	-	-	-	-	0.10	96.29
Osiris: 73_08 pyrite_3	early burial pyrite - rim	53.01	45.66	-	0.13	-	-	0.10	99.07
Osiris: 73_08 pyrite_4	ore-stage pyrite - rim	52.66	46.05	-	0.45	-	-	-	99.24
Osiris: 73_08 pyrite_5	Framboidal Pyrite	52.62	45.90	-	-	-	-	-	98.71
Osiris: 73_08 pyrite_6	Framboidal Pyrite	52.83	46.17	-	0.05	-	-	-	99.19
Isis: 57_67 pyrite_1	base metal pyrite - core	53.25	46.85	-	-	-	-	-	####
Isis: 57_67 pyrite_2	base metal pyrite - core	53.47	46.81	-	-	-	-	-	####
Isis: 57_67 pyrite_3	base metal pyrite - core	53.12	46.88	-	-	-	-	-	####
Isis: 57_67 pyrite_4	base metal pyrite - core	53.21	46.72	-	-	-	-	-	####
Isis: 57_67 pyrite_5	base metal pyrite - core	52.91	46.75	-	-	-	-	-	99.73
Isis: 57_67 pyrite_6	base metal pyrite - core	53.09	46.73	-	-	-	-	-	99.97
Isis: 57_67 pyrite_7	base metal pyrite - rim	52.45	46.25	0.32	-	-	-	-	99.13
Isis: 57_67 pyrite_8	base metal pyrite - core	52.54	46.49	-	-	-	-	-	99.22
Isis: 57_67 pyrite_9	base metal pyrite - rim	52.84	46.42	0.23	-	-	-	-	99.60
Osiris: 114_54 pyrite_1	early burial pyrite - rim	52.33	45.55	-	0.10	0.17	-	0.39	98.77
Osiris: 114_54 pyrite_2	early burial pyrite - core	51.92	45.50	-	0.05	0.18	-	0.18	98.11
Osiris: 114_54 pyrite_3	early burial pyrite - rim	51.91	45.90	-	0.14	0.13	-	-	98.16
Osiris: 114_54 pyrite_4	early burial pyrite - rim	51.50	45.62	-	0.17	0.18	-	-	97.74
Osiris: 114_54 pyrite_5	early burial pyrite - core	52.47	45.76	-	0.08	0.23	-	0.27	98.98
Osiris: 114_54 pyrite_6	early burial pyrite - core	52.37	45.47	-	0.09	0.13	-	0.48	98.76
Osiris: 114_54 pyrite_6	early burial pyrite - core	52.35	46.45	-	0.09	-	-	-	99.07
Osiris: 114_54 pyrite_8	early burial pyrite - core	53.05	46.72	-	0.07	-	-	-	99.98
Osiris: 114_54 pyrite_9	early burial pyrite - rim	51.74	45.86	-	0.13	0.13	-	-	98.01
Osiris: 285_05_py_1	base metal pyrite - core	53.70	46.88	-	0.11	-	-	-	####
Osiris: 285_05_py_2	base metal pyrite - core	52.68	46.96	-	-	-	-	-	99.72
Osiris: 285_05_py_3	base metal pyrite - core	52.56	46.47	-	0.06	-	-	-	99.25
Isis east: 101_44A_py_1	base metal pyrite - core	53.73	47.96	-	-	-	-	-	####
Isis east: 101_44A_py_2	base metal pyrite - core	53.31	45.97	-	0.10	-	-	0.12	99.60
Isis east: 101_44A_py_3	base metal pyrite - rim	51.63	45.23	-	0.68	-	-	-	97.64
Isis east: 101_44A_py_4	base metal pyrite - core	53.01	47.09	-	0.10	-	-	-	####
Osiris: 112_38_rlg_1	realgar	31.55	-	-	66.37	-	-	-	98.44
Osiris: 112_38_py_2	ore-stage pyrite - rim	52.24	45.97	-	1.18	-	-	-	99.49

Sample ID	Occurrence	Se	Zn	Cd	Mn	Hg	Ge	Co	Total
		0.01	0.04	0.14	0.02	0.11	0.01	0.01	
Isis: 72_219_73_sul_2	Sphalerite	0.03	65.01	-	-	-	0.02	0.03	98.25
Isis: 72_219_73_sul_3	Sphalerite	0.02	64.86	-	-	0.12	-	0.03	97.83
Isis: 72_219_73_sul_4	Sphalerite	0.02	66.03	0.16	0.02	-	-	0.03	99.85
Isis: 72_219_73_sul_6	Sphalerite	0.02	65.99	-	0.02	-	0.01	0.03	99.58
Isis: 72_219_73_sul_7	Sphalerite	0.01	65.98	-	-	-	-	0.02	99.64
Isis: 72_219_73_sul_8	Sphalerite	0.03	66.29	-	-	-	0.02	0.03	99.98
Isis: 72_219_73_sul_9	Sphalerite	0.02	66.01	-	-	-	-	0.02	100.20
Isis: 72_219_73_sul_10	Sphalerite	0.01	65.82	-	0.02	0.69	-	0.05	100.08
Isis: 72_219_73_sul_11	Sphalerite	0.01	64.18	-	-	0.48	-	0.03	97.30
Isis: 72_219_73_sul_12	Sphalerite	0.02	64.62	-	-	0.73	-	0.03	99.46
Isis: 72_219_73_sul_13	Sphalerite	0.01	65.63	-	-	0.41	0.01	0.03	99.47
Osiris: 61_401_20_sul_8	ore-stage pyrite - amorphot	0.03	-	-	-	-	-	-	98.67
Osiris: 61_401_20_sul_9	ore-stage pyrite - amorphot	0.04	-	-	-	-	-	-	99.01
Osiris: 61_393_60_sul_1	realgar	0.01	-	-	-	-	0.00	0.03	101.90
Osiris: 61_393_60_sul_4	realgar	0.07	-	-	-	-	-	0.05	98.42
Osiris: OS-11-61 393.60	ore-stage pyrite - amorphot	0.03	-	-	0.05	-	-	-	97.16

Sample ID	Occurrence	Ag	Se	Zn	Cd	Si	Tl	Total
		0.11	0.02	0.06	0.3	0.03	0.11	
Osiris: 73_08 pyrite_1	ore-stage pyrite - rim	-	0.03	-	-	0.04	-	99.12
Osiris: 73_08 pyrite_2	early burial pyrite - core	-	0.03	-	-	-	-	99.42
Osiris: 73_08 sphalerite_1	detrital sphalerite	-	0.04	61.61	-	0.03	-	96.29
Osiris: 73_08 pyrite_3	early burial pyrite - rim	-	0.07	-	-	0.06	-	99.07
Osiris: 73_08 pyrite_4	ore-stage pyrite - rim	-	0.02	-	-	0.03	-	99.24
Osiris: 73_08 pyrite_5	Framboidal Pyrite	-	-	-	-	0.03	-	98.71
Osiris: 73_08 pyrite_6	Framboidal Pyrite	-	-	-	-	0.07	-	99.19
Isis: 57_67 pyrite_1	base metal pyrite - core	-	0.04	-	-	-	-	####
Isis: 57_67 pyrite_2	base metal pyrite - core	-	0.02	-	-	-	-	####
Isis: 57_67 pyrite_3	base metal pyrite - core	-	-	-	-	-	-	####
Isis: 57_67 pyrite_4	base metal pyrite - core	-	-	-	-	-	-	####
Isis: 57_67 pyrite_5	base metal pyrite - core	-	0.02	-	-	-	-	99.73
Isis: 57_67 pyrite_6	base metal pyrite - core	-	-	-	-	-	-	99.97
Isis: 57_67 pyrite_7	base metal pyrite - rim	-	0.02	-	-	-	-	99.13
Isis: 57_67 pyrite_8	base metal pyrite - core	-	0.02	-	-	-	-	99.22
Isis: 57_67 pyrite_9	base metal pyrite - rim	-	0.02	-	-	-	-	99.60
Osiris: 114_54 pyrite_1	early burial pyrite - rim	-	0.07	-	-	0.06	-	98.77
Osiris: 114_54 pyrite_2	early burial pyrite - core	-	0.16	-	-	-	-	98.11
Osiris: 114_54 pyrite_3	early burial pyrite - rim	-	0.03	-	-	0.03	-	98.16
Osiris: 114_54 pyrite_4	early burial pyrite - rim	-	0.07	-	-	0.05	-	97.74
Osiris: 114_54 pyrite_5	early burial pyrite - core	-	0.11	-	-	0.03	-	98.98
Osiris: 114_54 pyrite_6	early burial pyrite - core	-	0.05	-	-	0.15	-	98.76
Osiris: 114_54 pyrite_6	early burial pyrite - core	-	0.03	-	-	-	-	99.07
Osiris: 114_54 pyrite_8	early burial pyrite - core	-	-	-	-	-	-	99.98
Osiris: 114_54 pyrite_9	early burial pyrite - rim	-	0.03	-	-	0.03	-	98.01
Osiris: 285_05_py_1	base metal pyrite - core	-	0.04	-	-	-	-	####
Osiris: 285_05_py_2	base metal pyrite - core	-	-	-	-	-	-	99.72
Osiris: 285_05_py_3	base metal pyrite - core	-	0.02	-	-	0.04	-	99.25
Isis east: 101_44A_py_1	base metal pyrite - core	-	-	-	-	-	-	####
Isis east: 101_44A_py_2	base metal pyrite - core	-	0.04	-	-	0.03	-	99.60
Isis east: 101_44A_py_3	base metal pyrite - rim	-	-	-	-	-	-	97.64
Isis east: 101_44A_py_4	base metal pyrite - core	-	0.05	-	-	-	-	####
Osiris: 112_38_rlg_1	realgar	-	-	-	-	0.05	-	98.44
Osiris: 112_38_py_2	ore-stage pyrite - rim	-	0.02	-	-	0.04	-	99.49

Sample ID	Occurrence	S 0.03	Fe 0.04	As 0.04	Sb 0.07	Zn 0.05	Total
Osiris: 294_22_py_1	base metal pyrite - rim	53.47	46.58	-	-	-	100.05
Osiris: 294_22_py_2	base metal pyrite - rim	53.45	46.49	0.23	-	-	100.19
Osiris: 294_22_py_3	base metal pyrite - core	54.65	46.87	-	-	-	101.54
Osiris: 294_22_py_4	base metal pyrite - rim	53.78	46.71	-	-	-	100.50
Osiris: 294_22_py_5	base metal pyrite - rim	54.42	46.69	-	-	-	101.12
Osiris: 294_22_py_6	base metal pyrite - rim	54.01	46.62	-	-	-	100.66
Osiris: 294_22_py_7	base metal pyrite - rim	53.96	46.55	-	-	-	100.55
Osiris: 294_22_py_8	base metal pyrite - rim	53.80	46.49	0.05	-	-	100.35
Osiris: 294_22_py_9	base metal pyrite - rim	53.55	46.34	-	-	-	99.93
Osiris: 294_22_py_10	base metal pyrite - core	53.68	46.41	-	-	-	100.11
Osiris: 294_22_py_11	base metal pyrite - core	53.35	46.47	-	-	-	99.86
Osiris: 294_22_py_12	base metal pyrite - core	53.60	46.36	-	-	-	99.97
Osiris: 294_22_py_13	base metal pyrite - rim	53.76	46.09	-	-	-	99.87
Osiris: 294_22_py_14	base metal pyrite - rim	53.84	46.20	-	-	-	100.08
Osiris: 294_22_py_15	base metal pyrite - rim	53.51	46.23	-	-	-	99.74
Osiris: 294_22_py_16	base metal pyrite - rim	53.59	46.39	-	-	-	100.02
Osiris: 294_22_py_17	base metal pyrite - core	53.82	46.46	-	-	-	100.30
Osiris: 294_22_py_19	fractured base metal pyrite	53.19	46.17	0.59	-	-	99.94
Osiris: 294_22_py_20	base metal pyrite - rim	53.30	46.12	-	-	-	99.43
Osiris: 294_22_py_21	base metal pyrite - rim	53.78	46.33	-	-	-	100.13
Osiris: 294_22_py_22	base metal pyrite - core	53.69	46.52	-	-	-	100.23
Osiris: 294_22_py_23	base metal pyrite - rim	53.40	46.33	-	-	-	99.76
Osiris: 294_22_py_24	base metal pyrite - rim	53.57	46.43	-	-	-	100.01
Osiris: 294_22_py_25	base metal pyrite - rim	53.39	46.29	-	-	-	99.68
Osiris: 294_22_py_26	base metal pyrite - rim	53.05	46.19	-	-	-	99.29
Osiris: Line 1 294_22_a5	base metal pyrite - rim	53.17	45.96	0.41	-	-	99.53
Osiris: Line 2 294_22_a5	base metal pyrite - core	53.58	46.36	-	-	-	99.98
Osiris: Line 3 294_22_a5	base metal pyrite - core	53.52	46.49	-	-	-	100.03
Osiris: Line 4 294_22_a5	base metal pyrite - core	53.74	46.51	-	-	-	100.31
Osiris: Line 5 294_22_a5	base metal pyrite - rim	53.71	46.47	-	-	-	100.20
Osiris: Line 1 294_22_a2	base metal pyrite - rim	53.44	46.02	-	-	-	99.49
Osiris: Line 2 294_22_a2	base metal pyrite - core	53.48	46.36	0.16	-	-	100.01
Osiris: Line 3 294_22_a2	base metal pyrite - core	53.74	46.29	-	-	-	100.06
Osiris: Line 4 294_22_a2	base metal pyrite - core	53.51	46.30	-	-	-	99.82
Osiris: Line 5 294_22_a2	base metal pyrite - core	53.60	46.24	-	-	-	99.85
Osiris: Line 6 294_22_a2	base metal pyrite - core	53.44	46.40	-	-	-	99.84
Osiris: Line 7 294_22_a2	base metal pyrite - core	53.57	46.29	-	-	-	99.90
Osiris: Line 8 294_22_a2	base metal pyrite - core	51.12	45.66	-	-	-	96.84
Osiris: Line 9 294_22_a2	base metal pyrite - core	53.38	46.27	-	-	-	99.68
Osiris: Line 10 294_22_a2	base metal pyrite - core	53.37	46.17	-	-	-	99.59
Osiris: Line 11 294_22_a2	base metal pyrite - core	53.55	46.19	-	-	-	99.76
Osiris: Line 12 294_22_a2	base metal pyrite - core	53.11	46.19	-	-	-	99.33
Osiris: Line 13 294_22_a2	base metal pyrite - core	53.44	46.22	-	-	-	99.67
Osiris: Line 14 294_22_a2	base metal pyrite - core	53.45	46.37	-	-	-	99.86
Osiris: Line 15 294_22_a2	base metal pyrite - rim	53.28	46.08	-	-	-	99.40

Sample ID	Occurrence	S 0.03	Fe 0.04	As 0.04	Sb 0.07	Zn 0.05	Total
Osiris: Line 1 294_22_a2B	base metal pyrite - rim	53.30	46.15	-	-	-	99.47
Osiris: Line 2 294_22_a2B	base metal pyrite - core	53.45	46.37	-	-	-	99.84
Osiris: Line 3 294_22_a2B	base metal pyrite - core	52.39	45.95	0.14	-	-	98.47
Osiris: Line 4 294_22_a2B	base metal pyrite - core	53.15	46.19	-	-	-	99.34
Osiris: Line 5 294_22_a2B	base metal pyrite - core	53.51	45.69	-	-	-	99.23
Osiris: Line 6 294_22_a2B	base metal pyrite - core	53.49	46.25	-	-	-	99.74
Osiris: Line 7 294_22_a2B	base metal pyrite - core	53.37	46.26	-	-	-	99.64
Osiris: Line 8 294_22_a2B	base metal pyrite - core	53.59	46.32	-	-	-	99.95
Osiris: Line 9 294_22_a2B	base metal pyrite - core	53.74	46.28	-	-	-	100.05
Osiris: Line 10 294_22_a2B	base metal pyrite - rim	53.56	46.14	-	-	-	99.72
Isis: Line 1 306_92_a3	base metal pyrite - rim	52.80	45.77	-	-	-	98.58
Isis: Line 3 306_92_a3	base metal pyrite - core	53.65	46.50	0.05	-	-	100.20
Isis: Line 4 306_92_a3	base metal pyrite - core	53.50	46.29	-	-	-	99.79
Isis: Line 5 306_92_a3	base metal pyrite - core	54.94	45.94	-	-	-	100.94
Isis: Line 6 306_92_a3	base metal pyrite - core	53.76	46.66	-	-	-	100.43
Isis: Line 7 306_92_a3	base metal pyrite - core	53.16	46.42	-	-	-	99.62
Isis: Line 9 306_92_a3	base metal pyrite - core	53.49	46.58	-	-	-	100.08
Isis: Line 10 306_92_a3	base metal pyrite - core	53.42	46.49	-	-	-	99.91
Isis: Line 11 306_92_a3	base metal pyrite - core	53.55	46.61	-	-	-	100.17
Isis: Line 12 306_92_a3	base metal pyrite - core	53.72	46.68	-	-	-	100.41
Isis: Line 13 306_92_a3	base metal pyrite - core	53.87	46.58	-	-	-	100.51
Isis: Line 14 306_92_a3	base metal pyrite - core	53.79	46.63	-	-	-	100.45
Isis: Line 15 306_92_a3	base metal pyrite - rim	53.80	46.61	-	-	-	100.42
Isis: 306_92_py_2	base metal pyrite - rim	52.89	45.35	0.05	-	-	98.33
Isis: 306_92_py_4	base metal pyrite - rim	53.24	46.18	-	-	-	99.44
Isis: 306_92_py_5	base metal pyrite - rim	53.58	46.33	-	-	-	99.93
Isis: 306_92_py_6	base metal pyrite - rim	53.91	46.13	-	-	-	100.07
Isis: 306_92_py_7	base metal pyrite - rim	53.91	46.65	-	-	-	100.56
Isis: 306_92_py_8	base metal pyrite - rim	53.26	46.51	-	-	-	99.80
Isis: 306_92_py_9	ore-stage pyrite - rim	52.77	45.48	0.67	-	-	98.93
Isis: 306_92_py_10	base metal pyrite - rim	53.60	46.50	-	-	-	100.11
Isis: 306_92_py_11	base metal pyrite - rim	53.78	46.58	-	-	-	100.37
Isis: 306_92_py_12	base metal pyrite - rim	53.81	46.25	-	-	-	100.08
Isis: 306_92_py_13	base metal pyrite - rim	53.60	46.63	-	-	-	100.25
Isis: 306_92_py_14	base metal pyrite - rim	53.55	46.55	-	-	-	100.14
Isis: 306_92_py_15	base metal pyrite - rim	54.41	46.43	-	-	-	100.88
Isis: 306_92_py_16	base metal pyrite - rim	53.68	46.21	-	-	-	99.89
Isis: 306_92_py_17	base metal pyrite - rim	53.32	46.20	-	-	-	99.53
Isis: 306_92_py_18	base metal pyrite - rim	53.29	46.03	-	-	-	99.34
Isis: 306_92_py_19	base metal pyrite - rim	53.62	46.21	-	-	-	99.86
Isis: 306_92_py_21	base metal pyrite - rim	53.14	45.94	0.09	-	-	99.19
Isis: 306_92_py_22	base metal pyrite - rim	53.48	46.44	-	-	-	99.93
Isis: 306_92_py_23	base metal pyrite - rim	53.06	46.31	-	-	-	99.40
Isis: 306_92_py_24	base metal pyrite - rim	53.52	46.54	-	-	-	100.07
Isis: 306_92_py_25	base metal pyrite - rim	53.51	46.41	-	-	-	99.94
Isis: 306_92_py_26	base metal pyrite - rim	53.86	46.31	-	-	-	100.19
Isis: 306_92_py_27	base metal pyrite - rim	53.62	46.57	-	-	-	100.24

Sample ID	Occurrence	S 0.03	Fe 0.04	As 0.04	Sb 0.07	Zn 0.05	Total
Isis: 306_92_py_28	base metal pyrite - rim	53.40	45.44	0.05	-	-	98.91
Isis: 306_92_py_29	base metal pyrite - rim	53.45	45.72	-	-	-	99.22
Isis: 306_92_py_30	base metal pyrite - rim	54.06	45.90	-	-	-	100.00
Isis: 306_92_py_31	base metal pyrite - rim	53.38	45.60	-	-	-	99.01
Isis: 306_92_py_32	base metal pyrite - rim	52.27	45.43	0.06	-	-	97.79
Isis: 306_92_py_33	base metal pyrite - rim	53.86	45.83	0.05	-	-	99.74
Isis: 306_92_py_33	base metal pyrite - rim	53.59	45.87	-	-	-	99.48
Isis: 306_92_py_34	base metal pyrite - rim	53.34	45.56	-	-	-	98.94
Isis: 306_92_py_35	base metal pyrite - rim	53.31	46.29	-	-	-	99.65
Isis: 306_92_py_36	base metal pyrite - rim	53.42	46.33	-	-	-	99.75
Isis: 306_92_py_37	base metal pyrite - rim	53.94	45.91	-	-	-	99.88
Isis: 306_92_py_38	base metal pyrite - rim	52.15	45.36	-	-	-	97.54
Isis: 306_92_py_39	base metal pyrite - rim	53.08	45.41	0.08	-	-	98.60
Isis: 306_92_py41	base metal pyrite - rim	53.02	45.70	-	-	-	98.73
Isis: 306_92_py42	base metal pyrite - core	53.66	46.29	-	-	-	99.98
Isis: 306_92_py43	base metal pyrite - core	53.68	46.47	-	-	-	100.16
Isis: 306_92_py44	base metal pyrite - core	53.64	46.38	-	-	-	100.03
Isis: 306_92_py45	base metal pyrite - rim	53.82	46.39	-	-	-	100.22
Isis: 306_92_area9	sphalerite	33.12	1.21	-	-	63.67	98.01
Isis: 306_92_area9a	sphalerite	33.00	1.42	-	-	68.08	102.54
Isis: 306_92_area9b	sphalerite	32.89	1.45	-	-	66.61	100.96
Isis: 306_92_area9c	sphalerite	32.79	1.69	-	-	67.69	102.18
Isis: Line 1 306_92_area1	base metal pyrite - core	53.14	46.25	-	-	-	99.42
Isis: Line 2 306_92_area1	base metal pyrite - core	53.32	46.58	-	-	-	99.91
Isis: Line 3 306_92_area1	base metal pyrite - core	53.47	46.73	-	-	-	100.21
Isis: Line 4 306_92_area1	base metal pyrite - core	53.46	46.56	-	-	-	100.02
Isis: Line 5 306_92_area1	base metal pyrite - core	53.42	46.51	-	-	-	99.99
Isis: Line 6 306_92_area1	base metal pyrite - core	53.36	46.46	-	-	-	99.87
Isis: Line 7 306_92_area1	base metal pyrite - core	53.71	46.41	-	-	-	100.13
Isis: Line 9 306_92_area1	base metal pyrite - core	52.71	46.06	-	-	-	98.77
Isis: Line 10 306_92_area1	base metal pyrite - core	52.44	45.88	-	-	-	98.36
Isis: Line 11 306_92_area1	base metal pyrite - core	53.66	46.44	-	-	-	100.11
Isis: Line 12 306_92_area1	base metal pyrite - core	53.40	46.47	-	-	-	99.88
Isis: Line 13 306_92_area1	base metal pyrite - core	52.68	45.84	-	-	-	98.55
Isis: Line 14 306_92_area1	base metal pyrite - rim	53.33	46.15	-	-	-	99.50
Isis: Line 15 306_92_area1	base metal pyrite - rim	53.63	46.44	-	-	-	100.11
Isis: Line 1 306_92_area5	base metal pyrite - core	53.39	46.17	-	-	-	99.58
Isis: Line 2 306_92_area5	base metal pyrite - core	52.86	45.97	-	-	-	98.86
Isis: Line 3 306_92_area5	base metal pyrite - core	53.02	46.10	-	-	-	99.14
Isis: Line 4 306_92_area5	base metal pyrite - core	53.44	46.36	-	-	-	99.82
Isis: Line 5 306_92_area5	base metal pyrite - core	53.38	46.38	-	-	-	99.78
Isis: Line 6 306_92_area5	base metal pyrite - core	53.48	46.40	-	-	-	99.89
Isis: Line 7 306_92_area5	base metal pyrite - core	53.14	46.35	-	-	-	99.51
Isis: Line 8 306_92_area5	base metal pyrite - core	53.39	46.39	-	-	-	99.79
Isis: Line 9 306_92_area5	base metal pyrite - core	53.35	46.41	-	-	-	99.79
Isis: Line 10 306_92_area5	base metal pyrite - core	53.26	46.37	-	-	-	99.64

Sample ID	Occurrence	S	Fe	As	Sb	Zn	Total
		0.03	0.04	0.04	0.07	0.05	
Isis: Line 11 306_92_area5	base metal pyrite - core	53.51	46.43	-	-	-	99.96
Isis: Line 12 306_92_area5	base metal pyrite - core	53.37	46.45	-	-	-	99.86
Isis: Line 13 306_92_area5	base metal pyrite - core	52.98	46.33	-	-	-	99.33
Isis: Line 14 306_92_area5	base metal pyrite - core	53.49	46.34	-	-	-	99.86
Isis: Line 15 306_92_area5	base metal pyrite - core	53.17	45.88	-	-	-	99.12
Isis: Line 16 306_92_area5	base metal pyrite - core	53.03	46.19	-	-	-	99.27
Isis: Line 17 306_92_area5	base metal pyrite - core	53.55	46.41	-	-	-	99.99
Isis: Line 18 306_92_area5	base metal pyrite - core	53.27	46.43	-	-	-	99.72
Isis: Line 19 306_92_area5	base metal pyrite - rim	53.21	46.31	-	-	-	99.55
Isis: Line 20 306_92_area5	base metal pyrite - rim	53.29	46.45	-	-	-	99.77
Osiris: Line 1 116_80B_a1	base metal pyrite - rim	52.90	46.00	0.23	-	-	99.14
Osiris: Line 2 116_80B_a1	base metal pyrite - rim	52.89	46.05	0.21	-	-	99.18
Osiris: Line 3 116_80B_a1	base metal pyrite - core	51.78	45.65	0.50	-	-	97.95
Osiris: Line 4 116_80B_a1	base metal pyrite - core	53.06	46.28	0.19	-	-	99.55
Osiris: Line 5 116_80B_a1	base metal pyrite - core	52.88	46.22	0.17	-	-	99.27
Osiris: Line 6 116_80B_a1	base metal pyrite - core	51.77	46.05	0.40	-	-	98.25
Osiris: Line 7 116_80B_a1	base metal pyrite - core	52.99	46.13	0.19	-	-	99.32
Osiris: Line 8 116_80B_a1	base metal pyrite - core	51.16	45.97	0.50	-	-	97.65
Osiris: Line 9 116_80B_a1	base metal pyrite - core	52.44	46.10	0.18	-	-	98.74
Osiris: Line 10 116_80B_a1	base metal pyrite - core	52.97	46.29	0.16	-	-	99.44
Osiris: Line 11 116_80B_a1	base metal pyrite - core	53.12	46.27	0.14	-	-	99.56
Osiris: Line 12 116_80B_a1	base metal pyrite - core	52.74	46.17	0.18	-	-	99.08
Osiris: Line 13 116_80B_a1	base metal pyrite - core	51.56	46.11	0.40	-	-	98.07
Osiris: Line 14 116_80B_a1	base metal pyrite - core	52.97	46.26	0.11	-	-	99.35
Osiris: Line 15 116_80B_a1	base metal pyrite - core	53.01	46.16	0.09	-	-	99.27
Osiris: Line 16 116_80B_a1	base metal pyrite - core	53.27	46.12	0.12	-	-	99.52
Osiris: Line 17 116_80B_a1	base metal pyrite - core	51.85	45.85	0.24	-	-	97.98
Osiris: Line 18 116_80B_a1	base metal pyrite - core	52.74	46.01	0.10	-	-	98.86
Osiris: Line 20 116_80B_a1	base metal pyrite - core	53.00	46.04	0.16	-	-	99.23
Osiris: Line 21 116_80B_a1	base metal pyrite - core	52.95	46.00	0.17	-	-	99.12
Osiris: Line 22 116_80B_a1	base metal pyrite - core	52.99	46.16	0.15	-	-	99.34
Osiris: Line 23 116_80B_a1	base metal pyrite - core	53.02	45.96	0.17	-	-	99.16
Osiris: Line 24 116_80B_a1	base metal pyrite - core	52.95	46.22	0.16	-	-	99.33
Osiris: Line 25 116_80B_a1	base metal pyrite - core	52.88	46.12	0.16	-	-	99.16
Osiris: Line 26 116_80B_a1	base metal pyrite - core	53.07	46.13	0.15	-	-	99.39
Osiris: Line 27 116_80B_a1	base metal pyrite - core	53.02	46.27	0.13	-	-	99.43
Osiris: Line 28 116_80B_a1	base metal pyrite - core	53.16	46.08	0.12	-	-	99.37
Osiris: Line 29 116_80B_a1	base metal pyrite - rim	53.07	46.08	0.15	-	-	99.31
Osiris: Line 30 116_80B_a1	base metal pyrite - rim	53.14	46.17	-	-	-	99.33
Osiris: Line 1 116_80B_a2	base metal pyrite - rim	53.21	45.95	0.11	-	-	99.30
Osiris: Line 2 116_80B_a2	base metal pyrite - rim	52.93	46.09	0.11	-	-	99.15
Osiris: Line 3 116_80B_a2	base metal pyrite - core	52.90	45.92	0.16	-	-	98.98
Osiris: Line 4 116_80B_a2	base metal pyrite - core	52.90	45.80	0.20	-	-	98.92
Osiris: Line 5 116_80B_a2	base metal pyrite - core	52.86	46.09	0.16	-	-	99.12
Osiris: Line 6 116_80B_a2	base metal pyrite - core	52.91	46.03	0.18	-	-	99.12
Osiris: Line 7 116_80B_a2	base metal pyrite - core	53.17	46.18	0.11	-	-	99.46

Sample ID	Occurrence	S	Fe	As	Sb	Zn	Total
		0.03	0.04	0.04	0.07	0.05	
Osiris: Line 9 116_80B_a2	base metal pyrite - core	52.92	46.02	0.12	-	-	99.06
Osiris: Line 10 116_80B_a2	base metal pyrite - core	53.05	46.06	0.12	-	-	99.23
Osiris: Line 11 116_80B_a2	base metal pyrite - core	52.40	45.80	0.25	-	-	98.45
Osiris: Line 12 116_80B_a2	base metal pyrite - core	52.96	46.03	0.14	-	-	99.16
Osiris: Line 13 116_80B_a2	base metal pyrite - core	52.97	46.06	0.13	-	-	99.16
Osiris: Line 14 116_80B_a2	base metal pyrite - core	52.85	46.07	0.17	-	-	99.09
Osiris: Line 15 116_80B_a2	base metal pyrite - core	52.74	45.91	0.17	-	-	98.82
Osiris: Line 16 116_80B_a2	base metal pyrite - core	52.32	45.47	0.44	-	-	98.23
Osiris: Line 17 116_80B_a2	base metal pyrite - core	52.86	46.01	0.16	-	-	99.03
Osiris: Line 18 116_80B_a2	base metal pyrite - core	52.97	46.08	0.13	-	-	99.20
Osiris: Line 19 116_80B_a2	base metal pyrite - rim	52.97	45.90	0.17	-	-	99.04
Osiris: Line 1 116_80B_ab	base metal pyrite - rim	52.49	45.61	0.43	-	-	98.55
Osiris: Line 2 116_80B_ab	base metal pyrite - rim	53.01	45.98	0.16	-	-	99.16
Osiris: Line 3 116_80B_ab	base metal pyrite - core	52.75	45.96	0.21	-	-	98.92
Osiris: Line 4 116_80B_ab	base metal pyrite - core	52.94	46.16	0.16	-	-	99.26
Osiris: Line 5 116_80B_ab	base metal pyrite - core	52.84	46.05	0.13	-	-	99.02
Osiris: Line 6 116_80B_ab	base metal pyrite - core	53.01	46.12	0.12	-	-	99.26
Osiris: Line 7 116_80B_ab	base metal pyrite - core	52.88	46.11	0.13	-	-	99.12
Osiris: Line 8 116_80B_ab	base metal pyrite - core	53.25	46.04	0.11	-	-	99.42
Osiris: Line 9 116_80B_ab	base metal pyrite - core	52.94	46.33	0.12	-	-	99.39
Osiris: Line 10 116_80B_ab	base metal pyrite - core	52.65	45.87	0.32	-	-	98.85
Osiris: Line 11 116_80B_ab	base metal pyrite - core	52.79	46.30	0.14	-	-	99.23
Osiris: Line 12 116_80B_ab	base metal pyrite - core	53.01	46.15	0.16	-	-	99.32
Osiris: Line 13 116_80B_ab	base metal pyrite - core	53.07	46.27	0.13	-	-	99.48
Osiris: Line 14 116_80B_ab	base metal pyrite - core	52.86	46.27	0.13	-	-	99.28
Osiris: Line 15 116_80B_ab	base metal pyrite - core	52.75	45.84	0.35	-	-	98.93
Osiris: Line 16 116_80B_ab	base metal pyrite - core	52.60	45.84	0.31	-	-	98.76
Osiris: Line 17 116_80B_ab	base metal pyrite - core	52.73	45.81	0.31	-	-	98.88
Osiris: Line 18 116_80B_ab	base metal pyrite - core	52.67	45.85	0.40	-	-	98.93
Osiris: Line 19 116_80B_ab	base metal pyrite - rim	52.62	45.98	0.20	-	-	98.80
Osiris: Line 20 116_80B_ab	base metal pyrite - rim	53.19	46.42	-	-	-	99.63
Isis: Line 1 306_92_area8	base metal pyrite - rim	53.19	46.34	-	-	-	99.56
Isis: Line 2 306_92_area8	base metal pyrite - rim	53.28	46.32	0.06	-	-	99.70
Isis: Line 3 306_92_area8	base metal pyrite - core	53.61	46.68	-	-	-	100.31
Isis: Line 4 306_92_area8	base metal pyrite - core	52.98	46.46	-	-	-	99.47
Isis: Line 5 306_92_area8	base metal pyrite - core	53.60	46.74	-	-	-	100.38
Isis: Line 6 306_92_area8	base metal pyrite - core	53.20	46.45	0.08	-	-	99.73
Isis: Line 7 306_92_area8	base metal pyrite - core	53.48	46.67	-	-	-	100.18
Isis: Line 8 306_92_area8	base metal pyrite - core	53.37	46.48	-	-	-	99.88
Isis: Line 9 306_92_area8	base metal pyrite - core	52.92	46.07	0.08	-	-	99.09
Isis: Line 10 306_92_area8	base metal pyrite - core	55.52	45.30	-	-	-	100.84
Isis: Line 11 306_92_area8	base metal pyrite - core	53.35	46.45	-	-	-	99.82
Isis: Line 12 306_92_area8	base metal pyrite - core	53.50	46.59	-	-	-	100.12
Isis: Line 13 306_92_area8	base metal pyrite - core	53.66	46.60	-	-	-	100.29
Isis: Line 14 306_92_area8	base metal pyrite - core	54.17	45.62	-	-	-	99.83

Sample ID	Occurrence	S	Fe	As	Sb	Zn	Total
		0.03	0.04	0.04	0.07	0.05	
Isis: Line 15 306_92_area8	base metal pyrite - core	52.10	45.74	-	-	-	97.86
Isis: Line 16 306_92_area8	base metal pyrite - core	53.45	46.61	-	-	-	100.09
Isis: Line 17 306_92_area8	base metal pyrite - core	53.43	46.66	-	-	-	100.11
Isis: Line 18 306_92_area8	base metal pyrite - core	53.03	46.43	-	-	-	99.48
Isis: Line 19 306_92_area8	base metal pyrite - core	51.55	46.24	-	-	-	97.80
Isis: Line 20 306_92_area8	base metal pyrite - core	53.60	46.36	-	-	-	99.97
Isis east: 104_75_py1	base metal pyrite - rim	53.34	46.50	-	-	-	99.86
Isis east: 104_75_py2	base metal pyrite - core	53.27	46.23	-	-	-	99.52
Isis east: 104_75_py3	base metal pyrite - rim	53.33	46.35	-	-	-	99.72
Isis east: 104_75_py4	base metal pyrite - rim	53.33	46.09	-	-	-	99.47
Isis east: 104_75_py5	base metal pyrite - rim	53.23	46.14	-	-	-	99.39
Isis east: 104_75_py6	base metal pyrite - core	53.43	46.38	-	-	-	99.83
Isis east: 104_75_py7	base metal pyrite - rim	53.38	46.07	-	-	-	99.46
Isis east: 104_75_py8	base metal pyrite - rim	53.49	46.18	-	-	-	99.70
Isis east: 104_75_py9	base metal pyrite - rim	53.31	46.34	-	-	-	99.66
Isis east: 104_75_py10	base metal pyrite - rim	53.49	46.10	-	-	-	99.62
Isis east: Line 1 117_19_a4	base metal pyrite - rim	53.05	46.13	0.14	-	-	99.35
Isis east: Line 2 117_19_a4	base metal pyrite - core	53.03	45.99	0.21	-	-	99.22
Isis east: Line 3 117_19_a4	base metal pyrite - core	53.13	46.01	0.24	-	-	99.38
Isis east: Line 4 117_19_a4	base metal pyrite - core	53.22	45.97	0.28	-	-	99.49
Isis east: Line 5 117_19_a4	base metal pyrite - core	53.12	46.01	0.21	-	-	99.35
Isis east: Line 6 117_19_a4	base metal pyrite - core	52.69	45.34	0.47	-	-	98.50
Isis east: Line 7 117_19_a4	base metal pyrite - core	52.98	45.62	0.43	-	-	99.05
Isis east: Line 8 117_19_a4	base metal pyrite - core	52.67	45.75	0.29	-	-	98.73
Isis east: Line 9 117_19_a4	base metal pyrite - core	53.23	46.24	0.22	-	-	99.69
Isis east: Line 10 117_19_a4	base metal pyrite - rim	53.26	46.35	-	-	-	99.64
Isis east: 117_19_py1	base metal pyrite - rim	53.26	46.34	-	-	-	99.62
Isis east: 117_19_py2	base metal pyrite - rim	53.02	45.91	0.15	-	-	99.09
Isis east: 117_19_py3	base metal pyrite - rim	53.43	46.41	-	-	-	99.86
Isis east: 117_19_py4	base metal pyrite - rim	53.13	46.02	-	-	-	99.19
Isis east: 117_19_py5	base metal pyrite - rim	53.28	45.75	-	-	-	99.08
Isis east: 117_19_py6	base metal pyrite - rim	53.30	46.16	-	-	-	99.49
Isis east: 117_19_py7	base metal pyrite - rim	53.40	45.95	-	-	-	99.38
Isis east: 117_19_py8	base metal pyrite - core	52.63	45.36	0.21	-	-	98.19
Isis east: 117_19_py9	base metal pyrite - core	52.72	45.85	0.29	-	-	98.88
Isis east: Line 1 117_19_a4a	base metal pyrite - rim	53.27	46.15	0.03	-	-	99.44
Isis east: Line 2 117_19_a4a	base metal pyrite - core	53.09	46.00	0.17	-	-	99.26
Isis east: Line 3 117_19_a4a	base metal pyrite - core	53.03	45.85	0.34	-	-	99.22
Isis east: Line 4 117_19_a4a	base metal pyrite - core	52.94	46.02	0.31	-	-	99.27
Isis east: Line 5 117_19_a4a	base metal pyrite - core	53.06	46.01	0.17	-	-	99.25
Isis east: Line 6 117_19_a4a	base metal pyrite - core	52.93	45.90	0.13	-	-	98.97
Isis east: Line 7 117_19_a4a	base metal pyrite - core	52.95	45.94	0.19	-	-	99.09
Isis east: Line 8 117_19_a4a	base metal pyrite - core	52.77	46.18	-	-	-	98.98
Isis east: Line 9 117_19_a4a	base metal pyrite - core	53.42	46.49	-	-	-	99.94
Isis east: Line 10 117_19_a4a	base metal pyrite - rim	53.29	46.04	-	-	-	99.35
Isis east: 115_26_py1	ore stage pyrite - rim	49.89	44.12	3.27	-	-	97.29

Sample ID	Occurrence	S	Fe	As	Sb	Zn	Total
		0.03	0.04	0.04	0.07	0.05	
Isis east: 115_26_py2	base metal pyrite - core	52.81	45.85	-	-	-	98.72
Isis east: 115_26_py3	base metal pyrite - core	53.60	45.93	0.06	-	-	99.60
Isis east: 115_26_py4	base metal pyrite - rim	53.45	45.92	-	-	-	99.39
Isis east: 115_26_py5	base metal pyrite - rim	53.22	46.20	-	-	-	99.46
Isis east: 115_26_py6	base metal pyrite - core	52.28	45.74	-	-	-	98.05
Isis east: 115_26_py7	base metal pyrite - rim	53.71	46.16	-	-	-	99.92
Isis east: 115_26_py8	base metal pyrite - rim	53.64	46.23	-	-	-	99.89
Isis east: 115_26_py9	base metal pyrite - rim	53.33	46.19	-	-	-	99.59
Isis east: 115_26_py10	base metal pyrite - rim	53.20	46.42	-	-	-	99.66
Isis east: 115_26_py11	base metal pyrite - rim	53.65	46.16	-	-	-	99.84
Isis east: 115_26_py12	base metal pyrite - rim	53.70	46.42	-	-	-	100.17
Isis east: 115_26_py13	base metal pyrite - core	52.96	46.39	-	-	-	99.41
Isis east: 115_26_py14	base metal pyrite - rim	53.58	46.01	-	-	-	99.61
Isis east: 115_26_py15	base metal pyrite - rim	53.49	46.28	-	-	-	99.80
Isis east: Line 1 115_26_a4	base metal pyrite - rim	53.30	46.00	-	-	-	99.34
Isis east: Line 2 115_26_a4	base metal pyrite - core	53.40	46.19	-	-	-	99.61
Isis east: Line 3 115_26_a4	base metal pyrite - core	53.44	46.30	-	-	-	99.79
Isis east: Line 4 115_26_a4	base metal pyrite - core	53.30	46.36	-	-	-	99.71
Isis east: Line 5 115_26_a4	base metal pyrite - core	53.52	46.28	-	-	-	99.81
Isis east: Line 6 115_26_a4	base metal pyrite - core	53.42	46.33	-	-	-	99.76
Isis east: Line 7 115_26_a4	base metal pyrite - core	53.61	46.33	-	-	-	99.95
Isis east: Line 8 115_26_a4	base metal pyrite - core	53.63	46.52	-	-	-	100.18
Isis east: Line 9 115_26_a4	base metal pyrite - rim	53.21	45.94	-	-	-	99.19
Isis east: Line 10 115_26_a4	base metal pyrite - rim	53.64	46.08	-	-	-	99.74
Isis east: Line 1 115_26_a4a	base metal pyrite - rim	53.49	45.86	-	-	-	99.38
Isis east: Line 2 115_26_a4a	base metal pyrite - core	53.30	45.92	-	-	-	99.23
Isis east: Line 3 115_26_a4a	base metal pyrite - core	53.22	45.77	-	-	-	99.02
Isis east: Line 4 115_26_a4a	base metal pyrite - core	53.56	45.74	-	-	-	99.33
Isis east: Line 5 115_26_a4a	base metal pyrite - rim	53.48	45.91	-	-	-	99.42
Osiris: 111_57A_py1	ore-stage pyrite - rim	53.37	46.14	-	-	-	99.59
Osiris: 111_57A_py2	ore-stage pyrite - core	52.57	45.45	1.36	-	-	99.41
Osiris: 111_57A_py3	ore-stage pyrite - rim	52.75	44.71	0.32	-	-	97.80
Osiris: 111_57A_py4	ore-stage pyrite - rim	52.95	45.41	0.08	-	-	98.44
Osiris: 111_57A_py5	ore-stage pyrite - core	53.67	45.65	0.09	-	-	99.42
Osiris: 111_57A_py6	ore-stage pyrite - core	53.31	45.63	-	-	-	98.97

Appendix E – LA-ICP-MS Data

LA-ICP-MS data for calcite and dolomite. Values are in ppm. Data below detection limit are indicated by (-) and other deleted data are indicated by an "X".

Sample ID	Phase	⁴⁵ Sc	⁴⁷ Ti	⁴⁹ Ti	⁵¹ V	⁵² Cr	⁵⁵ Mn	⁵⁷ Fe
696-1.FIN2	Cal 3	0.11	2.90	2.84	0.14	2.69	211.10	1764.00
696-2.FIN2	Cal 3	-	-	0.09	0.08	2.63	208.90	1653.00
696-3.FIN2	Cal 3	-	-	0.08	0.07	2.61	210.00	1770.00
696-4.FIN2	Dol 2	0.10	1.52	1.35	0.72	2.81	1041.00	32160.00
696-5.FIN2	Dol 2	0.05	0.72	0.89	0.43	2.90	857.00	30460.00
696-6.FIN2	Dol 2	0.12	1.24	1.57	1.52	2.87	936.00	29310.00
696-7.FIN2	Dol 2	-	0.18	-	1.09	2.95	468.10	31180.00
696-8.FIN2	Dol 2	-	-	-	0.94	2.85	458.00	31100.00
696-9.FIN2	Cal 3	-	-	-	0.15	2.65	201.20	1758.00
696-10.FIN2	Dol 2	-	-	0.61	1.52	3.96	619.00	40580.00
696-11.FIN2	Cal 3	-	-	0.69	0.07	2.63	137.10	1558.00
696-12.FIN2	Cal 3	-	-	0.12	0.05	2.75	137.00	1538.00
696-13.FIN2	Cal 3	-	-	-	0.05	2.87	160.20	1898.00
696-14.FIN2	Cal 3	-	-	0.09	-	2.74	100.70	1248.00
696-19.FIN2	Cal 3	0.04	-	0.88	0.21	2.63	143.60	1950.00
696-20.FIN2	Cal 3	-	-	-	0.05	2.60	156.10	2014.00
2991-25.FIN2	Cal 3	-	-	0.15	0.62	2.35	341.00	282.00
2991-24.FIN2	Cal 3	0.01	-	0.17	1.69	2.45	284.40	2157.00
2991-23.FIN2	Dol 2	0.05	1.83	1.76	1.79	2.66	1387.00	39350.00
2991-22.FIN2	Dol 2	-	0.77	0.59	0.53	2.58	993.00	53750.00
2991-21.FIN2	Dol 2	-	0.43	0.57	0.51	2.62	1031.00	54960.00
2991-20.FIN2	Cal 2	0.08	3.3	3.30	0.37	2.75	246.50	2826.00
2991-16.FIN2	Cal 2	0.28	4.3	4.40	0.51	2.75	230.30	3239.00
2991-15.FIN2	Cal 2	0.05	0.39	0.34	0.24	2.59	227.60	3860.00
2991-14.FIN2	Cal 2	0.16	2.13	2.27	0.38	2.68	230.40	3823.00
2991-13.FIN2	Cal 2	0.17	2.88	3.19	0.41	2.86	240.10	3870.00
2991-12.FIN2	Dol 2	-	0.63	0.68	0.31	2.72	1151.00	88900.00
2991-11.FIN2	Dol 2	0.15	1.63	1.66	2.82	3.15	1119.00	34980.00
2991-10.FIN2	Dol 2	0.15	1.63	1.81	2.64	3.24	1111.00	32750.00
2991-9.FIN2	Dol 2	0.03	1.62	1.76	0.90	2.54	1192.00	53680.00
2991-8.FIN2	Dol 2	0.32	1.43	1.69	4.45	3.36	1706.00	44850.00
2991-7.FIN2	Dol 2	0.16	1.25	1.35	2.12	2.93	900.00	26490.00
2991-6.FIN2	Cal 3	-	-	0.05	0.83	2.45	308.50	2206.00
2991-5.FIN2	Cal 3	-	-	0.30	0.67	2.51	427.00	156.20
2991-4.FIN2	Cal 3	-	-	-	0.65	2.48	360.60	291.00
2991-3.FIN2	Cal 3	0.09	-	-	1.38	2.50	223.30	1560.00
2991-2.FIN2	Cal 3	-	-	0.25	0.39	2.33	345.40	289.00
2991-1.FIN2	Cal 2	0.09	0.95	0.50	2.73	2.61	228.80	2530.00
13805-20	Dol 2	0.36	8.00	7.70	1.16	5.47	649.00	31760.00
13805-19	Dol 2	0.33	6.90	7.20	0.98	5.17	632.00	31670.00
13805-18	Dol 2	0.36	11.90	12.30	1.05	5.33	629.00	32700.00

LA-ICP-MS data for calcite and dolomite. Values are in ppm. Data below detection limit are indicated by (-) and other deleted data are indicated by an "X".

Sample ID Phase	⁵⁹ Co	⁶⁰ Ni	⁶¹ Ni	⁶⁵ Cu	⁶⁶ Zn	⁷⁵ As	⁸⁵ Rb	⁸⁸ Sr
696-1.FIN Cal 3	0.07	0.49	2.37	7.90	0.58	72.00	1.06	601.00
696-2.FIN Cal 3	0.03	0.17	1.75	0.12	0.05	5.00	0.03	385.30
696-3.FIN Cal 3	0.05	0.22	2.24	0.24	-	4.53	0.01	399.90
696-4.FIN Dol 2	2.00	4.36	5.58	3.60	5.66	429.00	0.14	92.50
696-5.FIN Dol 2	1.55	2.99	3.81	1.60	6.32	221.00	0.01	157.00
696-6.FIN Dol 2	1.66	4.20	5.95	2.64	4.24	381.40	0.01	416.00
696-7.FIN Dol 2	0.29	1.44	3.02	1.70	6.84	376.00	0.04	82.60
696-8.FIN Dol 2	0.24	1.39	2.53	1.19	6.51	302.00	0.02	80.70
696-9.FIN Cal 3	-	0.21	2.05	0.10	-	3.70	0.01	480.00
696-10.FI Dol 2	0.09	1.47	3.17	0.64	8.54	61.50	0.07	209.40
696-11.FI Cal 3	0.09	0.27	2.33	2.60	0.39	22.10	0.23	3059.00
696-12.FI Cal 3	-	0.19	1.66	0.60	-	4.30	0.05	2938.00
696-13.FI Cal 3	0.03	0.13	1.45	-	0.07	5.92	0.01	2454.00
696-14.FI Cal 3	-	0.20	2.22	0.27	-	1.15	0.02	4700.00
696-19.FI Cal 3	0.03	0.21	2.24	-	0.14	17.50	0.36	3460.00
696-20.FI Cal 3	0.04	0.20	2.17	-	0.05	2.37	0.01	2641.00
2991-25.F Cal 3	-	0.14	2.19	0.31	0.12	0.69	0.02	182.40
2991-24.F Cal 3	-	0.18	1.47	0.10	0.13	0.66	0.02	135.00
2991-23.F Dol 2	0.77	5.95	6.82	1.14	6.71	1.34	0.07	120.70
2991-22.F Dol 2	1.83	6.27	6.91	0.41	8.10	1.40	0.06	149.20
2991-21.F Dol 2	1.71	6.82	8.23	0.27	7.98	2.30	0.02	109.20
2991-20.F Cal 2	0.10	0.17	2.39	0.09	0.15	2.80	0.23	857.00
2991-16.F Cal 2	0.12	0.23	1.55	0.14	0.20	1.17	0.37	954.00
2991-15.F Cal 2	-	0.17	1.87	0.48	0.11	1.30	0.13	1026.00
2991-14.F Cal 2	0.09	0.23	1.95	0.07	0.15	0.86	0.18	989.00
2991-13.F Cal 2	0.13	0.31	1.72	1.64	0.40	8.00	0.29	965.00
2991-12.F Dol 2	1.53	4.87	6.14	0.72	8.13	5.60	0.04	106.90
2991-11.F Dol 2	-	0.51	1.82	0.18	2.89	0.39	0.02	144.50
2991-10.F Dol 2	0.10	1.30	2.65	0.18	2.85	0.38	0.01	205.00
2991-9.FI Dol 2	0.69	5.37	6.59	0.61	6.60	3.20	0.05	108.70
2991-8.FI Dol 2	0.28	2.42	3.25	0.28	4.38	1.64	0.01	106.40
2991-7.FI Dol 2	0.11	0.69	1.27	1.06	2.49	5.00	0.09	327.00
2991-6.FI Cal 3	0.01	0.13	1.99	-	0.13	0.86	0.02	109.40
2991-5.FI Cal 3	0.00	0.16	1.85	0.94	0.16	2.50	0.06	91.70
2991-4.FI Cal 3	-	0.14	1.19	0.23	0.07	1.14	0.01	137.30
2991-3.FI Cal 3	-	0.12	1.98	0.08	0.07	0.77	-	87.00
2991-2.FI Cal 3	-	0.12	1.78	2.40	0.12	3.10	0.11	105.70
2991-1.FI Cal 2	0.05	0.19	1.77	3.30	7.26	10.10	0.18	234.10
13805-20 Dol 2	0.14	1.80	2.61	0.73	5.92	2.40	0.45	108.90
13805-19 Dol 2	0.15	1.66	2.55	2.60	5.86	7.60	0.78	116.60
13805-18 Dol 2	0.22	1.86	2.55	4.10	6.10	6.70	0.45	118.40

LA-ICP-MS data for calcite and dolomite. Values are in ppm. Data below detection limit are indicated by (-) and other deleted data are indicated by an "X".

Sample ID	Phase	⁸⁹ Y	⁹⁰ Zr	⁹⁵ Mo	⁹⁸ Mo	¹⁰⁷ Ag	¹⁰⁹ Ag	¹¹¹ Cd
696-1.FIN2	Cal 3	0.60	0.98	0.02	0.02	-	0.01	-
696-2.FIN2	Cal 3	0.28	0.49	0.01	-	-	-	-
696-3.FIN2	Cal 3	0.30	0.21	0.01	-	-	-	0.01
696-4.FIN2	Dol 2	8.33	0.20	0.07	0.03	-	-	0.01
696-5.FIN2	Dol 2	7.54	0.07	0.05	0.01	-	-	0.02
696-6.FIN2	Dol 2	9.60	0.22	0.06	0.02	-	-	0.01
696-7.FIN2	Dol 2	4.53	0.19	0.05	0.04	-	-	-
696-8.FIN2	Dol 2	4.35	0.32	0.05	0.03	-	-	0.01
696-9.FIN2	Cal 3	0.57	1.74	0.01	-	-	-	0.01
696-10.FIN2	Dol 2	5.88	0.25	0.03	0.01	-	-	-
696-11.FIN2	Cal 3	0.16	0.33	0.06	0.04	-	-	-
696-12.FIN2	Cal 3	0.02	0.26	0.01	-	-	-	-
696-13.FIN2	Cal 3	0.08	0.76	-	-	-	-	-
696-14.FIN2	Cal 3	-	0.17	-	-	-	-	-
696-19.FIN2	Cal 3	1.07	0.39	0.02	0.01	-	-	-
696-20.FIN2	Cal 3	0.05	0.42	0.01	0.00	-	-	-
2991-25.FIN2	Cal 3	0.55	0.45	0.01	-	-	-	-
2991-24.FIN2	Cal 3	0.26	0.82	0.01	-	-	-	-
2991-23.FIN2	Dol 2	8.64	0.15	0.06	-	-	-	-
2991-22.FIN2	Dol 2	5.07	0.06	0.03	-	-	-	0.01
2991-21.FIN2	Dol 2	5.30	0.13	0.03	-	-	-	-
2991-20.FIN2	Cal 2	5.59	0.53	-	-	-	-	-
2991-16.FIN2	Cal 2	6.56	0.65	-	-	-	-	-
2991-15.FIN2	Cal 2	7.02	0.09	-	-	-	-	-
2991-14.FIN2	Cal 2	5.28	0.68	-	-	-	-	-
2991-13.FIN2	Cal 2	4.46	0.80	0.01	0.01	-	-	-
2991-12.FIN2	Dol 2	4.35	0.56	0.05	0.01	-	-	0.02
2991-11.FIN2	Dol 2	4.54	0.06	0.03	-	-	-	-
2991-10.FIN2	Dol 2	4.06	0.08	0.03	-	-	-	-
2991-9.FIN2	Dol 2	7.93	1.61	0.04	-	-	-	-
2991-8.FIN2	Dol 2	4.60	0.12	0.07	0.01	-	-	-
2991-7.FIN2	Dol 2	4.19	0.70	0.04	-	-	-	0.01
2991-6.FIN2	Cal 3	0.74	0.58	0.01	-	-	-	-
2991-5.FIN2	Cal 3	0.13	0.51	0.02	-	-	-	-
2991-4.FIN2	Cal 3	0.39	0.81	0.01	-	-	-	-
2991-3.FIN2	Cal 3	0.93	0.16	-	-	-	-	-
2991-2.FIN2	Cal 3	0.61	1.06	0.02	-	-	-	0.01
2991-1.FIN2	Cal 2	1.44	0.94	0.01	-	-	-	0.01
13805-20	Dol 2	4.96	0.41	0.05	0.03	-	-	0.01
13805-19	Dol 2	4.98	0.34	0.06	0.02	-	0.01	0.01
13805-18	Dol 2	5.43	0.28	0.06	0.05	-	-	0.01

LA-ICP-MS data for calcite and dolomite. Values are in ppm. Data below detection limit are indicated by (-) and other deleted data are indicated by an "X".

Sample #	Phase	¹¹⁴ Cd	¹²¹ Sb	¹²³ Sb	¹³⁷ Ba	¹³⁹ La	¹⁴⁰ Ce	¹⁴¹ Pr	¹⁴⁶ Nd
696-1.FIN	Cal 3	0.02	0.10	0.10	24.40	0.95	2.02	0.25	1.04
696-2.FIN	Cal 3	-	0.05	0.07	4.13	0.38	0.60	0.08	0.38
696-3.FIN	Cal 3	-	0.07	0.08	3.79	0.41	0.83	0.12	0.54
696-4.FIN	Dol 2	0.02	1.20	1.19	10.46	10.10	26.84	3.45	14.68
696-5.FIN	Dol 2	0.03	0.49	0.49	10.56	11.29	29.13	3.66	15.24
696-6.FIN	Dol 2	0.01	0.98	0.96	16.74	10.77	30.27	3.89	15.97
696-7.FIN	Dol 2	0.01	1.26	1.25	4.34	9.30	15.20	1.74	6.76
696-8.FIN	Dol 2	0.01	1.19	1.17	3.81	7.01	11.91	1.35	5.35
696-9.FIN	Cal 3	0.01	0.06	0.05	9.97	0.72	1.34	0.18	0.78
696-10.FI	Dol 2	0.01	0.31	0.31	10.66	9.95	16.44	1.96	7.80
696-11.FI	Cal 3	0.01	0.09	0.09	13.13	0.33	0.55	0.07	0.30
696-12.FI	Cal 3	-	-	0.06	9.17	0.07	0.11	0.02	0.06
696-13.FI	Cal 3	-	0.09	0.07	22.60	0.16	0.27	0.03	0.15
696-14.FI	Cal 3	0.01	-	-	10.49	0.08	-	-	0.13
696-19.FI	Cal 3	-	0.08	0.09	16.50	2.38	3.76	0.48	1.83
696-20.FI	Cal 3	-	0.03	-	17.18	0.10	0.16	0.02	0.11
2991-25.F	Cal 3	-	-	0.02	23.80	0.73	1.55	0.22	1.01
2991-24.F	Cal 3	-	0.01	-	11.94	0.41	1.07	0.15	0.60
2991-23.F	Dol 2	-	-	-	12.50	9.32	28.31	3.85	16.00
2991-22.F	Dol 2	0.02	-	0.01	20.50	5.31	15.92	2.24	9.84
2991-21.F	Dol 2	0.01	-	-	11.56	4.88	13.97	1.96	8.52
2991-20.F	Cal 2	-	-	-	24.10	14.52	22.49	2.70	11.12
2991-16.F	Cal 2	-	-	-	49.30	17.88	30.00	3.46	14.06
2991-15.F	Cal 2	-	0.01	-	14.30	26.70	37.40	4.18	16.30
2991-14.F	Cal 2	-	0.01	-	36.30	17.00	27.07	3.11	12.34
2991-13.F	Cal 2	0.02	-	0.02	42.40	13.18	22.56	2.54	10.06
2991-12.F	Dol 2	-	0.03	0.04	10.90	4.18	13.39	1.87	8.24
2991-11.F	Dol 2	-	-	-	15.70	7.85	16.27	2.02	8.00
2991-10.F	Dol 2	-	0.02	-	13.05	7.44	15.59	1.85	7.44
2991-9.FI	Dol 2	-	0.01	0.02	11.69	8.88	27.15	3.58	15.03
2991-8.FI	Dol 2	0.01	-	-	6.61	7.12	16.17	1.97	7.69
2991-7.FI	Dol 2	0.01	0.02	-	40.30	7.59	15.86	1.92	7.91
2991-6.FI	Cal 3	-	-	-	9.82	2.42	4.30	0.52	2.00
2991-5.FI	Cal 3	0.02	-	-	11.70	0.22	0.50	0.06	0.22
2991-4.FI	Cal 3	-	-	-	12.82	0.39	1.05	0.15	0.79
2991-3.FI	Cal 3	-	-	-	5.44	4.63	8.10	0.96	3.70
2991-2.FI	Cal 3	0.01	-	-	11.30	1.01	2.19	0.30	1.22
2991-1.FI	Cal 2	0.01	-	-	19.95	15.41	22.89	2.51	9.71
13805-20	Dol 2	0.01	0.01	-	9.75	5.15	15.14	2.08	8.79
13805-19	Dol 2	0.01	-	-	11.10	5.01	14.99	2.08	8.78
13805-18	Dol 2	0.01	0.01	0.02	13.28	4.97	15.38	2.13	9.14

LA-ICP-MS data for calcite and dolomite. Values are in ppm. Data below detection limit are indicated by (-) and other deleted data are indicated by an "X".

Sample ID	Phase	¹⁴⁷ Sm	¹⁵³ Eu	¹⁵⁷ Gd	¹⁵⁹ Tb	¹⁶³ Dy	¹⁶⁵ Ho	¹⁶⁶ Er
696-1.FIN2	Cal 3	0.20	0.04	0.16	0.02	0.09	0.02	0.04
696-2.FIN2	Cal 3	0.06	0.03	0.06	0.01	0.04	0.01	0.02
696-3.FIN2	Cal 3	0.09	0.03	0.08	0.01	0.05	0.01	0.02
696-4.FIN2	Dol 2	2.59	0.42	2.04	0.26	1.48	0.26	0.63
696-5.FIN2	Dol 2	2.63	0.42	2.04	0.23	1.30	0.21	0.54
696-6.FIN2	Dol 2	2.76	0.41	2.17	0.28	1.74	0.31	0.77
696-7.FIN2	Dol 2	1.12	0.18	1.03	0.12	0.76	0.13	0.33
696-8.FIN2	Dol 2	0.92	0.16	0.89	0.10	0.65	0.12	0.30
696-9.FIN2	Cal 3	0.16	0.05	0.13	0.02	0.11	0.02	0.05
696-10.FIN2	Dol 2	1.47	0.23	1.27	0.16	0.91	0.16	0.37
696-11.FIN2	Cal 3	0.05	0.03	0.04	0.01	0.03	0.01	0.01
696-12.FIN2	Cal 3	0.01	0.01	0.02	-	0.01	-	-
696-13.FIN2	Cal 3	-	0.02	0.03	-	0.02	-	0.01
696-14.FIN2	Cal 3	0.03	0.03	0.02	0.01	0.02	-	-
696-19.FIN2	Cal 3	0.29	0.24	0.27	0.03	0.18	0.03	0.05
696-20.FIN2	Cal 3	0.02	0.01	0.02	-	0.01	0.00	0.01
2991-25.FIN2	Cal 3	0.19	0.04	0.14	0.02	0.09	0.01	0.03
2991-24.FIN2	Cal 3	0.11	0.02	0.07	0.01	0.05	0.01	0.02
2991-23.FIN2	Dol 2	2.71	0.46	2.12	0.28	1.73	0.28	0.71
2991-22.FIN2	Dol 2	1.59	0.27	1.31	0.15	0.81	0.14	0.31
2991-21.FIN2	Dol 2	1.53	0.26	1.25	0.15	0.92	0.15	0.35
2991-20.FIN2	Cal 2	1.89	0.60	1.53	0.16	0.83	0.12	0.27
2991-16.FIN2	Cal 2	2.44	0.67	1.74	0.19	1.01	0.17	0.38
2991-15.FIN2	Cal 2	2.61	0.94	1.89	0.20	1.02	0.16	0.33
2991-14.FIN2	Cal 2	2.05	0.79	1.46	0.17	0.87	0.13	0.28
2991-13.FIN2	Cal 2	1.70	0.64	1.23	0.13	0.71	0.11	0.23
2991-12.FIN2	Dol 2	1.35	0.24	1.17	0.12	0.61	0.10	0.22
2991-11.FIN2	Dol 2	1.36	0.24	1.14	0.14	0.82	0.14	0.33
2991-10.FIN2	Dol 2	1.34	0.21	1.00	0.13	0.73	0.12	0.33
2991-9.FIN2	Dol 2	2.68	0.41	1.93	0.25	1.52	0.27	0.66
2991-8.FIN2	Dol 2	1.34	0.22	0.98	0.13	0.83	0.15	0.37
2991-7.FIN2	Dol 2	1.45	0.25	1.10	0.13	0.76	0.14	0.30
2991-6.FIN2	Cal 3	0.29	0.05	0.20	0.02	0.11	0.02	0.06
2991-5.FIN2	Cal 3	0.04	0.01	0.04	-	0.02	0.00	0.01
2991-4.FIN2	Cal 3	0.14	0.02	0.08	0.01	0.07	0.01	0.03
2991-3.FIN2	Cal 3	0.54	0.07	0.34	0.03	0.17	0.03	0.07
2991-2.FIN2	Cal 3	0.20	0.04	0.19	0.02	0.11	0.02	0.04
2991-1.FIN2	Cal 2	1.13	0.14	0.64	0.05	0.26	0.04	0.09
13805-20	Dol 2	1.45	0.23	1.20	0.14	0.77	0.14	0.31
13805-19	Dol 2	1.43	0.22	1.28	0.14	0.76	0.13	0.32
13805-18	Dol 2	1.43	0.24	1.33	0.15	0.84	0.14	0.33

LA-ICP-MS data for calcite and dolomite. Values are in ppm. Data below detection limit are indicated by (-) and other deleted data are indicated by an "X".

Sample	Phase	¹⁶⁹ Tm	¹⁷² Yb	¹⁷⁵ Lu	¹⁹⁷ Au	²⁰⁵ Tl	²⁰⁷ Pb	²⁰⁹ Bi	²³² Th	²³⁸ U
696-1	FIN Cal 3	0.01	0.02	-	-	0.01	0.56	-	0.01	0.22
696-2	FIN Cal 3	-	0.01	-	-	0.01	0.08	-	-	0.32
696-3	FIN Cal 3	-	0.02	-	-	-	0.07	-	0.01	0.17
696-4	FIN Dol 2	0.07	0.35	0.05	-	-	0.18	-	0.06	0.10
696-5	FIN Dol 2	0.05	0.29	0.04	-	0.04	0.09	-	0.03	0.06
696-6	FIN Dol 2	0.09	0.52	0.07	-	0.10	0.17	-	0.09	0.17
696-7	FIN Dol 2	0.03	0.15	0.02	-	0.06	0.24	-	0.03	0.16
696-8	FIN Dol 2	0.03	0.16	0.02	-	0.08	0.19	-	0.01	0.20
696-9	FIN Cal 3	0.01	0.03	0.01	-	-	0.08	-	0.05	1.10
696-10	FI Dol 2	0.04	0.20	0.03	-	-	0.26	-	0.03	0.20
696-11	FI Cal 3	-	0.01	-	-	0.01	0.34	-	0.01	0.34
696-12	FI Cal 3	-	-	-	-	0.01	0.18	-	0.00	0.12
696-13	FI Cal 3	-	-	-	-	0.01	0.20	-	0.00	0.82
696-14	FI Cal 3	-	0.01	-	-	-	0.18	-	-	0.08
696-19	FI Cal 3	0.01	0.04	-	-	0.01	0.38	-	0.01	0.34
696-20	FI Cal 3	-	-	-	-	-	0.14	-	-	0.38
2991-25	F Cal 3	-	0.02	-	-	-	0.05	-	0.01	0.19
2991-24	F Cal 3	0.01	0.02	-	-	0.01	0.07	-	0.01	0.73
2991-23	F Dol 2	0.08	0.42	0.05	-	-	0.24	-	0.06	0.12
2991-22	F Dol 2	0.03	0.15	0.02	-	0.01	0.31	-	0.01	0.09
2991-21	F Dol 2	0.03	0.14	0.02	-	0.01	0.20	-	0.02	0.18
2991-20	F Cal 2	0.03	0.15	0.02	-	0.01	0.57	-	0.04	0.21
2991-16	F Cal 2	0.04	0.23	0.03	-	0.01	0.68	-	0.12	0.36
2991-15	F Cal 2	0.03	0.13	0.01	-	-	0.64	-	0.03	0.05
2991-14	F Cal 2	0.03	0.17	0.02	-	0.01	0.82	-	0.11	0.50
2991-13	F Cal 2	0.03	0.14	0.02	-	0.02	0.84	-	0.10	0.37
2991-12	F Dol 2	0.02	0.09	0.01	-	-	0.28	-	0.01	0.10
2991-11	F Dol 2	0.04	0.20	0.03	-	-	0.14	-	0.16	0.13
2991-10	F Dol 2	0.04	0.21	0.02	-	-	0.15	-	0.14	0.12
2991-9	FI Dol 2	0.08	0.42	0.06	-	-	0.26	-	0.04	0.08
2991-8	FI Dol 2	0.04	0.21	0.03	-	-	0.17	-	0.10	0.08
2991-7	FI Dol 2	0.04	0.20	0.03	-	0.01	0.47	-	0.17	0.73
2991-6	FI Cal 3	0.01	0.03	-	-	0.01	0.11	-	0.01	0.28
2991-5	FI Cal 3	-	-	-	-	-	0.08	-	0.01	0.25
2991-4	FI Cal 3	-	0.02	-	-	0.01	0.08	-	-	0.28
2991-3	FI Cal 3	0.01	0.06	0.01	-	-	0.06	-	0.03	0.10
2991-2	FI Cal 3	0.00	0.02	-	-	0.01	0.15	-	-	0.25
2991-1	FI Cal 2	0.01	0.05	0.01	-	0.03	0.23	-	0.03	0.24
13805-20	Dol 2	0.03	0.18	0.02	-	0.01	0.15	-	0.30	1.20
13805-19	Dol 2	0.03	0.17	0.02	-	0.01	0.26	-	0.26	1.17
13805-18	Dol 2	0.04	0.19	0.03	-	0.02	0.24	-	0.29	1.32

LA-ICP-MS data for calcite and dolomite. Values are in ppm. Data below detection limit are indicated by (-) and other deleted data are indicated by an "X".

Sample ID	Phase	⁴⁵ Sc	⁴⁷ Ti	⁴⁹ Ti	⁵¹ V	⁵² Cr	⁵⁵ Mn	⁵⁷ Fe
13805-17	Cal 4	-	-	0.14	0.89	3.71	342.60	51.40
13805-16	Cal 4	-	-	0.25	0.36	3.66	469.00	39.50
13805-15	Cal 4	-	-	0.19	0.02	3.31	156.20	61.90
13805-14	Cal 4	0.05	1.10	1.19	0.56	3.77	3261.00	760.00
13805-13	Cal 4	0.01	-	0.16	1.61	3.54	523.00	42.20
13805-12	Cal 4	-	-	0.37	0.04	3.54	139.90	60.70
13805-11	Cal 4	-	0.48	0.98	0.01	3.54	141.90	111.40
13805-10	Dol 2	1.09	26.70	26.60	2.77	11.78	962.80	55090.00
13805-9	Dol 2	0.38	35.90	36.00	2.06	6.26	682.00	29580.00
13805-7	Dol 2	0.19	76.00	79.00	2.43	6.23	868.00	24420.00
13805-6	Dol 2	0.02	10.80	11.40	0.59	4.60	809.00	23580.00
13805-5	Dol 2	0.07	15.20	15.10	0.97	4.82	658.00	25410.00
13805-4	Dol 2	0.07	23.90	23.80	0.85	4.56	760.00	24310.00
13805-3	Dol 2	0.23	69.00	67.00	3.08	6.35	666.80	26100.00
13805-2	Dol 2	0.21	15.90	15.10	1.27	4.96	718.00	26990.00
13805-1	Cal 4	-	0.49	0.49	0.01	3.92	142.20	78.70
13805-1-1	Cal 4	-	-	0.29	-	3.79	139.50	53.70
17603-20.FIN2	Dol 3	0.46	3.27	3.44	9.79	5.25	1731.00	10200.00
17603-19.FIN2	Dol 3	0.49	7.00	6.90	13.78	5.82	1811.00	9730.00
17603-18.FIN2	Dol 3	0.14	4.40	5.60	6.30	4.57	1334.00	7740.00
17603-17.FIN2	Dol 3	0.16	4.47	5.70	9.90	4.64	1400.00	8780.00
17603-15.FIN2	Cal 4	0.79	0.12	0.34	11.93	3.83	2560.00	500.00
17603-14.FIN2	Cal 4	0.70	-	0.10	9.79	3.92	2400.00	71.00
17603-13.FIN2	Cal 4	0.51	0.56	0.59	7.17	3.81	3740.00	390.00
17603-12.FIN2	Cal 4	-	-	0.21	0.14	3.36	2263.00	270.00
17603-11.FIN2	Dol 2	-	1.96	2.07	0.70	3.30	410.00	982.00
17603-9.FIN2	Dol 2	0.05	1.18	1.25	2.29	3.51	423.60	1135.00
17603-8.FIN2	Dol 2	0.09	0.61	1.04	1.79	3.63	602.30	1677.00
17603-7.FIN2	Dol 2	0.03	0.70	0.84	2.36	3.53	365.50	356.00
17603-6.FIN2	Dol 2	0.05	0.77	1.09	3.40	3.37	323.50	659.00
17603-5.FIN2	Dol 2	0.04	0.51	0.80	3.14	3.76	324.00	667.00
17603-4.FIN2	Dol 2	0.04	1.19	1.55	3.58	3.95	309.20	1145.00
17603-3.FIN2	Cal 4	-	-	0.09	0.06	3.22	1541.00	101.00
17603-2.FIN2	Cal 4	-	0.34	0.34	0.17	3.32	1722.00	190.00
17603-1.FIN2	Cal 4	-	0.45	0.29	0.22	3.59	1645.00	420.00
12384-12.FIN2	Dol 1	40.80	12730.00	12560.00	421.00	227.00	876.00	52100.00
12384-11.FIN2	Dol 1	92.10	41200.00	41500.00	1126.00	612.00	910.00	127900.00
12384-10.FIN2	Dol 1	45.80	20400.00	20200.00	547.00	295.00	574.00	66300.00
12384-9.FIN2	Dol 1	44.70	14300.00	14600.00	485.00	261.00	850.00	60600.00
12384-8.FIN2	Dol 1	33.80	12900.00	12800.00	398.00	218.00	513.00	46600.00
12384-7.FIN2	Dol 1	88.90	27800.00	27500.00	944.00	504.00	1221.00	127600.00
12384-6.FIN2	Dol 1	105.40	49300.00	49000.00	1250.00	695.00	1269.00	151000.00
12384-5.FIN2	Dol 1	100.20	43600.00	44400.00	1114.00	646.00	1092.00	105000.00

LA-ICP-MS data for calcite and dolomite. Values are in ppm. Data below detection limit are indicated by (-) and other deleted data are indicated by an "X".

Sample	Phase	⁵⁹ Co	⁶⁰ Ni	⁶¹ Ni	⁶⁵ Cu	⁶⁶ Zn	⁷⁵ As	⁸⁵ Rb	⁸⁸ Sr
13805-17	Cal 4	-	0.19	1.54	-	-	0.39	-	160.30
13805-16	Cal 4	-	0.22	1.89	-	-	0.27	0.041	136.90
13805-15	Cal 4	-	0.17	1.48	-	-	0.84	0.013	112.50
13805-14	Cal 4	0.01	0.22	1.53	-	0.14	0.47	0.036	203.70
13805-13	Cal 4	0.06	0.17	1.81	-	-	0.37	0.016	106.70
13805-12	Cal 4	0.03	0.17	2.12	-	-	0.27	-	138.70
13805-11	Cal 4	0.06	0.23	2.37	0.45	0.14	3.50	0.13	212.00
13805-10	Dol 2	0.28	2.32	4.31	1.01	10.58	12.80	1.08	206.20
13805-9	Dol 2	0.66	2.91	3.66	2.50	5.60	11.10	2.66	108.20
13805-7	Dol 2	0.71	3.22	4.42	2.85	4.62	13.90	4.04	105.90
13805-6	Dol 2	0.15	1.84	2.55	0.31	4.16	2.80	0.46	79.10
13805-5	Dol 2	0.47	2.08	3.40	2.04	5.21	11.60	1.00	149.50
13805-4	Dol 2	0.12	1.88	2.75	1.16	4.09	6.10	0.70	79.60
13805-3	Dol 2	1.20	4.62	5.80	4.70	4.34	19.70	4.90	107.30
13805-2	Dol 2	0.20	1.99	2.81	1.03	4.73	8.00	1.63	127.30
13805-1	Cal 4	0.03	0.19	1.83	-	0.15	0.61	0.02	169.10
13805-1-1	Cal 4	0.03	0.26	2.12	3.30	0.10	9.80	0.21	114.00
17603-20	Dol 3	-	0.39	1.57	0.48	0.98	103.60	0.02	62.82
17603-19	Dol 3	-	0.75	1.82	0.58	0.85	7700.00	0.18	62.29
17603-18	Dol 3	0.06	0.30	1.44	0.65	0.73	77000.00	0.01	44.22
17603-17	Dol 3	0.09	0.37	1.30	1.33	1.01	-	0.09	51.70
17603-15	Cal 4	-	0.13	1.12	0.54	0.05	29.00	0.03	26.20
17603-14	Cal 4	-	0.13	1.14	0.71	0.04	169.00	0.02	23.56
17603-13	Cal 4	-	0.17	1.44	2.90	0.21	560.00	0.26	32.00
17603-12	Cal 4	-	0.24	1.64	0.86	0.05	50.00	0.02	54.10
17603-11	Dol 2	-	0.15	1.03	0.32	1.01	15.00	0.04	131.00
17603-9.F	Dol 2	-	0.05	0.70	0.28	0.78	4.30	0.13	67.30
17603-8.F	Dol 2	-	0.09	0.80	0.33	0.91	3.60	0.05	55.40
17603-7.F	Dol 2	-	0.07	1.00	0.30	0.63	1.00	0.02	73.40
17603-6.F	Dol 2	-	0.03	0.38	0.25	0.63	0.92	0.03	60.24
17603-5.F	Dol 2	-	0.06	0.27	0.38	0.97	3.70	0.02	57.80
17603-4.F	Dol 2	-	0.11	0.20	0.60	1.50	230.00	0.11	53.47
17603-3.F	Cal 4	-	0.14	1.57	0.26	0.04	7.20	0.03	47.01
17603-2.F	Cal 4	-	0.17	1.47	1.70	0.04	140.00	0.10	79.60
17603-1.F	Cal 4	0.11	0.22	1.50	4.40	0.22	610.00	0.43	49.70
12384-12	Dol 1	8.70	42.40	44.10	30.00	59.50	325.00	640.00	565.00
12384-11	Dol 1	16.20	108.70	122.00	63.20	128.90	871.00	1740.00	755.00
12384-10	Dol 1	9.60	56.00	50.10	42.40	65.40	447.00	880.00	508.00
12384-9.F	Dol 1	8.81	50.30	50.40	37.30	61.30	398.00	748.00	584.00
12384-8.F	Dol 1	6.40	37.50	47.90	37.00	74.00	323.00	620.00	541.00
12384-7.F	Dol 1	16.00	98.90	100.00	85.00	116.30	679.00	1440.00	478.00
12384-6.F	Dol 1	19.70	129.00	146.00	65.00	156.00	902.00	1960.00	580.00
12384-5.F	Dol 1	18.50	104.00	111.00	51.00	130.00	707.00	1780.00	674.00

LA-ICP-MS data for calcite and dolomite. Values are in ppm. Data below detection limit are indicated by (-) and other deleted data are indicated by an "X".

Sample ID	Phase	⁸⁹ Y	⁹⁰ Zr	⁹⁵ Mo	⁹⁸ Mo	¹⁰⁷ Ag	¹⁰⁹ Ag	¹¹¹ Cd
13805-17	Cal 4	6.84	0.09	-	-	-	-	-
13805-16	Cal 4	4.41	0.24	-	-	-	-	-
13805-15	Cal 4	0.31	0.11	-	-	-	-	-
13805-14	Cal 4	2.55	0.24	0.11	0.01	-	-	-
13805-13	Cal 4	6.92	0.13	0.02	-	-	-	-
13805-12	Cal 4	1.06	0.10	-	-	-	-	-
13805-11	Cal 4	0.26	0.15	-	-	-	-	-
13805-10	Dol 2	9.74	0.86	0.11	0.09	0.02	-	-
13805-9	Dol 2	4.71	1.44	1.20	1.50	-	-	-
13805-7	Dol 2	2.93	3.01	0.60	0.65	0.01	0.01	-
13805-6	Dol 2	2.16	0.51	0.06	0.03	-	-	-
13805-5	Dol 2	4.33	0.51	0.15	0.10	-	0.01	0.01
13805-4	Dol 2	2.81	0.56	0.08	0.04	0.01	-	0.01
13805-3	Dol 2	2.92	2.36	0.36	0.38	0.01	0.01	0.01
13805-2	Dol 2	4.60	0.69	0.06	0.04	-	0.01	0.01
13805-1	Cal 4	0.42	0.16	-	-	-	-	-
13805-1-1	Cal 4	0.44	0.11	-	-	-	-	-
17603-20.FIN2	Dol 3	2.86	0.22	0.07	0.01	-	-	0.01
17603-19.FIN2	Dol 3	2.91	0.25	0.08	0.03	-	-	0.01
17603-18.FIN2	Dol 3	1.59	0.38	0.05	0.01	0.01	-	0.02
17603-17.FIN2	Dol 3	2.84	0.38	0.07	0.02	0.01	-	0.03
17603-15.FIN2	Cal 4	9.18	4.56	0.10	-	0.01	-	0.01
17603-14.FIN2	Cal 4	5.79	2.23	0.08	0.01	-	-	-
17603-13.FIN2	Cal 4	3.29	0.79	0.12	0.01	-	-	-
17603-12.FIN2	Cal 4	0.16	0.04	0.07	0.02	-	-	-
17603-11.FIN2	Dol 2	2.15	0.02	0.02	0.01	-	-	0.01
17603-9.FIN2	Dol 2	1.85	0.06	0.01	-	-	-	0.01
17603-8.FIN2	Dol 2	1.68	0.03	0.02	-	-	-	0.01
17603-7.FIN2	Dol 2	1.78	0.04	-	-	-	-	-
17603-6.FIN2	Dol 2	2.32	0.02	0.01	-	-	-	0.01
17603-5.FIN2	Dol 2	2.67	0.04	0.01	-	0.01	-	0.01
17603-4.FIN2	Dol 2	2.69	0.06	0.01	0.01	-	-	0.01
17603-3.FIN2	Cal 4	0.05	0.05	0.05	0.00	-	-	0.01
17603-2.FIN2	Cal 4	0.02	0.05	0.05	0.00	-	-	0.01
17603-1.FIN2	Cal 4	0.08	0.11	0.08	0.01	0.01	-	0.01
12384-12.FIN2	Dol 1	44.80	337.00	0.73	0.73	0.06	0.07	0.15
12384-11.FIN2	Dol 1	94.20	899.00	1.47	1.29	0.12	0.13	0.47
12384-10.FIN2	Dol 1	89.00	443.00	0.64	0.63	-	-	0.13
12384-9.FIN2	Dol 1	71.10	500.00	0.71	0.59	0.09	-	0.15
12384-8.FIN2	Dol 1	34.10	300.00	-	0.41	0.05	-	0.11
12384-7.FIN2	Dol 1	81.80	810.00	1.10	1.09	0.19	0.09	0.27
12384-6.FIN2	Dol 1	130.00	1320.00	2.01	1.76	0.18	0.14	0.45
12384-5.FIN2	Dol 1	96.10	999.00	1.56	1.70	0.13	0.09	0.25

LA-ICP-MS data for calcite and dolomite. Values are in ppm. Data below detection limit are indicated by (-) and other deleted data are indicated by an "X".

Sample	Phase	¹¹⁴ Cd	¹²¹ Sb	¹²³ Sb	¹³⁷ Ba	¹³⁹ La	¹⁴⁰ Ce	¹⁴¹ Pr	¹⁴⁶ Nd
-		-							
13805-17	Cal 4	0.01	-	-	1.09	1.09	3.70	0.77	4.57
13805-16	Cal 4	-	-	0.01	3.60	1.74	3.52	0.59	3.47
13805-15	Cal 4	-	-	-	0.44	0.04	0.16	0.03	0.20
13805-14	Cal 4	-	-	0.010	7.04	1.74	3.38	0.53	2.57
13805-13	Cal 4	-	0.01	-	2.29	1.46	3.32	0.63	3.60
13805-12	Cal 4	-	-	-	0.70	0.09	0.44	0.11	0.72
13805-11	Cal 4	-	-	-	0.89	0.04	0.13	0.03	0.14
13805-10	Dol 2	0.02	0.04	0.04	15.80	10.27	30.22	4.19	17.81
13805-9	Dol 2	0.02	0.08	0.08	9.52	5.67	15.36	2.14	9.07
13805-7	Dol 2	0.02	0.08	0.10	12.99	3.46	8.03	1.10	4.58
13805-6	Dol 2	0.01	-	0.02	5.57	2.79	6.29	0.81	3.37
13805-5	Dol 2	0.01	0.03	0.03	10.14	4.42	12.89	1.79	7.62
13805-4	Dol 2	0.01	0.02	-	3.57	2.98	6.93	0.96	4.13
13805-3	Dol 2	0.01	0.09	0.08	18.00	3.00	7.18	1.03	4.37
13805-2	Dol 2	0.01	0.03	0.03	5.97	4.39	12.00	1.67	7.21
13805-1	Cal 4	-	-	-	0.38	0.05	0.17	0.03	0.15
13805-1-1	Cal 4	-	-	-	0.80	0.06	0.26	0.05	0.35
17603-20.	Dol 3	0.01	1.27	1.21	7.38	2.86	6.39	0.81	3.28
17603-19.	Dol 3	0.01	7.90	7.50	7.17	2.86	6.28	0.79	3.20
17603-18.	Dol 3	0.01	75.00	73.00	6.06	1.32	2.81	0.36	1.52
17603-17.	Dol 3	0.03	185.00	178.00	5.52	2.86	6.01	0.77	3.23
17603-15.	Cal 4	-	0.21	0.25	0.53	1.54	3.70	0.60	2.99
17603-14.	Cal 4	-	0.41	0.33	0.38	0.18	0.62	0.12	0.68
17603-13.	Cal 4	-	0.62	1.22	2.20	0.11	0.41	0.08	0.43
17603-12.	Cal 4	-	0.18	0.15	0.51	0.01	0.08	0.00	0.02
17603-11.	Dol 2	-	0.08	0.04	1.89	2.86	4.97	0.58	2.35
17603-9.F	Dol 2	-	0.08	0.08	4.07	2.22	3.99	0.48	1.95
17603-8.F	Dol 2	0.01	0.08	0.07	3.13	2.52	4.29	0.51	2.04
17603-7.F	Dol 2	0.01	0.04	0.05	3.76	2.16	4.08	0.48	2.03
17603-6.F	Dol 2	-	0.03	0.03	3.06	2.95	5.73	0.68	2.70
17603-5.F	Dol 2	0.01	0.13	0.14	3.39	2.52	5.08	0.63	2.63
17603-4.F	Dol 2	0.01	0.21	0.13	8.90	2.67	5.46	0.70	2.87
17603-3.F	Cal 4	-	0.06	0.03	0.48	-	0.01	-	-
17603-2.F	Cal 4	0.01	0.24	0.27	1.06	0.01	0.02	-	0.01
17603-1.F	Cal 4	0.01	1.14	0.68	1.23	0.01	0.07	0.00	0.01
12384-12.	Dol 1	0.47	0.81	0.53	1185.00	124.00	227.00	24.00	84.60
12384-11.	Dol 1	0.96	2.43	2.05	3220.00	339.00	577.00	55.70	178.00
12384-10.	Dol 1	0.57	0.75	0.73	1570.00	X	461.00	51.10	190.00
12384-9.F	Dol 1	0.53	0.45	0.58	1460.00	129.00	253.00	27.30	108.00
12384-8.F	Dol 1	0.48	0.39	0.67	1200.00	144.00	261.00	24.40	79.00
12384-7.F	Dol 1	0.95	1.61	2.25	2630.00	399.00	680.00	62.30	187.00
12384-6.F	Dol 1	1.37	2.74	4.23	3480.00	393.00	705.00	68.50	227.00
12384-5.F	Dol 1	1.15	1.88	2.65	3970.00	399.00	676.00	62.40	198.00

LA-ICP-MS data for calcite and dolomite. Values are in ppm. Data below detection limit are indicated by (-) and other deleted data are indicated by an "X".

Sample ID	Phase	¹⁴⁷ Sm	¹⁵³ Eu	¹⁵⁷ Gd	¹⁵⁹ Tb	¹⁶³ Dy	¹⁶⁵ Ho	¹⁶⁶ Er
13805-17	Cal 4	1.62	0.43	1.65	0.19	1.15	0.20	0.42
13805-16	Cal 4	1.09	0.34	1.29	0.12	0.62	0.09	0.14
13805-15	Cal 4	0.05	0.02	0.04	0.01	0.03	0.01	0.02
13805-14	Cal 4	0.67	0.17	0.65	0.08	0.42	0.07	0.14
13805-13	Cal 4	1.33	0.36	1.64	0.20	1.04	0.15	0.33
13805-12	Cal 4	0.23	0.06	0.18	0.03	0.18	0.03	0.07
13805-11	Cal 4	0.04	0.01	0.04	-	0.02	0.01	0.01
13805-10	Dol 2	3.01	0.48	2.39	0.30	1.56	0.29	0.60
13805-9	Dol 2	1.46	0.24	1.21	0.14	0.76	0.13	0.31
13805-7	Dol 2	0.85	0.15	0.66	0.08	0.42	0.08	0.18
13805-6	Dol 2	0.59	0.10	0.53	0.06	0.34	0.06	0.14
13805-5	Dol 2	1.30	0.22	1.03	0.12	0.69	0.12	0.27
13805-4	Dol 2	0.71	0.13	0.63	0.07	0.44	0.08	0.18
13805-3	Dol 2	0.82	0.12	0.70	0.08	0.45	0.08	0.19
13805-2	Dol 2	1.21	0.20	1.04	0.12	0.67	0.11	0.27
13805-1	Cal 4	0.05	0.02	0.06	0.01	0.04	0.01	0.02
13805-1-1	Cal 4	0.09	0.03	0.07	0.01	0.06	0.01	0.03
17603-20.FIN2	Dol 3	0.61	0.10	0.49	0.07	0.50	0.10	0.27
17603-19.FIN2	Dol 3	0.63	0.07	0.51	0.07	0.51	0.10	0.28
17603-18.FIN2	Dol 3	0.31	0.07	0.26	0.04	0.24	0.05	0.13
17603-17.FIN2	Dol 3	0.55	0.12	0.46	0.06	0.44	0.09	0.23
17603-15.FIN2	Cal 4	0.96	0.22	1.22	0.23	1.57	0.33	0.97
17603-14.FIN2	Cal 4	0.31	0.09	0.54	0.12	0.90	0.20	0.64
17603-13.FIN2	Cal 4	0.19	0.06	0.33	0.07	0.52	0.12	0.39
17603-12.FIN2	Cal 4	0.01	0.01	0.02	-	0.02	0.01	0.01
17603-11.FIN2	Dol 2	0.41	0.08	0.39	0.05	0.28	0.05	0.15
17603-9.FIN2	Dol 2	0.34	0.07	0.33	0.04	0.28	0.06	0.16
17603-8.FIN2	Dol 2	0.35	0.08	0.32	0.04	0.28	0.06	0.13
17603-7.FIN2	Dol 2	0.32	0.07	0.35	0.04	0.27	0.05	0.14
17603-6.FIN2	Dol 2	0.41	0.08	0.43	0.06	0.37	0.07	0.19
17603-5.FIN2	Dol 2	0.49	0.10	0.48	0.07	0.43	0.08	0.23
17603-4.FIN2	Dol 2	0.50	0.10	0.49	0.07	0.43	0.08	0.21
17603-3.FIN2	Cal 4	-	-	-	-	-	-	-
17603-2.FIN2	Cal 4	-	-	-	-	-	-	-
17603-1.FIN2	Cal 4	0.01	0.01	0.01	-	0.02	-	0.01
12384-12.FIN2	Dol 1	14.10	2.38	8.90	1.31	9.08	1.77	5.66
12384-11.FIN2	Dol 1	23.50	3.82	15.10	2.24	16.30	3.70	12.20
12384-10.FIN2	Dol 1	34.60	6.15	24.70	3.23	20.00	3.31	8.50
12384-9.FIN2	Dol 1	18.30	3.53	14.90	2.06	13.20	2.64	7.49
12384-8.FIN2	Dol 1	9.40	1.41	5.24	0.79	6.42	1.35	4.45
12384-7.FIN2	Dol 1	22.80	3.76	12.30	2.04	14.70	3.27	10.40
12384-6.FIN2	Dol 1	32.40	5.17	19.70	3.29	21.90	4.99	15.80
12384-5.FIN2	Dol 1	22.50	3.74	14.30	2.08	16.90	3.83	13.30

LA-ICP-MS data for calcite and dolomite. Values are in ppm. Data below detection limit are indicated by (-) and other deleted data are indicated by an "X".

Sample	Phase	¹⁶⁹ Tm	¹⁷² Yb	¹⁷⁵ Lu	¹⁹⁷ Au	²⁰⁵ Tl	²⁰⁷ Pb	²⁰⁹ Bi	²³² Th	²³⁸ U
13805-17	Cal 4	0.04	0.18	0.02	-	-	0.03	-	0.06	1.88
13805-16	Cal 4	0.01	0.04	-	-	-	0.00	-	0.01	0.57
13805-15	Cal 4	-	0.02	-	-	-	0.01	-	-	0.03
13805-14	Cal 4	0.01	0.07	0.01	-	-	0.02	-	0.08	1.74
13805-13	Cal 4	0.03	0.12	0.01	-	-	0.01	-	0.03	0.73
13805-12	Cal 4	0.01	0.05	0.01	-	-	0.03	-	0.03	0.38
13805-11	Cal 4	-	-	-	-	-	0.14	-	-	0.04
13805-10	Dol 2	0.07	0.34	0.05	-	0.03	0.45	-	0.74	3.43
13805-9	Dol 2	0.03	0.18	0.03	0.02	0.22	1.91	0.01	0.40	4.06
13805-7	Dol 2	0.02	0.10	0.01	0.04	0.26	1.79	0.01	0.32	7.52
13805-6	Dol 2	0.02	0.06	0.01	-	0.02	0.14	-	0.09	1.48
13805-5	Dol 2	0.03	0.15	0.02	-	0.04	0.61	-	0.15	1.99
13805-4	Dol 2	0.02	0.09	0.01	-	0.01	0.16	-	0.10	1.55
13805-3	Dol 2	0.02	0.10	0.01	0.01	0.22	2.00	0.01	0.26	5.33
13805-2	Dol 2	0.03	0.13	0.02	-	0.03	0.29	-	0.19	1.82
13805-1	Cal 4	-	0.01	-	-	-	0.06	-	0.02	0.20
13805-1-1	Cal 4	-	0.01	-	-	-	0.05	-	-	0.16
17603-20	Dol 3	0.03	0.21	0.03	1.75	0.03	0.70	-	0.14	2.59
17603-19	Dol 3	0.04	0.22	0.03	7.50	0.26	1.27	-	0.15	2.50
17603-18	Dol 3	0.02	0.08	0.01	3.90	0.26	0.37	-	0.03	1.72
17603-17	Dol 3	0.03	0.18	0.03	6.40	0.54	0.54	0.01	0.07	2.06
17603-15	Cal 4	0.13	0.94	0.14	2.00	0.31	0.43	-	0.17	6.80
17603-14	Cal 4	0.11	0.77	0.13	1.20	0.09	0.08	-	0.08	3.95
17603-13	Cal 4	0.06	0.48	0.08	8.40	0.13	0.49	-	0.03	2.69
17603-12	Cal 4	-	0.00	-	2.50	0.07	0.62	-	-	0.04
17603-11	Dol 2	0.02	0.09	0.01	0.08	0.02	0.06	-	0.01	0.09
17603-9.F	Dol 2	0.02	0.11	0.02	0.01	0.03	0.04	-	0.01	0.06
17603-8.F	Dol 2	0.01	0.10	0.01	0.02	0.05	0.31	-	0.01	0.09
17603-7.F	Dol 2	0.02	0.11	0.01	0.02	0.02	0.11	-	0.01	0.18
17603-6.F	Dol 2	0.02	0.14	0.02	-	0.02	0.13	-	0.01	0.07
17603-5.F	Dol 2	0.02	0.14	0.02	0.03	0.03	0.52	-	0.02	0.13
17603-4.F	Dol 2	0.03	0.16	0.02	2.40	0.11	0.22	-	0.01	0.09
17603-3.F	Cal 4	-	-	-	0.08	0.04	0.11	-	-	0.27
17603-2.F	Cal 4	-	-	-	2.00	0.05	0.17	-	-	0.14
17603-1.F	Cal 4	-	-	-	8.50	0.23	0.23	-	-	0.26
12384-12	Dol 1	0.77	5.87	0.80	0.63	3.12	8.78	0.14	42.40	18.80
12384-11	Dol 1	1.91	13.50	2.01	1.42	9.40	23.70	0.33	76.30	43.80
12384-10	Dol 1	1.23	7.70	0.98	0.92	4.44	9.60	0.12	103.00	25.80
12384-9.F	Dol 1	1.05	7.44	1.04	0.78	3.45	9.23	0.15	60.90	25.90
12384-8.F	Dol 1	0.67	5.31	0.79	0.69	2.95	7.70	0.07	27.50	16.30
12384-7.F	Dol 1	1.75	12.40	1.65	1.58	6.89	16.40	0.18	69.50	39.10
12384-6.F	Dol 1	2.52	18.30	2.72	3.43	8.90	18.90	0.16	108.00	49.00
12384-5.F	Dol 1	1.99	14.90	2.15	3.36	7.69	16.90	0.12	83.00	46.70

LA-ICP-MS data for calcite and dolomite. Values are in ppm. Data below detection limit are indicated by (-) and other deleted data are indicated by an "X".

Sample ID	Phase	⁴⁵ Sc	⁴⁷ Ti	⁴⁹ Ti	⁵¹ V	⁵² Cr	⁵⁵ Mn	⁵⁷ Fe
12384-4.FIN2	Dol 1	131.00	60800.00	61500.00	1560.00	950.00	1381.00	144000.00
12384-3.FIN2	Dol 1	82.00	34900.00	35400.00	900.00	525.00	891.00	79700.00
12384-2.FIN2	Host Rct	8.41	5.40	3.74	0.86	3.93	397.00	1419.00
12384-1.FIN2	Dol 1	119.00	43600.00	43300.00	1200.00	681.00	1008.00	X
4337-14.FIN2	Dol 1	11.27	2540.00	2530.00	80.80	48.20	545.00	33500.00
4337-13.FIN2	Host Rct	6.85	20.10	18.90	3.19	6.32	915.00	4780.00
4337-12.FIN2	Dol 1	20.06	6130.00	5980.00	172.50	96.60	731.00	56700.00
4337-11.FIN2	Dol 1	13.45	2690.00	2700.00	77.80	51.40	589.00	43000.00
4337-10.FIN2	Host Rct	0.36	8.60	5.40	2.51	3.39	567.20	13260.00
4337-9.FIN2	Dol 1	15.96	5430.00	5300.00	153.90	91.50	527.00	42400.00
4337-8.FIN2	Dol 1	15.21	4670.00	4540.00	136.70	85.40	528.00	40500.00
4337-7.FIN2	Dol 1	11.22	3670.00	3610.00	89.00	52.00	424.00	28800.00
4337-6.FIN2	Dol 1	10.70	2760.00	2730.00	87.60	51.90	452.60	30630.00
4337-5.FIN2	Dol 1	12.64	2750.00	2720.00	96.50	54.20	542.00	39900.00
4337-4.FIN2	Dol 1	15.58	5320.00	5200.00	143.80	83.10	455.00	38900.00
4337-3.FIN2	Dol 1	15.92	5990.00	5920.00	147.00	87.50	508.00	40640.00
4337-2.FIN2	Host Rct	0.41	7.70	7.70	1.94	3.83	54.90	2350.00
4337-1.FIN2	Host Rct	0.43	12.50	13.00	2.15	3.83	61.80	2050.00
34297-19.FIN2	Dol 3	0.98	2.30	2.76	3.76	4.76	676.00	4397.00
34297-18.FIN2	Dol 3	0.07	1.07	1.18	0.92	3.40	473.20	1541.00
34297-17.FIN2	Dol 3	0.88	1.36	1.61	2.45	3.96	613.00	2070.00
34297-15.FIN2	Dol 3	0.41	1.14	1.68	1.18	4.12	556.00	2020.00
34297-14.FIN2	Dol 3	0.08	2.65	2.86	0.85	4.00	750.00	7600.00
34297-13.FIN2	Dol 3	0.09	1.04	1.48	0.64	3.96	525.00	2680.00
34297-12.FIN2	Dol 3	0.52	1.89	2.13	1.64	3.93	649.00	4100.00
34297-11.FIN2	Dol 3	0.24	1.34	1.32	1.64	3.71	706.00	10100.00
34297-10.FIN2	Dol 3	0.06	1.25	1.26	0.56	3.46	515.00	1666.00
34297-9.FIN2	Dol 3	0.03	0.98	1.17	0.81	3.83	604.80	5010.00
34297-8.FIN2	Dol 3	0.02	0.85	1.12	0.89	4.05	558.30	1858.00
34297-7.FIN2	Dol 3	0.24	2.46	2.80	1.51	3.83	774.00	7047.00
34297-6.FIN2	Dol 3	0.40	2.40	2.66	1.60	3.93	779.60	7113.00
34297-5.FIN2	Dol 3	0.42	2.57	2.72	1.92	3.92	756.00	6879.00
34297-4.FIN2	Dol 3	0.33	2.26	2.62	1.66	4.06	736.70	7340.00
34297-3.FIN2	Dol 3	0.66	2.93	3.15	2.76	4.01	728.30	6703.00
34297-2.FIN2	Dol 3	0.26	2.60	2.86	1.42	3.53	708.00	6198.00
34297-1.FIN2	Dol 3	0.50	3.57	3.79	2.17	4.00	723.00	6990.00
7308-1.FIN2	Dol 1	74.80	31500.00	30700.00	848.00	640.00	858.00	123900.00
7308-2.FIN2	Dol 1	55.60	22900.00	22000.00	531.00	402.00	728.60	88500.00
7308-3.FIN2	Dol 1	68.50	36200.00	34600.00	748.00	820.00	807.00	105400.00
7309-4.FIN2	Dol 1	46.70	16900.00	16500.00	449.00	361.00	739.00	86800.00
7308-5.FIN2	Dol 1	67.10	28200.00	28100.00	741.00	543.00	775.00	99610.00
7308-6.FIN2	Dol 1	37.40	13500.00	13700.00	363.00	317.00	572.00	61100.00
7308-7.FIN2	Dol 1	26.10	9020.00	8710.00	216.00	169.00	491.00	43100.00
7308-8.FIN2	Dol 1	32.50	13300.00	13700.00	244.00	192.00	565.00	47500.00

LA-ICP-MS data for calcite and dolomite. Values are in ppm. Data below detection limit are indicated by (-) and other deleted data are indicated by an "X".

Sample ID Phase	⁵⁹ Co	⁶⁰ Ni	⁶¹ Ni	⁶⁵ Cu	⁶⁶ Zn	⁷⁵ As	⁸⁵ Rb	⁸⁸ Sr
12384-4.F Dol 1	24.50	147.00	128.00	102.00	176.00	1090.00	2630.00	794.00
12384-3.F Dol 1	14.60	85.70	88.00	63.00	105.00	666.00	1400.00	538.00
12384-2.F Host Rocl	0.53	0.53	0.99	24.30	1.37	26.30	0.69	287.00
12384-1.F Dol 1	X	X	X	X	X	X	1780.00	556.00
4337-14.F Dol 1	9.37	18.51	19.00	8.90	22.30	14.20	106.30	760.00
4337-13.F Host Rocl	0.67	1.89	2.74	1.83	3.94	4.30	X	1050.00
4337-12.F Dol 1	13.12	32.10	33.70	14.60	50.30	30.20	240.00	759.00
4337-11.F Dol 1	8.81	19.60	19.30	26.10	46.00	80.00	89.80	1257.00
4337-10.F Host Rocl	0.30	X	-	17.90	2.87	69.00	X	356.00
4337-9.FI Dol 1	16.03	32.80	34.00	17.30	44.00	23.00	221.00	689.00
4337-8.FI Dol 1	15.06	30.00	32.60	24.00	44.50	26.10	189.50	683.00
4337-7.FI Dol 1	9.30	21.06	21.80	10.80	29.60	14.70	124.70	842.00
4337-6.FI Dol 1	10.28	20.74	22.60	14.90	28.07	32.60	119.80	765.00
4337-5.FI Dol 1	13.42	24.40	23.90	19.20	44.70	36.20	133.20	730.00
4337-4.FI Dol 1	13.15	28.93	31.00	12.50	43.50	26.50	215.40	595.00
4337-3.FI Dol 1	12.65	29.53	30.70	10.90	46.80	18.60	208.40	542.00
4337-2.FI Host Rocl	3.42	2.83	3.59	9.20	2.07	12.20	0.78	2346.00
4337-1.FI Host Rocl	5.95	4.03	4.69	11.00	3.11	28.30	X	2338.00
34297-19. Dol 3	0.00	0.54	1.04	0.52	4.07	94.00	0.02	139.60
34297-18. Dol 3	-	0.14	0.82	1.16	3.27	5.60	0.07	43.91
34297-17. Dol 3	-	0.15	0.61	3.20	2.78	5.47	0.07	56.37
34297-15. Dol 3	0.05	0.25	1.20	0.88	1.28	11.20	0.03	92.50
34297-14. Dol 3	-	0.29	1.22	0.65	4.38	8.40	0.04	49.53
34297-13. Dol 3	0.09	0.26	0.91	1.83	2.35	14.40	0.08	51.99
34297-12. Dol 3	0.07	0.32	1.00	0.56	2.89	12.00	0.01	59.90
34297-11. Dol 3	0.23	0.52	1.20	0.33	5.93	41.90	0.02	85.00
34297-10. Dol 3	-	0.19	0.74	1.86	1.94	7.10	0.10	54.80
34297-9.F Dol 3	0.07	0.54	1.93	0.29	3.10	54.30	0.01	71.40
34297-8.F Dol 3	0.17	0.67	1.59	0.32	1.57	66.10	0.01	101.20
34297-7.F Dol 3	-	0.26	1.21	0.57	1.09	6.25	0.10	62.23
34297-6.F Dol 3	-	0.17	0.63	0.31	0.99	3.66	0.02	63.30
34297-5.F Dol 3	-	0.21	0.98	0.27	1.04	3.45	0.03	67.70
34297-4.F Dol 3	-	0.26	1.12	0.33	1.28	2.50	0.01	83.70
34297-3.F Dol 3	0.07	0.36	1.48	0.57	1.23	3.76	0.12	96.30
34297-2.F Dol 3	0.09	0.29	1.09	1.37	1.17	7.80	0.09	85.50
34297-1.F Dol 3	0.20	0.59	1.60	10.10	1.49	57.00	0.41	76.60
7308-1.FI Dol 1	19.70	110.40	112.00	770.00	116.60	X	1456.00	1270.00
7308-2.FI Dol 1	7.95	70.60	73.50	95.00	71.70	147.40	932.00	1070.00
7308-3.FI Dol 1	35.40	125.00	126.00	134.00	105.60	197.30	1308.00	1322.00
7309-4.FI Dol 1	13.80	87.20	80.90	X	78.50	134.00	826.00	1068.00
7308-5.FI Dol 1	15.00	102.00	111.60	294.00	95.60	391.00	1291.00	1267.00
7308-6.FI Dol 1	9.90	59.90	49.90	X	52.60	137.00	592.00	1028.00
7308-7.FI Dol 1	13.80	61.00	60.00	X	36.40	69.50	387.00	832.00
7308-8.FI Dol 1	4.89	34.60	34.80	158.00	37.80	60.40	363.00	742.00

LA-ICP-MS data for calcite and dolomite. Values are in ppm. Data below detection limit are indicated by (-) and other deleted data are indicated by an "X".

Sample ID	Phase	⁸⁹ Y	⁹⁰ Zr	⁹⁵ Mo	⁹⁸ Mo	¹⁰⁷ Ag	¹⁰⁹ Ag	¹¹¹ Cd
12384-4.FIN2	Dol 1	126.00	1300.00	2.04	1.88	0.14	0.10	0.35
12384-3.FIN2	Dol 1	100.00	780.00	0.88	1.01	0.15	0.05	0.21
12384-2.FIN2	Host R	6.32	0.82	0.02	0.01	0.01	0.01	0.04
12384-1.FIN2	Dol 1	193.00	NA	4.80	5.40	NA	NA	0.56
4337-14.FIN2	Dol 1	15.51	62.00	0.56	0.48	0.08	0.08	0.06
4337-13.FIN2	Host R	11.51	X	0.10	0.08	-	-	0.09
4337-12.FIN2	Dol 1	25.02	126.50	0.65	0.65	0.13	0.14	0.09
4337-11.FIN2	Dol 1	17.46	56.50	3.44	2.74	0.19	0.17	0.06
4337-10.FIN2	Host R	43.10	X	2.19	2.00	0.03	0.04	0.04
4337-9.FIN2	Dol 1	22.80	115.30	0.49	0.48	0.10	0.12	0.08
4337-8.FIN2	Dol 1	23.90	185.00	0.42	0.44	0.14	0.13	0.06
4337-7.FIN2	Dol 1	17.35	67.60	0.33	0.30	0.06	0.05	0.05
4337-6.FIN2	Dol 1	16.42	62.50	0.36	0.36	0.10	0.09	0.05
4337-5.FIN2	Dol 1	17.20	70.20	0.46	0.43	0.11	0.14	0.07
4337-4.FIN2	Dol 1	23.19	112.20	0.39	0.39	0.09	0.11	0.06
4337-3.FIN2	Dol 1	23.52	135.00	0.43	0.37	0.06	0.06	0.08
4337-2.FIN2	Host R	2.92	X	0.04	0.05	0.01	0.02	0.03
4337-1.FIN2	Host R	2.71	X	0.14	0.16	0.04	0.05	0.04
34297-19.FIN2	Dol 3	5.32	0.21	0.04	0.01	-	-	-
34297-18.FIN2	Dol 3	2.84	0.06	0.02	-	-	-	0.01
34297-17.FIN2	Dol 3	6.22	0.06	0.03	0.01	-	-	-
34297-15.FIN2	Dol 3	3.55	0.12	0.05	0.02	-	-	-
34297-14.FIN2	Dol 3	2.56	0.07	0.03	0.01	-	-	-
34297-13.FIN2	Dol 3	3.45	0.23	0.03	0.02	-	-	-
34297-12.FIN2	Dol 3	3.61	0.05	0.02	-	-	-	0.01
34297-11.FIN2	Dol 3	4.09	0.11	0.02	-	-	-	-
34297-10.FIN2	Dol 3	3.58	0.07	0.02	-	-	-	0.01
34297-9.FIN2	Dol 3	3.50	0.11	0.03	-	-	-	-
34297-8.FIN2	Dol 3	3.44	0.24	0.02	0.01	-	-	-
34297-7.FIN2	Dol 3	4.32	0.12	0.04	-	-	-	0.01
34297-6.FIN2	Dol 3	5.34	0.02	0.04	-	-	-	-
34297-5.FIN2	Dol 3	3.83	0.06	0.02	-	-	-	0.01
34297-4.FIN2	Dol 3	3.37	0.06	0.04	0.01	-	-	-
34297-3.FIN2	Dol 3	4.49	0.11	0.03	0.01	-	-	-
34297-2.FIN2	Dol 3	4.69	0.09	0.02	0.00	-	-	-
34297-1.FIN2	Dol 3	4.36	0.17	0.03	0.01	-	0.01	-
7308-1.FIN2	Dol 1	63.60	560.00	1.24	1.13	0.25	0.26	0.23
7308-2.FIN2	Dol 1	56.30	472.00	1.04	0.68	-	-	0.12
7308-3.FIN2	Dol 1	67.80	594.00	1.13	1.08	-	-	0.10
7309-4.FIN2	Dol 1	45.40	273.00	0.75	0.69	0.20	-	0.09
7308-5.FIN2	Dol 1	66.20	545.00	1.01	0.94	-	-	0.18
7308-6.FIN2	Dol 1	51.00	380.00	0.33	0.45	0.09	-	0.15
7308-7.FIN2	Dol 1	32.80	176.00	0.83	0.90	0.08	-	0.12
7308-8.FIN2	Dol 1	31.50	167.00	0.46	0.43	-	-	0.10

LA-ICP-MS data for calcite and dolomite. Values are in ppm. Data below detection limit are indicated by (-) and other deleted data are indicated by an "X".

Sample ID	Phase	¹⁴⁷ Sm	¹⁵³ Eu	¹⁵⁷ Gd	¹⁵⁹ Tb	¹⁶³ Dy	¹⁶⁵ Ho	¹⁶⁶ Er
12384-4.FIN2	Dol 1	35.80	4.94	20.60	2.73	20.80	4.62	15.70
12384-3.FIN2	Dol 1	30.50	5.10	20.70	2.71	18.00	3.71	11.10
12384-2.FIN2	Host Rct	1.56	0.30	1.18	0.19	1.21	0.22	0.61
12384-1.FIN2	Dol 1	25.90	4.66	18.70	3.46	28.70	7.00	27.30
4337-14.FIN2	Dol 1	3.73	0.64	2.71	0.40	2.68	0.52	1.46
4337-13.FIN2	Host Rct	2.56	0.49	2.11	0.32	2.08	0.41	1.07
4337-12.FIN2	Dol 1	7.25	1.20	4.84	0.67	4.47	0.88	2.55
4337-11.FIN2	Dol 1	4.17	0.79	3.26	0.49	3.12	0.59	1.67
4337-10.FIN2	Host Rct	11.87	2.15	9.55	1.31	7.55	1.23	2.86
4337-9.FIN2	Dol 1	5.94	1.10	4.24	0.62	3.97	0.79	2.44
4337-8.FIN2	Dol 1	5.43	1.05	3.74	0.59	4.25	0.86	2.55
4337-7.FIN2	Dol 1	4.64	0.82	3.26	0.48	3.19	0.59	1.75
4337-6.FIN2	Dol 1	4.33	0.79	3.22	0.47	3.02	0.57	1.63
4337-5.FIN2	Dol 1	4.35	0.83	3.19	0.46	3.15	0.61	1.75
4337-4.FIN2	Dol 1	5.88	1.05	4.32	0.61	4.10	0.81	2.44
4337-3.FIN2	Dol 1	5.47	1.04	4.01	0.60	4.01	0.78	2.35
4337-2.FIN2	Host Rct	0.71	0.12	0.57	0.08	0.53	0.10	0.25
4337-1.FIN2	Host Rct	0.66	0.12	0.55	0.08	0.45	0.09	0.26
34297-19.FIN2	Dol 3	0.74	0.17	0.72	0.11	0.72	0.15	0.47
34297-18.FIN2	Dol 3	0.30	0.07	0.27	0.04	0.32	0.07	0.24
34297-17.FIN2	Dol 3	1.06	0.23	0.94	0.13	0.87	0.18	0.53
34297-15.FIN2	Dol 3	0.38	0.11	0.43	0.06	0.44	0.10	0.30
34297-14.FIN2	Dol 3	0.30	0.08	0.28	0.04	0.34	0.07	0.21
34297-13.FIN2	Dol 3	0.50	0.14	0.47	0.06	0.42	0.08	0.28
34297-12.FIN2	Dol 3	0.43	0.08	0.41	0.06	0.46	0.10	0.32
34297-11.FIN2	Dol 3	0.49	0.10	0.42	0.07	0.49	0.11	0.33
34297-10.FIN2	Dol 3	0.44	0.12	0.42	0.06	0.44	0.09	0.28
34297-9.FIN2	Dol 3	0.38	0.09	0.43	0.06	0.42	0.09	0.29
34297-8.FIN2	Dol 3	0.34	0.08	0.37	0.05	0.41	0.09	0.28
34297-7.FIN2	Dol 3	0.48	0.09	0.51	0.08	0.58	0.12	0.37
34297-6.FIN2	Dol 3	0.50	0.10	0.60	0.10	0.77	0.17	0.49
34297-5.FIN2	Dol 3	0.49	0.09	0.45	0.07	0.54	0.12	0.32
34297-4.FIN2	Dol 3	0.48	0.10	0.46	0.07	0.48	0.10	0.28
34297-3.FIN2	Dol 3	0.63	0.12	0.54	0.09	0.65	0.13	0.41
34297-2.FIN2	Dol 3	0.46	0.09	0.54	0.08	0.64	0.14	0.43
34297-1.FIN2	Dol 3	0.54	0.10	0.53	0.09	0.58	0.14	0.40
7308-1.FIN2	Dol 1	15.80	2.66	11.80	1.64	11.93	2.15	7.37
7308-2.FIN2	Dol 1	14.07	2.41	10.90	1.56	10.79	2.07	6.56
7308-3.FIN2	Dol 1	16.30	2.80	12.25	1.85	12.36	2.45	7.76
7309-4.FIN2	Dol 1	13.90	2.19	9.50	1.39	8.95	1.66	4.89
7308-5.FIN2	Dol 1	16.70	2.91	12.41	1.69	12.38	2.35	7.29
7308-6.FIN2	Dol 1	9.94	1.83	8.11	1.29	9.70	1.78	5.40
7308-7.FIN2	Dol 1	8.80	1.38	6.26	0.87	5.91	1.22	3.47
7308-8.FIN2	Dol 1	8.90	1.53	6.68	0.89	5.74	1.16	3.47

LA-ICP-MS data for calcite and dolomite. Values are in ppm. Data below detection limit are indicated by (-) and other deleted data are indicated by an "X".

Sample ID	Phase	⁴⁵ Sc	⁴⁷ Ti	⁴⁹ Ti	⁵¹ V	⁵² Cr	⁵⁵ Mn	⁵⁷ Fe
7308-9.FIN2	Dol 1	30.90	10230.00	10100.00	279.00	249.30	574.00	61800.00
7308-10.FIN2	Dol 1	27.12	9350.00	9350.00	260.00	211.00	553.00	60900.00
7308-11.FIN2	Dol 1	30.20	10530.00	10370.00	276.00	234.00	578.00	58200.00
7308-12.FIN2	Dol 1	32.40	15600.00	14900.00	303.00	245.60	586.00	76200.00
7308-13.FIN2	Dol 1	14.43	3960.00	3980.00	118.10	95.40	335.30	41800.00
7308-14.FIN2	Dol 1	15.44	4660.00	4720.00	136.60	115.30	339.60	44500.00
7308-15.FIN2	Dol 1	31.90	10630.00	10430.00	297.00	250.00	534.00	81300.00
7308-16.FIN2	Dol 1	23.02	7520.00	7450.00	216.50	192.10	454.00	62500.00
7308-17.FIN2	Dol 1	21.05	6410.00	6240.00	175.50	159.60	415.00	58900.00
7308-18.FIN2	Dol 1	21.34	6810.00	6830.00	173.20	160.20	437.00	62500.00
7308-19.FIN2	Dol 1	9.20	1820.00	1830.00	33.00	32.00	156.00	9000.00
7308-20.FIN2	Dol 1	49.50	18100.00	18000.00	460.00	345.00	619.00	107000.00
7308-21.FIN2	Dol 1	34.93	11200.00	11200.00	306.00	291.00	629.80	102700.00
7308-22.FIN2	Dol 1	58.10	18400.00	18200.00	591.00	512.00	750.00	148900.00
7308-23.FIN2	Dol 1	40.50	15660.00	15860.00	391.00	375.00	645.00	109300.00
7308-24.FIN2	Dol 1	52.10	21800.00	21900.00	495.00	413.00	710.00	128800.00
7308-25.FIN2	Dol 1	50.90	20900.00	20800.00	500.00	381.00	692.00	119100.00
10816-25.FIN2	Dol 1	16.14	5920.00	5810.00	187.50	154.00	739.00	23100.00
10816-24.FIN2	Dol 1	12.18	4690.00	4640.00	151.00	128.40	554.00	28400.00
10816-23.FIN2	Dol 1	12.75	5280.00	5160.00	142.30	126.60	583.00	38600.00
10816-22.FIN2	Dol 1	14.85	5050.00	4950.00	179.70	155.60	643.00	34100.00
10816-21.FIN2	Dol 1	12.75	4470.00	4350.00	148.10	123.60	569.00	28800.00
10816-20.FIN2	Dol 1	17.74	7810.00	7720.00	218.50	188.10	761.00	27500.00
10816-19.FIN2	Dol 1	14.81	5060.00	5020.00	153.70	128.00	680.00	25300.00
10816-18.FIN2	Dol 1	15.29	4310.00	4230.00	145.10	121.60	755.00	39100.00
10816-17.FIN2	Dol 1	17.85	7950.00	7730.00	192.90	167.30	729.00	34100.00
10816-16.FIN2	Dol 1	15.84	6550.00	6430.00	174.60	154.60	662.00	31900.00
10816-15.FIN2	Dol 1	14.95	6720.00	6640.00	156.00	134.40	658.00	24600.00
10816-14.FIN2	Dol 1	16.62	6080.00	6020.00	171.80	151.40	713.00	45200.00
10816-13.FIN2	Dol 1	16.23	7400.00	7250.00	177.50	173.00	662.00	34700.00
10816-10.FIN2	Cal 1	0.49	5.40	5.70	3.27	4.14	208.40	756.00
10816-9.FIN2	Cal 1	0.25	2.40	2.70	4.27	3.74	191.60	721.00
10816-8.FIN2	Cal 1	0.41	4.60	5.20	5.85	4.55	187.80	711.00
10816-7.FIN2	Cal 1	2.31	9.40	13.20	5.87	11.55	290.00	927.00
10816-6.FIN2	Cal 1	1.03	3.70	4.30	9.25	7.09	251.80	1226.00
10816-5.FIN2	Cal 1	0.53	4.70	4.60	5.04	4.82	200.40	828.00
10816-4.FIN2	Cal 1	0.35	4.80	5.50	3.18	4.17	186.20	711.00
10816-3.FIN2	Cal 1	1.08	6.60	3.60	6.70	6.56	227.20	928.00
10816-2.FIN2	Cal 1	2.25	1.70	3.20	3.12	11.75	257.50	732.00
10816-1.FIN2	Cal 1	0.76	7.40	12.00	7.20	7.00	235.90	1107.00
15424-34.FIN2	Cal 2	0.06	-	0.41	0.42	2.05	76.80	815.00
15424-33.FIN2	Cal 2	-	-	0.27	0.59	2.06	94.60	216.00
15424-32.FIN2	Cal 2	0.05	-	0.64	0.56	2.28	98.40	286.00
15424-31.FIN2	Cal 2	-	-	-	0.95	2.09	111.70	338.00
15424-30.FIN2	Cal 2	-	-	0.60	1.93	2.01	108.60	313.00
15424-29.FIN2	Cal 2	-	-	0.23	0.76	2.20	87.00	197.00

LA-ICP-MS data for calcite and dolomite. Values are in ppm. Data below detection limit are indicated by (-) and other deleted data are indicated by an "X".

Sample	Phase	⁵⁹ Co	⁶⁰ Ni	⁶¹ Ni	⁶⁵ Cu	⁶⁶ Zn	⁷⁵ As	⁸⁵ Rb	⁸⁸ Sr
7308-9.FI	Dol 1	12.80	61.80	62.00	1540.00	45.20	127.20	439.00	920.00
7308-10.F	Dol 1	26.00	170.00	101.00	X	39.20	74.80	404.00	899.00
7308-11.F	Dol 1	12.40	50.50	60.00	200.00	48.20	69.70	434.00	863.00
7308-12.F	Dol 1	8.10	46.70	43.70	83.00	50.60	156.80	437.00	1005.00
7308-13.F	Dol 1	5.58	24.19	25.40	76.00	22.00	64.40	208.70	1128.00
7308-14.F	Dol 1	4.97	27.20	26.90	186.00	24.00	65.30	210.20	1143.00
7308-15.F	Dol 1	12.70	54.80	56.60	180.00	63.60	123.70	515.00	1009.00
7308-16.F	Dol 1	10.00	42.40	36.90	188.00	36.60	70.30	336.00	874.00
7308-17.F	Dol 1	5.85	33.70	34.00	53.00	27.80	60.60	285.00	797.00
7308-18.F	Dol 1	13.80	36.20	34.40	58.00	29.80	92.00	304.00	901.00
7308-19.F	Dol 1	1.57	9.50	6.90	15.80	12.70	6540.00	184.00	234.00
7308-20.F	Dol 1	10.30	64.90	61.50	222.00	63.70	310.00	743.00	824.00
7308-21.F	Dol 1	9.71	56.80	56.20	48.10	68.50	157.00	536.00	894.00
7308-22.F	Dol 1	24.40	112.30	114.00	116.00	124.00	245.00	1039.00	1362.00
7308-23.F	Dol 1	19.30	74.90	72.30	104.00	59.40	235.00	674.00	886.00
7308-24.F	Dol 1	41.40	100.40	96.00	200.00	74.60	217.00	833.00	1241.00
7308-25.F	Dol 1	9.70	69.40	72.60	115.00	67.80	139.30	942.00	1164.00
10816-25.	Dol 1	3.50	13.10	11.60	10.90	32.40	442.00	252.40	541.00
10816-24.	Dol 1	6.26	16.50	16.20	18.90	18.30	602.00	180.70	515.00
10816-23.	Dol 1	13.80	23.20	24.50	38.70	18.20	984.00	186.50	477.00
10816-22.	Dol 1	9.40	20.60	19.70	28.60	33.10	880.00	240.80	556.00
10816-21.	Dol 1	7.40	16.90	18.20	26.10	18.45	719.00	192.80	499.00
10816-20.	Dol 1	7.50	17.70	17.40	25.80	119.00	415.00	294.90	563.00
10816-19.	Dol 1	4.12	14.70	14.90	23.60	25.10	308.00	196.00	449.00
10816-18.	Dol 1	4.84	16.90	18.70	45.80	X	682.00	225.00	525.00
10816-17.	Dol 1	4.65	19.10	20.10	26.00	33.90	598.00	272.30	561.00
10816-16.	Dol 1	4.32	19.10	14.10	26.90	25.70	522.00	240.40	537.00
10816-15.	Dol 1	4.18	16.20	18.10	15.80	28.50	372.00	234.00	512.00
10816-14.	Dol 1	9.20	26.90	28.50	49.60	25.90	X	236.50	540.00
10816-13.	Dol 1	4.74	19.50	22.30	31.70	27.47	780.00	254.90	551.00
10816-10.	Cal 1	-	0.33	2.48	0.58	0.24	90.00	2.10	46.40
10816-9.F	Cal 1	-	0.22	2.69	0.18	0.04	27.00	0.70	49.20
10816-8.F	Cal 1	-	0.26	2.55	0.87	0.23	74.00	1.30	55.50
10816-7.F	Cal 1	0.02	0.32	2.24	0.86	0.41	100.00	1.80	74.70
10816-6.F	Cal 1	-	0.28	2.43	2.20	0.50	42.00	1.00	111.00
10816-5.F	Cal 1	-	0.30	2.01	1.10	0.25	57.00	1.20	55.00
10816-4.F	Cal 1	-	0.34	1.85	2.30	1.10	61.00	1.30	45.40
10816-3.F	Cal 1	-	0.36	1.99	1.60	0.36	71.00	0.89	69.10
10816-2.F	Cal 1	-	0.33	1.27	1.60	0.39	16.00	0.65	29.90
10816-1.F	Cal 1	-	0.35	1.67	3.40	0.70	42.00	1.40	87.10
15424-34.	Cal 2	-	0.23	0.98	0.28	0.19	8.60	0.11	567.00
15424-33.	Cal 2	-	0.14	1.20	0.18	0.15	34.00	0.05	159.00
15424-32.	Cal 2	-	0.13	0.94	0.19	0.12	4.60	0.09	106.70
15424-31.	Cal 2	-	0.12	0.67	0.07	0.10	1.28	0.02	85.20
15424-30.	Cal 2	-	0.10	1.15	0.16	0.14	1.70	0.03	184.30
15424-29.	Cal 2	-	0.11	1.58	0.28	0.09	1.80	0.04	216.70

LA-ICP-MS data for calcite and dolomite. Values are in ppm. Data below detection limit are indicated by (-) and other deleted data are indicated by an "X".

Sample ID	Phase	⁸⁹ Y	⁹⁰ Zr	⁹⁵ Mo	⁹⁸ Mo	¹⁰⁷ Ag	¹⁰⁹ Ag	¹¹¹ Cd
7308-9.FIN2	Dol 1	33.70	210.00	1.05	1.11	-	0.17	0.11
7308-10.FIN2	Dol 1	33.50	200.00	0.27	0.38	-	0.07	0.10
7308-11.FIN2	Dol 1	34.90	191.00	0.46	0.42	-	-	0.12
7308-12.FIN2	Dol 1	49.80	198.00	0.48	0.41	-	-	0.09
7308-13.FIN2	Dol 1	21.42	80.30	0.17	0.20	-	-	0.04
7308-14.FIN2	Dol 1	21.08	105.90	0.27	0.25	-	-	0.03
7308-15.FIN2	Dol 1	40.80	258.00	0.45	0.45	0.13	0.17	0.11
7308-16.FIN2	Dol 1	39.60	142.00	0.21	0.24	0.10	-	0.08
7308-17.FIN2	Dol 1	33.80	105.50	0.25	0.26	-	-	0.09
7308-18.FIN2	Dol 1	26.54	104.10	0.86	0.87	-	0.11	0.10
7308-19.FIN2	Dol 1	9.50	410.00	0.34	0.33	0.17	-	0.06
7308-20.FIN2	Dol 1	45.40	362.00	0.65	0.62	-	-	0.23
7308-21.FIN2	Dol 1	51.00	192.90	0.64	0.49	-	-	0.08
7308-22.FIN2	Dol 1	56.30	380.00	6.20	5.50	-	-	0.11
7308-23.FIN2	Dol 1	43.80	251.00	0.59	0.66	-	-	0.12
7308-24.FIN2	Dol 1	49.80	380.00	1.00	0.60	0.24	0.27	0.19
7308-25.FIN2	Dol 1	54.10	343.00	0.43	0.64	-	0.14	0.12
10816-25.FIN2	Dol 1	24.39	150.00	0.87	0.89	-	-	0.10
10816-24.FIN2	Dol 1	51.60	127.00	0.76	0.74	-	0.07	0.13
10816-23.FIN2	Dol 1	20.98	123.00	0.89	0.95	0.14	0.11	0.09
10816-22.FIN2	Dol 1	22.75	141.20	0.82	0.76	0.07	-	0.20
10816-21.FIN2	Dol 1	20.75	118.00	0.85	0.76	0.12	0.10	0.13
10816-20.FIN2	Dol 1	25.90	227.00	0.99	0.95	0.07	-	0.19
10816-19.FIN2	Dol 1	27.40	247.00	0.85	0.87	0.06	0.06	0.13
10816-18.FIN2	Dol 1	18.50	109.70	0.84	0.80	-	0.05	0.19
10816-17.FIN2	Dol 1	24.70	179.00	1.37	1.14	-	-	0.17
10816-16.FIN2	Dol 1	24.18	158.40	0.94	0.87	-	-	0.17
10816-15.FIN2	Dol 1	21.98	137.50	0.93	0.84	-	-	0.16
10816-14.FIN2	Dol 1	33.10	184.00	0.85	0.91	0.11	0.10	0.10
10816-13.FIN2	Dol 1	30.00	202.00	1.03	0.90	0.07	-	0.15
10816-10.FIN2	Cal 1	3.37	4.30	-	0.01	-	-	-
10816-9.FIN2	Cal 1	5.75	2.30	0.01	-	-	-	-
10816-8.FIN2	Cal 1	7.84	4.00	-	0.01	-	-	-
10816-7.FIN2	Cal 1	6.47	4.50	-	0.01	-	-	-
10816-6.FIN2	Cal 1	15.53	3.10	-	0.01	-	-	-
10816-5.FIN2	Cal 1	6.02	3.90	-	0.02	-	-	-
10816-4.FIN2	Cal 1	2.84	4.00	0.02	0.01	-	-	-
10816-3.FIN2	Cal 1	7.07	2.60	0.01	0.01	-	-	-
10816-2.FIN2	Cal 1	1.98	1.50	0.01	-	-	-	-
10816-1.FIN2	Cal 1	10.18	2.30	0.01	-	-	-	-
15424-34.FIN2	Cal 2	1.51	1.04	-	0.01	-	-	-
15424-33.FIN2	Cal 2	1.52	0.63	-	-	-	-	-
15424-32.FIN2	Cal 2	0.69	0.68	-	-	-	-	-
15424-31.FIN2	Cal 2	1.76	0.29	-	-	-	-	-
15424-30.FIN2	Cal 2	0.90	0.43	-	0.01	-	-	-
15424-29.FIN2	Cal 2	1.01	0.48	0.01	-	-	-	-

LA-ICP-MS data for calcite and dolomite. Values are in ppm. Data below detection limit are indicated by (-) and other deleted data are indicated by an "X".

Sample ID	Phase	¹¹⁴ Cd	¹²¹ Sb	¹²³ Sb	¹³⁷ Ba	¹³⁹ La	¹⁴⁰ Ce	¹⁴¹ Pr	¹⁴⁶ Nd
7308-9.FI	Dol 1	0.31	0.82	0.72	858.00	72.60	127.00	13.30	49.90
7308-10.F	Dol 1	0.24	0.51	0.55	725.00	57.80	99.00	11.70	42.10
7308-11.F	Dol 1	0.28	0.48	0.47	764.00	53.20	101.30	11.05	46.00
7308-12.F	Dol 1	0.34	-	-	811.00	250.00	560.00	57.00	240.00
7308-13.F	Dol 1	0.16	0.23	0.16	407.00	30.80	55.90	6.36	26.30
7308-14.F	Dol 1	0.15	0.18	0.22	2640.00	22.70	48.20	5.34	21.60
7308-15.F	Dol 1	0.49	0.65	0.62	1040.00	106.00	191.00	18.40	66.00
7308-16.F	Dol 1	0.24	0.35	0.37	531.00	62.50	152.00	17.80	77.00
7308-17.F	Dol 1	0.19	0.25	0.41	474.00	42.40	90.00	10.80	45.90
7308-18.F	Dol 1	0.17	0.38	0.57	552.00	65.50	117.00	11.20	42.40
7308-19.F	Dol 1	0.15	1.21	1.35	1155.00	13.90	24.30	2.52	10.90
7308-20.F	Dol 1	0.65	0.77	-	1800.00	76.00	145.00	15.70	64.00
7308-21.F	Dol 1	0.51	0.39	0.53	852.00	71.90	160.00	19.60	89.00
7308-22.F	Dol 1	0.59	0.79	1.47	2520.00	120.00	201.00	21.10	81.50
7308-23.F	Dol 1	0.35	0.73	0.76	1311.00	61.80	117.00	13.41	57.60
7308-24.F	Dol 1	0.55	1.31	1.43	1550.00	93.00	158.00	16.90	66.30
7308-25.F	Dol 1	0.47	0.89	0.68	1662.00	107.00	187.00	19.10	76.70
10816-25.	Dol 1	0.21	2.10	2.15	318.00	X	220.00	22.00	X
10816-24.	Dol 1	0.15	3.34	3.31	265.00	X	183.00	26.50	X
10816-23.	Dol 1	0.19	4.48	4.35	291.00	28.70	59.60	6.39	26.10
10816-22.	Dol 1	0.23	4.12	4.22	336.00	32.00	67.80	7.22	30.63
10816-21.	Dol 1	0.18	3.54	3.35	233.00	33.10	66.90	7.29	30.90
10816-20.	Dol 1	0.31	3.08	3.01	381.00	35.50	73.20	7.59	31.40
10816-19.	Dol 1	0.19	2.68	2.62	236.00	27.80	59.30	6.37	27.30
10816-18.	Dol 1	0.22	3.59	3.50	343.00	30.20	57.20	5.80	23.90
10816-17.	Dol 1	0.19	3.85	3.78	401.00	34.90	71.30	7.69	32.44
10816-16.	Dol 1	0.25	2.83	3.07	302.00	37.10	75.70	7.66	31.80
10816-15.	Dol 1	0.21	2.87	3.10	405.00	30.90	65.40	6.80	28.50
10816-14.	Dol 1	0.22	3.55	3.72	312.00	58.00	124.00	12.90	54.00
10816-13.	Dol 1	0.28	3.29	3.33	335.00	38.70	83.20	9.00	39.40
10816-10.	Cal 1	-	-	0.04	13.00	0.14	0.34	0.05	0.35
10816-9.F	Cal 1	-	-	-	7.20	0.13	0.32	0.07	0.57
10816-8.F	Cal 1	0.01	-	0.04	12.00	0.19	0.51	0.11	0.83
10816-7.F	Cal 1	-	-	0.05	15.00	0.49	1.30	0.17	1.02
10816-6.F	Cal 1	-	-	-	10.00	0.24	0.78	0.17	1.36
10816-5.F	Cal 1	-	-	-	11.00	0.11	0.39	0.07	0.55
10816-4.F	Cal 1	-	-	-	12.00	0.11	0.31	0.07	0.35
10816-3.F	Cal 1	0.01	-	-	10.30	0.33	0.75	0.12	0.79
10816-2.F	Cal 1	0.01	-	-	3.80	0.06	0.17	0.04	0.23
10816-1.F	Cal 1	0.01	-	-	8.30	0.17	0.51	0.10	0.89
15424-34.	Cal 2	-	-	-	47.80	1.59	2.89	0.39	1.61
15424-33.	Cal 2	-	-	-	19.70	1.42	2.88	0.42	1.83
15424-32.	Cal 2	-	-	-	5.60	1.18	2.01	0.25	1.06
15424-31.	Cal 2	-	-	-	7.82	1.50	2.66	0.37	1.74
15424-30.	Cal 2	-	-	-	21.30	1.08	1.93	0.29	1.26
15424-29.	Cal 2	-	-	-	17.20	0.88	1.77	0.27	1.19

LA-ICP-MS data for calcite and dolomite. Values are in ppm. Data below detection limit are indicated by (-) and other deleted data are indicated by an "X".

Sample ID	Phase	¹⁴⁷ Sm	¹⁵³ Eu	¹⁵⁷ Gd	¹⁵⁹ Tb	¹⁶³ Dy	¹⁶⁵ Ho	¹⁶⁶ Er
7308-9.FIN2	Dol 1	9.05	1.44	7.16	0.96	6.36	1.25	3.73
7308-10.FIN2	Dol 1	8.64	1.50	6.90	0.94	6.29	1.18	3.70
7308-11.FIN2	Dol 1	8.48	1.42	6.95	0.96	6.79	1.22	3.72
7308-12.FIN2	Dol 1	31.00	3.70	17.60	2.03	12.30	1.95	5.03
7308-13.FIN2	Dol 1	5.51	0.87	4.07	0.61	3.93	0.71	2.12
7308-14.FIN2	Dol 1	4.58	0.81	3.68	0.54	3.79	0.70	2.10
7308-15.FIN2	Dol 1	10.60	1.71	7.41	1.08	8.20	1.54	5.20
7308-16.FIN2	Dol 1	13.70	2.04	10.90	1.20	7.90	1.36	3.87
7308-17.FIN2	Dol 1	9.40	1.50	7.36	1.03	6.38	1.21	3.46
7308-18.FIN2	Dol 1	7.65	1.21	5.85	0.75	5.01	0.95	2.78
7308-19.FIN2	Dol 1	1.82	0.79	1.84	0.26	1.62	0.33	1.01
7308-20.FIN2	Dol 1	10.90	2.04	8.40	1.19	8.37	1.69	5.26
7308-21.FIN2	Dol 1	17.90	2.95	14.30	1.81	10.31	1.81	4.93
7308-22.FIN2	Dol 1	15.60	2.88	11.80	1.59	11.14	2.17	6.43
7308-23.FIN2	Dol 1	12.20	2.06	8.92	1.32	8.34	1.56	4.95
7308-24.FIN2	Dol 1	12.69	2.16	9.77	1.36	9.88	1.82	5.88
7308-25.FIN2	Dol 1	14.70	2.61	11.20	1.54	10.24	2.10	5.90
10816-25.FIN2	Dol 1	10.60	1.45	5.60	0.70	4.35	0.83	2.36
10816-24.FIN2	Dol 1	X	X	X	X	11.90	1.76	3.81
10816-23.FIN2	Dol 1	5.38	0.93	4.00	0.56	3.77	0.72	2.11
10816-22.FIN2	Dol 1	5.97	1.02	4.69	0.59	4.32	0.81	2.36
10816-21.FIN2	Dol 1	6.04	1.05	4.72	0.62	3.93	0.70	1.95
10816-20.FIN2	Dol 1	6.24	1.12	4.91	0.68	4.73	0.87	2.66
10816-19.FIN2	Dol 1	5.71	1.03	4.48	0.69	4.26	0.98	3.06
10816-18.FIN2	Dol 1	4.62	0.82	3.70	0.52	3.39	0.64	1.92
10816-17.FIN2	Dol 1	6.46	1.09	4.84	0.66	4.51	0.84	2.64
10816-16.FIN2	Dol 1	6.31	1.05	4.74	0.64	4.36	0.79	2.40
10816-15.FIN2	Dol 1	5.71	0.99	4.22	0.58	3.95	0.73	2.26
10816-14.FIN2	Dol 1	9.70	1.94	6.80	0.89	5.94	1.09	3.47
10816-13.FIN2	Dol 1	8.30	1.47	6.41	0.86	5.41	1.03	2.93
10816-10.FIN2	Cal 1	0.18	0.05	0.37	0.06	0.48	0.08	0.23
10816-9.FIN2	Cal 1	0.33	0.09	0.63	0.11	0.81	0.15	0.37
10816-8.FIN2	Cal 1	0.47	0.12	0.84	0.16	1.15	0.20	0.50
10816-7.FIN2	Cal 1	0.48	0.12	0.82	0.14	0.91	0.17	0.44
10816-6.FIN2	Cal 1	0.86	0.23	1.88	0.31	2.10	0.37	0.92
10816-5.FIN2	Cal 1	0.31	0.08	0.61	0.11	0.77	0.14	0.34
10816-4.FIN2	Cal 1	0.16	0.05	0.32	0.05	0.40	0.08	0.22
10816-3.FIN2	Cal 1	0.37	0.10	0.77	0.13	1.00	0.17	0.45
10816-2.FIN2	Cal 1	0.12	0.03	0.27	0.05	0.30	0.05	0.18
10816-1.FIN2	Cal 1	0.53	0.15	1.15	0.20	1.30	0.24	0.61
15424-34.FIN2	Cal 2	0.27	0.06	0.32	0.03	0.24	0.04	0.10
15424-33.FIN2	Cal 2	0.35	0.07	0.35	0.04	0.26	0.04	0.12
15424-32.FIN2	Cal 2	0.18	0.03	0.16	0.02	0.14	0.02	0.05
15424-31.FIN2	Cal 2	0.40	0.07	0.36	0.04	0.25	0.04	0.13
15424-30.FIN2	Cal 2	0.22	0.03	0.21	0.02	0.12	0.02	0.06
15424-29.FIN2	Cal 2	0.24	0.05	0.22	0.02	0.14	0.03	0.06

LA-ICP-MS data for calcite and dolomite. Values are in ppm. Data below detection limit are indicated by (-) and other deleted data are indicated by an "X".

Sample #	Phase	¹⁶⁹ Tm	¹⁷² Yb	¹⁷⁵ Lu	¹⁹⁷ Au	²⁰⁵ Tl	²⁰⁷ Pb	²⁰⁹ Bi	²³² Th	²³⁸ U
7308-9.FI	Dol 1	0.54	4.06	0.49	0.13	1.65	290.00	0.15	28.24	14.14
7308-10.F	Dol 1	0.53	3.63	0.47	0.12	1.59	13.20	0.09	28.30	13.60
7308-11.F	Dol 1	0.53	3.90	0.50	0.07	1.57	9.60	0.13	26.10	13.29
7308-12.F	Dol 1	0.69	4.39	0.59	0.07	1.73	10.30	0.15	92.00	23.00
7308-13.F	Dol 1	0.29	2.04	0.27	0.06	0.81	5.42	0.06	12.47	6.30
7308-14.F	Dol 1	0.29	2.01	0.29	0.04	0.80	4.88	0.05	13.19	8.19
7308-15.F	Dol 1	0.64	6.40	0.81	0.15	1.91	11.40	0.21	38.80	22.80
7308-16.F	Dol 1	0.57	3.75	0.56	0.05	1.31	9.90	0.23	25.90	13.16
7308-17.F	Dol 1	0.46	3.04	0.43	0.04	1.08	7.90	0.08	19.60	11.36
7308-18.F	Dol 1	0.38	2.59	0.38	0.05	1.21	14.90	0.32	18.66	10.43
7308-19.F	Dol 1	0.14	1.21	0.15	-	0.74	30.40	0.04	4.70	2.46
7308-20.F	Dol 1	0.79	5.97	0.74	1.80	2.88	21.60	0.17	42.10	23.10
7308-21.F	Dol 1	0.68	4.29	0.57	-	2.15	16.80	0.11	42.40	17.17
7308-22.F	Dol 1	0.87	6.10	0.86	0.19	3.98	34.20	1.15	51.20	30.00
7308-23.F	Dol 1	0.62	4.37	0.65	0.12	2.72	23.10	0.24	41.30	22.34
7308-24.F	Dol 1	0.81	5.94	0.79	0.35	3.14	31.30	0.93	41.80	26.10
7308-25.F	Dol 1	0.87	6.22	0.88	0.12	3.42	34.70	0.16	51.70	21.80
10816-25.	Dol 1	0.33	2.38	0.32	0.06	4.77	8.64	0.04	21.50	7.43
10816-24.	Dol 1	0.43	2.55	0.34	0.21	7.63	9.77	0.12	X	9.59
10816-23.	Dol 1	0.29	1.99	0.28	0.35	12.70	17.80	0.34	15.20	5.93
10816-22.	Dol 1	0.34	2.28	0.32	0.29	11.15	13.95	0.16	16.84	6.76
10816-21.	Dol 1	0.28	1.95	0.25	0.21	9.10	12.90	0.22	16.98	6.06
10816-20.	Dol 1	0.37	2.80	0.39	0.16	7.00	9.53	0.09	20.96	8.60
10816-19.	Dol 1	0.43	2.94	0.45	0.13	5.59	7.61	0.08	19.70	8.50
10816-18.	Dol 1	0.27	1.83	0.25	0.28	10.40	20.70	0.11	13.47	5.35
10816-17.	Dol 1	0.36	2.57	0.37	0.26	8.33	9.95	0.06	20.10	7.80
10816-16.	Dol 1	0.33	2.34	0.32	0.21	7.64	8.38	0.05	17.72	6.57
10816-15.	Dol 1	0.31	2.23	0.31	0.13	5.63	10.17	0.06	16.76	5.87
10816-14.	Dol 1	0.51	3.32	0.47	0.35	12.10	14.10	0.16	22.00	7.67
10816-13.	Dol 1	0.39	2.72	0.38	0.24	9.38	10.36	0.07	28.70	7.59
10816-10.	Cal 1	0.03	0.15	0.02	-	0.02	0.50	-	0.10	0.07
10816-9.F	Cal 1	0.04	0.21	0.02	-	0.01	0.23	-	0.02	0.03
10816-8.F	Cal 1	0.05	0.30	0.03	-	0.03	0.34	-	0.06	0.06
10816-7.F	Cal 1	0.05	0.34	0.05	-	0.03	0.61	-	0.19	0.17
10816-6.F	Cal 1	0.09	0.46	0.06	-	0.02	0.39	-	0.10	0.14
10816-5.F	Cal 1	0.03	0.17	0.02	-	0.01	0.33	-	0.10	0.14
10816-4.F	Cal 1	0.02	0.12	0.02	-	0.01	0.20	-	0.05	0.07
10816-3.F	Cal 1	0.05	0.25	0.03	-	0.02	0.25	-	0.17	0.15
10816-2.F	Cal 1	0.02	0.16	0.03	-	0.01	0.14	0.01	0.11	0.09
10816-1.F	Cal 1	0.07	0.32	0.04	-	0.03	0.23	0.01	0.09	0.12
15424-34.	Cal 2	0.01	0.05	0.01	-	0.01	0.63	-	0.04	1.83
15424-33.	Cal 2	0.01	0.06	0.01	-	0.01	0.12	-	0.01	0.88
15424-32.	Cal 2	-	0.04	-	-	-	0.11	-	0.02	0.62
15424-31.	Cal 2	0.01	0.06	0.01	-	-	0.04	-	-	0.52
15424-30.	Cal 2	0.01	0.04	0.01	-	-	0.12	-	-	0.40
15424-29.	Cal 2	0.01	0.03	-	-	-	0.14	-	0.01	0.70

LA-ICP-MS data for calcite and dolomite. Values are in ppm. Data below detection limit are indicated by (-) and other deleted data are indicated by an "X".

Sample ID	Phase	⁴⁵ Sc	⁴⁷ Ti	⁴⁹ Ti	⁵¹ V	⁵² Cr	⁵⁵ Mn	⁵⁷ Fe
15424-28.FIN2	Cal 2	-	-	-	0.96	2.16	92.00	136.40
15424-27.FIN2	Cal 2	-	-	0.14	1.20	2.30	99.40	317.00
15424-26.FIN2	Cal 2	0.04	-	0.31	0.35	1.96	67.70	793.00
15424-25.FIN2	Cal 2	0.04	-	0.37	0.47	2.17	103.60	394.00
15424-24.FIN2	Cal 2	-	-	0.87	0.85	2.34	100.80	558.00
15424-23.FIN2	Cal 2	-	-	1.70	2.05	2.21	93.20	232.00
15424-22.FIN2	Cal 2	-	-	0.73	1.79	2.18	116.40	455.00
15424-21.FIN2	Cal 2	-	-	0.36	1.18	1.97	89.90	204.00
15424-20.FIN2	Cal 2	-	-	1.28	0.57	2.55	100.40	303.00
15424-19.FIN2	Cal 2	0.58	57.00	61.00	5.19	5.09	89.90	9200.00
15424-18.FIN2	Cal 2	0.79	30.80	29.80	3.57	4.29	122.70	4500.00
15424-17.FIN2	Cal 2	0.59	46.00	44.00	4.69	5.15	91.50	1640.00
15424-16.FIN2	Cal 2	0.81	48.00	47.00	4.75	6.03	98.40	3000.00
15424-14.FIN2	Cal 2	0.90	83.00	84.00	5.31	5.10	84.10	1250.00
15424-13.FIN2	Cal 2	0.65	51.10	52.00	7.19	5.69	71.30	801.00
15424-12.FIN2	Cal 2	0.67	66.90	64.50	7.82	5.67	79.60	833.00
15424-11.FIN2	Cal 2	0.67	52.60	53.20	7.41	5.32	77.40	1007.00
15424-10.FIN2	Cal 2	0.62	100.00	101.00	8.10	5.94	77.70	1190.00
15424-9.FIN2	Cal 2	0.68	69.00	69.30	7.61	5.82	73.50	1480.00
15424-8.FIN2	Cal 2	0.34	86.00	86.00	4.56	4.90	76.70	1275.00
15424-7.FIN2	Cal 2	0.19	3.70	3.90	1.45	2.52	79.10	1103.00
15424-6.FIN2	Cal 2	0.33	8.70	7.80	2.17	3.23	76.90	1007.00
15424-5.FIN2	Cal 2	0.17	3.60	3.90	1.16	2.54	77.00	1103.00
15424-4.FIN2	Cal 2	0.17	6.10	6.20	1.43	3.08	77.40	1068.00
15424-3.FIN2	Cal 2	0.16	8.60	9.00	1.07	2.85	78.20	1109.00
15424-2.FIN2	Cal 2	0.17	10.80	11.80	1.54	3.37	81.60	1187.00
15424-1.FIN2	Cal 2	0.25	17.90	17.10	2.72	3.99	73.6	910.00

LA-ICP-MS data for calcite and dolomite. Values are in ppm. Data below detection limit are indicated by (-) and other deleted data are indicated by an "X".

Sample	Phase	⁵⁹ Co	⁶⁰ Ni	⁶¹ Ni	⁶⁵ Cu	⁶⁶ Zn	⁷⁵ As	⁸⁵ Rb	⁸⁸ Sr
15424-28	Cal 2	-	-	-	-	-	1.08	-	102.20
15424-27	Cal 2	-	0.09	-	0.09	0.11	4.50	0.04	162.00
15424-26	Cal 2	-	0.14	-	0.19	0.12	3.80	0.06	541.00
15424-25	Cal 2	-	0.11	-	0.33	0.13	1.71	0.05	136.30
15424-24	Cal 2	-	-	-	0.33	0.25	9.90	0.12	383.00
15424-23	Cal 2	-	0.15	-	0.26	0.29	8.00	0.23	89.00
15424-22	Cal 2	-	0.17	-	0.10	0.18	20.00	0.05	191.40
15424-21	Cal 2	-	0.11	-	0.18	-	2.40	0.06	112.30
15424-20	Cal 2	-	0.20	-	1.62	0.37	12.90	0.33	157.00
15424-19	Cal 2	1.28	4.70	7.00	5.20	1.30	250.00	5.20	374.00
15424-18	Cal 2	0.67	1.43	2.17	4.20	0.93	123.00	3.80	452.00
15424-17	Cal 2	0.40	1.31	2.05	2.40	1.23	106.00	5.30	393.00
15424-16	Cal 2	0.60	1.94	1.80	6.60	1.73	230.00	7.10	448.00
15424-14	Cal 2	0.20	0.50	1.40	2.60	1.53	63.00	5.40	539.00
15424-13	Cal 2	-	0.41	-	1.38	0.82	37.00	4.70	567.00
15424-12	Cal 2	0.10	0.41	-	1.30	0.91	30.00	4.96	563.00
15424-11	Cal 2	0.08	0.41	-	0.89	0.99	42.00	5.00	588.00
15424-10	Cal 2	0.42	1.06	-	2.30	0.76	38.00	5.50	626.00
15424-9.F	Cal 2	0.50	1.42	1.90	4.00	0.97	47.00	4.96	608.00
15424-8.F	Cal 2	0.25	0.78	1.70	1.07	0.55	10.80	3.26	787.00
15424-7.F	Cal 2	-	0.12	-	0.06	0.13	4.00	0.35	811.00
15424-6.F	Cal 2	-	0.17	-	0.18	0.23	4.40	0.70	782.00
15424-5.F	Cal 2	-	0.17	1.19	0.16	0.20	9.10	0.51	797.00
15424-4.F	Cal 2	-	0.20	1.41	0.16	0.28	10.80	0.75	833.00
15424-3.F	Cal 2	-	0.14	-	0.13	0.27	10.00	0.58	848.00
15424-2.F	Cal 2	0.11	0.42	-	0.56	0.26	13.00	0.84	852.00
15424-1.F	Cal 2	0.10	0.37	-	2.10	0.46	23.00	1.37	700.00

LA-ICP-MS data for calcite and dolomite. Values are in ppm. Data below detection limit are indicated by (-) and other deleted data are indicated by an "X".

Sample ID	Phase	⁸⁹ Y	⁹⁰ Zr	⁹⁵ Mo	⁹⁸ Mo	¹⁰⁷ Ag	¹⁰⁹ Ag	¹¹¹ Cd
15424-28.FIN2	Cal 2	0.81	0.22	-	-	-	-	-
15424-27.FIN2	Cal 2	1.56	0.58	0.01	-	-	-	0.01
15424-26.FIN2	Cal 2	1.06	0.58	-	-	-	-	-
15424-25.FIN2	Cal 2	1.28	0.46	-	-	-	-	-
15424-24.FIN2	Cal 2	1.16	1.04	-	-	-	-	-
15424-23.FIN2	Cal 2	1.29	0.70	0.05	-	-	-	-
15424-22.FIN2	Cal 2	1.10	0.54	-	-	-	-	-
15424-21.FIN2	Cal 2	1.82	0.16	-	-	-	-	-
15424-20.FIN2	Cal 2	1.11	1.02	0.03	-	-	-	-
15424-19.FIN2	Cal 2	2.26	6.60	0.11	0.11	0.04	0.03	-
15424-18.FIN2	Cal 2	3.40	6.60	0.06	0.06	-	-	-
15424-17.FIN2	Cal 2	2.21	8.80	-	0.05	-	-	0.01
15424-16.FIN2	Cal 2	2.46	11.40	0.06	0.05	-	0.03	-
15424-14.FIN2	Cal 2	2.66	8.70	0.06	0.07	-	-	0.01
15424-13.FIN2	Cal 2	2.95	10.60	0.08	0.04	-	-	-
15424-12.FIN2	Cal 2	3.15	7.90	0.05	0.04	-	-	0.01
15424-11.FIN2	Cal 2	2.75	8.20	0.05	0.06	-	-	-
15424-10.FIN2	Cal 2	2.84	7.30	0.17	0.17	-	-	-
15424-9.FIN2	Cal 2	2.69	7.80	0.13	0.11	-	-	-
15424-8.FIN2	Cal 2	2.34	4.13	0.11	0.10	0.04	-	-
15424-7.FIN2	Cal 2	2.04	1.62	-	-	-	-	-
15424-6.FIN2	Cal 2	2.49	11.80	-	0.01	-	-	-
15424-5.FIN2	Cal 2	1.72	1.97	-	-	-	-	-
15424-4.FIN2	Cal 2	1.84	1.55	0.02	0.01	-	-	-
15424-3.FIN2	Cal 2	1.66	1.21	-	-	-	-	-
15424-2.FIN2	Cal 2	1.82	0.83	0.04	0.03	-	-	-
15424-1.FIN2	Cal 2	2.76	2.40	-	-	-	-	-

LA-ICP-MS data for calcite and dolomite. Values are in ppm. Data below detection limit are indicated by (-) and other deleted data are indicated by an "X".

Sample #	Phase	¹¹⁴ Cd	¹²¹ Sb	¹²³ Sb	¹³⁷ Ba	¹³⁹ La	¹⁴⁰ Ce	¹⁴¹ Pr	¹⁴⁶ Nd
15424-28.	Cal 2	-	-	-	7.69	0.85	1.60	0.25	1.17
15424-27.	Cal 2	-	-	-	13.10	1.33	2.42	0.36	1.55
15424-26.	Cal 2	-	-	-	27.10	0.83	1.45	0.21	0.81
15424-25.	Cal 2	-	-	-	19.81	2.90	4.85	0.61	2.38
15424-24.	Cal 2	-	-	-	38.40	1.34	2.49	0.34	1.58
15424-23.	Cal 2	-	-	-	7.00	0.91	1.56	0.25	1.09
15424-22.	Cal 2	-	-	-	18.04	1.39	2.64	0.35	1.58
15424-21.	Cal 2	-	-	-	8.00	1.02	2.16	0.33	1.59
15424-20.	Cal 2	-	0.05	-	12.80	1.20	2.54	0.36	1.58
15424-19.	Cal 2	0.02	0.20	0.12	37.00	4.04	6.73	0.84	3.39
15424-18.	Cal 2	0.01	0.08	0.06	38.00	4.53	10.23	1.45	6.36
15424-17.	Cal 2	-	0.05	0.04	48.00	4.01	6.83	0.80	3.12
15424-16.	Cal 2	0.03	0.10	0.10	61.00	4.51	7.52	0.85	3.31
15424-14.	Cal 2	0.01	-	0.02	42.00	4.06	6.76	0.82	3.18
15424-13.	Cal 2	-	-	-	36.00	3.49	5.71	0.73	2.79
15424-12.	Cal 2	-	-	-	31.10	3.58	6.07	0.76	3.12
15424-11.	Cal 2	-	-	-	36.00	3.71	6.07	0.76	3.14
15424-10.	Cal 2	-	-	0.07	37.00	3.61	5.77	0.75	2.88
15424-9.F	Cal 2	-	0.10	0.15	36.10	3.54	5.64	0.72	2.91
15424-8.F	Cal 2	-	0.23	0.19	21.20	1.78	3.23	0.42	1.72
15424-7.F	Cal 2	-	-	-	17.90	1.49	2.59	0.36	1.50
15424-6.F	Cal 2	0.01	-	-	18.30	1.64	2.80	0.40	1.65
15424-5.F	Cal 2	-	-	-	15.40	1.21	2.14	0.30	1.30
15424-4.F	Cal 2	-	-	-	18.90	1.41	2.49	0.35	1.47
15424-3.F	Cal 2	-	-	-	17.90	1.16	2.09	0.29	1.29
15424-2.F	Cal 2	0.01	-	0.10	16.93	1.13	2.18	0.29	1.18
15424-1.F	Cal 2	-	0.16	0.18	32.00	1.98	3.51	0.49	2.12

LA-ICP-MS data for calcite and dolomite. Values are in ppm. Data below detection limit are indicated by (-) and other deleted data are indicated by an "X".

Sample ID	Phase	¹⁴⁷ Sm	¹⁵³ Eu	¹⁵⁷ Gd	¹⁵⁹ Tb	¹⁶³ Dy	¹⁶⁵ Ho	¹⁶⁶ Er
15424-28.FIN2	Cal 2	0.23	0.04	0.19	0.02	0.13	0.02	0.05
15424-27.FIN2	Cal 2	0.31	0.06	0.31	0.04	0.21	0.04	0.11
15424-26.FIN2	Cal 2	0.14	0.04	0.15	0.02	0.13	0.02	0.06
15424-25.FIN2	Cal 2	0.40	0.07	0.34	0.05	0.22	0.04	0.12
15424-24.FIN2	Cal 2	0.25	0.07	0.26	0.03	0.19	0.03	0.07
15424-23.FIN2	Cal 2	0.23	0.04	0.26	0.03	0.17	0.03	0.08
15424-22.FIN2	Cal 2	0.28	0.04	0.22	0.02	0.15	0.02	0.06
15424-21.FIN2	Cal 2	0.35	0.07	0.37	0.04	0.24	0.04	0.11
15424-20.FIN2	Cal 2	0.36	0.07	0.24	0.03	0.17	0.04	0.08
15424-19.FIN2	Cal 2	0.60	0.10	0.45	0.06	0.40	0.07	0.18
15424-18.FIN2	Cal 2	1.22	0.20	0.85	0.10	0.61	0.11	0.26
15424-17.FIN2	Cal 2	0.56	0.11	0.40	0.06	0.35	0.07	0.20
15424-16.FIN2	Cal 2	0.56	0.14	0.49	0.07	0.37	0.07	0.18
15424-14.FIN2	Cal 2	0.57	0.12	0.48	0.06	0.39	0.07	0.21
15424-13.FIN2	Cal 2	0.55	0.12	0.55	0.07	0.52	0.09	0.23
15424-12.FIN2	Cal 2	0.59	0.12	0.52	0.07	0.51	0.09	0.24
15424-11.FIN2	Cal 2	0.59	0.11	0.54	0.06	0.46	0.09	0.23
15424-10.FIN2	Cal 2	0.50	0.12	0.51	0.07	0.46	0.09	0.21
15424-9.FIN2	Cal 2	0.48	0.13	0.40	0.06	0.42	0.07	0.21
15424-8.FIN2	Cal 2	0.36	0.09	0.37	0.05	0.29	0.05	0.15
15424-7.FIN2	Cal 2	0.33	0.08	0.35	0.04	0.25	0.06	0.14
15424-6.FIN2	Cal 2	0.37	0.09	0.35	0.06	0.32	0.06	0.17
15424-5.FIN2	Cal 2	0.27	0.07	0.26	0.03	0.25	0.04	0.14
15424-4.FIN2	Cal 2	0.30	0.08	0.25	0.04	0.24	0.04	0.13
15424-3.FIN2	Cal 2	0.25	0.07	0.20	0.03	0.24	0.04	0.11
15424-2.FIN2	Cal 2	0.25	0.07	0.24	0.04	0.25	0.05	0.11
15424-1.FIN2	Cal 2	0.46	0.11	0.45	0.06	0.42	0.06	0.20

LA-ICP-MS data for calcite and dolomite. Values are in ppm. Data below detection limit are indicated by (-) and other deleted data are indicated by an "X".

Sample ID	Phase	¹⁶⁹ Tm	¹⁷² Yb	¹⁷⁵ Lu	¹⁹⁷ Au	²⁰⁵ Tl	²⁰⁷ Pb	²⁰⁹ Bi	²³² Th	²³⁸ U
15424-28	Cal 2	0.01	0.02	-	-	-	0.05	-	0.00	0.71
15424-27	Cal 2	0.01	0.05	0.01	-	0.01	0.08	-	0.01	0.94
15424-26	Cal 2	0.01	0.03	-	-	0.01	0.38	-	0.02	0.88
15424-25	Cal 2	0.01	0.08	0.01	-	0.01	0.13	-	0.02	1.14
15424-24	Cal 2	0.01	0.05	-	-	0.01	0.32	-	0.02	1.09
15424-23	Cal 2	0.01	0.04	0.01	-	-	0.21	-	0.01	0.61
15424-22	Cal 2	0.01	0.04	0.01	-	0.01	0.13	-	0.01	0.68
15424-21	Cal 2	0.01	0.05	0.01	-	-	0.07	-	0.00	0.45
15424-20	Cal 2	0.01	0.06	0.01	-	0.01	0.24	-	0.01	1.41
15424-19	Cal 2	0.02	0.19	0.03	-	0.28	5.60	0.01	0.47	7.87
15424-18	Cal 2	0.03	0.21	0.03	-	0.11	2.72	0.01	0.31	6.56
15424-17	Cal 2	0.02	0.15	0.02	-	0.06	2.40	-	0.41	6.63
15424-16	Cal 2	0.02	0.17	0.02	-	0.10	3.53	0.01	0.43	6.37
15424-14	Cal 2	0.03	0.15	0.03	-	0.13	1.70	0.01	0.44	8.59
15424-13	Cal 2	0.03	0.21	0.02	-	0.14	0.99	0.01	0.48	11.59
15424-12	Cal 2	0.03	0.22	0.02	-	0.13	0.97	0.01	0.49	13.42
15424-11	Cal 2	0.03	0.16	0.02	-	0.12	1.23	-	0.53	12.53
15424-10	Cal 2	0.03	0.18	0.03	-	0.22	1.70	-	0.51	11.90
15424-9	F Cal 2	0.03	0.16	0.02	-	0.26	2.15	0.02	0.46	10.36
15424-8	F Cal 2	0.02	0.13	0.02	-	0.09	1.59	0.02	0.16	4.69
15424-7	F Cal 2	0.02	0.10	0.02	-	0.01	0.47	-	0.07	3.13
15424-6	F Cal 2	0.02	0.13	0.02	-	0.01	0.52	-	0.13	7.75
15424-5	F Cal 2	0.01	0.07	0.01	-	0.01	0.49	-	0.06	2.18
15424-4	F Cal 2	0.01	0.12	0.01	-	0.01	0.61	-	0.09	2.35
15424-3	F Cal 2	0.01	0.07	0.01	-	0.01	0.59	-	0.05	1.14
15424-2	F Cal 2	0.01	0.10	0.01	-	0.02	0.60	-	0.05	1.46
15424-1	F Cal 2	0.03	0.13	0.02	-	0.04	0.71	0.01	0.19	3.82

LA-ICP-MS data for pyrite. Values are in ppm. Data below detection limit are indicated by (-) and other discarded data (due to interference) are indicated by an "X".
LLQ = below limit of quantitation (see section 2.4.3)

Sample ID	Phase	⁵¹ V	⁵² Cr	⁵⁵ Mn	⁵⁹ Co	⁶⁰ Ni
7308-1.FIN2	Early diagenesis	580.00	390.00	14800.00	X	X
7308-2.FIN2	Early diagenesis	435.00	250.00	20200.00	X	X
7308-3.FIN2	Early diagenesis	X	3.40	X	1035.00	3390.00
7308-4.FIN2	Early diagenesis	0.90	2.30	X	740.00	1350.00
7308-5.FIN2	Early diagenesis	0.23	3.00	X	670.00	1900.00
7308-6.FIN2	Early diagenesis	X	X	50500.00	141.00	1000.00
7308-7.FIN2	Early diagenesis	710.00	220.00	19700.00	X	X
7308-8.FIN2	Early diagenesis	910.00	370.00	7470.00	X	X
7308-9.FIN2	Early diagenesis	X	130.00	-	1320.00	1830.00
7308-10.FIN2	Early diagenesis	481.00	190.00	10500.00	X	X
7308-11.FIN2	Early diagenesis	423.00	160.00	11440.00	X	X
7308-12.FIN2	Early diagenesis	549.00	620.00	43000.00	X	X
7308-13.FIN2	Early diagenesis	1810.00	510.00	6600.00	X	560.00
11454-6.FIN2	Early diagenesis	1.80	X	19.00	182.00	1270.00
11454-7.FIN2	Early diagenesis	23.30	X	82.00	368.00	1750.00
11454-9.FIN2	Early diagenesis	17.00	12.00	1460.00	53.00	420.00
11454-10.FIN2	Early diagenesis	LLQ	8.90	1840.00	34.80	660.00
11680B-2.FIN2	Base metal	-	0.42	1.53	4.40	227.00
11680B-3.FIN2	Base metal	0.08	-	3.24	13.73	376.60
11680B-4.FIN2	Base metal	0.06	-	6.25	47.70	828.00
11680B-5.FIN2	Base metal	0.16	X	10.20	107.20	1465.00
11680B-6.FIN2	Base metal	-	0.53	1.53	2.27	200.10
11680B-7.FIN2	Base metal	-	LLQ	0.64	5.18	225.30
11680B-8.FIN2	Base metal	0.17	0.45	14.20	6.00	88.10
11680B-9.FIN2	Base metal	0.09	-	4.65	202.40	2290.00
11680B-10.FIN2	Base metal	LLQ	-	1.08	24.30	510.00
11680B-11.FIN2	Base metal	LLQ	0.62	1.14	11.60	300.00
11680B-12.FIN2	Base metal	0.12	X	2.20	1.10	175.00
11680B-14.FIN2	Base metal	LLQ	0.29	2.60	10.65	319.00
11680B-15.FIN2	Base metal	-	0.43	1.23	41.40	652.00
11680B-16.FIN2	Base metal	-	0.52	0.67	1.45	313.00
11680B-17.FIN2	Base metal	0.07	LLQ	13.60	120.30	1163.00
11238-11.FIN2	Base metal	1.66	0.22	3.25	143.00	830.00
11238-12.FIN2	Base metal	1.37	3.80	201.00	126.00	517.00
21931-1.FIN2	Base metal	0.81	LLQ	2.40	93.00	310.00
21931-2.FIN2	Base metal	0.38	X	4.80	2.56	18.60
21931-3.FIN2	Base metal	-	13.00	-	14.40	32.60
21931-4.FIN2	Base metal	-	X	3.90	2.60	20.10
21931-5.FIN2	Base metal	LLQ	3.10	9.50	12.00	18.10
21931-6.FIN2	Base metal	-	X	LLQ	4.90	28.90
21931-7.FIN2	Base metal	X	2.10	1.60	9.00	25.00
21931-8.FIN2	Base metal	0.41	1.26	18.80	0.91	10.00
21931-9.FIN2	Base metal	0.64	3.20	2.20	7.00	9.00
21931-10.FIN2	Base metal	0.40	X	0.90	8.80	36.00
21931-11.FIN2	Base metal	LLQ	X	4.80	5.02	31.00
21931-12.FIN2	Base metal	-	11.00	7.00	3.06	11.20
21931-13.FIN2	Base metal	-	0.40	LLQ	1.51	9.80
10144a-1.FIN2	Base metal	X	11.50	21.60	X	X

LA-ICP-MS data for pyrite. Values are in ppm. Data below detection limit are indicated by (-) and other discarded data (due to interference) are indicated by an "X".
LLQ = below limit of quantation (see section 2.4.3)

Sample ID	Phase	⁶¹ Ni	⁶⁵ Cu	⁶⁶ Zn	⁷⁵ As	⁹⁵ Mo	⁹⁸ Mo
7308-1.FIN2	Early diagenesis	840.00	LLQ	820.00	1440.00	121.00	102.00
7308-2.FIN2	Early diagenesis	1900.00	212.00	1210.00	5030.00	99.00	120.00
7308-3.FIN2	Early diagenesis	3240.00	297.00	X	2350.00	217.00	214.00
7308-4.FIN2	Early diagenesis	1250.00	138.00	X	1450.00	LLQ	0.49
7308-5.FIN2	Early diagenesis	1940.00	450.00	LLQ	2400.00	1.71	1.42
7308-6.FIN2	Early diagenesis	X	260.00	X	X	X	X
7308-7.FIN2	Early diagenesis	X	-	221.00	1050.00	4.00	-
7308-8.FIN2	Early diagenesis	X	72.00	206.00	1960.00	X	-
7308-9.FIN2	Early diagenesis	1930.00	1870.00	X	7200.00	LLQ	LLQ
7308-10.FIN2	Early diagenesis	X	139.00	360.00	2300.00	11.00	-
7308-11.FIN2	Early diagenesis	X	114.00	530.00	3050.00	37.00	LLQ
7308-12.FIN2	Early diagenesis	X	-	-	800.00	-	-
7308-13.FIN2	Early diagenesis	X	136.00	600.00	2060.00	22.00	LLQ
11454-6.FIN2	Early diagenesis	1210.00	177.00	31.70	2350.00	194.00	204.00
11454-7.FIN2	Early diagenesis	1720.00	286.00	X	3520.00	223.00	232.00
11454-9.FIN2	Early diagenesis	400.00	3700.00	67.70	14600.00	123.00	134.00
11454-10.FIN2	Early diagenesis	580.00	2040.00	51.30	2540.00	65.50	68.00
11680B-2.FIN2	Base metal	214.00	35.30	7.01	1681.00	75.40	76.80
11680B-3.FIN2	Base metal	353.00	17.50	6.95	2552.00	172.00	173.00
11680B-4.FIN2	Base metal	773.00	1.23	6.86	2530.00	109.80	114.10
11680B-5.FIN2	Base metal	1328.00	4.69	6.48	3026.00	138.00	140.30
11680B-6.FIN2	Base metal	206.00	33.10	7.27	1970.00	78.60	79.40
11680B-7.FIN2	Base metal	216.00	4.21	6.01	2250.00	100.60	99.20
11680B-8.FIN2	Base metal	82.00	14.00	4.64	3820.00	231.60	235.30
11680B-9.FIN2	Base metal	2129.00	3.98	8.23	4890.00	333.00	341.00
11680B-10.FIN2	Base metal	485.00	33.50	7.24	2020.00	92.70	94.90
11680B-11.FIN2	Base metal	295.00	23.50	7.07	2129.00	96.30	100.40
11680B-12.FIN2	Base metal	175.00	22.60	6.89	1740.00	65.30	65.60
11680B-14.FIN2	Base metal	314.10	13.20	6.34	2250.00	111.00	111.20
11680B-15.FIN2	Base metal	628.00	6.14	8.68	4770.00	431.00	444.00
11680B-16.FIN2	Base metal	319.00	29.70	7.25	1624.00	80.50	81.60
11680B-17.FIN2	Base metal	1136.00	3.11	6.89	2650.00	108.20	109.30
11238-11.FIN2	Base metal	880.00	41.00	6.36	3220.00	115.00	110.00
11238-12.FIN2	Base metal	460.00	66.00	37.00	-	88.00	88.00
21931-1.FIN2	Base metal	300.00	53.00	2.10	7300.00	14.20	15.30
21931-2.FIN2	Base metal	24.00	2.50	1.17	47.00	4.27	4.23
21931-3.FIN2	Base metal	16.00	4.20	-	134.00	3.80	2.24
21931-4.FIN2	Base metal	20.00	1.33	LLQ	49.00	3.10	3.53
21931-5.FIN2	Base metal	18.00	3.10	1.59	134.00	10.00	10.30
21931-6.FIN2	Base metal	24.40	LLQ	0.96	57.70	2.84	2.90
21931-7.FIN2	Base metal	-	26.00	1.10	150.00	4.65	4.34
21931-8.FIN2	Base metal	-	8.20	3.00	25.10	3.15	3.01
21931-9.FIN2	Base metal	-	24.00	2.60	1600.00	3.36	4.00
21931-10.FIN2	Base metal	47.00	15.00	0.98	500.00	3.00	2.82
21931-11.FIN2	Base metal	31.00	1.00	2.40	600.00	2.18	1.98
21931-12.FIN2	Base metal	47.00	4.50	2.40	1000.00	2.33	1.90
21931-13.FIN2	Base metal	15.20	2.32	1.90	20.30	2.07	2.15
10144a-1.FIN2	Base metal	X	83.00	7.50	1520.00	X	-

LA-ICP-MS data for pyrite. Values are in ppm. Data below detection limit are indicated by (-) and other discarded data (due to interference) are indicated by an "X".
LLQ = below limit of quantation (see section 2.4.3)

Sample ID	Phase	⁵¹ V	⁵² Cr	⁵⁵ Mn	⁵⁹ Co	⁶⁰ Ni
10144a-2.FIN2	Base metal	X	11.70	35.00	2.20	25.00
10144a-3.FIN2	Base metal	-	-	3.90	X	LLQ
10144a-4.FIN2	Base metal	LLQ	-	X	3.40	71.00
10144a-5.FIN2	Base metal	LLQ	-	X	X	X
10144a-6.FIN2	Base metal	-	6.20	12.71	X	-
10144a-7.FIN2	Base metal	X	1.80	10.40	8.40	58.00
10144a-8.FIN2	Base metal	-	-	-	X	9.40
10144a-9.FIN2	Base metal	X	-	LLQ	3.70	5.90
10144a-10.FIN2	Base metal	X	-	9.60	X	6.50
10144a-11.FIN2	Base metal	0.62	-	45.00	4.50	15.00
10144a-12.FIN2	Base metal	5.40	1100.00	X	20.60	220.00
10144a-13.FIN2	Base metal	-	73.00	X	-	17.30
10144a-14.FIN2	Base metal	-	5.00	17.70	-	5.40
10144a-15.FIN2	Base metal	-	-	17.20	X	-
11238-1.FIN2	Ore Stage	91.00	34.00	121.00	550.00	2870.00
11238-2.FIN2	Ore Stage	0.53	1.00	4.10	52.40	1430.00
11238-3.FIN2	Ore Stage	117.00	X	1150.00	53.00	460.00
11238-4.FIN2	Ore Stage	33.00	390.00	1050.00	4.00	1900.00
11238-5.FIN2	Ore Stage	144.00	420.00	2420.00	212.00	1920.00
11238-6.FIN2	Ore Stage	500.00	2400.00	11600.00	240.00	200.00
11238-7.FIN2	Ore Stage	25.00	X	1110.00	211.00	1220.00
11238-10.FIN2	Ore Stage	160.00	1100.00	5500.00	78.00	1800.00
11680B-1.FIN2	Ore stage	0.65	0.91	5.98	346.00	441.00
11680B-13.FIN2	Ore stage	0.34	0.99	25.70	76.00	676.00
11454-1.FIN2	Ore stage	9.50	X	10.60	421.00	1300.00
11454-2.FIN2	Ore stage	13.80	27.50	73.00	140.00	840.00
11454-3.FIN2	Ore stage	2.01	6.90	45.90	349.00	1530.00
11454-4.FIN2	Ore stage	1.13	X	80.00	252.00	1640.00
11454-5.FIN2	Ore stage	3.70	X	6.30	193.00	1170.00
11454-8.FIN2	Ore stage	0.68	X	X	50.00	940.00

LA-ICP-MS data for pyrite. Values are in ppm. Data below detection limit are indicated by (-) and other discarded data (due to interference) are indicated by an "X".
LLQ = below limit of quantation (see section 2.4.3)

Sample ID	Phase	⁵¹ V	⁵² Cr	⁵⁵ Mn	⁵⁹ Co	⁶⁰ Ni		
10144a-2.FIN2	Base metal		26.00	350.00	8.60	8900.00	-	-
10144a-3.FIN2	Base metal		16.40	124.00	23.40	7710.00	-	-
10144a-4.FIN2	Base metal		45.00	560.00	102.00	30200.00	LLQ	0.20
10144a-5.FIN2	Base metal		X	540.00	15.20	4400.00	LLQ	LLQ
10144a-6.FIN2	Base metal		-	119.00	17.70	3790.00	X	X
10144a-7.FIN2	Base metal		60.00	122.00	15.40	2620.00	-	-
10144a-8.FIN2	Base metal		17.00	52.10	6.40	720.00	LLQ	-
10144a-9.FIN2	Base metal		7.00	32.20	19.50	2680.00	-	X
10144a-10.FIN2	Base metal		15.00	87.00	14.70	2460.00	X	-
10144a-11.FIN2	Base metal		4.00	6.60	6.60	1800.00	0.80	0.80
10144a-12.FIN2	Base metal		X	42.00	25.00	24000.00	10.00	3.10
10144a-13.FIN2	Base metal		19.40	3.40	2.96	350.00	-	X
10144a-14.FIN2	Base metal		5.30	42.00	29.50	6470.00	-	-
10144a-15.FIN2	Base metal		10.10	18.20	26.60	3510.00	-	-
11238-1.FIN2	Ore Stage		2500.00	317.00	23.50	X	143.00	146.00
11238-2.FIN2	Ore Stage		1210.00	68.00	17.10	16800.00	266.00	265.00
11238-3.FIN2	Ore Stage		500.00	140.00	130.00	X	2.00	9.00
11238-4.FIN2	Ore Stage		2400.00	136.00	120.00	X	X	X
11238-5.FIN2	Ore Stage		4500.00	960.00	320.00	X	X	14.00
11238-6.FIN2	Ore Stage		X	3800.00	1300.00	X	220.00	240.00
11238-7.FIN2	Ore Stage		X	310.00	50.00	X	X	X
11238-10.FIN2	Ore Stage		1400.00	2190.00	400.00	X	60.00	55.00
11680B-1.FIN2	Ore stage		450.00	109.00	5.07	4600.00	50.60	50.90
11680B-13.FIN2	Ore stage		652.00	27.00	5.57	17000.00	93.40	96.00
11454-1.FIN2	Ore stage		1170.00	267.00	32.30	2890.00	242.00	258.00
11454-2.FIN2	Ore stage		700.00	206.00	41.00	2900.00	100.00	121.00
11454-3.FIN2	Ore stage		1285.00	216.00	106.00	2390.00	256.00	272.00
11454-4.FIN2	Ore stage		1380.00	214.00	107.00	2660.00	271.00	280.00
11454-5.FIN2	Ore stage		1100.00	142.00	85.00	3230.00	223.00	232.00
11454-8.FIN2	Ore stage		880.00	2290.00	109.90	2230.00	75.90	76.50

LA-ICP-MS data for pyrite. Values are in ppm. Data below detection limit are indicated by (-) and other discarded data (due to interference) are indicated by an "X".
LLQ = below limit of quantitation (see section 2.4.3)

Sample ID	Phase	¹⁰⁷ Ag	¹⁰⁹ Ag	¹¹¹ Cd	¹¹⁴ Cd	¹²¹ Sb	¹²³ Sb
7308-1.FIN2	Early diagenesis	X	-	-	16.00	6.80	-
7308-2.FIN2	Early diagenesis	X	-	-	27.00	-	-
7308-3.FIN2	Early diagenesis	10.80	12.00	-	-	6.48	6.40
7308-4.FIN2	Early diagenesis	0.37	0.49	X	X	0.64	0.64
7308-5.FIN2	Early diagenesis	1.16	1.57	0.14	X	6.60	6.60
7308-6.FIN2	Early diagenesis	X	X	93.00	150.00	-	-
7308-7.FIN2	Early diagenesis	-	-	15.00	-	4.60	X
7308-8.FIN2	Early diagenesis	X	-	-	-	2.10	-
7308-9.FIN2	Early diagenesis	5.40	4.70	-	0.50	10.30	8.30
7308-10.FIN2	Early diagenesis	-	X	11.00	12.00	-	-
7308-11.FIN2	Early diagenesis	-	-	-	8.00	-	X
7308-12.FIN2	Early diagenesis	-	-	-	-	-	-
7308-13.FIN2	Early diagenesis	-	-	-	11.90	-	6.70
11454-6.FIN2	Early diagenesis	3.80	3.67	0.56	0.74	7.50	7.10
11454-7.FIN2	Early diagenesis	5.23	5.25	1.08	1.63	7.07	7.23
11454-9.FIN2	Early diagenesis	6.80	6.90	1.84	2.01	45.00	42.00
11454-10.FIN2	Early diagenesis	7.40	8.10	0.89	1.36	43.00	38.30
11680B-2.FIN2	Base metal	1.76	1.84	LLQ	0.04	8.22	8.33
11680B-3.FIN2	Base metal	0.33	0.43	0.05	0.03	12.31	12.16
11680B-4.FIN2	Base metal	X	-	-	0.04	28.50	27.42
11680B-5.FIN2	Base metal	0.05	LLQ	0.05	0.06	36.58	36.70
11680B-6.FIN2	Base metal	0.96	0.83	LLQ	0.04	9.16	8.97
11680B-7.FIN2	Base metal	LLQ	LLQ	LLQ	LLQ	12.23	12.40
11680B-8.FIN2	Base metal	0.08	0.08	-	0.04	7.21	7.52
11680B-9.FIN2	Base metal	-	-	0.08	-	33.37	34.50
11680B-10.FIN2	Base metal	1.72	1.62	LLQ	0.03	12.24	11.75
11680B-11.FIN2	Base metal	0.62	0.59	-	LLQ	10.43	10.39
11680B-12.FIN2	Base metal	1.15	1.22	LLQ	-	7.37	7.52
11680B-14.FIN2	Base metal	0.26	0.23	LLQ	LLQ	11.67	11.85
11680B-15.FIN2	Base metal	0.21	0.23	-	0.03	25.73	25.18
11680B-16.FIN2	Base metal	2.29	2.02	LLQ	0.04	12.51	12.49
11680B-17.FIN2	Base metal	LLQ	0.04	LLQ	0.03	19.25	19.09
11238-11.FIN2	Base metal	1.60	1.37	0.64	0.57	21.60	21.60
11238-12.FIN2	Base metal	3.40	4.49	-	0.71	9.00	8.34
21931-1.FIN2	Base metal	0.64	0.30	1.09	0.39	15.80	17.30
21931-2.FIN2	Base metal	0.02	X	-	0.21	3.87	3.54
21931-3.FIN2	Base metal	0.06	0.28	X	-	0.76	0.25
21931-4.FIN2	Base metal	-	-	-	0.23	4.69	4.59
21931-5.FIN2	Base metal	-	LLQ	-	0.29	5.70	5.02

LA-ICP-MS data for pyrite. Values are in ppm. Data below detection limit are indicated by (-) and other discarded data (due to interference) are indicated by an "X".
LLQ = below limit of quantation (see section 2.4.3)

Sample ID	Phase	¹⁹⁷ Au	²⁰² Hg	²⁰⁵ Tl	²⁰⁴ Pb	²⁰⁷ Pb	²⁰⁹ Bi
7308-1.FIN2	Early diagenesis	-	-	2.20	77.00	200.00	-
7308-2.FIN2	Early diagenesis	X	-	X	77.00	391.00	-
7308-3.FIN2	Early diagenesis	0.69	7.10	5.40	29.20	141.00	15.70
7308-4.FIN2	Early diagenesis	-	0.18	LLQ	6.60	43.00	0.65
7308-5.FIN2	Early diagenesis	0.18	0.65	LLQ	42.00	270.00	1.12
7308-6.FIN2	Early diagenesis	X	140.00	21.00	X	X	16.00
7308-7.FIN2	Early diagenesis	-	-	1.90	-	36.00	-
7308-8.FIN2	Early diagenesis	-	-	2.40	27.00	122.00	-
7308-9.FIN2	Early diagenesis	0.80	3.20	2.00	58.00	321.00	12.70
7308-10.FIN2	Early diagenesis	X	13.90	2.30	-	129.00	-
7308-11.FIN2	Early diagenesis	-	-	LLQ	60.00	257.00	-
7308-12.FIN2	Early diagenesis	X	-	3.00	-	44.00	-
7308-13.FIN2	Early diagenesis	X	-	7.90	21.00	96.00	-
11454-6.FIN2	Early diagenesis	0.89	4.99	9.70	25.00	91.00	0.31
11454-7.FIN2	Early diagenesis	0.66	12.10	18.50	61.20	226.00	1.70
11454-9.FIN2	Early diagenesis	0.61	34.40	13.20	141.00	500.00	7.30
11454-10.FIN2	Early diagenesis	0.70	33.60	4.59	92.00	278.00	5.20
11680B-2.FIN2	Base metal	0.03	1.57	8.04	2.02	2.30	-
11680B-3.FIN2	Base metal	0.08	1.74	7.71	2.35	1.72	-
11680B-4.FIN2	Base metal	0.28	1.45	14.92	3.42	10.20	-
11680B-5.FIN2	Base metal	0.39	2.11	21.90	7.33	24.60	-
11680B-6.FIN2	Base metal	0.03	2.32	7.28	4.25	9.40	-
11680B-7.FIN2	Base metal	0.77	2.04	6.42	2.68	0.82	-
11680B-8.FIN2	Base metal	0.09	2.47	30.70	9.10	27.30	-
11680B-9.FIN2	Base metal	0.52	3.41	13.50	9.73	27.00	LLQ
11680B-10.FIN2	Base metal	0.06	2.14	8.62	2.59	2.56	-
11680B-11.FIN2	Base metal	0.05	2.13	6.23	2.89	3.30	-
11680B-12.FIN2	Base metal	0.04	2.61	6.35	3.02	1.69	-
11680B-14.FIN2	Base metal	0.06	1.98	6.46	2.53	1.50	-
11680B-15.FIN2	Base metal	0.21	3.84	10.82	5.25	4.00	LLQ
11680B-16.FIN2	Base metal	0.06	3.71	9.79	3.94	0.04	-
11680B-17.FIN2	Base metal	0.23	3.79	15.19	6.81	10.60	-
11238-11.FIN2	Base metal	0.50	16.90	28.00	63.00	178.00	3.80
11238-12.FIN2	Base metal	0.43	6.80	22.00	22.60	49.30	1.56
21931-1.FIN2	Base metal	LLQ	5.10	13.20	18.20	68.00	0.47
21931-2.FIN2	Base metal	0.05	-	0.60	0.49	1.27	X
21931-3.FIN2	Base metal	LLQ	1.90	1.90	3.70	11.30	0.13
21931-4.FIN2	Base metal	0.07	0.53	2.80	0.84	1.42	-
21931-5.FIN2	Base metal	LLQ	0.37	2.60	1.70	5.20	0.03

LA-ICP-MS data for pyrite. Values are in ppm. Data below detection limit are indicated by (-) and other discarded data (due to interference) are indicated by an "X".
LLQ = below limit of quantation (see section 2.4.3)

Sample ID	Phase	¹⁰⁷ Ag	¹⁰⁹ Ag	¹¹¹ Cd	¹¹⁴ Cd	¹²¹ Sb	¹²³ Sb
21931-6.FIN2	Base metal	-	-	0.08	-	4.43	4.27
21931-7.FIN2	Base metal	-	X	0.29	0.64	1.74	1.71
21931-8.FIN2	Base metal	-	-	0.22	0.16	1.46	1.59
21931-9.FIN2	Base metal	LLQ	0.14	LLQ	0.63	3.70	3.20
21931-10.FIN2	Base metal	-	-	0.24	-	1.90	2.19
21931-11.FIN2	Base metal	X	-	-	0.28	1.64	2.22
21931-12.FIN2	Base metal	X	X	-	X	2.31	2.11
21931-13.FIN2	Base metal	X	-	-	-	0.75	0.68
10144a-1.FIN2	Base metal	0.15	0.09	0.21	-	0.12	0.14
10144a-2.FIN2	Base metal	0.56	0.35	NA	NA	2.20	2.50
10144a-3.FIN2	Base metal	0.48	0.55	0.32	0.33	1.60	1.55
10144a-4.FIN2	Base metal	1.93	1.85	0.39	-	9.20	9.60
10144a-5.FIN2	Base metal	0.51	0.66	0.29	0.34	1.39	1.30
10144a-6.FIN2	Base metal	0.16	0.20	0.51	-	0.53	0.52
10144a-7.FIN2	Base metal	0.21	0.27	LLQ	LLQ	2.51	2.41
10144a-8.FIN2	Base metal	X	X	-	0.20	0.05	-
10144a-9.FIN2	Base metal	-	0.09	0.40	0.40	0.44	0.51
10144a-10.FIN2	Base metal	0.13	0.11	-	0.27	0.95	0.97
10144a-11.FIN2	Base metal	0.51	0.41	X	X	1.27	0.78
10144a-12.FIN2	Base metal	X	X	-	1.60	15.00	7.40
10144a-13.FIN2	Base metal	-	0.08	0.11	0.40	0.36	0.32
10144a-14.FIN2	Base metal	0.36	0.28	0.39	0.34	1.34	1.35
10144a-15.FIN2	Base metal	0.22	0.12	0.32	0.37	0.20	0.26
11238-1.FIN2	Ore Stage	21.00	15.10	2.40	1.97	690.00	670.00
11238-2.FIN2	Ore Stage	2.40	2.62	LLQ	0.21	43.00	42.00
11238-3.FIN2	Ore Stage	17.00	2.10	X	4.50	40.00	44.00
11238-4.FIN2	Ore Stage	30.00	18.00	21.00	7.00	29.00	21.00
11238-5.FIN2	Ore Stage	34.00	74.00	4.90	26.00	174.00	200.00
11238-6.FIN2	Ore Stage	200.00	X	50.00	53.00	4000.00	4000.00
11238-7.FIN2	Ore Stage	45.00	36.00	1.83	X	96.00	83.00
11238-10.FIN2	Ore Stage	15.00	4.30	-	36.00	1330.00	1320.00
11680B-1.FIN2	Ore stage	1.75	1.71	0.14	0.14	20.30	20.50
11680B-13.FIN2	Ore stage	0.34	0.33	0.10	0.10	19.07	18.97
11454-1.FIN2	Ore stage	5.60	6.60	-	LLQ	6.10	6.70
11454-2.FIN2	Ore stage	7.60	7.80	0.26	-	10.80	11.30
11454-3.FIN2	Ore stage	9.40	8.30	0.25	0.31	13.40	13.00
11454-4.FIN2	Ore stage	12.80	12.50	0.40	0.51	10.50	10.80
11454-5.FIN2	Ore stage	2.79	2.82	0.94	0.99	8.50	9.20
11454-8.FIN2	Ore stage	12.70	11.40	3.20	3.40	15.90	16.10

LA-ICP-MS data for pyrite. Values are in ppm. Data below detection limit are indicated by (-) and other discarded data (due to interference) are indicated by an "X".

LLQ = below limit of quantation (see section 2.4.3)

Sample ID	Phase	¹⁹⁷ Au	²⁰² Hg	²⁰⁵ Tl	²⁰⁴ Pb	²⁰⁷ Pb	²⁰⁹ Bi
21931-6.FIN2	Base metal	0.04	-	0.67	0.87	2.08	-
21931-7.FIN2	Base metal	0.04	0.90	3.40	2.00	7.60	0.01
21931-8.FIN2	Base metal	-	0.23	0.86	0.55	1.89	X
21931-9.FIN2	Base metal	0.12	4.10	2.70	26.00	36.00	0.33
21931-10.FIN2	Base metal	-	0.13	1.90	1.50	6.60	LLQ
21931-11.FIN2	Base metal	-	1.40	0.68	3.50	3.60	-
21931-12.FIN2	Base metal	-	1.80	0.55	2.40	4.90	-
21931-13.FIN2	Base metal	-	0.07	0.42	0.54	2.02	X
10144a-1.FIN2	Base metal	X	-	7.40	140.00	700.00	-
10144a-2.FIN2	Base metal	0.16	6.00	25.00	119.00	490.00	0.01
10144a-3.FIN2	Base metal	0.01	0.34	22.80	785.00	3560.00	-
10144a-4.FIN2	Base metal	0.39	11.40	49.10	60.00	217.00	0.01
10144a-5.FIN2	Base metal	0.13	1.75	18.70	344.00	1680.00	0.01
10144a-6.FIN2	Base metal	NA	0.17	19.41	476.00	2306.00	-
10144a-7.FIN2	Base metal	-	0.53	11.40	250.00	1110.00	0.01
10144a-8.FIN2	Base metal	X	-	4.05	67.00	350.00	-
10144a-9.FIN2	Base metal	-	0.34	22.40	569.00	2620.00	-
10144a-10.FIN2	Base metal	0.03	1.02	16.00	295.00	1270.00	0.01
10144a-11.FIN2	Base metal	0.02	3.50	23.90	24.00	79.00	0.02
10144a-12.FIN2	Base metal	0.10	19.00	105.00	80.00	330.00	0.02
10144a-13.FIN2	Base metal	-	0.62	10.50	6.20	27.00	-
10144a-14.FIN2	Base metal	-	0.34	31.70	1028.00	4310.00	-
10144a-15.FIN2	Base metal	X	0.19	22.20	694.00	2810.00	X
11238-1.FIN2	Ore Stage	54.00	360.00	1380.00	470.00	490.00	4.20
11238-2.FIN2	Ore Stage	2.70	18.50	75.00	37.00	68.00	0.39
11238-3.FIN2	Ore Stage	0.80	55.00	490.00	610.00	1750.00	0.19
11238-4.FIN2	Ore Stage	-	164.00	600.00	2000.00	7600.00	0.55
11238-5.FIN2	Ore Stage	15.00	320.00	780.00	1570.00	7300.00	6.60
11238-6.FIN2	Ore Stage	203.00	5800.00	X	6700.00	5000.00	1.70
11238-7.FIN2	Ore Stage	X	101.00	250.00	1390.00	4600.00	0.46
11238-10.FIN2	Ore Stage	37.00	2250.00	6600.00	3100.00	4200.00	6.80
11680B-1.FIN2	Ore stage	3.07	15.80	73.90	42.70	153.00	0.05
11680B-13.FIN2	Ore stage	2.40	35.00	58.00	44.00	22.00	0.06
11454-1.FIN2	Ore stage	1.04	7.80	10.80	84.40	395.00	1.14
11454-2.FIN2	Ore stage	1.98	6.10	7.40	116.00	570.00	0.43
11454-3.FIN2	Ore stage	1.13	9.06	47.30	63.30	276.00	0.84
11454-4.FIN2	Ore stage	5.20	9.87	45.90	97.40	434.00	0.58
11454-5.FIN2	Ore stage	1.27	7.06	13.60	24.50	82.50	0.33
11454-8.FIN2	Ore stage	1.00	57.30	4.61	121.20	256.00	5.40

Appendix F – SIMS Data

SIMS Data for host rocks and all carbonate phases. Values are in ‰. FeO data is from EMPA on adjacent spot ("-" denotes values below detection). $\delta^{18}\text{O}$ (SMOW)* column is Fe-corrected data as described in Chapter 2.4.5. NA denotes spots which were not analyzed.

Comment	Phase	$\delta^{13}\text{C}$ (PDB)	$\delta^{18}\text{O}$ (SMOW)	FeO (wt%)	$\delta^{18}\text{O}$ (SMOW)*
P1419B_M1299_IP14070_18O160_S3104B_3_calh@1 (OS-11-80 73.08)	Host rock	-12.32	20.54	0.13	NA
P1419B_M1299_IP14070_18O160_S3104B_3_Cal4@2 (OS-11-80 73.08)	Host rock		20.60	NA	NA
P1419B_M1299_IP14070_18O160_S3106A_3_Calh@1 (OS-11-83 123.84)	Host rock	-9.57	21.61	-	NA
P1419B_M1299_IP14070_18O160_S3106A_3_Calh@2 (OS-11-83 123.84)	Host rock	-8.48	21.75	-	NA
P1419B_M1299_IP14070_18O160_S3107A_2_Calh@1 (OS-12-120 43.37)	Host rock	-8.49	20.16	0.13	NA
P1419B_M1299_IP14070_18O160_S3107A_2_Calh@2 (OS-12-120 43.37)	Host rock	-8.47	20.08	0.05	NA
P1419B_M1299_IP14070_18O160_S3107A_4_Calh@1 (OS-12-120 43.37)	Host rock	-8.95	19.81	0.08	NA
P1419B_M1299_IP14070_18O160_S3107A_4_Calh@2 (OS-12-120 43.37)	Host rock	-8.96	19.57	0.38	NA
P1419B_M1299_IP14070_18O160_S3107A_4_Calh@3 (OS-12-120 43.37)	Host rock	-3.53	19.62	0.94	NA
P1419B_M1299_IP14070_18O160_S3107C_1_Calh@1 (OS-12-120 43.37)	Host rock	-6.73	20.40	1.22	NA
P1419B_M1299_IP14070_18O160_S3107C_1_Calh@2 (OS-12-120 43.37)	Host rock	-8.06	20.09	-	NA
P1419D_M1299_IP14078E_13C12C_S3104B_3_Calh@3 (OS-11-80 73.08)	Host rock	-12.12	NA	0.18	NA
P1419D_M1299_IP14078E_13C12C_S3107C_1_Calh@3 (OS-12-120 43.37)	Host rock	-8.19	NA	0.14	NA
P1419B_M1299_IP14070_18O160_S3106B_3_Calh@1 (OS-11-83 123.84)	Host rock	-9.51	21.47	NA	NA
P1419B_M1299_IP14070_18O160_S3106B_1_Calh@1 (OS-11-83 123.84)	Host rock		21.91	NA	NA
P1419B_M1299_IP14070_18O160_S3106B_3_Calh@2 (OS-11-83 123.84)	Host rock	-9.34	20.88	NA	NA
P1419A_M1299_IP14070_18O160_S3106B_2_Doll@1 (OS-11-83 123.84)	Dol 1	-6.59	27.81	6.32	23.83
P1419A_M1299_IP14070_18O160_S3106A_3_Doll@1 (OS-11-83 123.84)	Dol 1	-5.39	27.84	4.07	25.28
P1419A_M1299_IP14070_18O160_S3106B_1_Doll@1 (OS-11-83 123.84)	Dol 1	-4.82	28.04	4.65	25.12
P1419A_M1299_IP14070_18O160_S3106A_2_Doll@1 (OS-11-83 123.84)	Dol 1	-4.90	30.91	3.10	28.95
P1419A_M1299_IP14070_18O160_S3106A_1_Doll@1 (OS-11-83 123.84)	Dol 1	-4.72	33.77	1.06	33.10
P1419A_M1299_IP14070_18O160_S3106B_2_Doll@3 (OS-11-83 123.84)	Dol 1	-5.38	25.46	7.27	20.88
P1419A_M1299_IP14070_18O160_S3106B_3_Doll@2 (OS-11-83 123.84)	Dol 1	-6.55	25.24	2.45	23.69
P1419A_M1299_IP14070_18O160_S3104A_1_Doll@2 (OS-11-80 73.08)	Dol 1	NA	24.20	NA	NA
P1419A_M1299_IP14070_18O160_S3104A_2_Doll@1 (OS-11-80 73.08)	Dol 1	NA	24.50	NA	NA
P1419A_M1299_IP14070_18O160_S3106B_1_Doll@2 (OS-11-83 123.84)	Dol 1	NA	26.38	7.57	21.61
P1419C_M1299_IP14070_18O160_S3104A_1_Doll@1 (OS-11-80 73.08)	Dol 1	NA	27.01	NA	NA
P1419C_M1299_IP14078_13C12C_S3104A_1_Doll@4 (OS-11-80 73.08)	Dol 1	-8.16	NA	NA	NA
P1419C_M1299_IP14078_13C12C_S3104A_1_Doll@3 (OS-11-80 73.08)	Dol 1	-8.66	NA	NA	NA
P1419C_M1299_IP14078_13C12C_S3104A_2_Doll@3 (OS-11-80 73.08)	Dol 1	-4.09	NA	4.70	NA
P1419C_M1299_IP14078_13C12C_S3106B_3_Doll@3 (OS-11-83 123.84)	Dol 1	-7.47	NA	5.72	NA
P1419C_M1299_IP14078_13C12C_S3106A_2_Doll@3 (OS-11-83 123.84)	Dol 1	-1.94	NA	3.34	NA
P1419C_M1299_IP14078_13C12C_S3106A_2_Doll@2 (OS-11-83 123.84)	Dol 1	-4.65	NA	NA	NA

SIMS Data for host rocks and all carbonate phases. Values are in ‰. FeO data is from EMPA on adjacent spot ("-" denotes values below detection). $\delta^{18}\text{O}$ (SMOW)* column is Fe-corrected data as described in Chapter 2.4.5. NA denotes spots which were not analyzed.

Comment	Phase	$\delta^{13}\text{C}$ (PDB)	$\delta^{18}\text{O}$ (SMOW)	FeO (wt%)	$\delta^{18}\text{O}$ (SMOW)*
P1419B_M1299_IP14070_18O160_S3109A_1_Cal@1 (OS-11-80 108.16)	Cal 1	-0.02	10.17	0.10	NA
P1419B_M1299_IP14070_18O160_S3109A_1_Cal@2 (OS-11-80 108.16)	Cal 1	-0.46	10.34	0.12	NA
P1419B_M1299_IP14070_18O160_S3109A_1_Cal@3 (OS-11-80 108.16)	Cal 1	-0.87	10.07	0.09	NA
P1419B_M1299_IP14070_18O160_S3109A_1_Cal@4 (OS-11-80 108.16)	Cal 1	-1.11	10.21	0.08	NA
P1419A_M1299_IP14070_18O160_S3105B_1_Dol2@1 (OS-11-80 176.03)	Dol 2	-0.72	19.34	-	19.34
P1419A_M1299_IP14070_18O160_S3105B_2_Dol2@1 (OS-11-80 176.03)	Dol 2	-5.48	19.61	0.70	19.17
P1419A_M1299_IP14070_18O160_S3103A_1_Dol2@1 (OS-11-41 342.97)	Dol 2	-4.51	22.78	0.35	22.56
P1419A_M1299_IP14070_18O160_S3103A_2_Dol2@1 (OS-11-41 342.97)	Dol 2	-7.58	22.93	0.64	22.52
P1419A_M1299_IP14070_18O160_S3103A_2_Dol2@3 (OS-11-41 342.97)	Dol 2	-2.55	22.94	0.76	22.46
P1419A_M1299_IP14070_18O160_S3103A_1_Dol2@3 (OS-11-41 342.97)	Dol 2	-2.37	23.04	0.68	22.61
P1419A_M1299_IP14070_18O160_S3103A_1_Dol2@4 (OS-11-41 342.97)	Dol 2	-6.29	23.35	0.50	23.03
P1419A_M1299_IP14070_18O160_S3103A_1_Dol2@5 (OS-11-41 342.97)	Dol 2	-7.44	23.44	0.71	22.99
P1419A_M1299_IP14070_18O160_S3103A_2_Dol2@2 (OS-11-41 342.97)	Dol 2	-3.40	23.45	0.78	22.96
P1419A_M1299_IP14070_18O160_S3103A_1_Dol2@2 (OS-11-41 342.97)	Dol 2	-2.14	23.67	0.58	23.30
P1419A_M1299_IP14070_18O160_S3103B_3_Dol2@1 (OS-11-41 342.97)	Dol 2	-4.98	24.02	0.92	23.44
P1419A_M1299_IP14070_18O160_S3103B_2_Dol2@1 (OS-11-41 342.97)	Dol 2	-3.98	24.02	1.69	22.96
P1419A_M1299_IP14070_18O160_S3103B_1_Dol2@1 (OS-11-41 342.97)	Dol 2	-4.36	24.11	1.28	23.30
P1419A_M1299_IP14070_18O160_S3105A_2_Dol2@1 (OS-11-80 176.03)	Dol 2	-2.94	26.71	3.46	24.53
P1419A_M1299_IP14070_18O160_S3112B_2_Dol2@2 (OS-12-120 138.05)	Dol 2	-7.60	24.53	3.01	22.63
P1419A_M1299_IP14070_18O160_S3112B_3_Dol2@3 (OS-12-120 138.05)	Dol 2	-7.92	25.43	2.48	23.87
P1419A_M1299_IP14070_18O160_S3112B_2_Dol2@1 (OS-12-120 138.05)	Dol 2	-7.54	25.12	3.87	22.68
P1419A_M1299_IP14070_18O160_S3112A_5_Dol2@2 (OS-12-120 138.05)	Dol 2	-7.28	24.85	2.92	23.01
P1419A_M1299_IP14070_18O160_S3112B_3_Dol2@1 (OS-12-120 138.05)	Dol 2	-7.98	25.56	4.30	22.85
P1419A_M1299_IP14070_18O160_S3111A_1_Dol2@2 (OS-11-83 29.91)	Dol 2	-7.61	27.19	4.25	24.51
P1419A_M1299_IP14070_18O160_S3111A_1_Dol2@5 (OS-11-83 29.91)	Dol 2	-7.64	27.63	3.15	25.65
P1419A_M1299_IP14070_18O160_S3112B_2_Dol2@3 (OS-12-120 138.05)	Dol 2	-7.52	25.53	4.02	23.00
P1419A_M1299_IP14070_18O160_S3112A_2_Dol2@2 (OS-12-120 138.05)	Dol 2	-8.89	24.94	2.90	23.11
P1419A_M1299_IP14070_18O160_S3111A_2_Dol2@1 (OS-11-83 29.91)	Dol 2	-8.66	26.59	2.83	24.81
P1419A_M1299_IP14070_18O160_S3111A_2_Dol2@2 (OS-11-83 29.91)	Dol 2	-7.43	26.79	2.99	24.91
P1419A_M1299_IP14070_18O160_S3112A_1_Dol2@2 (OS-12-120 138.05)	Dol 2	-7.02	25.39	3.03	23.49
P1419A_M1299_IP14070_18O160_S3108A_1_Dol2@2 (OS-11-52 6.96)	Dol 2	-7.59	25.56	3.88	23.12
P1419A_M1299_IP14070_18O160_S3112A_5_Dol2@1 (OS-12-120 138.05)	Dol 2	-7.76	24.80	2.98	22.93
P1419A_M1299_IP14070_18O160_S3112B_2_Dol3@3 (OS-12-120 138.05)	Dol 2	-8.39	25.40	3.32	23.31

SIMS Data for host rocks and all carbonate phases. Values are in ‰. FeO data is from EMPA on adjacent spot ("-" denotes values below detection). $\delta^{18}\text{O}$ (SMOW)* column is Fe-corrected data as described in Chapter 2.4.5. NA denotes spots which were not analyzed.

Comment	Phase	$\delta^{13}\text{C}$ (PDB)	$\delta^{18}\text{O}$ (SMOW)	FeO (wt%)	$\delta^{18}\text{O}$ (SMOW)*
P1419A_MI299_IP14070_180160_S3112A_2_Dol2@3 (OS-12-120 138.05)	Dol 2	-8.12	25.52	3.22	23.49
P1419A_MI299_IP14070_180160_S3111A_1_Dol2@1 (OS-11-83 29.91)	Dol 2	-7.37	25.60	3.67	23.29
P1419A_MI299_IP14070_180160_S3112A_1_Dol2@4 (OS-12-120 138.05)	Dol 2	-8.76	24.58	2.94	22.73
P1419A_MI299_IP14070_180160_S3108A_1_Dol2@4 (OS-11-52 6.96)	Dol 2	-7.90	25.89	5.67	22.32
P1419A_MI299_IP14070_180160_S3112A_3_Dol2@1 (OS-12-120 138.05)	Dol 2	-8.39	24.62	3.40	22.48
P1419A_MI299_IP14070_180160_S3112A_1_Dol2@5 (OS-12-120 138.05)	Dol 2	-8.58	24.43	3.08	22.49
P1419A_MI299_IP14070_180160_S3108A_2_Dol2@2 (OS-11-52 6.96)	Dol 2	-7.32	25.83	4.84	22.78
P1419A_MI299_IP14070_180160_S3112A_3_Dol2@2 (OS-12-120 138.05)	Dol 2	-8.15	25.07	4.00	22.55
P1419A_MI299_IP14070_180160_S3103A_1_Dol3@1 (OS-11-41 342.97)	Dol 2	-3.90	22.69	0.04	22.66
P1419A_MI299_IP14070_180160_S3112A_3_Dol3@1 (OS-12-120 138.05)	Dol 2	-7.10	25.38	4.35	22.64
P1419A_MI299_IP14070_180160_S3112A_1_Dol3@1 (OS-12-120 138.05)	Dol 2	-7.29	25.21	4.24	22.54
P1419A_MI299_IP14070_180160_S3112A_2_Dol2@1 (OS-12-120 138.05)	Dol 2	-7.30	25.36	4.32	22.64
P1419A_MI299_IP14070_180160_S3111A_1_Dol2@4 (OS-11-83 29.91)	Dol 2	NA	24.98	4.03	22.44
P1419A_MI299_IP14070_180160_S3111A_1_Dol2@3 (OS-11-83 29.91)	Dol 2	NA	26.68	NA	NA
P1419A_MI299_IP14070_180160_S3108A_2_Dol2@3 (OS-11-52 6.96)	Dol 2	NA	26.19	5.70	22.59
P1419A_MI299_IP14070_180160_S3108A_2_Dol2@1 (OS-11-52 6.96)	Dol 2	NA	26.54	4.89	23.46
P1419A_MI299_IP14070_180160_S3112A_5_Dol2@3 (OS-12-120 138.05)	Dol 2	NA	25.57	3.83	23.16
P1419A_MI299_IP14070_180160_S3108A_1_Dol2@3 (OS-11-52 6.96)	Dol 2	NA	26.25	6.23	22.33
P1419A_MI299_IP14070_180160_S3112A_1_Dol2@1 (OS-12-120 138.05)	Dol 2	NA	25.70	3.49	23.51
P1419A_MI299_IP14070_180160_S3112B_3_Dol3@3 (OS-12-120 138.05)	Dol 2	NA	24.66	NA	NA
P1419A_MI299_IP14070_180160_S3112A_1_Dol2@3 (OS-12-120 138.05)	Dol 2	NA	24.76	3.21	22.74
P1419A_MI299_IP14070_180160_S3112A_3_Dol2@3 (OS-12-120 138.05)	Dol 2	NA	24.91	NA	24.91
P1419A_MI299_IP14070_180160_S3112A_1_Dol2@3 (OS-12-120 138.05)	Dol 2	NA	24.76	NA	24.76
P1419C_MI299_IP14078_13C12C_S3112B_2_Dol3@1 (OS-12-120 138.05)	Dol 2	-7.56	NA	NA	NA
P1419C_MI299_IP14078_13C12C_S3112B_2_Dol3@2 (OS-12-120 138.05)	Dol 2	-9.43	NA	NA	NA
P1419C_MI299_IP14078_13C12C_S3112B_3_Dol2@2 (OS-12-120 138.05)	Dol 2	-7.94	NA	NA	NA
P1419C_MI299_IP14078_13C12C_S3105A_3_Dol2@1 (OS-11-80 176.03)	Dol 2	-3.19	NA	3.99	NA
P1419B_MI299_IP14070_180160_S3110A_1_Cal@1 (OS-11-80 154.24)	Cal 2	-8.93	19.94	-	NA
P1419B_MI299_IP14070_180160_S3110A_1_Cal@2 (OS-11-80 154.24)	Cal 2	-9.18	20.27	-	NA
P1419B_MI299_IP14070_180160_S3110A_1_Cal@3 (OS-11-80 154.24)	Cal 2	-9.39	20.42	-	NA
P1419B_MI299_IP14070_180160_S3111A_1_Cal@1 (OS-11-83 29.91)	Cal 2	-4.94	19.30	0.61	NA
P1419B_MI299_IP14070_180160_S3111A_1_Cal@2 (OS-11-83 29.91)	Cal 2	-4.08	20.92	0.47	NA
P1419B_MI299_IP14070_180160_S3111A_1_Cal@3 (OS-11-83 29.91)	Cal 2	-4.35	20.88	0.24	NA
P1419B_MI299_IP14070_180160_S3108A_1_Cal@1 (OS-11-52 6.96)	Cal 3	-7.19	18.43	0.15	NA

SIMS Data for host rocks and all carbonate phases. Values are in ‰. FeO data is from EMPA on adjacent spot ("-" denotes values below detection). $\delta^{18}\text{O}$ (SMOW)* column is Fe-corrected data as described in Chapter 2.4.5. NA denotes spots which were not analyzed.

Comment	Phase	$\delta^{13}\text{C}$ (PDB)	$\delta^{18}\text{O}$ (SMOW)	FeO (wt%)	$\delta^{18}\text{O}$ (SMOW)*
P1419B_M1299_IP14070_18O160_S3108A_1_Cal@2 (OS-11-52 6.96)	Cal 3	-6.91	18.70	0.17	NA
P1419B_M1299_IP14070_18O160_S3108A_2_Cal@1 (OS-11-52 6.96)	Cal 3	-8.74	19.23	0.24	NA
P1419B_M1299_IP14070_18O160_S3108A_2_Cal@2 (OS-11-52 6.96)	Cal 3	-8.87	17.89	0.31	NA
P1419B_M1299_IP14070_18O160_S3108B_1_Cal@1 (OS-11-52 6.96)	Cal 3	-8.45	20.27	0.19	NA
P1419B_M1299_IP14070_18O160_S3108B_1_Cal@2 (OS-11-52 6.96)	Cal 3	-8.62	20.59	0.19	NA
P1419B_M1299_IP14070_18O160_S3108B_1_Cal@3 (OS-11-52 6.96)	Cal 3	-8.05	20.65	0.21	NA
P1419B_M1299_IP14070_18O160_S3108B_3_Cal@1 (OS-11-52 6.96)	Cal 3	-8.23	20.33	0.19	NA
P1419B_M1299_IP14070_18O160_S3108B_3_Cal@2 (OS-11-52 6.96)	Cal 3	-7.27	20.32	0.16	NA
P1419B_M1299_IP14070_18O160_S3108B_3_Cal@3 (OS-11-52 6.96)	Cal 3	-8.04	18.73	0.09	NA
P1419B_M1299_IP14070_18O160_S3108B_3_Cal@4 (OS-11-52 6.96)	Cal 3	-7.51	20.25	0.11	NA
P1419A_M1299_IP14070_18O160_S3103A_2_Dol3@3 (OS-11-41 342.97)	dol 3	-2.85	18.82	0.16	18.72
P1419A_M1299_IP14070_18O160_S3103A_2_Dol3@1 (OS-11-41 342.97)	dol 3	-3.98	19.54	0.13	19.45
P1419A_M1299_IP14070_18O160_S3105B_1_Dol3@1 (OS-11-80 176.03)	dol 3	-6.08	19.66	0.22	19.52
P1419A_M1299_IP14070_18O160_S3105B_2_Dol3@1 (OS-11-80 176.03)	dol 3	-4.65	19.77	-	19.77
P1419A_M1299_IP14070_18O160_S3103A_1_Dol3@4 (OS-11-41 342.97)	dol 3	-3.84	19.95	0.09	19.89
P1419A_M1299_IP14070_18O160_S3103A_2_Dol3@2 (OS-11-41 342.97)	dol 3	-1.99	19.97	0.68	19.55
P1419A_M1299_IP14070_18O160_S3103A_1_Dol3@3 (OS-11-41 342.97)	dol 3	-3.92	20.10	0.09	20.04
P1419A_M1299_IP14070_18O160_S3103A_1_Dol3@2 (OS-11-41 342.97)	dol 3	-3.92	20.35	0.26	20.19
P1419A_M1299_IP14070_18O160_S3103B_3_Dol3@1 (OS-11-41 342.97)	dol 3	-3.18	20.48	0.16	20.38
P1419A_M1299_IP14070_18O160_S3103B_2_Dol3@1 (OS-11-41 342.97)	dol 3	-1.55	20.96	0.20	20.83
P1419A_M1299_IP14070_18O160_S3103B_1_Dol3@1 (OS-11-41 342.97)	dol 3	-5.30	21.15	-	21.15
P1419A_M1299_IP14070_18O160_S3106B_1_Dol3@1 (OS-11-83 123.84)	dol 3	-7.08	24.32	0.34	24.10
P1419A_M1299_IP14070_18O160_S3106A_3_Dol3@1 (OS-11-83 123.84)	dol 3	0.08	31.38	0.09	31.32
P1419A_M1299_IP14070_18O160_S3107B_1_Dol3@3 (OS-12-120 43.37)	dol 3	-7.76	22.14	0.75	21.67
P1419A_M1299_IP14070_18O160_S3107C_2_Dol3@3 (OS-12-120 43.37)	dol 3	0.42	27.64	0.14	27.55
P1419A_M1299_IP14070_18O160_S3112B_3_Dol3@1 (OS-12-120 138.05)	dol 3	-6.50	22.18	0.32	21.98
P1419A_M1299_IP14070_18O160_S3112A_2_Dol3@1 (OS-12-120 138.05)	dol 3	-8.28	23.68	3.14	21.70
P1419A_M1299_IP14070_18O160_S3107B_1_Dol3@5 (OS-12-120 43.37)	dol 3	-5.97	19.54	0.14	19.45
P1419A_M1299_IP14070_18O160_S3112B_3_Dol3@2 (OS-12-120 138.05)	dol 3	-6.88	18.40	1.12	17.69
P1419A_M1299_IP14070_18O160_S3105A_1_Dol2@1 (OS-11-80 176.03)	dol 3	-0.76	19.43	0.46	19.14
P1419A_M1299_IP14070_18O160_S3105A_1_Dol2@2 (OS-11-80 176.03)	dol 3	-2.62	18.14	0.13	18.06
P1419A_M1299_IP14070_18O160_S3112A_3_Dol3@2 (OS-12-120 138.05)	dol 3	-8.85	20.19	0.65	19.78
P1419A_M1299_IP14070_18O160_S3106A_2_Dol3@1 (OS-11-83 123.84)	Dol 3	3.15	34.28	NA	NA

SIMS Data for host rocks and all carbonate phases. Values are in ‰. FeO data is from EMPA on adjacent spot ("-" denotes values below detection). $\delta^{18}\text{O}$ (SMOW)* column is Fe-corrected data as described in Chapter 2.4.5. NA denotes spots which were not analyzed.

Comment	Phase	$\delta^{13}\text{C}$ (PDB)	$\delta^{18}\text{O}$ (SMOW)	FeO (wt%)	$\delta^{18}\text{O}$ (SMOW)*
P1419A_M1299_IP14070_18O160_S3112A_2_Dol3@2 (OS-12-120 138.05)	dol 3	-6.52	22.52	1.10	21.83
P1419A_M1299_IP14070_18O160_S3106A_2_Dol3@2 (OS-11-83 123.84)	dol 3	-1.13	25.35	NA	NA
P1419A_M1299_IP14070_18O160_S3105A_2_Dol3@1 (OS-11-80 176.03)	dol 3	NA	18.98	0.39	18.74
P1419A_M1299_IP14070_18O160_S3106A_3_Dol3@2 (OS-11-83 123.84)	dol 3	NA	25.64	0.15	25.54
P1419A_M1299_IP14070_18O160_S3107B_1_Dol3@4 (OS-12-120 43.37)	dol 3	NA	22.94	0.18	22.82
P1419A_M1299_IP14070_18O160_S3107C_2_Dol3@4 (OS-12-120 43.37)	dol 3	NA	21.82	0.28	21.64
P1419A_M1299_IP14070_18O160_S3112B_2_Dol3@1 (OS-12-120 138.05)	dol 3	NA	22.65	0.50	22.34
P1419A_M1299_IP14070_18O160_S3112B_2_Dol3@2 (OS-12-120 138.05)	dol 3	NA	22.30	1.07	21.62
P1419C_M1299_IP14078_13C12C_S3105A_3_Dol3@1 (OS-11-80 176.03)	dol 3	-2.17	NA	NA	NA
P1419C_M1299_IP14078_13C12C_S3105A_2_Dol3@2 (OS-11-80 176.03)	dol 3	3.55	NA	NA	NA
P1419B_M1299_IP14070_18O160_S3105A_1_Cal4@2 (OS-11-80 176.03)	cal 4	-0.59	18.59	-	NA
P1419B_M1299_IP14070_18O160_S3105B_1_Cal4@1 (OS-11-80 176.03)	cal 4	-7.20	17.89	-	NA
P1419B_M1299_IP14070_18O160_S3105B_1_Cal4@2 (OS-11-80 176.03)	cal 4	-6.62	18.00	0.19	NA
P1419B_M1299_IP14070_18O160_S3105B_1_Cal4@3 (OS-11-80 176.03)	cal 4	-7.36	17.82	-	NA
P1419B_M1299_IP14070_18O160_S3105B_1_Cal4@4 (OS-11-80 176.03)	cal 4	-6.16	18.03	-	NA
P1419B_M1299_IP14070_18O160_S3105B_2_Cal4@1 (OS-11-80 176.03)	cal 4	-6.92	19.39	-	NA
P1419B_M1299_IP14070_18O160_S3105B_2_Cal4@2 (OS-11-80 176.03)	cal 4	-7.25	19.44	-	NA
P1419B_M1299_IP14070_18O160_S3105B_2_Cal4@3 (OS-11-80 176.03)	cal 4	-6.21	19.33	-	NA
P1419B_M1299_IP14070_18O160_S3105B_2_Cal4@4 (OS-11-80 176.03)	cal 4	-5.00	17.37	-	NA
P1419B_M1299_IP14070_18O160_S3105A_1_Cal4@1 (OS-11-80 176.03)	cal 4	NA	13.30	NA	NA
P1419D_M1299_IP14078E_13C12C_S3105A_1_Cal4@3 (OS-11-80 176.03)	cal 4	0.19	1	0.08	NA